Two-Ion Control and Polarization Forces for Precise Mass Comparisons

by

James K. Thompson

Submitted to the Department of Physics
in partial fulfillment of the requirements for the degree of

Doctor of Philosophy

at the

MASSACHUSETTS INSTITUTE OF TECHNOLOGY

September 2003

Author .....
Department of Physics
July 31, 2003

Certified by .....
David E. Pritchard
Cecil and Ida Green Professor of Physics
Thesis Supervisor

Accepted by .....
Thomas J. Greytak
Professor of Physics, Associated Department Head for Education

Two-Ion Control and Polarization Forces for Precise Mass Comparisons

by

James K. Thompson

Submitted to the Department of Physics
on July 31, 2003, in partial fulfillment of the
requirements for the degree of
Doctor of Philosophy

Abstract

We have improved the ability to compare the masses of single ions by an order of magnitude to a fractional accuracy of $\sim 7 \times 10^{-12}$. This is done by simultaneously confining two ions in a Penning trap, and simultaneously comparing their cyclotron frequencies which are inversely proportional to the masses. The precision of the previous technique of alternately trapping the two ions was completely limited by magnetic field noise. Our new technique reduces the impact of both magnetic field and trap voltage noise by more than three orders of magnitude.

We can measure and control the relative motion of the two ions in the Penning trap. We have developed a new mode coupling technique to park the ions on a shared magnetron orbit of diameter 1 mm but on opposite sides of the trap. We superpose on top of this magnetron motion the small cyclotron orbits of 150 μm diameter needed to simultaneously compare the cyclotron frequencies. The Coulomb interaction keeps the separation of the cyclotron guiding centers constant, thus minimizing cyclotron frequency perturbations due to ion-ion interactions. The ions spatially average magnetic field inhomogeneities and electrostatic imperfections at the magnetron frequency of 5 kHz. We have developed techniques to precisely measure and systematically vary the ion-ion separation. The control techniques are critical for exploring systematic errors.

We discovered that we are sensitive to induced charge distributions within our molecular ions. As an ion moves on its cyclotron motion, it experiences a motional electric field which can polarize the ion. The induced charge distribution then leads to a systematic cyclotron frequency shift. Since the polarizability of the ion depends on its quantum state, we can monitor the quantum rotational state of a single CO^+ molecule by measuring its cyclotron frequency. From the size of the observed cyclotron frequency shifts between rotational states, we determine the electric dipole moment of the CO^+ to be 1.025(15) $ea_\circ$. This novel example of a polarization force has not been observed previously.

Thesis Supervisor: David E. Pritchard
Title: Cecil and Ida Green Professor of Physics

To my parents
John and Noreen

for your unconditional love and support....

Acknowledgments

My time at MIT has been a wonderful experience. I would like to thank the many people who helped to make it so.

The RLE staff have been beyond friendly and are always willing to go the extra mile to help you. At the top of the list is Carol Costa, who from the very start was there to guide me through the local bureaucracy and to remind me of deadlines, talks, and especially cookie hour. But more than anything else, she always expressed a genuine concern in my (and everyone's) personal well being, and she was always ready to offer encouragement and perspective. Thank you, Carol!

The other members of the RLE staff have also been fantastic. In particular, Maxine Samuels and Lorraine Simmons always made purchasing materials a breeze. Gerry Power, Al McGurl, and Dave Foss kept the facilities and network running in great shape. I feel very lucky that the RLE staff were both excellent professionals and genuinely nice people.

Throughout my time here, I was able to interact with many excellent colleagues who collectively helped to foster the creative and friendly atmosphere in the AMO group. I have many good memories of breaks from the lab to play basketball or soccer with Stephen Moss, Tony Roberts, Joel De Vries and a host of others. Thanks goes to Deep Gupta and Ananth Chikkatur for time spent together figuring out problem sets. David Kokorowski, Alex Cronin, and Rich Rubenstein were members of Dave Pritchard's interferometer lab who were always helpful for perspective or just the right screw or tool.

I have had the opportunity to work with many excellent undergraduates including Roland Nguyen, Baruch Feldman, Sidney Burks, Miranda Priebe, Josh Jackson, and Nisha Nath. They always brought eagerness and a freshness to the lab. Claudiu Stan brought his studied approach to problem solving in his first year of graduate school.

Ed Myers has taken over this experiment and moved it to Florida State University. He is a really excellent physicist who came up to speed amazingly fast. I am appreciative of all of his efforts to continue this experiment, and I feel quite confident that it has found a great home with him. I would also like to thank him for comments and feedback on this thesis, and most of all for being such a great mentor for me as an undergraduate.

Simon and I owe much to our predecessors. Our results are the culmination of work by many people. Bob Flannagan got the cryogenic aspect of the experiment up and running in the mid-'80's. Robert Weisskoff and Eric Cornell demonstrated most of the single-ion techniques still used today. Eric Cornell really laid the foundation for the two-ion technique and deserves special thanks for having gotten so much of the theory correct. Kevin Boyce made several crucial technical improvements including a very stable yet flexible voltage source for the trap. Vassant Natarajan and Frank DiFillippo demonstrated the ability to make a mass table. Fred Palmer (postdoc), Michael Bradley, and Trey Porto (postdoc) set the stage for our present work by building the experimental insert we currently use.

I would like to single out Mike and Trey for special thanks. When I joined the lab,

Mike and Trey were heroically hunting down spurious noise sources. They managed to get the cryogenic apparatus working only to realize that the trap voltage source was no longer working. Trey took the task of building a new voltage source on his shoulders and left us with a fantastically stable source that was crucial for our present work. Trey was also a wonderful source of subtle insight into physics. Mike led the charge to measure the alkali masses, which I believe to be the scientifically most important measurements to date. In the end, Simon and I were left with an apparatus in great shape, and we owe both of them many thanks for this. Trey and Mike also spent a considerable amount of time patiently answering my questions. To top it all off, they were both exceptionally nice guys whom I am glad to still call friends.

Simon Rainville has been a fabulous collaborator and friend. Some of the brightest and darkest hours of graduate school were spent together. Simon is a really excellent physicist with an amazing amount of patience and an eye for detail. He has the unique ability to shrug off pressures of the immediate and aim for the long term payoff. He is also one of the most organized people I know. In fact, I owe my very enrollment in graduate school to him since I could never quite remember to register on my own. I have enjoyed our many lunches together sitting in the shade of the MIT chapel. Simon's broad curiosity always made for great discussions and got our minds off the lab for a while. It has been an absolute pleasure to work together. I wish him all the best as he tests the waters of biophysics. I would also like to thank his wife Catherine who was always ready to offer a smile and encouragement.

Dave Pritchard has been leading this experiment for close to 20 years. When you join his group, he really gives you the keys and lets you set the direction. This reflects a deep trust in his students, and I consider myself lucky to have joined a world class experiment and been given such free reign. He was always there with suggestions and subtle insights. Of course, his insights must usually be aged a day or two before you actually realize just how clever they are. I would like to thank him for all of his advice and support.

Lastly, I would like to thank my family. I was blessed to have such special parents in John and Noreen. They always encouraged my curiosity and gave me a sense of grounding in life. My siblings Joneen and Billy have been a constant source of encouragement. They too are headed towards the Ph.D. finish line, and I can't wait to have my own copy of their theses. Of course, the person who has actually put up with the day to day inconveniences of my graduate school experience is my wife Debbie. She has consistently dealt with my late nights and long hours while trying to finish her own thesis. Her proofing talents also made this a much more readable thesis. I appreciate you so very much, and look forward to our next step together.

This work was supported by the National Science Foundation, the Joint Services Electronics Program, and a National Institute of Science and Technology Precision Measurement Grant.

Contents

Chapter 1

Introduction

1.1 Elegance

Elegance. This is the word I choose to start my thesis. A casual reader will no doubt be overwhelmed by the technical details necessary for a deep understanding of this work. But at the heart of this thesis is a very elegant set of simple ideas which should not be lost sight of and which I hope to introduce in this brief opening section. To convey the elegance of this experiment, I have aimed to make these first few pages accessible to a more general audience including my family and friends. The remainder of the thesis will be aimed at future graduate students who wish to become experts.

The goal of my efforts over many years has been to compare the masses of single atoms more accurately than has ever been achieved before. We have succeeded. We can now compare masses to 11 digits, making our measurements the most accurate in the world. There are many excellent reasons to do this. Some of the reasons have to do with testing our fundamental understanding of nature. One example is our attempt to discover exactly how correct Einstein was in placing an equal sign between E and mc^2. We have measured the m, a mass difference, by carefully measuring the difference in mass between two different types of silicon atoms. The two particular silicon atoms we have chosen to compare differ because one of them has had an extra neutron particle dropped into its core or nucleus. As the neutron falls into the center of the atom, it releases energy in the form of γ-rays. γ-rays are just a very energetic form of light. By measuring the color (or wavelength) of this light, one can determine the amount of energy released E. We can then simply multiply our measured mass difference times the speed of light squared, and see if this is equal to the energy released as γ-rays. This is how we can test the Einstein mass-energy equivalence relationship $E = mc^2$. On the other hand, if we trust that Einstein was exactly correct and $E = mc^2$, then our mass measurements are a way to precisely determine how much energy the released γ-rays carry away.

There are other fundamental but slightly more esoteric tests of our understanding of nature which we can perform with our mass measurements. One such test is of Quantum

Electrodynamics or QED, which describes how all charged particles (such as the particles of which you and I are composed) push and pull on one another. QED predicts that there are particles continually popping into existence and disappearing almost as quickly as they appeared. The theory allows us to precisely predict how this sea of transient particles changes the strength of the little magnet attached to every electron. But to do this calculation, one needs a fundamental number called the fine structure constant, or more usually α. The value of α is approximately $1/137$ and carries no units much like the mathematical constant $\pi = 3.14159....$ Unlike π however, α is a number which must be measured since it is specific to the particular universe in which we live (or at least our current level of understanding leads us to think this). Our mass measurements fit together with four other extremely precise measurements to determine the value of α out to eight digits: $\alpha = 1/(137.03600)$. Using this value, the theory of Quantum Electrodynamics can predict how strong an electron's little magnet ought to be. Another experiment (also using a Penning trap like our work) has measured the strength of a single electron's magnet. The measurement and prediction currently agree to eight digits! This means that the predicted sea of transient or virtual particles has very real effects which we can precisely measure and predict.

One other fundamental application of accurately comparing masses is to determine how much a little ghostly particle called a neutrino weighs. There are three known types of neutrinos called the electron-neutrino, muon-neutrino, and tau-neutrino because of their association with a particular type of particle. It was only recently discovered that neutrinos have nonzero mass. This was done using a several-story tall detector full of very pure water and buried deep inside of a mine to shield it from cosmic radiation. Essentially, this experiment and several others afterward showed that muon-neutrinos turn into another type of neutrino and then back again. This is akin to a cat turning into a dog and then back into a cat—strange indeed. It is not obvious, but this oscillation between neutrino types indicates that the neutrinos have different masses. Since the masses are different and $0 - 0 = 0$, this proves that the mass of at least one of the neutrinos cannot be zero.

This nonzero neutrino mass has an impact not only on our understanding of how particles interact with one another but also at the larger scale of how the universe evolves. As I sit here writing or as you sit there reading, there are approximately 10 000 000 000 000 000 neutrinos passing through our bodies every second. If neutrinos have even a tiny mass, the sum of the masses of all of the neutrinos in the universe could be larger than the sum of all of the other known matter in the universe. This has a profound effect on how the universe expands or contracts because of the gravitational force of these nonzero mass neutrinos.

By measuring the mass difference between special types of helium and hydrogen atoms (^{3}He and ^{3}H), we can help to determine the mass of the electron-neutrino. This can be done because the hydrogen atom spontaneously emits a single electron and a single electron-neutrino. Several groups around the world are carefully measuring the energy distribution of

the emitted electrons. From conservation of energy, the maximum energy that the electron can carry away is just the mass difference between the two atoms (converted into an energy with $E = mc^2$!) minus the mass of the electron-neutrino. By knowing the maximum energy carried away by an electron and our mass difference, the electron-neutrino mass can be determined. The techniques that we have developed, and which are presented in this thesis, leave the experiment poised to perform the ^{3}He versus ^{3}H mass comparison with unprecedented accuracy.

Clearly, our mass measurements can have an important impact on humanity's basic understanding of the universe. Of course, we cannot use a simple balance or spring scale to "weigh" these single atoms. Instead we use the very powerful experimental technique of turning the mass comparison into a counting comparison. To do this, we must remove one or several electrons from the atom so that it has a net charge. When we place the charged atom (called an ion) in a magnetic field, the ion moves in circles. We call this circular motion the cyclotron motion. The number of revolutions per second is proportional to the size of the magnetic field and inversely proportional to the ion's mass. We can place one ion in the magnetic field and count how many revolutions per second it executes. We can then place a different ion in the same magnetic field and measure how many revolutions per second that it executes. The ratio of the two numbers of revolutions then gives the ratio of the masses. This is the central idea of the technique.*

Of course, the magnetic field cancels from the ratio of the measured revolutions per second only if the magnetic field does not change between the measurements. If the magnetic field does change then the ratio of the two masses which we quote will be incorrect. In fact, the magnetic field is constantly changing. Here at MIT, the Boston subway creates enormous magnetic field fluctuations. We must also worry about the metal laboratory door opening and closing or the elevator down the hall moving from one floor to another.

To eliminate the effect of magnetic field noise on our mass measurements, I have spent the past three years with Simon Rainville implementing a technique which allows us to measure the revolutions per second of both ions *at the same time*. Any change in the magnetic field is then common to both ions and so cancels when we take the ratio of the two simultaneous measurements. We call this the two-ion technique to contrast it to all of the previous work in which only one ion at a time was used. The two-ion technique has been spectacularly successful, leading to a factor of 10 improvement in our ability to compare the masses of single atoms. This makes our mass comparisons currently the most accurate in the world. In addition, we no longer have to take all of our data between 1 am and 5 am when the subway is not running.

*For macroscopic objects, the unit of mass is the kilogram which is defined by a hunk of platinum-iridium metal stored in France. For small objects such as our atoms, it is more convenient to use a particular isotope of carbon ^{12}C as our mass reference. We can perform a chain of mass ratio comparisons relating a particular type of atom to the mass of ^{12}C. The mass of ^{12}C is defined to be exactly 12 u where u is the abbreviation of atomic mass unit. The atomic mass unit is related to the kilogram by the Avogadro constant $N_A = 6.022\,141\,99 \times 10^{23}$ and the statement that a N_A number of ^{12}C atoms has a mass of 0.012 kilograms.

When we have a pair of ions, we wish to hold on to them for several weeks so that we can carefully perform our measurements. To do this, we must add a set of specially shaped metal plates or electrodes which we bias with approximately 15 Volts (slightly more than your typical 9 Volt battery). The electric fields created by the electrodes provide confinement of the ions along the direction of the magnetic field. The magnetic field provides confinement in the radial direction (i.e. perpendicular to the magnetic field lines). Thus, the ion is trapped and cannot escape. This combination of electric and magnetic fields is called a Penning trap. We have held onto a single ion for more than a month in our Penning trap.

In order to "see" the ions, we have a very sensitive current detector which allows us to measure the tiny currents induced in the electrodes as the ion bounces up and down in the trap. We call this up and down motion the axial motion. The axial motion typically has an amplitude slightly less than a millimeter. In order to count how many times per second the ions revolve on their cyclotron motions, we use a coupling technique that allows us to convert the circular cyclotron motion into the up and down axial motion that we can detect. From the axial motion, we can determine where the ion was on its circular cyclotron orbit to about 1/40 of a revolution. To measure the revolutions per second, we set each ion in motion and allow them to orbit freely for some amount of time after which we measure their positions on their separate orbits. In between the start of the motion and the measurement of the final position, many complete orbits go by. We can keep track of these extra revolutions when the time interval is very short. From this we get a better estimate of the revolutions per second. We then repeat the measurement, but allow the ions to revolve for a slightly longer period of time. This technique is extremely powerful, allowing us to obtain the mass ratio to 10 digits in about one minute.[†]

We cannot haphazardly place two ions in the same trap at the same time. If the ions get too close to one another, they would interact very strongly. The interactions would cause us to inaccurately measure the mass ratio. To avoid this perturbation of the mass ratio, we keep the ions about 1 mm apart from one another. We exploit an extra mode of motion in our Penning trap called the magnetron mode to accomplish this.

The magnetron motion is a circular motion like the cyclotron mode but it is much slower. Typically, the cyclotron motion occurs at about 5 million revolutions per second while the magnetron motion occurs at about 5 thousand revolutions per second. The remaining up and down axial motion occurs at about 200 thousand bounces per second. See Fig. 2-3 for how the cyclotron, axial and magnetron mode occur all at once for a single ion in the trap.

We park the two ions we want to measure on a shared magnetron orbit but on opposite sides of the trap. Figure 1-1 shows what this would look like if viewed from above. The diameter of the motion about the center of the trap is set to about 1 mm. This relatively large separation is needed to avoid strong ion-ion interactions. We can then excite on top of this motion the smaller cyclotron orbits of radius $\sim$ 0.1 mm (about the width of two

[†]In one minute, the ion orbits once for every American!

human hairs) that we need to compare the masses.

One of the biggest challenges was to park the ions on a shared magnetron orbit. To do this, we first developed sensitive tools to watch each ion's magnetron motion so that we would know when we had achieved our goal. We developed a novel mode coupling technique that allows us to place the ions on the ideal shared magnetron orbit about the center of the trap. We can also move the ion pair onto a smaller or larger diameter magnetron orbit as desired. This control allows us to explore how our measured mass ratio changes as the ions interact more or less strongly. It is remarkable to think that we accomplish all of this simply by watching how the ions bounce up and down in the trap.

In the end, our control of the pair of ions was so complete that we were able to load a pair of silicon atoms into the trap and move them around for two weeks performing almost continuous measurements. We completed the entire series of measurements having made only one of the rarer of the two silicon atoms ever. This was no fluke as we were able to do the same for a pair of sulfur atoms.

We can now compare masses to slightly better than 11 digits with the two-ion technique. This is a factor of ten improvement over all previous work. With further tweaking and optimization, it should be possible to do even better in the future. The extreme sensitivity of these comparisons brought about something which was quite unexpected.

We found that our measurements are sensitive to the positions of the electrons inside the atom or molecule we are measuring. In fact, we are so sensitive that we can measure the charge distribution (or electric dipole moment) to a few percent. Such a direct measurement is a first for molecules with a net charge. In addition, the charge distribution depends on the quantum state of the molecule. By measuring the cyclotron frequency, we can continuously and nondestructively monitor the quantum state of a single molecule for weeks. For instance, by observing the cyclotron frequency, we can determine whether a single CO^+ molecule is rotating end-over-end like a dumbbell with one "quanta of rotation." If the molecule is rotating, then we can also determine whether the rotation axis is parallel to the magnetic field direction or not. We can observe when the molecule jumps from one quantum rotational state to another. These jumps occur when the CO^+ molecule absorbs or emits a quanta of rotation from or into the microwave radiation which is present in the background. This is quite a neat trick.

This gives a sample of the things I have worked on for the past six years of my life. I will now turn to a more technical discussion of these ideas beginning with a quick survey of similar experiments. To this point, I have tried to avoid using the usual technical jargon, but now I will shift gears and proceed at full steam.

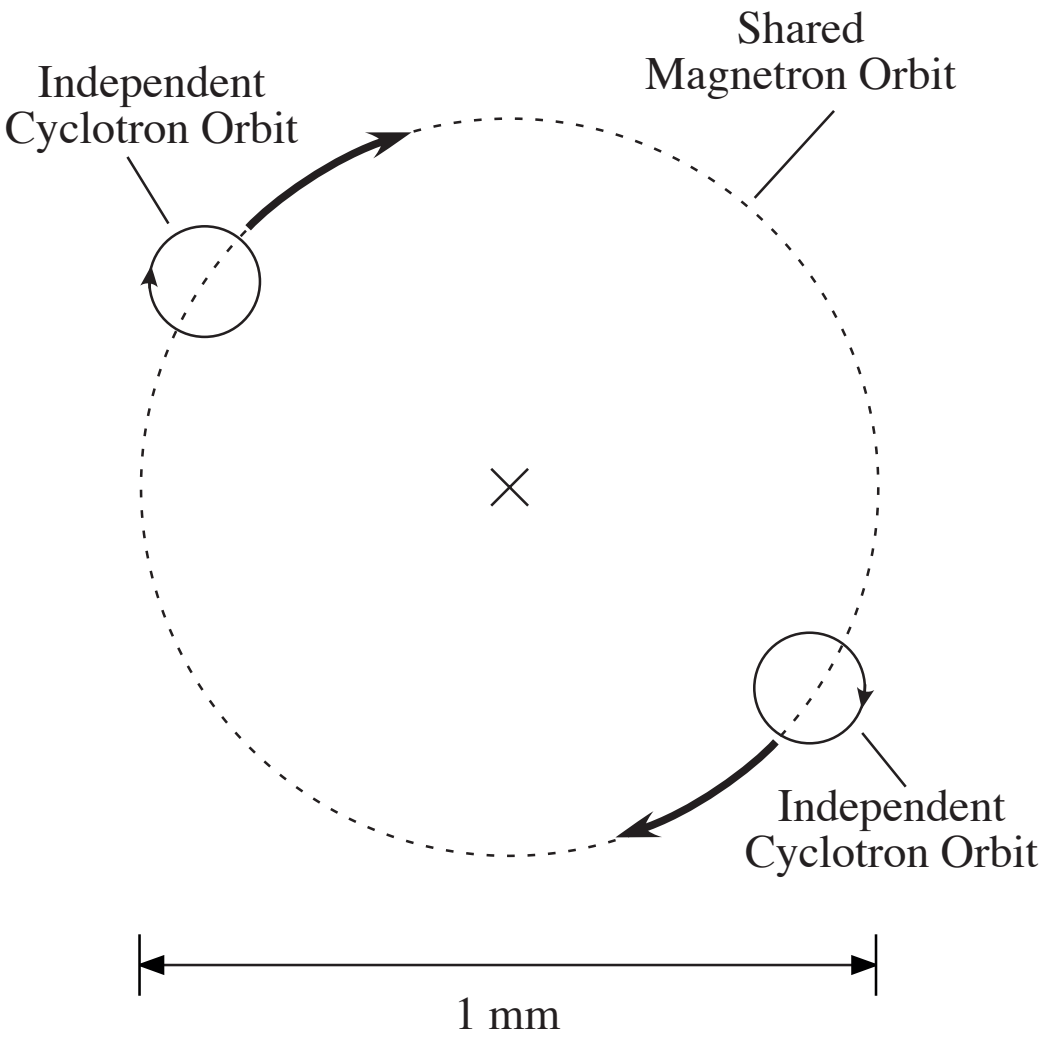

Figure 1-1: The two ions parked on a shared magnetron orbit, but on opposite sides of the trap. The x marks the center of the trap. The ions are too small to see so only their paths are shown. The ions complete about 5 thousand orbits per second on the large magnetron motion orbit indicated by the dashed line. We can then create much smaller circular cyclotron motions on top of this comparatively slow motion, as is shown by the solid circles. Each ion completes about 5 million orbits per second on the smaller cyclotron paths. By counting how many orbits per second each ion executes on its cyclotron path, we can determine the ratio of their masses. This configuration makes us completely insensitive to magnetic field variation since it is the same for both of them and cancels when we take the ratio of the measured orbits per second.

1.2 Oh, the Places We'll Go

This thesis represents work which was done in constant collaboration with Simon Rainville. The amount of material was so large that we were forced to make some arbitrary divisions of the material. Simon's thesis [1]^G focuses on a detailed examination of the experimental systematic errors associated with the two-ion technique, and the reader should go there for the full details on this material. Throughout this thesis, Simon's work will be referenced whenever it provides more detail on a particular subject. In addition, any reference originating from our lab will be denoted with a "Group" superscript ^{G}, as was done for the reference to Simon's thesis above. The remainder of this chapter will provide a quick overview of our field and then a more detailed discussion of the scientific applications of precise mass comparisons.

In Chapter 2, we introduce the physics of a single ion in a Penning trap. Some of this is standard to many ICR lab theses, but is useful to include here since much of the two-ion discussion will be built upon this foundation. In the first half of the chapter, we will discuss the physics of a perfect Penning trap. Section 2.1.3 aims to provide some physical intuition with regards to the radial modes of motion, which we feel was perhaps neglected in previous theses. Section 2.1.6 reinforces the analogy to a pseudo quantum system for building intuition about the physics behind the sideband couplings. An experimental demonstration of adiabatic conversion of motion from one radial mode to another will also be presented. In the second half of the chapter, we will provide some intuition regarding the effects of trap field imperfections on the cyclotron motion. The last part of the chapter contains a discussion of several experimental modifications and advances. Chief among these will be an explanation in Sect. 2.3.3 of the PhaseLock technique for continuously monitoring the axial frequency of a single ion.

Chapter 3 turns to an examination of the physics behind the two-ion technique. Some of this will be a restatement of previous results in the original two-ion technique proposal of Ref. [2]^G. The results are restated in a way that we feel gives more physical intuition regarding the underlying physics. Also, based on words of advice from Eric A. Cornell, who performed the majority of the original calculations, the results have been independently recalculated. In some cases such as the ion-ion nonlinear perturbation (Sect. 3.5.3), small errors were found and the correct results are presented. The accuracy of the perturbative estimate of the cyclotron-cyclotron frequency shift is confirmed by carrying the expansion to higher order in Sect. 3.5.3. The collective magnetron motion is presented in Sect. 3.3.2 with modified orbits which more accurately account for the nonlinear ion-ion interaction. These new orbits are confirmed by numerical simulation. In Sect. 3.3.4, an estimate is given of the effect of trap field imperfections on the collective magnetron motion. We conclude the chapter with an examination of the effect of nonzero axial orbits on the normal modes of motion.

Chapter 4 lies at the heart of this thesis. It describes the tools and techniques used

to measure and control the collective magnetron motion of the ions. The chapter begins by describing how we load the ions and the several techniques that were developed to coarsely park the ions on a shared magnetron orbit. We then turn to a discussion of how we measure the ion-ion separation and rms radius of each ion. We also show that we can sensitively measure the difference in the rms magnetron radii of the two ions. This is critical for increasing confidence in the size of the estimated systematic errors discussed in Simon Rainville's thesis. Lastly, the chapter concludes with a detailed demonstration and explanation of a coupling technique which allows us to move canonical angular momentum between the two collective magnetron modes. This coupling technique allows us to precisely park the ions on a shared magnetron orbit as well as to vary the ion-ion separation as we desire.

Chapter 5 is a summary of the fruits of our labor. Here, we describe our reduced sensitivity to both magnetic field and trap voltage noise. We also discuss how the two-ion technique reduces the effect of measurement noise and certain systematic errors. Improvements in the axial detector are discussed. The improvements allow us to simultaneously detect the two axial signals of the ions. We will then show the dramatic experimental increase in precision that results from simultaneous cyclotron frequency comparisons. We then present experimental confirmation of the predicted nonlinear cyclotron-cyclotron perturbation. Finally, the chapter concludes with a demonstration of our control of systematic errors by measuring the cyclotron frequency ratio versus ion-ion separation. This chapter has the greatest overlap with Simon Rainville's thesis $[1]^G$. As a result, I have strived to avoid simply duplicating his work, and instead try to give a slightly different perspective on some of the subjects. My intent is for Chap. 5 to serve as a complement to Simon's thesis.

Chapter 6 discusses the unexpected observation of cyclotron frequency variations (or jumps) arising from polarization forces, which were unaccounted for in all previous work comparing cyclotron frequencies. The experimental observations are presented first, along with an overview of other possible sources of cyclotron frequency jumps that we carefully eliminated. We then dicuss the theory of polarization forces and how these forces give rise to a new effective mass. The resulting cyclotron frequency shift had not been previously predicted, so some time is spent presenting several physical pictures of the origin of this force. A detailed comparison between the experimental and theoretical spectrum of measured cyclotron frequency ratios for CO^+ versus N_2^+ is performed and found to be in excellent agreement. From the data, the mass ratio of CO^+ versus N_2^+ is determined to 2×10^{-11}. The body-frame electric dipole moment of the CO^+ molecule is directly determined to a few percent, demonstrating a very novel probe of the structure of molecular ions.

Chapter 7 wraps things up with a summary and a brief discussion of possible future directions. The prospects and challenges of comparing $^3He^+$ vs. $^3H^+$ will be discussed. This mass ratio will be important for helping to determine the electron neutrino mass. In addition, a proposed method will be given to tune the magnetron radius imbalance to

zero. This has the potential to reduce systematic errors from trap field imperfections by an order of magnitude. Lastly, the thesis will conclude with a brief discussion of using two independent Penning traps to perform simultaneous cyclotron frequency comparisons.

1.3 Other Experiments

Our single ion mass spectrometry work is part of a larger community of Penning trap physics around the world. The pioneering work on trapping single ions was performed by Dehmelt and VanDyck at the University of Washington during the 1980s.[‡] Besides mass comparisons, work in Penning traps includes: electron g-factor measurement at Harvard [3], bound-state electron g-factor measurements at Mainz [4], and formation of antihydrogen by both the ATHENA [5] and ATRAP [6] groups at CERN.

The group of Robert S. VanDyck at the University of Washington (UW) is the only other group in the world that can perform mass comparisons with accuracy significantly greater than 1 part in 10^{10}. As such their work is our only direct competition. The UW approach is based on carefully engineering their magnetic field to be stable to $\leq 1 \times 10^{-11}$/hour. To do this, they designed a new magnet which eliminates all materials with temperature dependent magnetic susceptibilities. They also ensure that all surfaces surrounding the magnet are maintained at a constant temperature. This is done by direct cooling with the LHe rather than the previous He vapor provided by the variable rate boil off. They also use external magnetometers and feedback to compensate for external magnetic field fluctuations [7]. The UW group has used this apparatus to measure the atomic mass of the proton and ^{16}O to 1.4×10^{-10} and 1×10^{-11} respectively [8]. To achieve a relative precision of 10^{-11}, they require approximately 200 hours of integration, compared to only 5 hours with our technique (a factor of 40 difference.) They predict that it will be difficult to do better than 1×10^{-11} because of systematic errors associated with measuring the axial frequency of the ions. As will be shown in Chap. 5, our technique does not require ultra-precise axial frequency measurements, even for mass ratios with accuracies of 10^{-12}. The UW group should also be mentioned for their measurement of the atomic mass of the electron to 2×10^{-9} [9]. This is currently the most accurate experimental value in existence that does not rely on complex QED calculations as part of the determination [10].

The group of Gerry Gabrielse at Harvard has performed a comparison of the proton/antiproton mass to charge ratio as a test of CPT. The measured ratio differs from one by $-0.9(9) \times 10^{-10}$ [11]. This comparison was performed by simultaneously confining a single antiproton and an H^- ion in the same trap. They placed the ion not being measured on a 2 mm cyclotron orbit to store it while the other ion's cyclotron frequency was measured at the center of the trap. They would then cool the outer ion to the center of the trap and store the other ion on a large cyclotron orbit. The small cyclotron damping rate meant

[‡]Dehmelt received the Nobel prize for his work. The award could have legitimately been shared with VanDyck for his contribution to the determination of the electron and positron g-factors.

that it took 1 to 2 hours to accomplish the switching.[§] This time scale is to be compared to their magnetic field drifts of 0.4 to 2.0×10^{-9}/hour. Additionally, they were restricted to taking data at night when magnetic field noise was reduced. This storage technique for making alternating comparisons is a much simpler technique than our two-ion technique. But as a result, their technique lacks the true power of simultaneous cyclotron frequency comparisons, which eliminates magnetic and trap voltage noise and also reduces measurement and systematic errors.[¶] On a separate point, the polarization force shift, which we discovered and which will be discussed in Chapter 6, impacts their comparison at the level of the quoted error. This is the result of the large polarizability of the H^- ion.

The SMILETRAP group in Stockholm is the only other group to demonstrate mass comparisons with precision below 10^{-9}. Their most accurate measurements have accuracies $\sim 5 \times 10^{-10}$ [12], [13]. Many other groups are pushing toward higher precision mass spectrometry. Most of these groups are seeking to perform measurements of radioactive nuclei and spend much of their time worrying about creating and loading the ions to be measured before they decay.

1.4 Scientific Applications: Overview

In work prior to the two-ion technique, we measured a total of 13 neutral masses[‖], ranging from the mass of the proton to the mass of ^{133}Cs all with accuracies one to three orders of magnitude higher than the previously accepted values. This advance in accuracy has allowed important contributions in both fundamental physics and metrology, including:

- an 80-fold improvement of the current γ-ray wavelength standard by using $E = \Delta mc^2$ to determine the energies of ^{14}N neutron capture γ-rays (widely used as γ-ray calibration lines) $[15]^G$,
- opening the way for an atomic standard of mass by replacing the artifact kilogram mass standard with a crystal of pure silicon and our accurate determination of the atomic mass of ^{28}Si $[15]^G$,
- new determinations of the molar Planck constant, $N_A h$, with precision ~ 10 ppb $[14]^G$,
- new determinations of the fine structure constant, α, with precision ~ 5 ppb $[14]^G$,

[§]For comparison, our typical switch time between ion species is ~ 10 minutes when performing alternating measurements.

[¶]The two-ion technique described in this thesis could be used to compare the mass to charge of the proton and antiproton to $\sim 10^{-12}$. The modifications necessary for such a measurement are similar to those described in Sect. 7.2 for the comparison of $^3He^+$ versus $^3H^+$. The main challenge would lie in loading the antiproton. But once the antiproton is loaded, we could potentially hold on to it for quite some time.

[‖]I significantly contributed to the data taking, analysis, and writing of the publication for approximately 1/3 of them: ^{133}Cs, ^{87}Rb, ^{85}Rb, and ^{23}Na $[14]^G$.

- providing reference masses for mass comparisons of radioactive nuclei that are important for testing models of astrophysical heavy element formation [16].

By improving our accuracy using the two-ion technique we have opened the door to further contributions to fundamental physics, including:

- checking the relationship $E = mc^2$ to a few parts in 10^7 by weighing γ-rays from neutron capture by ^{32}S and ^{28}Si [17]; this could also provide an independent determination of $N_A h$ and the fine structure constant α,
- measurement of the ^{3}H - ^{3}He mass difference, which is important in ongoing experiments to determine the electron neutrino rest mass [18], [19],
- determination of excitation and binding energies of atomic and molecular ions by weighing the associated small decrease in mass, $\Delta m = E_{binding}/c^2$ (we must reach our ultimate goal of a few parts in 10^{12} to make this a generally useful technique),
- improvement of traditional applications of mass spectrometry resulting from our orders of magnitude improvement in both accuracy and sensitivity.

In addition, we have discovered a cyclotron frequency shift arising from polarization forces that allows

- nondestructive quantum state measurement of a single molecule over the extremely long time scales of weeks,
- determination of the molecular electric dipole moment of ions such as CO^+ to a few percent,
- the possibility of single molecule spectroscopy using nondestructive state detection provided by cyclotron frequency measurements.

1.5 Molar Planck Constant $N_A h$ and the Fine Structure Constant α

Soon after I joined the lab, we measured the masses of ^{133}Cs, ^{87,85}Rb, and ^{23}Na [14]^G, [20]^G as part of a program to determine the Molar Planck constant $N_A h$ and the fine structure constant α from measurements of h/m_{atom}. A further motivation for our measurements is that Cs and Rb are used as reference masses for measurements of heavy radioactive nuclei that are important for modeling astrophysical heavy element formation [21], [16]. As shown in Table 1.1, we improved the accuracy with which these masses are known by one to two orders of magnitude.

Table 1.1: Measured neutral alkali masses.

Species	MIT Mass (u)	ppb	1995 Mass (u) [22]	ppb	$difference/\sigma_{1993}$
^{133}Cs	132.905 451 931 (27)	0.20	132.905 446 800 (3200)	24.0	1.6
^{87}Rb	86.909 180 520 (15)	0.17	86.909 183 500 (2700)	31.0	-1.1
^{85}Rb	84.911 789 732 (14)	0.16	84.911 789 300 (2500)	29.0	0.2
^{23}Na	22.989 769 280 7 (28)	0.12	22.989 769 670 0 (2300)	9.8	-1.7

1.5.1 Molar Planck Constant $N_A h$

The Molar Planck constant $N_A h$ is an important quantity in metrology and for fundamental physics.** New values of $N_A h$ at the few ppb level in combination with measurements of h (such as a recent 87 ppb measurement [24]) can yield values of N_A with ppb level accuracy. Precise values of $N_A h$ would also provide a way to check QED and test the unity of physics across disciplines by accurately determining the fine structure constant α.

Avogadro's number N_A is the ratio of the SI and atomic units of mass [25]. The unified atomic mass unit is defined by setting the atomic mass of ^{12}C to be exactly 12 u. N_A is defined as the number of elementary entities in one mole (the amount of substance whose mass in grams equals its atomic mass) and has an approximate value of $N_A \approx 6.022 \times 10^{23}$/mole. Avogadro's number can then be written as the ratio of any atom's mass in atomic mass units denoted by M_{atom} and in SI units denoted by m_{atom}

$$N_A = \frac{M_{atom}}{m_{atom}} \times 10^{-3} \tag{1.1}$$

where the factor of 10^{-3} arises because of the definition of Avogadro's constant in terms of grams rather than the SI unit kilogram.

Transposing Eq. 1.1 shows that $1/N_A$ can be regarded as the universal mass quantum (in grams). The mass of any elementary entity is then its atomic mass (i.e. mass quantum number) times this mass quantum. (Unlike most other quantized quantities, the mass quantum number is not a simple rational number.)

Thus, $N_A h$ is the ratio of h to the mass quantum, a universal h/m. It can be obtained from a particular value of h/m_{atom} by multiplying by M_{atom}

$$N_A h = \frac{h}{m_{atom}} M_{atom} \times 10^{-3} \ . \tag{1.2}$$

Our technique for measuring M_{atom} therefore allows measurements of h/m_{atom} using different atoms to be compared with $\approx 10^{-10}$ accuracy.

In both Schroedinger's equation for a free particle and the expression for magnetic moments of elementary entities, h and m always occur in the ratio h/m. Thus h/m is often measured in experiments involving simple quantum expressions. By equating the classical

**This section is a direct quote from Ref. [23]^G. The first half of the article that is used here was co-written by David E. Pritchard and myself.

($p = m_x v$) and quantum ($p = h/\lambda_{dB}$) expressions for the momentum of a particle, we see that measurements in SI units of the deBroglie wavelength λ_{dB} and the velocity v of a particle combine to measure h/m_X in SI units,

$$v\lambda_{dB} = \frac{h}{m_X} \ . \tag{1.3}$$

Comparison of the energy and wavelength of a photon would also yield a value of $N_A h$, but at accuracies of ≈ 100 ppb [15]^G.

Precision mass spectrometry now allows several independent determinations of $N_A h$ from several independent measurements of h/m_{atom} using different atoms. The values of h/m_{atom} for different species can be compared with no reduction in accuracy at the 0.1 ppb level. Using *different* atoms possessing very *different* systematic measurement errors will provide a strong constraint on experimental errors.

1.5.2 Fine Structure Constant α

An accurate value of the Molar Planck constant leads to a new determination of the fine structure constant α. Noting the definitions of $\alpha \equiv e^2/\hbar c$ and the infinite-nuclear-mass Rydberg constant $R_\infty \equiv (2\pi^2 m_e e^4)/(h^3 c) \approx 1.09 \times 10^5$ cm^{-1} (cgs units) makes it easy to see that

$$\alpha^2 = \frac{2R_\infty}{c}\frac{h}{m_e} = \frac{2R_\infty}{c}\frac{m_p}{m_e}\frac{N_A h}{M_p}10^3 \ . \tag{1.4}$$

R_∞ is known with an accuracy of 0.008 ppb [26]. m_p/m_e has been measured to 2 ppb [9]. The mass of the proton in atomic units M_p has been measured by our group to 0.5 ppb [15]^G, and VanDyck *et al.* have reported a value of M_p accurate to 0.14 ppb [27]. The speed of light c is a defined constant. Thus an independent measurement of $N_A h$ is capable of determining α to 1 ppb.

The possibility of redundancy in the experimental determination of $N_A h$ would greatly enhance the confidence in determinations of α from Eq. 1.4. This is not a trivial point since it would take a considerable weight of evidence to believe that disagreement between the QED and $N_A h$ determinations of α signifies some error in QED. The mass ratio m_p/m_e is the only quantity without more than a single direct measurement at the ppb level (a recent value of $m_e/m_{^{12}C}$ extracted from QED theory and boundstate electron g factor measurements in hydrogenic ^{12}C has confirmed the value to about 2 ppb [28]).

1.5.3 Update

Since the initial measurement of the alkali masses, the predicted progress on measurements of h/m_{atom} has been made. The Stanford group under the direction of Chu recently published a preliminary value of h/m_{Cs} with a quoted fractional accuracy of about 15×10^{-9}

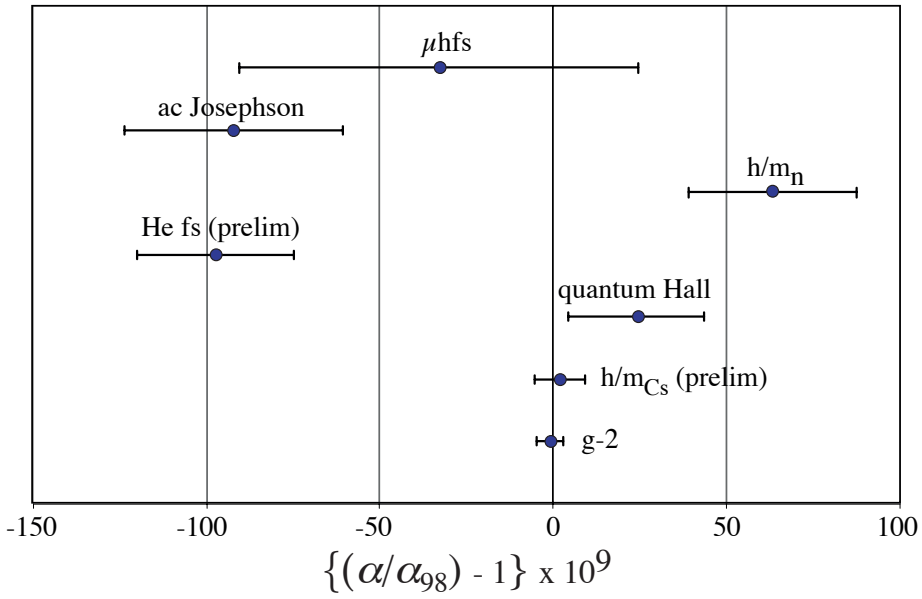

Figure 1-2: Current determinations of the fine structure constant α. The figure shows the fractional deviation from the CODATA98 value of $\alpha_{98}^{-1} = 137.035\ 999\ 76(50)$. Our mass measurements are integral parts of the two determinations $h/m_{\rm Cs}$ and $h/m_{\rm n}$. The values were taken from references [29], [30], and [31].

[30]. This will determine the Molar Planck constant to the same accuracy and the fine structure constant to twice the accuracy, or 7.5×10^{-9}. A reanalysis of the data is presently underway to more carefully examine shifts of the absorbed photon's wavelength due to the index of refraction created by the surrounding cloud of cold atoms. This has the possibility of decreasing the final quoted uncertainty on α to 3.1×10^{-9}. The agreement of this preliminary result with the value from the electron g-2 (combined with QED calculations) is well within the errors, but we should wait for the final result before drawing conclusions.

The Stanford group has ceased operation of the apparatus used to obtain the latest results. They are beginning construction of a second apparatus using a double interferometer geometry to reduce their sensitivity to noise from vibration of the optical elements. The rather ambitious goal is to improve the current measurement by one to two orders of magnitude. This would make the uncertainty on the atomic mass of the electron the dominant source of error in determining α (if we wish to use the QED-independent measurement of the electron mass) [9],[10].

In addition to the work on Cs, the challenges of measuring h/m_{atom} for Rb and Na have been taken up by two other groups. These groups not only work with different atomic species than the Stanford Group, but they also use extremely different experimental approaches. This will provide a powerful check of the systematic errors on $N_A h$ and the associated fine structure constant α. A measurement of $h/m_{\rm Rb}$ is currently underway at the Laboratoire Kastler Brossel, Ecole Normale Supérieure under the direction of Biraben

[32]. They estimate a final accuracy of 60 ppb on $h/m_{\rm Rb}$ and therefore 30 ppb on α. An initial measurement of $h/m_{\rm Na}$ with 7 ppm precision has been performed at MIT under the direction of Pritchard [33]. The work at MIT demonstrated a new type of double interferometer that is insensitive to the vibrations and ac Stark shifts that were large sources of noise and error in the Stanford work. This technique also has the advantage that the measured phase shift goes quadratically with the number of absorbed photons compared to the linear dependence of the Stanford interferometer. Because the systematic errors associated with measuring $h/m_{\rm Rb}$ are predicted to be lower, there is a possibility that the MIT group will switch to working with Rb. The MIT group estimates that a final precision of a few ppb is possible with their demonstrated technique.

1.6 Testing $E = mc^2$

The relationship $E = mc^2$ will be tested using our newly measured mass ratios for the pairs $^{29}{\rm Si}^+/^{28}{\rm SiH}^+$ and $^{33}{\rm S}^+/^{32}{\rm SH}^+$. These ratios were measured with the two-ion technique to a fractional accuracy of 7×10^{-12} which represents an order of magnitude improvement on our previous best mass comparisons. The test of $E = mc^2$ will be accomplished by comparing the mass differences $\Delta M_{\rm Si} = (M[^{28}{\rm Si}]+M[{\rm n}]-M[^{29}{\rm Si}])$ and $\Delta M_{\rm S} = (M[^{32}{\rm S}]+M[{\rm n}]-M[^{33}{\rm S}])$ to the energy of the emitted γ-rays in the neutron capture processes converting ^{28}Si to ^{29}Si and ^{32}S to ^{33}S [17]. The energy of the emitted γ-rays is determined by measuring their wavelengths using Bragg diffraction. The wavelength measurements, which are still being analyzed, were performed by NIST at the ILL in France [34].

We expect that the ultimate sensitivity of this comparison will be limited by the precision of the γ-ray wavelength measurements to 3 parts in 10^7. This test of special relativity does not depend on measuring spatial anisotropy as do most other tests such as the Michelson-Morley and Hughes-Drever experiments. As a result, this test does not require the assumption that the Cosmic Microwave Background is a preferred frame of reference in order to set limits on various parameters quantifying the violation of special relativity [35].

A violation of mass-energy equivalence can be thought to signify two different fundamental speeds in the theory of special relativity: an electromagnetic speed of light c_{em}, which is the speed with which light propagates in a vacuum, and a distinct mechanical speed of light c_m, which is the limiting speed of a massive particle [17]. Introducing these labels, the comparison can be expressed in terms of accurately measured quantities using

$$\frac{\Delta M_x^\circ}{10^3 N_A h} c_m^2 = c_{em}\left(\frac{1}{\lambda_x} - \frac{1}{\lambda_{\rm D}}\right) \quad . \tag{1.5}$$

The x refers to either the Si or S comparison. The mass difference is defined as $\Delta M_{\rm Si}^\circ = (M[^{28}{\rm Si}] + M[{\rm D}] - M[^{29}{\rm Si}] - M[{\rm H}])$ and similarly for the sulfur comparison. This is slightly different from the original mass difference defined above since we cannot directly measure the mass of the neutral neutron. The mass difference $\Delta M_{\rm Si}^\circ$ is determined from our measured

mass ratios at 10^{-11}, combined with the measured mass ratio of hydrogen and deuterium [36]. The ratio $2 \times M[\mathrm{H}]/M[\mathrm{D}]$ is only known to a relative accuracy of a few 10^{-10}, but to a similar absolute accuracy as our measurements. The modified mass difference $\mathbf{\Delta} M^{\circ}_{\mathrm{Si}}$ includes the neutron mass up to the deuteron binding energy. To account for this, the deuteron binding energy is subtracted from the right hand side of Eq. 1.5. The deuteron binding energy is determined from the wavelength λ_{D} of the emitted γ-rays in its own neutron capture process [37]. Lastly, the Planck constant h (used to convert frequency to energy) and the Avogadro constant N_A (used to convert the mass difference from u to kg), are combined to form the Molar-Planck constant, which is known to better than 10^{-8} from measurements of the fine structure constant as discussed in the previous section. The combined uncertainty on the mass difference is $\sim 5 \times 10^{-8}$ compared to the expected uncertainty on the wavelengths of 3×10^{-7}. The comparison of the two hypothetical fundamental speeds of light c_{em} and c_m is limited by the accuracy of the wavelength measurements. The accuracy of our latest measurements completely removes the mass measurements as a source of error for this comparison.

Of course, we can also turn things around by assuming the correctness of the mass-energy relationship. We could then solve Eq. 1.5 for the Molar Planck constant $N_A h$. This would yield a new determination of both the Molar-Planck and fine structure constants as was discussed in the previous section. Unfortunately, unless the wavelength measurements are significantly improved, the accuracy will not be competitive with other measurements of these fundamental constants.

Chapter 2

Single Ion Physics

2.1 Perfect Penning Trap Physics

2.1.1 Normal Modes

A Penning Trap is used to hold our ions in a small region of space $\sim$ 1 mm^3 for up to several weeks. The trap consists of a very uniform magnetic field of 8.5 T provided by a superconducting magnet (see Fig. 2-1). The magnetic field provides both a cyclotron mode to measure and the radial confinement. Axial confinement is provided by a much weaker quadrupole electric field established by a set of three electrodes called the Upper Endcap, the Lower Endcap and the Ring. To achieve a purely quadrupolar field, the electrodes form a set of hyperbola of rotation as shown in the cross section of Fig. 2-2. The Ring electrode is biased with respect to the Endcap electrodes by an amount V_{r}, typically -15 V for positive ions of mass to charge 30 u/e. Three normal modes of motion result from this combination of fields called the trap cyclotron, axial, and magnetron modes with a typical hierarchy of mode frequencies $\omega_{\mathrm{ct}} \sim 2\pi$ 5 MHz $\gg \omega_{\mathrm{z}} \sim 2\pi$ 0.2 MHz $\gg \omega_{\mathrm{m}} \sim 2\pi$ 5 kHz. Figure 2-3 shows the three normal modes of motion moving simultaneously. The trap cyclotron motion is so much faster than the other modes that it is represented as a solid ring. We can independently control the amplitude of each mode, and the situation shown here is just one particular example.

To examine the physics behind the normal modes, we explicitly write the magnetic field and electrostatic potential as

$$\vec{B} = B_0 \hat{z} \quad , \tag{2.1}$$

and

$$V(z, \rho) = \frac{V_{\mathrm{r}}}{2} \frac{z^2 - \frac{1}{2}\rho^2}{d^2} \quad . \tag{2.2}$$

The effective trap size d is given by

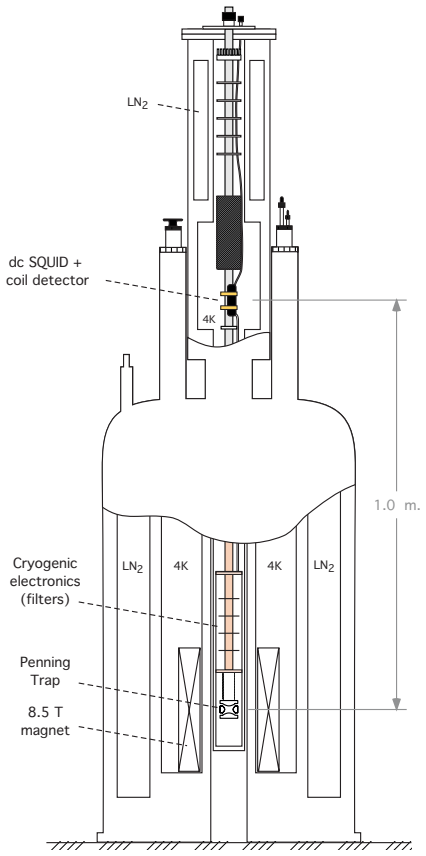

Figure 2-1: Experimental apparatus including the superconducting magnet.

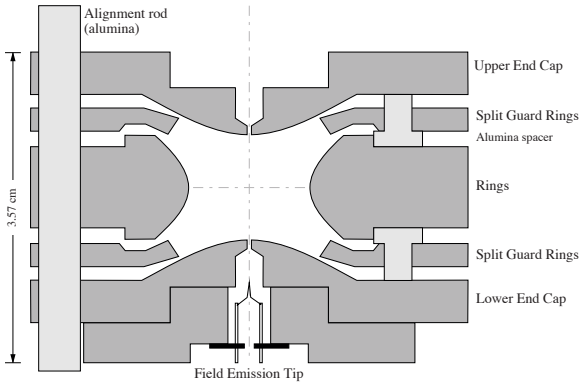

Figure 2-2: Penning trap electrodes used to provide axial confinement. The Ring electrode is biased with respect to the Endcaps using ~ 15 V. An 8.5 T magnetic field provides radial confinement as well as the cyclotron motion we will measure. The Guard Ring electrodes are biased with a common DC voltage to shim the electrostatic anharmonicity C_4. At rf frequencies, the Guard Rings are split in order to apply resonant dipole drive and quadrupole coupling fields. The field emission point (FEP) can be biased to provide an electron beam to ionize neutral gas that enters through the hole in the Upper Endcap.

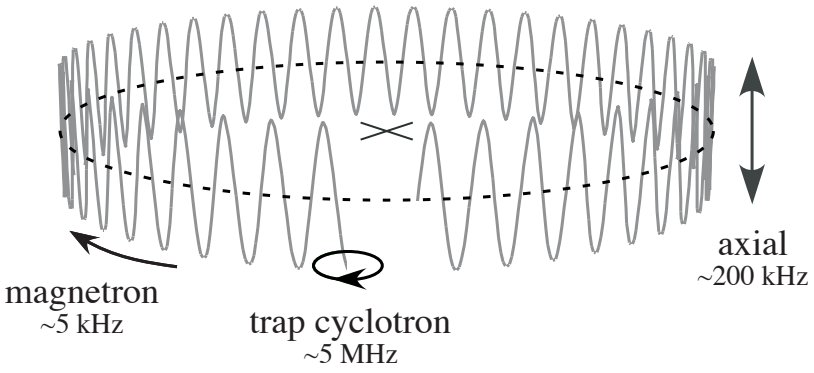

Figure 2-3: Penning trap normal modes of motion.

$$d^2 = \frac{1}{2}\left(z_0^2 + \frac{\rho_0^2}{2}\right) \quad . \tag{2.3}$$

The parameter z_0 is the distance from the center of the trap to the Upper/Lower Endcap electrode, and ρ_0 is the distance to the Ring electrode. For our trap, d= 5.49 mm.

These fields give rise to classical equations of motion that separate for the axial and radial motions. The axial equation of motion is just that for a classical harmonic oscillator

$$\ddot{z} + \omega_z^2 z = 0 \quad , \tag{2.4}$$

with angular frequency

$$\omega_z^2 = \frac{qV_r}{md^2} \quad . \tag{2.5}$$

The radial equation of motion (after dividing by the mass) is given by

$$\ddot{\vec{\rho}} = \omega_c \dot{\vec{\rho}} \times \hat{z} + \frac{1}{2}\omega_z^2 \vec{\rho}^2 \quad , \tag{2.6}$$

with ω_c just the free space cyclotron frequency qB_0/mc. Assuming circular motion at a frequency ω to be determined, one can make the substitution

$$\vec{\rho} = \Re\left\{(\hat{x} + \imath\hat{y})\, e^{\imath\omega t}\right\} \quad , \tag{2.7}$$

yielding a quadratic equation in ω with solutions

$$\omega_{ct} = \frac{\omega_c + \sqrt{\omega_c^2 - 2\omega_z^2}}{2} \quad , \tag{2.8}$$

$$\omega_m = \frac{\omega_c - \sqrt{\omega_c^2 - 2\omega_z^2}}{2} \quad . \tag{2.9}$$

The first motion with eigenfrequency $\omega_{\rm ct}/2\pi \sim 5$ MHz is called the trap cyclotron mode since it returns to the free space cyclotron frequency in the limit that the trapping potential and hence $\omega_{\rm z}$ go to zero. The other circular mode with frequency $\omega_{\rm m}/2\pi \sim 5$ kHz is called the magnetron mode and satisfies the condition $\omega_{\rm m} \ll \omega_{\rm ct}$ when $\omega_{\rm z} \ll \omega_{\rm ct}$ as is typically the case in our experiment. The trap cyclotron mode can be thought of as normal cyclotron motion slightly perturbed by the radial electric field of the trap. In contrast, the much slower magnetron motion should be thought of as a quasi-linear motion in which the force due to the radial electric field is balanced by the Lorentz force. The centrifugal force acts only as a small perturbation to the motion. In the limit $\omega_{\rm c} \gg \omega_{\rm z}$, the magnetron frequency $\omega_{\rm m}$ can be expanded to next leading order in $\omega_{\rm z}/\omega_{\rm c}$ as

$$\omega_{\rm m} = \frac{\omega_{\rm z}^2}{2\omega_{\rm c}} \left(1 + \frac{1}{2}\left(\frac{\omega_{\rm z}}{\omega_{\rm c}}\right)^2 + \mathcal{O}\left(\left(\frac{\omega_{\rm z}}{\omega_{\rm c}}\right)^4\right)\right) \quad . \tag{2.10}$$

The first term has no mass or charge dependence. In fact, it is just proportional to the ratio of the radial trap electric field and the axial magnetic field $E_{\rm rad}/B_0$. This is quite similar to what one finds for a so-called E cross B drift. The fact that the magnetron frequency $\omega_{\rm m}$ is at lowest order independent of both the charge and the mass is a key result for our present work. The second term is a mass dependent correction due to the centrifugal force and is typically of order 10^{-3}. For two ions with a fractional mass difference of $\leq 10^{-3}$, the fractional difference in the magnetron frequencies is $\leq 10^{-6}$. This is a frequency difference of ≤ 5 mHz for typical magnetron frequencies.

If the trap voltage is increased, eventually the ion cannot move on a stable orbit that generates a strong enough Lorentz force to balance the force from the radial trap electric field. As a result, the cyclotron orbit size will exponentially decrease while the magnetron orbit size will exponentially increase. The threshold for this behavior corresponds to the point at which the eigenfrequencies become complex, which happens when $2\omega_{\rm z}^2 > \omega_{\rm c}^2$. Equivalently, the threshold for this behavior can be expressed as $\omega_{\rm m} \simeq \omega_{\rm ct}$.

Ultimately, we wish to compare the free space cyclotron frequencies of single ions. We can determine the free space cyclotron frequency using either of two relationships involving the measured normal mode frequencies

$$\omega_{\rm c} = \omega_{\rm ct} + \omega_{\rm m} \tag{2.11}$$

or

$$\omega_{\rm c}^2 = \omega_{\rm ct}^2 + \omega_{\rm z}^2 + \omega_{\rm m}^2 \quad . \tag{2.12}$$

The first expression is useful for order of magnitude estimates of frequency shifts associated with imperfections in the trap electric fields. The second expression is much more important since it has been shown to be invariant with respect to trap tilt (i.e., misalignment of the

axial electric field and magnetic field) and trap ellipticity (i.e., the electrodes are slightly elliptical instead of perfectly circular) [38].

With the typical hierarchy of mode frequencies $\omega_{ct} \gg \omega_z \gg \omega_m$, we typically need to measure the axial and magnetron frequencies to much lower relative accuracy compared to the trap cyclotron frequency. If $\Delta\omega_{ct}$, $\Delta\omega_z$, and $\Delta\omega_m$ are the uncertainties on each mode frequency, then the uncertainty on the free space cyclotron frequency $\Delta\omega_c$ is given by

$$\left(\frac{\Delta\omega_c}{\omega_c}\right)^2 = \left(\frac{\Delta\omega_{ct}}{\omega_{ct}}\right)^2 + \left(\frac{\omega_z}{\omega_c}\right)^4 \left(\frac{\Delta\omega_z}{\omega_z}\right)^2 + \left(\frac{\omega_m}{\omega_c}\right)^4 \left(\frac{\Delta\omega_m}{\omega_m}\right)^2 \quad . \tag{2.13}$$

The axial and magnetron frequencies therefore need to be determined with $(\omega_z/\omega_c)^2 \sim 10^{-3}$ and $(\omega_m/\omega_c)^2 \sim 10^{-6}$ less relative precision than the trap cyclotron frequency. In terms of absolute precision for a typical ion with $m/q = 28$ u/e, we must measure the mode frequencies to $\Delta\omega_{ct}/2\pi \sim 5$ μHz, $\Delta\omega_z/2\pi \sim 200$ μHz, and $\Delta\omega_m/2\pi \sim 5$ mHz in order to determine ω_c to 1 part in 10^{12}. Achieving this accuracy is quite difficult for the axial mode. The two-ion technique relaxes the precision with which the axial and magnetron frequencies must be known by the fractional mass difference between the ions, which is typically $\leq 10^{-3}$ (see Sect. 5.2). Thus, the two-ion technique allows us to focus on measuring the trap cyclotron frequency very precisely, and more specifically the difference of the two trap cyclotron frequencies, thus returning us closer to the ideal situation in which only a magnetic field is present.

2.1.2 Axial Detection

We detect a single ion's axial motion by measuring the image currents induced between the Lower and Upper Endcaps as the ion moves up and down at 200 kHz. The detector consists of a self-resonant superconducting transformer, with $Q = 4 \times 10^5$ and center frequency 212 kHz, which is coupled to a dc SQUID. The SQUID is operated as a sensitive current detector. The self-resonant transformer is often referred to as the "coil" since it is a hand wound toroidal inductor with windings made of niobium wire.

In the current configuration discussed in Sect. 5.3, the signal to noise is dominated by the 4.2 K Johnson noise currents of the transformer. To achieve adequate signal to noise, we typically need to excite the ion to an axial amplitude between 200 and 1000 μm depending on the experimental details. It is also important that the axial frequency be very stable during the measurement, since we must rely on the narrow band nature of the signal to attain adequate signal to noise. From a typical axial signal integrated over 4 s, we can determine the phase, frequency, and amplitude of the axial motion to $\pm 10°$, ± 10 mHz, and $\pm 5\%$ respectively.

As the image currents flow through the transformer, a voltage is induced across the endcaps of the trap. This induced voltage acts back on the ion to damp its axial motion.

When the ion is resonant with the coil, a typical damping time is $\tau \sim 1$ s for an N_2^+ ion.* The damping allows us to quickly cool the axial motion to 4.2 K. The final axial temperature is set by the temperature of the Johnson noise currents in the transformer. The coupling of the ion to the transformer provides the only damping in our system, but we can use sideband coupling techniques discussed below to cool the radial modes by coupling them to the damped axial mode.

2.1.3 Pushing on the Radial Modes

The cyclotron and magnetron modes of motion are only distinguished by their frequencies since they are both clockwise rotations about the magnetic field lines.† Since the cyclotron motion moves at a much higher frequency, to first order one can assume that all the momentum is carried by the cyclotron mode and that the magnetron mode simply characterizes the guiding center of this cyclotron motion as it slowly drifts about the trap center. Practically, this is equivalent to obeying the classical boundary conditions on position and momentum at some time t in two steps. First, draw a circular motion tangent to the ion's velocity and with a radius ρ_c satisfying $v = \omega_c \rho_c$. Of course, there are two such circles that can be drawn, but only one of them corresponds to the correct clockwise motion. The radial vector specifying the magnetron motion $\vec{\rho}_m$ is just the center of this cyclotron motion with respect to the center of the trap. Having decomposed the motion into normal modes, the position at some later time t is trivially expressed as the sum of the two mode vectors $\vec{\rho} = \vec{\rho}_c + \vec{\rho}_m$ with each vector rotating clockwise at their normal mode frequencies ω_{ct} and ω_m. There is some error in this decomposition because the magnetron mode does carry some momentum, but the error is of order $(\omega_m/\omega_{ct})(\rho_m/\rho_c) \sim 10^{-3}(\rho_m/\rho_c)$.‡

Now imagine that we apply an instantaneous impulse $\vec{I}$ along some direction in the $x-y$ plane at $t = 0$. (For some reason, it is helpful for me to envision this as taking my finger and giving a fast poke to the ion.) The resulting change in momentum creates a small change in the cyclotron vector $\Delta\vec{\rho}_c$ satisfying

$$\vec{I} = -m\omega_c \left(\Delta\vec{\rho}_c \times \hat{z}\right) \quad . \tag{2.14}$$

Because the impulse is instantaneous, the ion's position is unchanged. The change in the magnetron vector $\Delta\vec{\rho}_m$ must be chosen to cancel the change in the cyclotron vector

$$\Delta\vec{\rho}_m = -\Delta\vec{\rho}_c \quad . \tag{2.15}$$

*The damping time increases as $\tau = \tau^\circ(1 + \delta^{*2})$ where τ° is the resonant value and δ^* is the ion-coil detuning in units of HWHM of the coil resonance.

†Clockwise here is as viewed with the magnetic field lines pointing out of the page. This perspective will be used throughout this thesis when discussing clockwise or counterclockwise motion.

‡In the case of infinitesimal *changes* of the two mode amplitudes to be discussed below, the change in amplitudes are equal in magnitude and the error is of order (ω_m/ω_{ct}).

The guiding center of the cyclotron motion is now given by the magnetron vector

$$\vec{\rho}_{\rm m} = \vec{\rho}_{\rm m0} + \Delta\vec{\rho}_{\rm m} \quad , \tag{2.16}$$

and the position of the ion on its cyclotron motion with respect to the guiding center is given by

$$\vec{\rho}_{\rm c} = \vec{\rho}_{\rm c0} + \Delta\vec{\rho}_{\rm c} \quad . \tag{2.17}$$

It is not possible to "push" on one radial mode without pushing on the other one as well. However, one can arrange the timing of our "pushes" so that they constructively add for one mode and average to zero for the other mode. It is possible to arrange for constructive interference for one mode and destructive interference for the other mode because of the different frequencies with which the two mode vectors rotate in between the pushes. This is precisely what happens when an rf dipole electric field resonant at one of the mode frequencies is applied. For a dipole drive at $\omega_{\rm ct}$, each $\Delta\vec{\rho}_{\rm c}$ adds constructively while each $\Delta\vec{\rho}_{\rm m}$ adds quasi-randomly to zero.

2.1.4 Coupling the Modes

The radial and axial modes move independently of one another under normal conditions. But as shown in [39]^G, a quadrupole electric field of the form $(z\hat{x} + x\hat{z})$ can couple either of the radial normal modes to the axial mode. The field is produced by applying an rf voltage to one of the four segments of the split Guard Ring electrodes. For now, let us just consider coupling of the cyclotron and axial modes. If the coupling were at DC, motion in the cyclotron mode would create a driving force along the axial direction at the cyclotron frequency. The response of the axial mode is suppressed by the large detuning of this axial force from resonance. By using an rf field with frequency $\omega_{\rm p} = \omega_{\rm ct} - \omega_{\rm z}$, a frequency component of the axial force is generated at $\omega_{\rm z}$. This resonant force causes growth of the axial motion. In turn, this axial motion will beat against the quadrupole rf field to generate a back-action force at $\omega_{\rm ct}$ along the $\hat{x}$ direction. This back-action force is out of phase with the original cyclotron motion. As a result, the cyclotron motion decreases until its amplitude is driven "through zero" and picks up a negative sign. Because of this negative sign, the cyclotron motion now creates a force along the axial direction out of phase with the original force, causing the axial amplitude to start to decrease.

The result is continuous oscillation of the motion between the modes, which can be described as classical Rabi oscillations with the quantum mechanical phase and amplitude replaced by the phase and classical action ($\oint \vec{p}_{can} \cdot d\vec{q}$) of each mode.[§] In the time domain,

[§]It is interesting to note that the classical action is precisely what is quantized in the Bohr-Sommerfeld approximation. This is especially striking when you realize that a π-pulse exchanges the harmonic oscillator quantum numbers between the two coupled modes.

this mode coupling appears as amplitude modulation of each mode. In the frequency domain, we observe the single peak in a power spectrum of the detected axial motion split into two peaks with a separation equal to the Rabi frequency ω_{R}.

We can form a π-pulse by applying the coupling for a time given by the relation $t_{\pi}\omega_{\mathrm{R}} = \pi$ so that the radial and axial modes completely swap classical actions and phases. Most importantly, the phase of the axial motion at the end of the π-pulse is just the phase of the cyclotron motion before the π-pulse up to several constant phase offsets.[¶]

It should be noted that if the rf field had been chosen to be $\omega_{\mathrm{p}} = \omega_{\mathrm{ct}} + \omega_{\mathrm{z}}$, then the back-action of the axial motion on the cyclotron motion would have been in phase with the original motion. This would lead to exponential growth of both the axial and cyclotron modes, which might be useful as a parametric amplifier in future work.[‖]

To couple the axial and magnetron modes, the correct coupling frequency is at $\omega_{\mathrm{p}} = \omega_{\mathrm{z}} + \omega_{\mathrm{m}}$. The sum frequency for this coupling is intimately related to the minus sign of Eq. 2.15. Exponential amplification of the modes occurs when the coupling is at the mode difference frequency $\omega_{\mathrm{p}} = \omega_{\mathrm{z}} - \omega_{\mathrm{m}}$.

2.1.5 PNP Cyclotron Frequency Measurement

The Pulse aNd Phase (PNP) technique is used to measure the trap cyclotron frequency ω_{ct}. This is a very elegant technique that allows the precision of the measurement to increase as the inverse of the measurement time $1/T_{\mathrm{evol}}$. The PNP technique is described in references [39][G] and [40][G]. The basic idea is to measure how much phase the cyclotron motion accumulates versus time. To accomplish this, the cyclotron motion is initially set to zero amplitude using a continuous coupling to the damped axial mode.[**] A dipole rf electric field resonant at ω_{ct} is applied for approximately 30 ms, creating cyclotron motion with amplitude ~ 100 μm.[††] The cyclotron motion then freely evolves phase for some time T_{evol} completely undetected and undamped so that perturbations are minimized. A π-pulse

[¶]The phase offsets include the phase of the coupling rf field and the translation of the time-coordinate to the end of the coupling pulse.

[‖]This second application is very commonly referred to as a heating drive, implying some uncertainty or increase in entropy, which is not true. This coupling can be thought of as a coherent amplifier for one of the quadratures, and would be most useful for decoupling the cyclotron orbit size from the size of the axial motion necessary for good detection S/N. For this to work though, it is first necessary to reduce the ion's effective temperature below the thermal limit set by the detection circuit.

[**]The sideband coupling technique does not conserve energy, and one finds that the temperature of the cyclotron mode is related to the temperature of the axial mode by $T_{\mathrm{c}} = (\omega_{\mathrm{c}}/\omega_{\mathrm{z}})T_{\mathrm{z}}$. Because the axial frequency is fixed, the effective thermal radius is independent of ion mass and corresponds to a thermal cyclotron radius of ~ 7 μm. The thermal magnetron radius is also ~ 7 μm. This is the level at which we can set the radial amplitudes to zero.

[††]The phase of the cyclotron motion at $t = 0$ is set by the phase of the drive field. For the experiment to be reproducible, it is important that the cyclotron drive phase at $t = 0$ be constant relative to the phase of the sideband coupling drive at $t = 0$. This is accomplished by using integer drive and coupling frequencies. This ensures that the two independent frequencies always come back around to the same relative phase every second. We then start each measurement based on a one Hz clock which is phaselocked to the frequency reference distributed to all the frequency synthesizers.

lasting ~ 300 ms is applied, transferring the cyclotron action and phase to the axial mode. The axial motion is recorded for 8 s by measuring the image currents induced between the trap endcaps. From the phase of the axial motion, we determine the phase of the cyclotron motion just before the π-pulse to $\pm 10^{\circ}$.

The experiment is repeated several times varying the phase evolution time $T_{\rm evol}$ between 0.1 and several 100 s. Extra points are taken at short $T_{\rm evol}$ to help unwrap the extra integer number of 2π, which we cannot measure with a single PNP since the cyclotron phase is measured modulo 2π. After this phase unwrapping, the frequency is determined from the variation of phase with $T_{\rm evol}$. For $f_{\rm ct} = 5$ MHz and a measurement phase noise of 10°, an evolution time $T_{\rm evol} = 100$ s yields the cyclotron frequency to 6 parts in 10^{11}.

2.1.6 Mode Coupling Revisited and Adiabatic Passage

Having talked about the mode coupling problem from a largely classical perspective, I will emphasize the analogy to a quantum mechanical problem. We will often refer to ac Stark shifts, avoided crossings, and π-pulses with this analogy in mind. Rather than simply repeating previous results, I will discuss an extension of the results of Ref. [39][G] to simultaneous couplings between both the axial-cyclotron and axial-magnetron modes.

To begin, the force generated by two independent quadrupole coupling fields can be written as

$$\vec{F}_p = q\left(z\hat{x} + x\hat{z}\right)\Re\left\{E_{pc}e^{\imath\omega_{\rm pc}t} + E_{pm}e^{\imath\omega_{\rm pm}t}\right\} \quad . \tag{2.18}$$

We assume the case in which $\omega_{\rm pc}$ is near $\omega_{\rm ct} - \omega_{\rm z}$ and $\omega_{\rm pm}$ is near $\omega_{\rm z} + \omega_{\rm m}$. We can simplify the resulting equations of motion by dropping nonresonant terms and making the adiabatic approximation that any new variation is slow compared to the unperturbed motion. The results can be summarized in matrix form as

$$\imath\hbar\frac{\partial}{\partial t}\begin{pmatrix} C \\ Z \\ M^* \end{pmatrix} = \frac{\hbar}{2}\begin{pmatrix} 0 & \Omega_c e^{\imath\delta t} & 0 \\ \Omega_c^* e^{-\imath\delta t} & -\imath\gamma & \Omega_m e^{\imath\eta t} \\ 0 & \Omega_m^* e^{-\imath\eta t} & 0 \end{pmatrix}\begin{pmatrix} C \\ Z \\ M^* \end{pmatrix} \tag{2.19}$$

where the amplitudes are related to the Penning trap modes by the definitions

$$\vec{\rho}_{\rm c}(t) = \Re\left\{\frac{C(t)}{\sqrt{\pi m\omega_{\rm c}}}(\hat{x} + \imath\hat{y})e^{\imath\omega_{\rm ct}t}\right\} \tag{2.20}$$

$$z(t) = \Re\left\{\frac{Z(t)}{\sqrt{\pi m\omega_{\rm z}}}e^{\imath\omega_{\rm z}t}\right\} \tag{2.21}$$

$$\vec{\rho}_{\rm m}(t) = \Re\left\{\frac{M(t)}{\sqrt{\pi m\omega_{\rm c}}}(\hat{x} + \imath\hat{y})e^{\imath\omega_{\rm m}t}\right\} \quad , \tag{2.22}$$

the mode coupling strengths are related to the quadrupole field strengths by

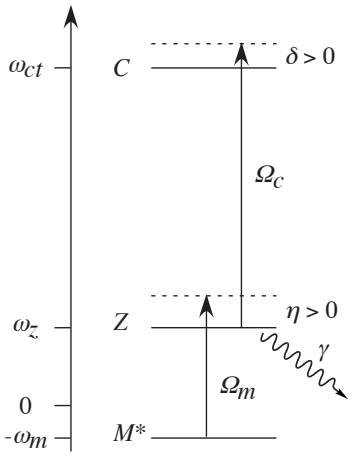

Figure 2-4: The analogous quantum system to our classical equations of motion. The picture shown includes couplings between the axial mode and the two radial modes.

$$\Omega_c = \frac{qE_{pc}}{2m\sqrt{\omega_z \omega_c}} \tag{2.23}$$

$$\Omega_m = \frac{qE_{pm}}{2m\sqrt{\omega_z \omega_c}} \quad , \tag{2.24}$$

and the detunings of the couplings from resonance are given by

$$\delta = \omega_{pc} - (\omega_{ct} - \omega_z) \tag{2.25}$$

$$\eta = \omega_{pm} - (\omega_z + \omega_m) \quad . \tag{2.26}$$

The damping of the axial mode is phenomenologically introduced through the imaginary diagonal term $-\imath\gamma$. The factor of $\hbar$ is completely superfluous. It is present simply to stress how much these reduced classical equations of motion appear to mirror a system of coupled quantum mechanical states with complex amplitudes. In the absence of damping $\gamma = 0$, the effective Hamiltonian is Hermitian so the mode amplitudes evolve via a Unitary transformation and the sum of the square of the mode amplitudes is a conserved quantity

$$|C(t)|^2 + |Z(t)|^2 + |M(t)|^2 = |C(0)|^2 + |Z(0)|^2 + |M(0)|^2 \quad . \tag{2.27}$$

The uncoupled energy levels for this fictitious quantum system are shown in Fig. 2-4 along with the various couplings.

In the limit of resonant couplings $\delta = \eta = 0$, there exists an eigenvector dubbed the dark state. It is called the dark state because it has no overlap with the damped axial mode and so is completely undamped. In general, the dark state is given by

$$|\psi_d\rangle = \frac{1}{\sqrt{|\Omega_c|^2 + |\Omega_m|^2}} \begin{pmatrix} \Omega_m \\ 0 \\ -\Omega_c \end{pmatrix} = \begin{pmatrix} e^{\imath\phi_m} \cos\theta \\ 0 \\ -e^{-\imath\phi_c} \sin\theta \end{pmatrix} \quad . \tag{2.28}$$

In the second expression we have parameterized using the cyclotron-magnetron mixing angle θ defined by

$$\tan\theta = \left| \frac{\Omega_c}{\Omega_m} \right| \quad , \tag{2.29}$$

and the coupling phases defined by

$$e^{\imath\phi_x} = \frac{\Omega_x}{|\Omega_x|} \quad . \tag{2.30}$$

In the limit of a single applied coupling to the axial mode, the dark state corresponds to the remaining uncoupled mode. For concreteness, assume that $\Omega_m = 0$. The mixing angle is then $\theta = \pi/2$, and the magnetron mode is the dark state. Using the adiabatic theorem of quantum mechanics, we can continuously transform the dark state into the cyclotron mode by slowly ramping up Ω_m and ramping down Ω_c as is shown in Fig. 2-5. The exact form of the ramps is unimportant. It is only important that the couplings be large since this sets the scale for adiabaticity.

The adiabatic transformation of the dark state has been experimentally observed. To start, all three modes were initially cooled to zero and then 150 μm of magnetron motion was created with a standard resonant dipole drive. The couplings were varied as shown in Fig. 2-5, but both couplings were simultaneously set to zero before completion of the sequence (as in (b)). The shut-off of the couplings is chosen to be very fast compared to the inverse Rabi frequencies just before the shut-off. This violates adiabaticity in the maximal sense, and we expect the dark state to be projected onto the usual magnetron and cyclotron normal modes. The amplitudes of the cyclotron and magnetron modes were subsequently measured using sequential π-pulses to the detected axial mode.

Figure 2-6 shows the results. The measured cyclotron and magnetron amplitudes squared are plotted against the final mixing angle just before shut-off. The mixing angle is determined from the final coupling strengths, which are measured using an avoided crossing technique [39]^G. This clearly demonstrates the adiabatic transformation of pure magnetron motion into pure cyclotron motion. The reverse sequence was demonstrated as well. A Ramsey SOF measurement scheme could be implemented using adiabatic passage to perform $\pi/2$-pulses between the cyclotron and magnetron modes as a way of measuring the free space cyclotron frequency from the sum of the two mode frequencies $\omega_c = \omega_{ct} + \omega_m$.

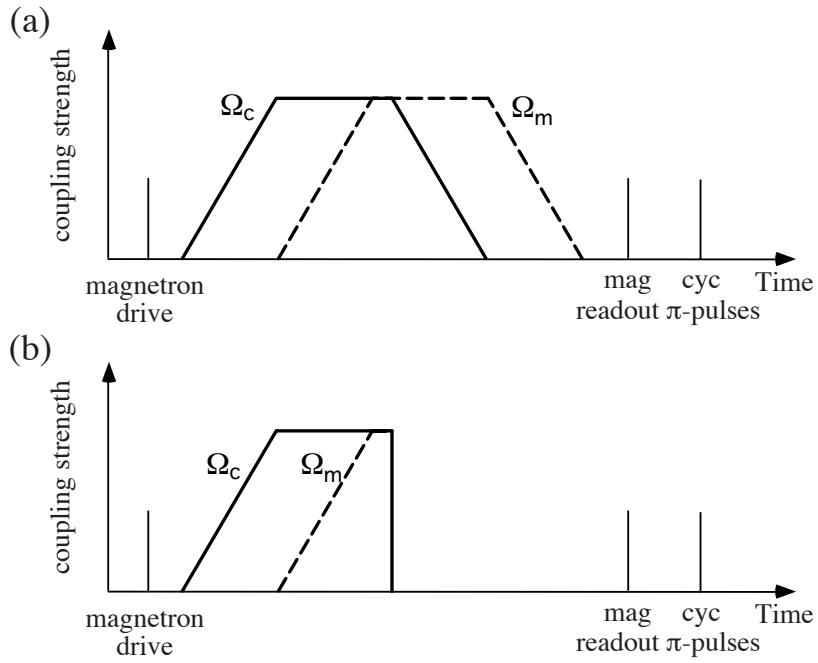

Figure 2-5: Adiabatic Transfer sequence. Initially a small magnetron motion is created. The magnetron motion is then adiabatically transformed into cyclotron motion by varying the strengths of the couplings between each mode and the intermediate axial mode as shown. By simultaneously sending the coupling strengths to zero at various points in the ramp sequence as shown in (b), the initial magnetron motion is projected onto both magnetron and cyclotron motion with the ratio determined by the ratio of the final coupling strengths. The mixing angle is 45° when the couplings are sent to zero in the example of (b), meaning that we would measure equal magnetron and cyclotron amplitudes.

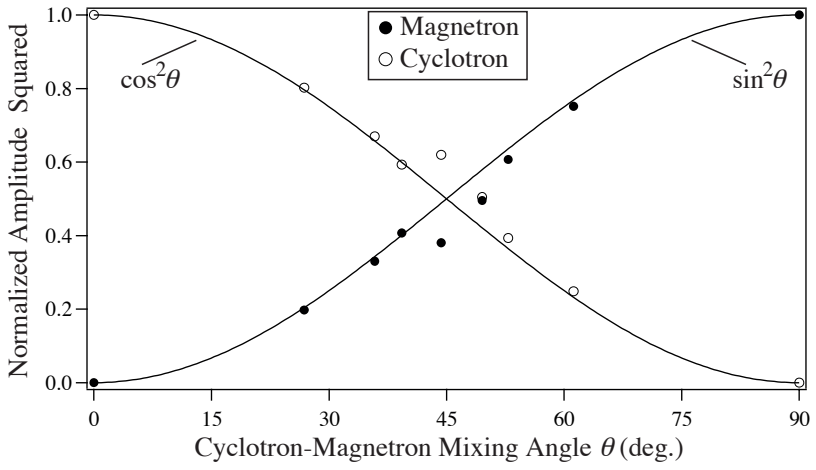

Figure 2-6: Experimental demonstration of the transfer of classical action from the magnetron mode to the cyclotron mode by adiabatic transformation of the dark state.

2.2 Imperfect Penning Trap Physics

2.2.1 Trap Field Imperfections

The magnetic field and electric fields in an actual Penning trap do not consist only of a perfectly uniform magnetic field and a perfectly quadrupole electric field. The magnetic field is not perfectly uniform because of the finite length of the superconducting solenoid and the presence of the experimental apparatus in the bore of the solenoid. The electric field is not purely quadrupolar because of imperfections in machining, alignment of the electrodes, and pernicious patches of charge which freeze to the electrode surfaces.*

In both cases we have shims which allow us to make the fields more ideal. For the magnetic field, a set of superconducting shims built into the magnet allow us to null the first few moments of the magnetic field inhomogeneity. For the electric field, a set of electrodes called the Guard Rings sit between the Ring and Endcap electrodes. By varying the voltage on the Guard Rings, we can shim the second azimuthally symmetric term in the expansion of the electric field beyond the quadrupole term, which is characterized by its multipole expansion coefficient C_4 defined below. The next lower order term characterized by C_3 is not symmetric under reflection about the plane $z = 0$ and so will be shown to have a much smaller impact on our measurements. Shimming the magnet takes a day's work and causes large drifts of the average field for many days afterward, presumeably due to thermal relaxation. As a result, this is not done very often. In contrast, the Guard Ring electrode can be adjusted in milliseconds without any associated relaxation time.

The trap fields are normally characterized by a multipole expansion about the trap center. The natural expansion parameter for the electric field is the characteristic trap size d. In most cases and especially in the two-ion technique, we are concerned with imperfections that are azimuthally symmetric and are symmetric about reflection through the plane $z = 0$. The contribution to the total potential from such terms can be written as

$$V = \frac{1}{2} V_{\mathrm{r}} \sum_{k=0}^{\infty} C_{\mathrm{k}} \left(\frac{r}{d}\right)^k P_k\left(\cos\theta\right) \quad . \tag{2.31}$$

The $P_k(x)$ are the standard Legendre polynomials with the sign convention $P_0(0) = 1$. The potential is specified by this relation at a position $\vec{r}$ expressed in the standard spherical coordinates r, θ and ϕ. The unitless expansion parameters C_{x} express the contribution to the potential of each term as a fraction of the Ring voltage V_{r}. An ideal Penning trap has all expansion coefficients zero except for C_2=1. This is why the factor of 1/2 sits in front of the expansion. This expansion follows the conventions of Ref. [38]. Odd terms such as C_3 can be included in the above expansion, but Ref. [38] argues that it is more convenient to expand in terms of the trap dimension along the axial direction z_0. We will not concern

*A thin layer of graphite is applied to the inner surfaces of the trap electrodes to minimize these charge patches. The current form is sold under the name Aerodag, and comes as an aerosol.

ourselves with this point since we will not be referring in this thesis to odd terms except for order of magnitude estimates for which the above expansion will suffice.

The magnetic field does not have a definite length scale to use in a multipole expansion. One could reasonably choose the trap size or the solenoid size. By convention, we will not impose a scale and simply allow the expansion coefficient $B_{\rm n}$ to carry units of magnetic field/length^n. Because there is no current flowing in the region in which the field will be expanded, the magnetic field can be written in terms of a scalar potential. We will expand this scalar potential in a multipole expansion as

$$\Psi = -\sum_{l=1}^{\infty} \frac{B_{l-1} r^l}{l} P_l\left(\cos\theta\right) \quad . \tag{2.32}$$

Taking the gradient of the scalar potential gives the magnetic field $\vec{B} = -\nabla\Psi$. In explicit form, the magnetic field is given by

$$\vec{B} = \sum_{l=0}^{\infty} B_l r^l [P_l\left(\cos\theta\right)\hat{z} - \frac{1}{l+1} P_l^1\left(\cos\theta\right)\hat{\phi}] \quad . \tag{2.33}$$

Note that the associated Legendre polynomial P_l^1 now appears in the expansion. Either of these equations can be taken to define the expansion coefficients $B_{\rm n}$. These definitions are just those of Ref. [38].

We have developed new techniques to accurately measure the expansion terms B_2, B_4, C_4, and C_6. We do not actually measure C_4, but rather the value of the Guard Ring voltage $V_{\rm gr}^{\circ}$ which sets C_4=0. We then measure the geometric coefficient D_4, which relates a change in the Guard Ring voltage to a change in C_4. We can use these two measured values and the relationship

$$C_4 = \frac{D_4}{V_{\rm r}} \left(V_{\rm gr} - V_{\rm gr}^{\circ}\right) \tag{2.34}$$

to calculate the C_4 for a given Guard Ring voltage $V_{\rm gr}$.

The measurements are accomplished by taking advantage of the frequency shifts of the various modes caused by these trap anharmonicities. To measure D_4, $V_{\rm gr}^{\circ}$, and C_6, we measure the change in axial frequency versus magnetron radius or $\Delta f_{\rm z}$ vs $\rho_{\rm m}$. We can also perform the equivalent of a PNP measurement, but on the magnetron mode. This allows us to measure the magnetron frequency shift versus magnetron radius $\Delta f_{\rm m}$ vs $\rho_{\rm m}$. We find very good agreement between the two independent techniques in determining D_4, $V_{\rm gr}^{\circ}$, and C_6.

The second technique of measuring $\Delta f_{\rm m}$ vs $\rho_{\rm m}$ has the extremely small systematic errors associated with the PNP measurement because only one mode is nonzero during the measurement. In addition, the magnetron mode is not damped, making the analysis of the signal less complicated. On the other hand, the signal to noise of the $\Delta f_{\rm m}$ vs $\rho_{\rm m}$ technique is lower because the fractional frequency shifts of $f_{\rm z}$ and $f_{\rm m}$ are the same, but the absolute

Table 2.1: Measured Trap Field Parameters

m/q u/e	Species	V_r V	V_{gr}° - $V_r/2$ mV	D_4	C_6	B_2/B_0 $10^{-9}/\mathrm{mm}^2$	B_4/B_0 $10^{-9}/\mathrm{mm}^4$
33	$^{32}SH^+$, $^{33}S^+$	18.55	89.9(7)	-0.082(4)	0.0011(1)	6.1(6)	1.2(5)
29	$^{29}Si^+$, $^{28}SiH^+$	16.18	84.0(7)	-0.082(4)	0.0011(1)	6.1(6)	1.2(5)
28	N_2^+, CO^+, $^{13}C_2H_2^+$	15.64	82.3(7)	-0.082(4)	0.0011(1)	6.1(6)	1.2(5)
16	CD_2^+, CH_4^+	8.952	66.8(7)	-0.082(4)	0.0011(1)	6.1(6)	1.2(5)

shift Δf_m is smaller by approximately $f_m/f_z \sim 1/40$.

In all previous work, the electrostatic anharmonicity was minimized by tuning the Guard Ring voltage to make the axial resonance line shape as symmetric as possible [41]^G. Practically, this trap tuning technique was always found to be ambiguous and difficult to interpret. For instance, it was never clear whether C_4 had been tuned to zero or if we were tuning C_4 against C_6 to some kind of balance. In addition, we could not accurately measure D_4. This is because axial amplitude calibrations are much more difficult to be certain of as a result of the damping. For instance, we have measured the chirping of the slowly damped axial mode when detuned from resonance with the coil. We found that it was quite difficult to be certain of the exact amplitudes involved.

To measure the magnetic field inhomogeneities B_2 and B_4, we measure the axial frequency shift versus cyclotron radius or Δf_{ct} versus ρ_c. The axial frequency shift arising from B_2 is often called a bottle shift. This is in direct analogy to the confinement of plasmas in magnetic field gradients. The confinement force arises because of the interaction of the magnetic dipole moment of the cyclotron motion with the magnetic field gradient.

Table 2.1 summarizes our best estimates of the trap fields and will be used to make estimates throughout this thesis. For scale, the value of the quadratic magnetic field inhomogeneity B_2 means that the cyclotron frequency changes by about 3 parts in 10^9 when the frequency is measured on a 1 mm magnetron orbit as compared to at the trap center. A detailed discussion of these measurements is provided in Simon Rainville's thesis [1]^G, Sect. 2.5.

2.2.2 Calculating Frequency Shifts

The effect of a small nonlinear force on an oscillator is to slightly shift its frequency and to introduce small harmonics of the motion. Consider first a linear oscillator such as the axial mode with an additional force that varies as z^3

$$\ddot{z} + \omega_{z0}^2 z + \lambda z^3 = 0 \ . \tag{2.35}$$

(In this section, we will use subscript 0 to refer to the unperturbed frequency or motion

and subscript 1 to refer to the first order perturbation. These are not ion labels.) This perturbation is exactly the form of the modification introduced by a C_4 term in the electrostatic potential. One's first instinct is to pull out a common factor of z and write the new frequency as

$$\omega_{z1}^2 = \omega_{z0}^2 + \lambda z_0^2 \quad . \tag{2.36}$$

This is correct at the order of magnitude level, but it is incorrect at the level of factors of 1/2 that are important for our purposes. The reason is that this does not properly account for correlations between the extra force and the motion. A way to systematically deal with these correlations is to substitute

$$z\left(t\right) = z_0 \cos\left(\left(\omega_{z0} + \Delta\omega_z\right) t + \phi\right) \quad , \tag{2.37}$$

and express the nonlinear force as a Fourier sum. To conveniently accomplish this for any power of nonlinearity, simply substitute

$$\theta = \left(\omega_{z0} + \Delta\omega_z\right) t + \phi \quad , \tag{2.38}$$

and use the ability of software such as Mathematica[†] to reduce the nonlinear term to a sum of linear trigonometric functions. In our example, this will yield an equation of the form

$$\ddot{z} + (\omega_{z0}^2 + \frac{3}{4}\lambda z_0^2)z + \frac{1}{4}\lambda z_0^3 \cos\left(3\left(\omega_{z0} + \Delta\omega_z\right) t + 3\phi\right) = 0 \quad . \tag{2.39}$$

The modified frequency to lowest order is given by

$$\omega_{z1}^2 = \omega_{z0}^2 + \frac{3}{4}\lambda z_0^2 \quad . \tag{2.40}$$

The additional force at frequency $3\omega_{z1}$ drives a small harmonic response at $3\omega_{z1}$, which we ignore to first order.

Second order perturbation would begin by assuming motion of the form

$$z\left(t\right) = z_0 \cos\left(\left(\omega_{z0} + \Delta\omega_z\right) t + \phi\right) + \frac{\beta}{2\omega_{z0}}\lambda z_0^3 \cos\left(3\left(\omega_{z0} + \Delta\omega_z\right) t + 3\phi\right) \quad . \tag{2.41}$$

I have parameterized the harmonic such that the coefficient to be solved for β is of order unity. Substitution into the equations of motion will result in an additional frequency shift of second order in the small quantity λ/ω_z.

In the case of the circular radial motion of an ion in a Penning trap, the force that contributes to a frequency shift is the average force directed along the radial vector of the

[†]The command TrigReduce writes functions of nonlinear trigonometric functions as a sum of linear trigonometric functions. In the case above, this is done easily by hand, but this gets more difficult as the power of the nonlinearity grows.

motion averaged around a single orbit of both radial modes. This is made clear by a concrete example. Imagine an additional force of the form

$$\vec{F} = \lambda x \hat{x} \ . \tag{2.42}$$

We simply assume circular orbits and average the force around one orbit each of the cyclotron and magnetron orbits. We will specify the two phases of the motion by ϕ_c and ϕ_m.

$$\vec{F}_{\rm c} = \frac{\hat{\rho}_{\rm c}}{(2\pi)^2} \int_0^{2\pi} \int_0^{2\pi} \vec{F} \cdot \hat{\rho}_{\rm c} d\phi_c d\phi_m = \frac{\lambda}{2} \vec{\rho}_{\rm c} \tag{2.43}$$

$$\vec{F}_{\rm m} = \frac{\hat{\rho}_{\rm m}}{(2\pi)^2} \int_0^{2\pi} \int_0^{2\pi} \vec{F} \cdot \hat{\rho}_{\rm m} d\phi_c d\phi_m = \frac{\lambda}{2} \vec{\rho}_{\rm m} \tag{2.44}$$

These averaged forces are used in separate equations of motion for the cyclotron and magnetron motion

$$\ddot{\vec{\rho}}_{\rm c} = \omega_{\rm c} \dot{\vec{\rho}}_{\rm c} \times \hat{z} + \frac{1}{2} \omega_{\rm z}^2 \vec{\rho}_{\rm c} + \frac{\lambda}{2m} \vec{\rho}_{\rm c} \tag{2.45}$$

$$\ddot{\vec{\rho}}_{\rm m} = \omega_{\rm c} \dot{\vec{\rho}}_{\rm m} \times \hat{z} + \frac{1}{2} \omega_{\rm z}^2 \vec{\rho}_{\rm m} + \frac{\lambda}{2m} \vec{\rho}_{\rm m} \ . \tag{2.46}$$

It is trivial to solve each equation for the modified frequency resulting from the additional force. As will be discussed in the following section, odd order terms in the multipole expansion such as C_3 generate radial forces which are even in the coordinates and so average to zero.

Of course, the previous machinery of expressing the force as a Fourier series can also be used to calculate the frequency shifts of the radial modes. In fact, the two approaches are actually the same upon further examination. The math for calculating perturbations of the radial modes is more complicated because of the two dimensions and two normal modes, but the same logic applies as for the one-dimensional oscillator. One substitutes the zeroth order motion and keeps only the forces generated by the anharmonicities at the fundamental frequency of each mode. For instance, the correct substitution would be of the form

$$\begin{aligned} \vec{\rho}_0 \ = \ & +\hat{x} \left\{ \rho_{\rm c} \cos\left(\omega_{\rm ct} + \Delta\omega_{\rm ct}\right) t + \rho_{\rm m} \cos\left(\omega_{\rm m} + \Delta\omega_{\rm m}\right) t \right\} \\ & -\hat{y} \left\{ \rho_{\rm c} \sin\left(\omega_{\rm ct} + \Delta\omega_{\rm ct}\right) t + \rho_{\rm m} \sin\left(\omega_{\rm m} + \Delta\omega_{\rm m}\right) t \right\} \ . \end{aligned} \tag{2.47}$$

The axial motion is completely uncorrelated in time with the radial motion. So, we can simply replace terms and coefficients in the radial forces that are proportional to z^n by the time averaged value $\langle z^n \rangle$.

2.2.3 Odd Orders Do Not Matter (Much)

In most discussions of anharmonicities, we will ignore terms $C_{\rm n}$ with n odd. The reason for this is that they generate forces which average to zero around a complete orbit. As a result, they produce no frequency shift to first order. For the two-ion technique, we do not need to worry too much about the dc forces generated by these odd terms since on average they are the same for both ions. See previous theses such as Weisskoff's [41]^G for more detail on the effects of the dc forces generated by these odd order terms.

One might imagine, however, that for a term such as C_3, the second order perturbation would give rise to a frequency shift of the same magnitude as the higher order electrostatic term C_6. This is not the case because the harmonic motions that give rise to the second order frequency shift are generated by nonresonant forces. The size of the harmonic at integer multiple frequency n is suppressed by an additional factor of $1/((n-1)\omega_{\rm z})$ and not simply by $\left(C_3 z_0^3/d^3\right)^2$. For instance, consider the case of a one-dimensional harmonic oscillator with an additional quadratic force as would be produced by C_3

$$\ddot{z} + \omega_{\rm z0}^2 z + \lambda z^2 = 0 \ . \tag{2.48}$$

The first order frequency shift vanishes and the second order shift is given by

$$\omega_{\rm z2}^2 = \omega_{\rm z0}^2 - \frac{5}{6}\frac{\lambda^2 z_0^2}{\omega_{\rm z0}^2} \ . \tag{2.49}$$

2.2.4 Perturbation Matrix to Higher Order

Because the two-ion technique requires exploring a larger fraction of the trap, we need to know the frequency shifts associated with higher order terms in the expansions of the fields. In previous theses, only expressions for frequency shifts up to B_2 and C_4 were presented. These shifts also do not exist in the literature. Somewhat simplified expressions are presented here that are correct up to small corrections of order $\omega_{\rm m}/\omega_{\rm c}$. The expressions presented here were calculated independently of those in Simon Rainville's thesis [1]^G and they are found to agree with one another.[‡] Simon Rainville's thesis [1]^G also contains expressions to higher order that are not given here for space and since we are not yet sensitive to these terms. His higher order terms were also found to agree with my calculations.

$$\frac{\Delta\omega_{ct}}{\omega_{ct}} = -\frac{3\,C_4}{2}\,\frac{\omega_m}{\omega_c}\,\frac{\left(2{z_0}^2 - {\rho_c}^2 - 2{\rho_m}^2\right)}{d^2} \tag{2.50}$$

$$\frac{\Delta\omega_m}{\omega_m} = \frac{3\,C_4}{2}\,\frac{\left(2\,{z_0}^2 - 2\,\rho_c^2 - \rho_m^2\right)}{d^2} \tag{2.51}$$

[‡]Small errors may have crept into previous theses, but the expressions presented here and in Simon Rainville's thesis have been carefully proofed.

$$\frac{\Delta\omega_z}{\omega_z} = \frac{3\,C_4}{4}\,\frac{\left(z_0{}^2 - 2\,\rho_c{}^2 - 2\,\rho_m{}^2\right)}{d^2} \tag{2.52}$$

$$\frac{\Delta\omega_{ct}}{\omega_{ct}} = \frac{-15\,C_6}{8}\,\frac{\omega_m}{\omega_c}\,\frac{\left(3z_0{}^4 - 6z_0{}^2\rho_c{}^2 + \rho_c{}^4 - 12z_0{}^2\rho_m{}^2 + 6\rho_c{}^2\rho_m{}^2 + 3\rho_m{}^4\right)}{d^4} \tag{2.53}$$

$$\frac{\Delta\omega_m}{\omega_m} = \frac{15\,C_6}{8}\,\frac{\left(3\,z_0{}^4 - 12\,z_0{}^2\,\rho_c{}^2 + 3\,\rho_c{}^4 - 6\,z_0{}^2\,\rho_m{}^2 + 6\,\rho_c{}^2\,\rho_m{}^2 + \rho_m{}^4\right)}{d^4} \tag{2.54}$$

$$\frac{\Delta\omega_z}{\omega_z} = \frac{15\,C_6}{16}\,\frac{\left(z_0{}^4 - 6\,z_0{}^2\,\rho_c{}^2 + 3\,\rho_c{}^4 - 6\,z_0{}^2\,\rho_m{}^2 + 12\,\rho_c{}^2\,\rho_m{}^2 + 3\,\rho_m{}^4\right)}{d^4} \tag{2.55}$$

The frequency shifts due to magnetic field inhomogeneities are:

$$\frac{\Delta\omega_{ct}}{\omega_{ct}} = \frac{B_2\,\left(z_0{}^2 - \rho_c{}^2 - \rho_m{}^2\right)}{2\,B_0} \tag{2.56}$$

$$\frac{\Delta\omega_m}{\omega_m} = \frac{B_2\,\left(\rho_c{}^2\,\omega_c + \left(-z_0{}^2 + \rho_m{}^2\right)\,\omega_m\right)}{2\,B_0\,\omega_m} \tag{2.57}$$

$$\frac{\Delta\omega_z}{\omega_z} = \frac{B_2\,\left(\rho_c{}^2\,\omega_c + \rho_m{}^2\,\omega_m\right)}{4\,B_0\,\omega_m} \tag{2.58}$$

$$\frac{\Delta\omega_{ct}}{\omega_{ct}} = \frac{3\,B_4\,\left(z_0{}^4 + \rho_c{}^4 + 4\,\rho_c{}^2\,\rho_m{}^2 + \rho_m{}^4 - 4\,z_0{}^2\,\left(\rho_c{}^2 + \rho_m{}^2\right)\right)}{8\,B_0} \tag{2.59}$$

$$\frac{\Delta\omega_m}{\omega_m} = \frac{-3B_4\left(2\rho_c^4\,\omega_c + 2\rho_c^2\,\rho_m^2\,\omega_c + z_0^4\,\omega_m + \rho_m^4\,\omega_m - 4z_0^2\,\left(\rho_c^2\,\omega_c + \rho_m^2\,\omega_m\right)\right)}{8\,B_0\,\omega_m} \tag{2.60}$$

$$\frac{\Delta\omega_z}{\omega_z} = \frac{3\,B_4\,\left(-\left(\rho_c{}^4\,\omega_c\right) - 2\,\rho_c{}^2\,\rho_m{}^2\,\omega_c - \rho_m{}^4\,\omega_m + z_0{}^2\,\left(\rho_c{}^2\,\omega_c + \rho_m{}^2\,\omega_m\right)\right)}{8\,B_0\,\omega_m} \tag{2.61}$$

Lastly, it is important to recognize that the cyclotron frequency is perturbed by the relativistic mass shift

$$\frac{\Delta\omega_{\rm ct}}{\omega_{\rm ct}} = -\frac{\omega_{\rm ct}^2\rho_{\rm c}^2}{2c^2} \quad . \tag{2.62}$$

This relativistic shift was used to calibrate the cyclotron drive strength by measuring the trap cyclotron frequency shift versus cyclotron radius.

2.2.5 Definitions of fctOpt, fzOpt, fmOpt

We will now introduce the concept of an optimal C_4 that makes a single-ion mode frequency independent of magnetron radius to first order about some selected radius. This will be a tremendously useful concept when controlling systematic errors in the two-ion technique, as described in Sect. 5.6.

Since we can precisely measure the values of B_2, B_4, C_4, and C_6 in our trap, we can then plot the perturbation of the trap cyclotron frequency as a function of magnetron radius, i.e., $\Delta f_{\rm ct}$ vs $\rho_{\rm m}$. The contributions from C_4 and B_2 scale as $\rho_{\rm m}^2$ while the contributions from B_4 and C_6 scale as $\rho_{\rm m}^4$. We can easily modify C_4 by changing the voltage on the Guard Ring. We can also modify B_2 using superconducting shims built into the magnet, although

this is more painful and is not done very often. On the other hand, we do not have control over C_6 or B_4.[§] We must simply live with the measured values. As a result, we cannot make the trap cyclotron frequency perturbation exactly zero $\Delta f_{\rm ct}$=0 for all $\rho_{\rm m}$.

On the other hand, by tuning C_4 we can make $\Delta f_{\rm ct}$ at a given magnetron radius independent of small variations about that radius. This turns out to be good enough in the two-ion technique, where we are usually only concerned with differential shifts. The value of C_4 that provides local flatness of the trap cyclotron frequency at a given magnetron radius $\rho_{\rm m}^{\circ}$ is given by the solution of

$$\left.\frac{\partial \Delta f_{\rm ct}}{\partial \rho_{\rm m}}\right|_{\rho_{\rm m}^{\circ}} = 0 \tag{2.63}$$

where for emphasis $\Delta f_{\rm ct}$ is the frequency shift of the trap cyclotron mode of a single ion as a function of $\rho_{\rm m}$ due to the trap field imperfections alone, i.e., not including ion-ion interactions. We can then convert this optimal C_4 into an equivalent Guard Ring voltage using Eq. 2.34. We will refer to this optimal value of C_4 as a function of ion-ion separation as fctOpt. In other situations we will refer to this optimal tuning in terms of a Guard Ring voltage $V_{\rm gr}^{\rm optct}$.

The same concept applies to examination of the other two single ion modes $f_{\rm z}$ and $f_{\rm m}$. The optimum value of C_4 at a given magnetron radius that makes the axial (magnetron) frequency independent of magnetron radius to first order will be referred to as fzOpt (fmOpt). The equivalent Guard Ring voltages are $V_{\rm gr}^{\rm optz}$ and $V_{\rm gr}^{\rm optm}$. The expressions for these optimum values can be easily calculated from Eq. 2.63 and the shifts in the preceding Sect. 2.2.4. The expressions are explicitly given in Simon Rainville's thesis [1]^G, Sect. 5.2.

2.3 Improvements

2.3.1 General Notes

The vast majority of the cryogenic apparatus is unchanged from that described in the thesis of Michael P. Bradley [20]^G. The current high-Q detection coil is new since the previous one used to measure the alkali masses developed a short when we attempted to increase its coupling to the SQUID. Two new coils were wound. An attempt was made to improve the design of the coils by introducing tabs to guide the winding process with the goal of increasing the uniformity of the windings. It was believed that this would better confine the magnetic field to the interior of the teflon winding mold where losses should be low. Despite our attempts (some of which risked limb and possibly life) the process of winding a high-Q coil remains closer to sorcery than we would like to admit. Roland Nguyen's MIT senior thesis [42]^G is a good reference for what is known about winding coils.

[§]Actually, we might have control over B_4. We could use it to partially cancel the effect of C_6. But, this is not trivial to do, and it should be carefully weighed before being attempted.

A minor technical improvement was made with the removal of a series of carbon film resistors previously used to monitor the LHe level in the insert dewar. The wires to these resistors were strung along the outside of the insert. We removed all but the last resistor, which is located well above the location of the SQUID and high-Q coil. It was found that this eliminated an intermittent and very troublesome source of noise that had plagued us for the previous few years.

At one point, we found that the effective trap size increased. The trap size was determined by measuring the slope of the Ring voltage versus the mass to charge of the ion. The Ring voltage here is that necessary to keep each ion at different mass to charge resonant with the fixed frequency axial detector. Pulling up the insert and breaking vacuum revealed that a nut had fallen off of the trap so that the Lower Endcap had dropped by a small amount. Most likely, the nut had worked loose while thermally cycling the insert. The trap was probably unsupported at the nut's nominal position but was held in place by friction until it slipped. We had to recompress the trap, put the nut back in place, and realign the trap. I mention this only to maintain a record of the various sorts of silly things that can happen.

The largest change to the experiment is the complete replacement of the data acquisition computer and all of its software with new code written from scratch. The early stages of this work was performed by Simon Rainville while I was winding new detection coils for the apparatus. With time, however, we realized that the two-ion technique was largely a problem of controlling complexity. Advanced automation and control became a major task for both of us. Two of the highlights of the data acquisition system were a custom macro language for scripting various actions, and online analysis of data for fast debugging of experimental problems.

2.3.2 Guard Ring Control

A modular extension of the trap voltage source was built, allowing computer control of the Guard Ring voltage. The design is very similar to the circuit used to add computer controlled voltages to the Ring voltage. The circuit accepts a ± 10 V signal that can be generated by a DAC. The voltage is divided down by a factor of 400, 100, 4, or 1, and then added using an AMP01 operational amplifier to the gross Guard Ring voltage provided by the VBox. The division factor is selected via digital bits controlled by the computer. In addition, the voltages were sent to a multiplexed precision voltmeter for automatic reading and logging of trap voltages by the data acquisition computer. The main challenge of building this system was to avoid introducing a new source of noise since our detector is extremely sensitive.

Practically, this was a major experimental advance. This allowed us to accurately measure the trap anharmonicities and geometric coefficients for many hours while completely under computer control. This would have been physically impossible if manual adjustments

were necessary.* The computer control of the Guard Ring also allowed us to adjust the anharmonicities to speed up or slow down the processes used to measure and control the relative magnetron motion. It was also used to separately optimize the simultaneous cyclotron frequency measurements for the phase evolution period and the axial measurement period. This was key when exploring systematic errors at large ion-ion separations. The capability to control the Guard Ring became so ubiquitous in everyday operation that it is hard to imagine that we ever lived without it. This addition allowed us to fully automate the many hours of data taking, but it should be emphasized that it also opened new measurement possibilities that were not possible if human intervention were required.

2.3.3 PhaseLocking the Axial Mode

PhaseLocking is a technique we use to measure very small changes in the axial frequency of a single ion. In most cases PhaseLock is used to monitor the size and frequency at which the axial motion is frequency modulated by the beating of the separation and common modes. This frequency modulation occurs when electrostatic anharmonicities are present as is discussed in Sect. 4.3.2. PhaseLock is a Proportional Integral, Derivative (PID) feedback loop that seeks to hold the axial frequency constant in time by applying a small additional voltage to the Ring electrode. The size of this additional voltage tells us by how much other sources would have changed the axial frequency in its absence.

The error signal for this feedback system is derived by measuring the phase response of the ion's axial motion relative to the phase of the drive field, which is held at a fixed frequency. The ion's axial response leads or lags the drive depending on whether the center frequency of the axial resonance is below or above the drive frequency.† Based on the sign and magnitude of the measured relative phase and the width of the axial mode's resonance, we can predict the relative frequency detuning of the drive and the axial mode. It should be pointed out that this is a very general experimental technique with direct analogies such as optical systems where the frequency of an optical cavity is locked to an external laser (or, as is usually the case, vice versa).

As discussed in previous theses [41]^G, we do not directly drive the axial motion with a resonant drive at ω_z. The capacitance between the Lower Endcap and the Upper Endcap would cause the drive to directly excite our detector. We could not discriminate the ion and drive signals since they would be at the same frequency. To avoid this, the axial frequency is modulated at several hundred Hz, and the drive is applied at the frequency of one of the resulting sidebands. The frequency modulation is created by applying a small ac voltage to the Ring at $\omega_{\rm mod}/2\pi \approx 200$ Hz. The drive is then applied near $\omega_z \pm \omega_{\rm mod}$. The drive acts on the axial motion through the motional sideband and produces a response at all other

*Trey and I tried to manually adjust the Guard Ring for such a measurement. The results were not reproducible and the statistics were much too low.

†See Fig. 4-4 for an example of this general phenomena of phase lead and lag in which the oscillator is the self-resonant detector.

orders. In the limit of small modulation index such as we use, the majority of the ion's motion is at the fundamental near ω_z. So, this technique allows us to apply the drive at one frequency and detect the ion's response at another frequency. This can be understood as a mixing technique, and one should see Weisskoff's thesis [41]^G for an illuminating discussion of the perturbative regime of axial frequency modulation.

Figure 2-7 shows the current implementation of PhaseLock. The portion inside the dashed box is performed in software. The bank of synthesizers are phase locked to one another by a common stable 10 MHz clock signal from which the digitizing clock at 1 kHz is also derived. The phase measurements are made by mixing the digitized fixed-frequency signals (only the phases vary in time!) to dc for both the sine and cosine quadratures. Each quadrature amplitude is then separately low pass filtered. The arctangent of the ratio of quadrature amplitudes yields the phase. As explained below, three phases at three different frequencies are measured and subtracted to yield the ion's phase response. The three frequencies are the mixed-down lock frequency at $\omega_L = \omega_{\rm drive} \mp \omega_{\rm mod} - \omega_{\rm mixer} \sim 250$ Hz, the mixed-down drive frequency at $\omega_D = \omega_{\rm drive} - \omega_{\rm mixer} \sim 250 \pm 200$ Hz, and the Ring modulation frequency $\omega_{\rm mod} \sim 200$ Hz.

Since the various filters in the system limit the bandwidth of the signal to ≤ 1 Hz, we can decimate the measured phases so that only one point per 100 ms is carried further in the calculation (i.e. 99 of every 100 points are discarded). This sets the rate at which we actually update the Ring voltage. Using the known damping time of the ion, the ion-drive detuning can be estimated from the measured phase response of the ion. In turn, the voltage needed to set this detuning to zero is calculated from knowledge of the change in axial frequency for a small change in the Ring voltage. A PID system is used to stabilize the feedback loop with the strength of each term set by user-optimized coefficients. A DAC then creates a voltage that is summed inside of the VBox with the gross Ring voltage to gently push the axial frequency into resonance with the drive.

Some of the phase offsets in our system vary from one measurement session to the next and need to be controlled or measured. This variation results from the need to change the frequencies of the synthesizer used. In addition, we set the amplitude of the drive and Ring modulation synthesizers to zero between measurement sessions. Both of these operations randomize the phase of the synthesizer output. To control these shot-to-shot random phases, we use a new technique to "carry our phase reference with us."[‡]

With $\omega_{\rm mod}/2\pi \approx 200$ Hz, the Lower Endcap drive frequency is close enough to our detector to create a significant response at $\omega_{\rm D}$, which we measure with high signal to noise. This allows us to subtract the measured drive phase $\omega_{\rm D}$ from the phase of the measured axial response. As mentioned above, this makes the system robust against a randomization

[‡]In spirit, this is similar to the Pound-Drever technique of locking optical cavities and lasers in which the laser is frequency modulated to create sidebands that serve as phase references. This reduces the sensitivity of the system to perturbations such as mirror vibration from the optical wavelength to the much longer rf wavelength used to create the sidebands.

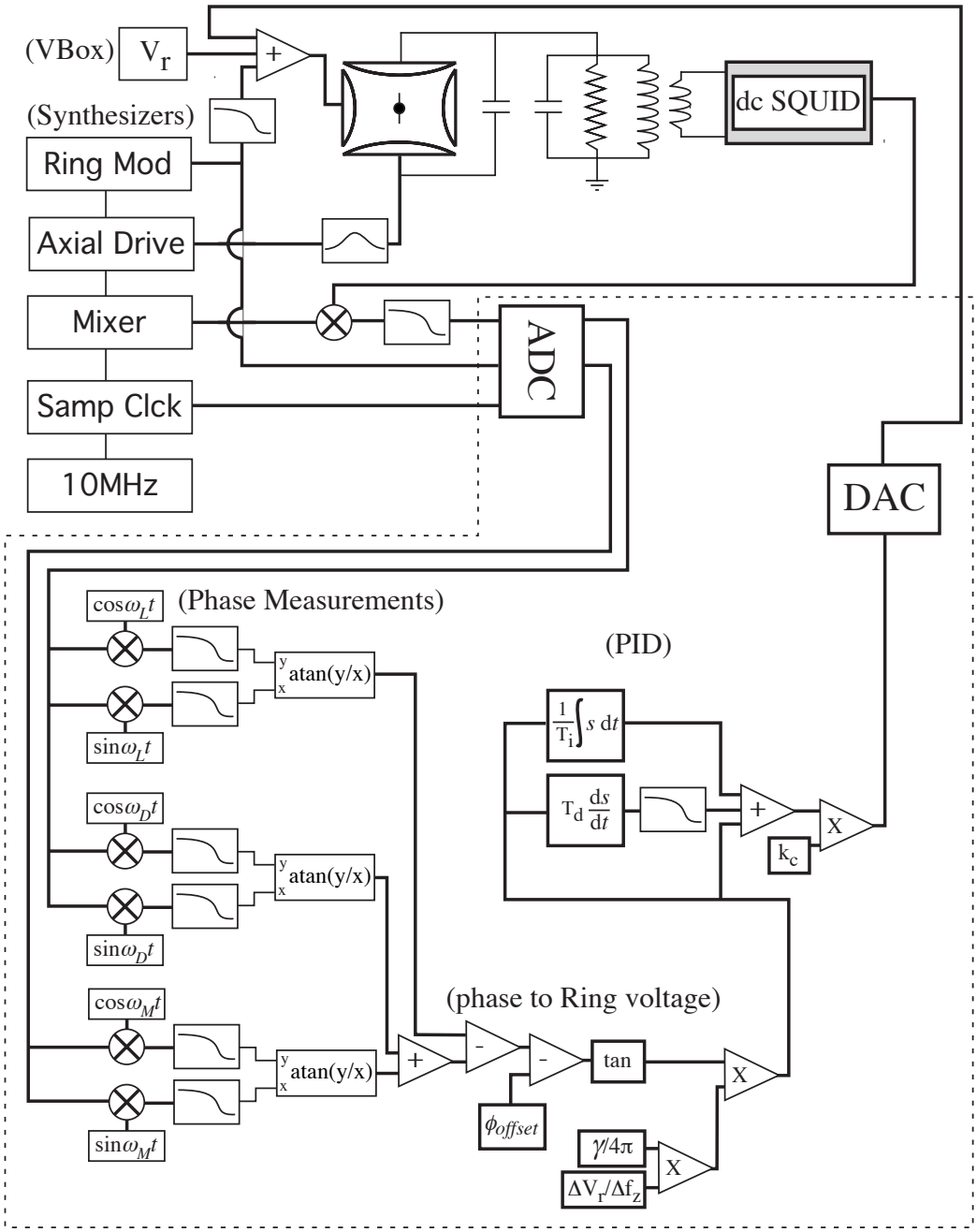

Figure 2-7: Implementation of the PhaseLock Technique for measuring small variations of the axial frequency of a single ion. The axial frequency variation in the absence of the feedback loop is determined from the small voltage that must be added to the Ring to lock the axial frequency to that of an external fixed-frequency drive.

of the drive synthesizer's phase between measurement sessions. Since the detected drive and ion signal are mixed down to lower frequency for digitizing by a common mixer synthesizer, this technique also makes the system robust against randomization of the mixer phase. In addition, because the signal is so close in frequency to the ion's, any changes in the phase shifts of the intermediate electronics or SQUID are common to both the directly detected drive and the signal produced by the ion's response. The only element with a significant frequency response on this scale is the coil, so we choose the modulation frequency to be much larger than the coil width $\omega_{\mathrm{mod}} \gg \gamma_{\mathrm{coil}}$. At a large detuning of the drive from resonance with the coil, the variation of the phase response of the coil to the direct drive is small for variations of the detuning of even several Hz.

The only remaining phase that varies from one execution to the next is the phase of the Ring modulation synthesizer. To remedy this, we directly measure the synthesizer phase. Because the frequency is less than our digitizer's Nyquist frequency of 500 Hz, we directly sample this signal on a separate ADC channel. The measured Ring modulation phase is then subtracted from the measured ion phase.

The detected phase is turned into an estimate of the relative detuning of the drive from resonance δ_d using

$$\delta_d = \frac{\gamma}{2} \tan\left(\psi_C - \phi_{offset}\right) \tag{2.64}$$

where γ is the FWHM of the axial mode, ψ_C is the measured ion phase with the two synthesizer offsets subtracted, and ϕ_{offset} is a net phase offset that accounts for sundry phase shifts in the system that are found to be very stable over many months. To determine ϕ_{offset}, we slowly scan the ion's axial resonance across the fixed axial drive and determine the value of ψ_C when the detected axial power is a maximum. ϕ_{offset} is set to this value so that the predicted axial-drive detuning is $\delta_d = 0$ at this peak power. Using this method, the offset phase can be determined to $\pm 5^\circ$. While this offset phase introduces a small error in our knowledge of the ion's axial frequency ($\sim$ 2 mHz), we are chiefly interested in observing variation of the axial frequency and so this offset is not a concern. Since the predicted detuning becomes infinitely sensitive to noise in the measurement of the phases as $(\psi_C - \phi_{offset})$ approaches $\pm 90^\circ$, the value of $(\psi_C - \phi_{offset})$ is constrained in-software to lie between $\pm 80^\circ$, thus limiting the maximum size of the predicted correction voltage.

The finite measurement signal to noise of our detection circuit means that we must integrate the signal for some finite amount of time before we can make an accurate estimate of the axial-drive detuning from the measured phase. Roughly, the present signal to noise sets this time scale at about one damping time $\tau = 1$ s or in terms of a frequency $\gamma/2\pi \sim$ 0.15 Hz. This sets a soft upper limit on the bandwidth of the feedback loop. In contrast, the *desired* bandwidth of the feedback loop is determined by the range of ion-ion separations of interest. Assuming a minimum ion-ion separation of $\rho_{\mathrm{s}} =$ 500 μm, one needs a bandwidth from dc to 0.4 Hz (or periods of 2.5 s to ∞). Empirically, we find that careful choice of

the various terms in our PID feedback loop allows us to do slightly better than the soft limit given above. We have locked to the axial frequency modulation caused by ion-ion interactions for separations as small as 500 μm.

The low detection signal-to-noise also limited the gain of the feedback loop. The signal-to-noise can be increased by using larger axial amplitudes, but we tried to work with axial amplitudes ≤ 300 μm so that with two ions in the trap $\rho_s \geq z$. Close to DC, the system was tuned to reduce the amplitude of frequency variations by 3.8 with this reduction factor falling off to 1.8 at 0.2 Hz. To keep the derivative term of the PID correction signal from introducing large amounts of noise into the feedback loop, it was decided to limit its frequency response with an additional low pass filter.

The total processing time for the feedback loop is typically 5 ms out of every update period of 100 ms. This allows us to introduce various control niceties such as the ability to calculate power spectra of specified ranges of the time data. We can perform fits to these power spectra to extract the amplitude and frequency of any axial frequency modulation. Automatic corrections for C_4, C_6, and the finite axial amplitude are applied to the frequency modulations extracted from the power spectrum so that the ion-ion separation ρ_s is accurately determined in real time. The results of these fits are sent to a running log so the user can carefully track the separation and common magnetron amplitudes of the two ions versus time. In addition, the Guard Ring voltage can be controlled along with an offset voltage to account for the small C_2 coefficient of the Guard Ring or the rms magnetron radius of the ion. Each of the terms of the PID feedback loop are separately plotted, which is quite useful when tuning the PID loop. For testing the frequency response of the system, various Ring voltage waveforms at a fixed frequency can be added to the PID output voltage and the relative phase and amplitude of each PID term calculated over a specified number of cycles. In a similar manner, the system can create an amplitude modulated magnetron drive for adiabatically modulating the magnetron radius of a single ion in the trap. An event sequencer allows the user to specify times at which parameters such as the Guard Ring voltage should be automatically changed. These sequences can be read and written to file. There are several other bells and whistles that will not be discussed. These bells and whistles are very important for reducing costly mistakes and allowing more automated data taking.

Chapter 3

Two-Ion Theory

We wish to place two ions of very similar mass in our Penning trap and perform simultaneous cyclotron frequency comparisons to eliminate the effect of magnetic field noise, which is our dominant source of noise when alternately comparing cyclotron frequencies. We cannot haphazardly introduce two ions in the trap since the Coulomb interaction could significantly perturb the cyclotron frequency ratio. Instead, we wish to exploit the heretofore unused magnetron mode to keep the ions ~ 1 mm apart from one another. As will be shown in this chapter, at this separation the perturbation of the cyclotron ratio is well below 1 part in 10^{11}. The chief concern then becomes magnetic field inhomogeneities and trap electrostatic imperfections. Due to these imperfections, the cyclotron frequency of one ion can vary by as much as 1 part in 10^9 depending on whether it is measured with the ion at the center of the trap or on a 1 mm magnetron orbit.

The ideal configuration to suppress the effect of magnetic field inhomogeneities is to park each ion on a common magnetron orbit but on opposite sides of the trap (see Fig. 1-1). We can then superpose on top of this large and slow motion the small and fast cyclotron and axial motions needed to measure the cyclotron frequency ratio using the previously demonstrated PNP technique. In this ideal configuration, the ions maintain a constant ion-ion separation but swap positions in the trap at the magnetron frequency $\omega_{\mathrm{m}}/2\pi \approx 5$ kHz. It is essential that the magnetron radii of the two ions be the same to a few percent so that the radially dependent cyclotron frequency shifts are common to both ions and cancel in the ratio to better than 1 part in 10^{11}.

In this chapter, we will show that this ideal magnetron configuration actually turns out to be a normal mode of the system when the Coulomb interaction between the ions is included. In addition, the strength of this interaction will ensure that the rms magnetron radii are the same to a few percent as required. We will also calculate the perturbations of the trap cyclotron and axial frequencies that are crucial for understanding and minimizing systematic errors due to ion-ion interactions.

Much of this discussion will be built on our lab's initial proposal for comparing the cyclotron frequencies of two ions in a single Penning trap by Eric A. Cornell, Kevin R.

Boyce, Deborah L.K. Fygenson and David E. Pritchard [2]^G. Certain portions of the theory will be more complete or discussed in a way that we hope gives a more intuitive feel for the physics behind the various results. We believe this will be instructive for future graduate students. We will also discuss how a proper treatment of the nonlinear interaction gives rise to elliptical magnetron normal modes. We will include an estimate of the effect of electrostatic anharmonicities on the collective magnetron orbits. Numerical simulations of the magnetron motions are performed for comparison with the perturbation theory, and will be shown to be in excellent agreement. We believe that this really nails down that we understand collective magnetron orbits in a self-consistent way, which was not the case previously.

Before starting, let us define some notation that will be used throughout this chapter and those following it. The two ions we will compare have very similar masses denoted by m_0 and m_1. Because the masses are similar it is useful to also define their average mass $\bar{m}$ and fractional mass difference 2η such that

$$\bar{m} \equiv \frac{1}{2}\left(m_1 + m_0\right) \tag{3.1}$$

and

$$\begin{aligned} m_0 &= \bar{m}\left(1+\eta\right) \\ m_1 &= \bar{m}\left(1-\eta\right) \quad . \end{aligned} \tag{3.2}$$

We will *always* use the convention $m_0 \geq m_1$ so that $\eta \geq 0$. In addition, we will define cyclotron, axial, and magnetron frequencies for a hypothetical ion of mass $\bar{m}$ as

$$\bar{\omega}_{\rm c} \equiv \frac{qB}{\bar{m}c} \tag{3.3}$$

$$\bar{\omega}_{\rm z} \equiv \sqrt{\frac{qV_{\rm r}}{\bar{m}d^2}} \tag{3.4}$$

$$\bar{\omega}_{\rm m} \equiv \frac{\bar{\omega}_{\rm c} - \sqrt{\bar{\omega}_{\rm c}^2 - 2\bar{\omega}_{\rm z}^2}}{2} \quad . \tag{3.5}$$

These definitions are slightly different from the average of each ion's frequencies (for instance $\bar{\omega}_{\rm c} \neq (\omega_{\rm c1} + \omega_{\rm c0})/2$) although in the limit that $\eta \ll 1$ the difference is quite small.

Lastly, and most importantly, we will define the magnetron separation $\vec{\rho}_{\rm s}$ and common $\vec{\rho}_{\rm com}$ vectors as

$$\vec{\rho}_{\rm s} \equiv \vec{\rho}_{\rm m1} - \vec{\rho}_{\rm m0} \tag{3.6}$$

$$\vec{\rho}_{\rm com} \equiv \frac{1}{2}\left(\vec{\rho}_{\rm m1} + \vec{\rho}_{\rm m0}\right) \tag{3.7}$$

with corresponding magnitudes $\rho_s \equiv |\vec{\rho}_s|$ and $\rho_{com} \equiv |\vec{\rho}_{com}|$. To be clear, when cyclotron motion is present the vectors $\vec{\rho}_{m0,1}$ refer to the guiding centers of the much faster cyclotron motion. We will find that the $\vec{\rho}_s$ and $\vec{\rho}_{com}$ vectors are the normal modes of the coupled magnetron system for equal masses $\eta = 0$ and approximate normal modes for very similar masses $\eta \ll 1$.

It should be noted that the common vector is approximately the center of mass of the magnetron motions when $\eta \ll 1$. For most of the mass doublets we work with $2\eta < 10^{-3}$, and the fractional error in referring to the common mode as the center of mass mode is of the same order. In most day-to-day usage we referred to the common mode as the center of mass mode. But in this thesis (and I encourage this in future use as well), I will strive to refer to this mode as the common mode since it is more correct and avoids some confusion in the discussion of the imbalance of the magnetron orbits in the limit that the common-like mode amplitude goes to zero.

3.1 The Big Picture

The dynamics of two ions in a Penning trap can be understood as independent ion motion slightly perturbed by the relatively weak Coulomb interaction. Each ion will move on orbits that look like the usual cyclotron, axial, and magnetron motions with slightly perturbed frequencies or with modulated amplitudes over time scales of many seconds. At lowest order, the perturbations are only significant between nearly frequency-degenerate modes. If we use ions with similar masses, then the hierarchy of mode frequencies $\omega_c \gg \omega_z \gg \omega_m$ means that only like modes are nearly degenerate with one another. For instance, we will find that the cyclotron mode of one ion is most strongly perturbed by the cyclotron mode of the other ion. This pair-wise interaction between modes greatly reduces the complexity of the problem. Whether the interaction between two modes simply causes frequency shifts or actually mixes the modes is determined by the degree of degeneracy between the modes relative to the interaction strength. We will find that the cyclotron and axial motions remain independent with small frequency perturbations that will be important to understand for accurate mass comparisons. In contrast, the frequency degeneracy of the magnetron modes will cause them to completely mix into two new collective modes that are just the common and separation vectors defined in the previous section. The separation mode consists of a rotation of the separation vector at a slightly higher frequency than the average uncoupled magnetron frequency $\bar{\omega}_m$. The length of the separation vector remains constant in order to conserve energy and canonical angular momentum. The common mode corresponds to a rotation of the sum vector about the center of the trap at $\bar{\omega}_m$. These collective modes will beat against one another because of the slight frequency difference. The beating produces modulation of each ion's magnetron amplitude on time scales of 5 to 50 s. This is favorable for averaging away the differential frequency shifts due to trap field imperfections when

comparing the cyclotron frequencies of the ions.

The Coulomb force between the ions is extremely weak compared to the forces from the trapping fields. For scale, at a separation of 1 mm the electric field that one ion sees due to the other ion is 14.4 μV/cm compared to the radial trap electric field of ~ 1.2 V/cm for $V_{\rm r}$= 15 V and $\rho_{\rm m}$= $\rho_{\rm s}/2$. An alternative and quite useful way to express the strength of the Coulomb force is to express its magnitude in units of frequency squared

$$\Omega_{\rm E}^2 = \frac{q^2}{m\rho_{\rm s}^3} \quad . \tag{3.8}$$

Of course, this frequency must be compared to the other frequency scales in our trap. A convenient way to characterize this is to imagine that each pair of modes are degenerate in frequency. We can then calculate the normal modes of the system (which look like some version of sum and difference modes) and identify the frequency splitting between the modes as an effective Rabi frequency. The axial Rabi frequency is

$$\Omega_{\rm z} \equiv \frac{\Omega_{\rm E}^2}{\omega_{\rm z}} = \frac{qd^2}{\rho_{\rm s}^3 V_{\rm r}\sqrt{m}} \quad . \tag{3.9}$$

The cyclotron Rabi frequency is

$$\Omega_{\rm c} \equiv \frac{\Omega_{\rm E}^2}{\omega_{\rm c}} = \frac{c}{\rho_{\rm s}}\frac{(q/\rho_{\rm s}^2)}{B} \quad . \tag{3.10}$$

The magnetron Rabi frequency is

$$\Omega_{\rm m} \equiv \frac{2\Omega_{\rm E}^2}{\omega_{\rm c}} = \frac{c}{\rho_{\rm s}/2}\frac{(q/\rho_{\rm s}^2)}{B} \quad . \tag{3.11}$$

See Eq. 3.15 for typical magnitudes. These Rabi frequencies have a common dependence on the ion-ion separation of $1/\rho_{\rm s}^3$. The two radial Rabi frequencies do not depend on mass, while the axial Rabi frequency varies like $1/\sqrt{m}$. The expansions of the two radial Rabi frequencies are written to look like the electric field produced by one ion at the other ion's location divided by the trap magnetic field. It is then easy to see that the quantities $\rho_{\rm s}\Omega_{\rm c}$ and $\rho_{\rm s}\Omega_{\rm m}/2$ look like the velocity with which a particle would move through the perpendicular (or crossed) trap magnetic field and ion-ion electric fields without deflection. In the case of the magnetron motion, this will in fact turn out to be the correct interpretation.

To determine the behavior resulting from the couplings above and the case of nondegenerate masses, we will compare these Rabi frequencies to the frequency differences between modes, which we can write in terms of the fractional mass difference 2η and the mode frequencies of a hypothetical ion of the average mass $\bar{m}$

$$\delta_{\rm z2} \equiv \omega_{\rm z1} - \omega_{\rm z0} \approx \eta\bar{\omega}_{\rm z} \tag{3.12}$$

$$\delta_{\rm c2} \equiv \omega_{\rm ct1} - \omega_{\rm ct0} \approx 2\eta\bar{\omega}_{\rm ct} \tag{3.13}$$

$$\delta_{\mathrm{m2}} \equiv \omega_{\mathrm{m1}} - \omega_{\mathrm{m0}} \approx -2\eta \frac{\bar{\omega}_{\mathrm{m}}^2}{\bar{\omega}_{\mathrm{c}}} \ . \tag{3.14}$$

See Eq. 3.16 for typical magnitudes. The first two expressions are trivial to derive. The magnetron difference frequency can be arrived at from Eq. 2.10. The magnetron frequencies are independent of mass at first approximation because the centrifugal force is so small. For scale, the centrifugal force is of order $\omega_{\mathrm{m}}^2 \rho_{\mathrm{m}}$ compared to the Lorentz and electrostatic forces of order $\omega_{\mathrm{c}} \omega_{\mathrm{m}} \rho_{\mathrm{m}}$ and $\omega_{\mathrm{z}}^2 \rho_{\mathrm{m}}$ respectively.

How do these frequency scales compare to one another? As a concrete example, consider the pair $^{13}C_2H_2^+$ vs N_2^+ for which the fractional mass difference is $2\eta = 5.79 \times 10^{-4}$, the average mass is $\bar{m}$= 28.0137 u, and the axial and cyclotron frequencies are $\omega_{\mathrm{z}}/2\pi = 212$ kHz and $\omega_{\mathrm{c}}/2\pi = 4.67 \times 10^6$ MHz. If the ions are 1 mm apart then we find that the Rabi frequencies and mode differences evaluate to

$$\begin{array}{rcrcl} \Omega_{\mathrm{z}}/2\pi\,|_{\rho_{\mathrm{s}}=1\ \mathrm{mm}} & = & 593\ \mathrm{mHz} & = & \frac{1}{1.69\ \mathrm{s}} \\ \Omega_{\mathrm{c}}/2\pi\,|_{\rho_{\mathrm{s}}=1\ \mathrm{mm}} & = & 26.9\ \mathrm{mHz} & = & \frac{1}{37.2\ \mathrm{s}} \\ \Omega_{\mathrm{m}}/2\pi\,|_{\rho_{\mathrm{s}}=1\ \mathrm{mm}} & = & 53.8\ \mathrm{mHz} & = & \frac{1}{18.6\ \mathrm{s}} \end{array} \tag{3.15}$$

and

$$\begin{array}{rcr} \delta_{\mathrm{z2}}/2\pi & = & 61.4\ \mathrm{Hz} \\ \delta_{\mathrm{c2}}/2\pi & = & 2700\ \mathrm{kHz} \\ \delta_{\mathrm{m2}}/2\pi & = & -2.9\ \mathrm{mHz} \end{array} \tag{3.16}$$

For both the axial and cyclotron modes $\delta \gg \Omega$, and the modes will remain independent ion modes with only a small perturbation of the mode frequencies. In contrast, the magnetron frequencies are almost identical so that $\Omega_{\mathrm{m}} \gg \delta_{\mathrm{m2}}$. In this regime, we find that the independent magnetron modes will mix into collective modes.

Let us further examine in a very general manner what we expect for each regime. Essentially each normal mode in our Penning trap can be thought of as an harmonic oscillator interacting with another harmonic oscillator. First, consider the scenario such as for our magnetron modes in which the two oscillators have identical resonant frequencies. It might help to imagine two pendula of equal length and mass. The smallest interaction between the oscillators mixes the normal modes into a common and a stretch mode. If one pendula oscillates with amplitude A and the other oscillator is at zero amplitude, then at some later time the other oscillator will have amplitude A and the original oscillator will have zero amplitude. This swapping of amplitudes can be described with many terms that will be used throughout this thesis including: beating between normal modes, amplitude swapping, and Rabi oscillations. We can characterize the strength of the interaction between the ions in terms of a Rabi frequency that is given by the frequency with which the amplitude swaps between the oscillators. A larger Rabi frequency indicates a larger interaction. On time scales much shorter than a Rabi cycle, the modes should be thought of as independent

harmonic oscillators, but for longer time scales the motions are best described in terms of the common and separation modes. For a given problem, it is important to first decide which time scale is relevant.

The second regime of coupling is when the frequency difference between the oscillators is so large that exciting the motion of one oscillator will not cause any significant excitation of the second oscillator at later times. This is the regime of the cyclotron-cyclotron and axial-axial interactions. Physically, each oscillator drives the motion of the other oscillator nonresonantly so that the amplitude of the response is down by $\Omega_{\rm R}/(2\delta)$. This means that the interaction of the oscillators is chiefly at second order and appears as a frequency pulling (actually pushing or repelling). For instance, the lower frequency oscillator with amplitude a_0 drives the higher frequency oscillator below resonance, creating motion at the same frequency with amplitude $b_1 = -a_0\Omega_{\rm R}/|2\delta|$. The induced motion of the higher frequency oscillator then acts back on the lower frequency oscillator generating a resonant force proportional to $-a_0\Omega_{\rm R}^2/|4\delta|$ that lowers its frequency. The higher frequency oscillator experiences a similar reaction force, but because it drives the other oscillator above resonance, the reaction force is proportional to $b_0\Omega_{\rm R}^2/|4\delta|$ and shifts its frequency up. The nondegenerate oscillators repel one another in frequency. This is a second order interaction with direct analogy to the ac Stark shift in quantum mechanics.

3.2 Impact of Conserved Quantities

The rotational symmetry of the trap leads to conservation of canonical angular momentum for the two-ion system

$$L_{\rm z} = \frac{qB}{2c}\left(\vec{\rho}_1^{\,2} + \vec{\rho}_0^{\,2}\right) + m_1\,\vec{\rho}_1 \times \dot{\vec{\rho}}_1 + m_0\,\vec{\rho}_0 \times \dot{\vec{\rho}}_0 \quad . \tag{3.17}$$

The canonical angular momentum differs from the kinetic angular momentum by the large contribution from the magnetic field.* If the axial motions are taken to be zero amplitude then there is no damping in the system and the energy is also conserved. The total energy can be written as

$$E = -\frac{1}{4}\frac{qV_{\rm r}}{d^2}\left(\vec{\rho}_1^{\,2} + \vec{\rho}_0^{\,2}\right) + \frac{1}{2}m_1\,\dot{\vec{\rho}}_1^{\,2} + \frac{1}{2}m_0\,\dot{\vec{\rho}}_0^{\,2} + \frac{q^2}{\rho_{\rm s}} \quad . \tag{3.18}$$

For cyclotron motion, the kinetic energy dominates over the potential energy associated with the radial electric fields. For magnetron motion, the situation is reversed and the energy is mostly stored as potential energy. Together, these conserved quantities constrain the possible motion near the magnetron frequency for ions of nearly equal mass because of

*For a single ion in a Penning trap, the canonical angular momentum for a cyclotron orbit is $L_{\rm z} = (-m\omega_{\rm c}/2 + m\omega_{\rm m})\rho_{\rm c}^2$ while for a magnetron orbit it is $L_{\rm z} = (m\omega_{\rm c}/2 - m\omega_{\rm m})\rho_{\rm m}^2$. For equal size orbits, the canonical angular momentum in each mode is equal but opposite in sign. This is a great way to quickly remember the contribution of the magnetic field to the canonical angular momentum.

the similarity of the uncoupled magnetron frequencies. In contrast, motions near the axial and cyclotron frequencies are not constrained because of the large frequency difference of the uncoupled modes.

It was shown in the initial proposal for working with two ions in a Penning trap ([2]^G equations 2.12 and 2.13) that these conserved quantities lead to the ion-ion separation and the common amplitude being approximate constants of the motion when only magnetron motion is considered. The derivation of the constraints assumes the motions are the independent magnetron motions with adiabatically varying amplitudes and phases. This is necessary in order to ignore interactions with the cyclotron modes. The interactions are strongly suppressed by the large difference in frequencies $\bar{\omega}_{\rm c} \gg \bar{\omega}_{\rm m}$. It is further assumed and verified that the kinetic energy and angular momentum associated with the small changes in velocities do not significantly contribute to the energy or angular momentum. This second step is a bit of a cheat since it assumes some knowledge of the dynamics.

The first constraint on the sum of the magnetron amplitudes squared follows directly from conservation of canonical angular momentum and is completely independent of even whether the ions are interacting or not. To derive the constraint, we approximate that the ions move at the average magnetron frequency $\bar{\omega}_{\rm m}$ and that the magnetron amplitudes are only slowly varying in time with characteristic frequency $\Omega_{\rm m} \ll \bar{\omega}_{\rm m}$. Then to leading order in η, we can write

$$\delta L_{\rm z}\left(\frac{2}{\bar{m}}\right) = \delta\left(\rho_{\rm m1}^2 + \rho_{\rm m0}^2\right)(\bar{\omega}_{\rm c} - 2\bar{\omega}_{\rm m}) + \delta\left(\rho_{\rm m0}^2 - \rho_{\rm m1}^2\right)2\eta\bar{\omega}_{\rm m} = 0 \quad . \tag{3.19}$$

This can be simplified using Eq. 3.14 to give the first constraint

$$\frac{\delta\left(\rho_{\rm m1}^2 + \rho_{\rm m0}^2\right)}{\rho_{\rm s}^2} \approx \frac{\delta_{\rm m2}}{\bar{\omega}_{\rm m}}\frac{\delta(\rho_{\rm m1}^2 - \rho_{\rm m0}^2)}{\rho_{\rm s}^2} \quad . \tag{3.20}$$

The second constraint is on the maximum possible change in the ion-ion separation and follows from first constraint combined with conservation of energy. The stringency of the constraint is inversely proportional to the strength of the ion-ion interaction:

$$\frac{\delta\rho_{\rm s}}{\rho_{\rm s}} \approx \delta_{\rm mag}\frac{\delta(\rho_{\rm m1}^2 - \rho_{\rm m0}^2)}{\rho_{\rm s}^2} = \frac{-\delta_{\rm m2}}{2\Omega_{\rm m}}\frac{\delta(\rho_{\rm m1}^2 - \rho_{\rm m0}^2)}{\rho_{\rm s}^2} \quad . \tag{3.21}$$

The parameter $\delta_{\rm mag}$ will show up in a different context, but for now one can take the second expression as a defining relation. The second constraint was derived using a similar set of assumptions as the first constraint. Combining the two constraints sets a limit on changes in the common mode amplitude similar to the second constraint.

For the example pair of $^{13}C_2H_2^+$ vs N_2^+ of the previous section, the constraint on changes in the sum of the squares of the magnetron amplitudes is quite stringent since the fractional difference in the magnetron frequencies is $\delta_{\rm m2} \sim 5 \times 10^{-7}$ and the second factor can only assume a maximum value of unity. The second expression constraining the change in the

ion-ion separation is more fragile with the leading factor $\delta_{\rm mag} = 0.03$ at $\rho_{\rm s} = 1$ mm. This is still a small range of possible change in $\rho_{\rm s}$ so that we may consider the ion-ion separation an approximate constant of the motion. This will allow us to more confidently linearize the equations of motion in the following sections.

3.3 Coupled Magnetron Modes

3.3.1 Equal Masses

The radial equations of motion for two ions in a Penning trap can be written starting from Eq. 2.6 for a single ion and adding the Coulomb repulsion

$$(1-\eta)\,\ddot{\vec{\rho}}_1 = \bar{\omega}_{\rm c}\dot{\vec{\rho}}_1 \times \hat{z} + \frac{1}{2}\bar{\omega}_{\rm z}^2\,\vec{\rho}_1 + \frac{q^2\,(\vec{\rho}_1 - \vec{\rho}_0)}{\bar{m}\rho_{\rm s}^3} \tag{3.22}$$

$$(1+\eta)\,\ddot{\vec{\rho}}_0 = \bar{\omega}_{\rm c}\dot{\vec{\rho}}_0 \times \hat{z} + \frac{1}{2}\bar{\omega}_{\rm z}^2\,\vec{\rho}_0 - \frac{q^2\,(\vec{\rho}_1 - \vec{\rho}_0)}{\bar{m}\rho_{\rm s}^3} \tag{3.23}$$

where we have divided by the average mass $\bar{m}$, the fractional mass difference is 2η, $\rho_{\rm s} = |\,\vec{\rho}_{\rm m1} - \vec{\rho}_{\rm m0}|$, and the cyclotron and axial frequencies are those of a hypothetical ion of mass $\bar{m}$ (see the chapter introduction for more on these definitions). For equal mass ions $\eta = 0$, taking the sum and difference of Eqs. 3.22 and 3.23 yields uncoupled equations of motion for the sum and difference magnetron vectors

$$\ddot{\vec{\rho}}_{\rm s} = \bar{\omega}_{\rm c}\dot{\vec{\rho}}_{\rm s} \times \hat{z} + \frac{1}{2}\bar{\omega}_{\rm z}^2\left(1 + \frac{4\Omega_{\rm E}^2}{\bar{\omega}_{\rm z}^2}\right)\vec{\rho}_{\rm s} \tag{3.24}$$

$$\ddot{\vec{\rho}}_{\rm com} = \bar{\omega}_{\rm c}\dot{\vec{\rho}}_{\rm com} \times \hat{z} + \frac{1}{2}\bar{\omega}_{\rm z}^2\,\vec{\rho}_{\rm com} \tag{3.25}$$

where the magnetron common $\vec{\rho}_{\rm com}$ and separation $\vec{\rho}_{\rm s}$ vectors are defined previously by Eq. 3.6. The solutions of these equations are identical to that of a single ion, and the mode frequencies can be arrived at by analogy to Eq. 2.9. Using the approximation that $\omega_{\rm m} \approx \omega_{\rm z}^2/(2\omega_{\rm c})$, it is easy to show that to first order the normal mode frequencies are given by

$$\omega_{\rm ms} \approx \bar{\omega}_{\rm m} + \Omega_{\rm m} \tag{3.26}$$

$$\omega_{\rm mc} = \bar{\omega}_{\rm m} \quad . \tag{3.27}$$

The only assumption we have made in our derivation is that the denominator of the Coulomb interaction is well approximated by the magnetron difference vector. This means that our solutions are only accurate when the cyclotron and axial amplitudes are much less

than ρ_s. I want to emphasize that the decoupling of the equations of motion is exact for equal mass ions and gives us the exact normal modes of the system. These exact modes will be used in the next section as the starting point for perturbatively calculating the normal modes when the ions have slightly different masses.

Figure 3-1 shows both (a) the original uncoupled magnetron positions and (b) the new normal modes. The collective mode vectors $\vec{\rho}_s$ and $\vec{\rho}_{com}$ both rotate clockwise at nearly identical frequencies. If the frequencies were truly identical then the magnetron radius of each ion would be constant in time. The slight frequency difference between the modes leads to modulation of the magnetron amplitudes at the beat frequency between the modes Ω_m. We will often refer to this beating as a swapping motion since the two ions take turns with one ion closer to and the other ion further from the trap center with the roles swapped after half a beat period.

The swapping motion is very convenient for making accurate mass comparisons since the magnetic field inhomogeneities and electrostatic imperfections are averaged by the swapping motion on a time scale of 5 to 40 s, which is typically much less than the integration time $T_{evol} \sim 300$ s used to measure the cyclotron frequency ratio. In general, we will work to place the common mode (or center of mass) at the center of the trap (ρ_{com}=0) so that the ions are very nearly parked on a shared magnetron orbit but on opposite sides of the trap. Even if this ideal situation is not exactly achieved, the swapping ensures that the residual imbalance in the rms magnetron radii averages to zero. This behavior will be slightly modified for unequal mass ions, as will be discussed in the next section 3.3.2.

Before continuing, we will briefly consider the nature of the separation mode that maintains the ion-ion separation constant in spite of (because of!) the repulsive Coulomb interaction. The separation mode can be understood as an $E \times B$ drift about the common mode vector. The magnetic field B is the usual 8.5 T trap field, and the electric field E is that generated by the other ion located on the opposite side of the common position. The ions move with just the correct velocity to generate a Lorentz force that just balances the repulsive electric field between them.

One can derive the beat frequency between the two modes using this model. This is easiest to imagine in a rotating frame at $\bar{\omega}_m$ such that the common mode vector $\vec{\rho}_{com}$ is stationary. In this frame, the trap electric fields have been cancelled by the Lorentz force generated by motion at $\bar{\omega}_m$. The only remaining net force is generated by each ion's electric field. Assuming circular motion about the stationary common mode position, then the radius of the orbit is $\rho_s/2$. The equation of motion for one of the ions gives an expression which can be solved for Ω_m

$$-\Omega_m^2 \frac{\rho_s}{2} = -\Omega_m \bar{\omega}_c \frac{\rho_s}{2} + \Omega_E^2 \rho_s \quad . \tag{3.28}$$

Because the orbit is so slow, the centrifugal force on the left hand side of the equation is a tiny correction that we can ignore. Solving for Ω_m with this approximation gives the

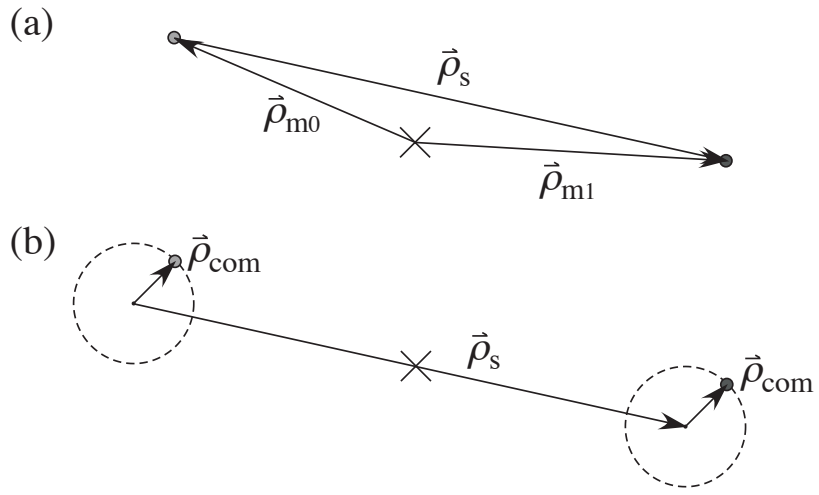

Figure 3-1: The magnetron motion of ion 0 on the left and ion 1 on the right. In the uncoupled basis shown in (a), the individual magnetron vectors $\vec{\rho}_{\rm m0}$ and $\vec{\rho}_{\rm m1}$ rotate clockwise near $\bar{\omega}_{\rm m}$with constant magnitudes. In the Coulomb coupled system shown in (b), each ion's magnetron motion should be written in terms of the new normal modes $\vec{\rho}_{\rm s}$ and $\vec{\rho}_{\rm com}$. Both vectors rotate clockwise near $\bar{\omega}_{\rm m}$, but the separation vector rotates at a slightly higher frequency, leading to a modulation of each ion's magnetron amplitude at the beat frequency $\Omega_{\rm m}$.

previously defined value

$$\Omega_{\rm m} = \frac{2\Omega_{\rm E}^2}{\bar{\omega}_{\rm c}} \ . \tag{3.29}$$

3.3.2 Nearly Equal Masses

When the masses are nearly but not exactly equal, the equations of motion 3.22 and 3.23 can be added and subtracted to yield

$$\ddot{\vec{\rho}}_{\rm s} = \bar{\omega}_{\rm c}\dot{\vec{\rho}}_{\rm s} \times \hat{z} + \frac{1}{2}\bar{\omega}_{\rm z}^2\left(1 + \frac{4\Omega_{\rm E}^2}{\bar{\omega}_{\rm z}^2}\right)\vec{\rho}_{\rm s} - \frac{\eta}{2}\ddot{\vec{\rho}}_{\rm com} \tag{3.30}$$

$$\ddot{\vec{\rho}}_{\rm com} = \bar{\omega}_{\rm c}\dot{\vec{\rho}}_{\rm com} \times \hat{z} + \frac{1}{2}\bar{\omega}_{\rm z}^2\,\vec{\rho}_{\rm com} - \eta\ddot{\vec{\rho}}_{\rm s} \ . \tag{3.31}$$

The equations of motion are now slightly coupled to one another by the last term that arises from the finite mass splitting. The symmetry of the couplings is broken by the difference of 1/2 in the definition of the common and separation vectors and is not of real interest. Since the last terms in each equation are of order $\eta\bar{\omega}_{\rm m}^2\rho$, which is small compared to all the other terms, they can be treated as a perturbation. Of course if $\rho_{\rm s} = |\,\vec{\rho}_{\rm s}|$ is constant then the Coulomb interaction parameter $\Omega_{\rm E}$ is also constant. One can then simply assume two circular modes of different frequencies that can be exactly calculated. We will return to

this point shortly, but push ahead for now.

Magnetron Orbits at First Pass

Although these coupled equations can be exactly solved, I have found that it is more enlightening to solve for the small mode mixing by calculating the perturbation of the motions starting from the exact normal modes for equal mass ions. This calculation is akin to the first order perturbation theory of quantum mechanics, in which a small perturbation causes a small mixing of the original eigenstates. To proceed, we will treat the coupling terms as drives originating from the zeroth order estimates of the orbits $\vec{\rho}_{\rm s}^{(0)}$ and $\vec{\rho}_{\rm com}^{(0)}$ that in turn excite motions $\vec{\rho}_{\rm com}^{(1)}$ and $\vec{\rho}_{\rm s}^{(1)}$. We ignore the reaction force since it will be of second order in the coupling. The chief effect of the reaction force would be a fractional shift of the difference frequency $\Omega_{\rm m}$, which is of order $(\delta_{\rm m2}/\Omega_{\rm m})^2 \leq 10^{-3}$. Evaluating the time derivatives of the zeroth order solutions and ignoring the difference between $\omega_{\rm ms}$ and $\omega_{\rm mc}$ we find

$$\ddot{\vec{\rho}}_{\rm s}^{(1)} = \bar{\omega}_{\rm c}\dot{\vec{\rho}}_{\rm s}^{(1)} \times \hat{z} + \frac{1}{2}\bar{\omega}_{\rm z}^2\left(1 + \frac{4\Omega_{\rm E}^2}{\bar{\omega}_{\rm z}^2}\right)\vec{\rho}_{\rm s}^{(1)} + \frac{\eta\bar{\omega}_{\rm m}^2}{2}\vec{\rho}_{\rm com}^{(0)} \tag{3.32}$$

$$\ddot{\vec{\rho}}_{\rm com}^{(1)} = \bar{\omega}_{\rm c}\dot{\vec{\rho}}_{\rm com}^{(1)} \times \hat{z} + \frac{1}{2}\bar{\omega}_{\rm z}^2\vec{\rho}_{\rm com}^{(1)} + \eta\bar{\omega}_{\rm m}^2\vec{\rho}_{\rm s}^{(0)} \tag{3.33}$$

The first order induced motions are at the frequencies of the drive terms, and it is straightforward to find that the separation and common modes are given by

$$\begin{array}{rcl} \vec{\rho}_{\rm s} = \vec{\rho}_{\rm s}^{(0)} + \vec{\rho}_{\rm s}^{(1)} & = & \Re\left\{(\hat{x} + \imath\hat{y})\, e^{\imath\omega_{\rm ms}t}\left[\tilde{\rho}_{\rm s} - 2\delta_{\rm mag}\tilde{\rho}_{\rm com}e^{-\imath\Omega_{\rm m}t}\right]\right\} \\ \vec{\rho}_{\rm com} = \vec{\rho}_{\rm com}^{(0)} + \vec{\rho}_{\rm com}^{(1)} & = & \Re\left\{(\hat{x} + \imath\hat{y})\, e^{\imath\omega_{\rm mc}t}\left[\tilde{\rho}_{\rm com} + \frac{1}{2}\delta_{\rm mag}\tilde{\rho}_{\rm s}e^{+\imath\Omega_{\rm m}t}\right]\right\} \end{array} \quad . \tag{3.34}$$

with the unitless mixing parameter $\delta_{\rm mag}$ given by

$$\delta_{\rm mag} = \frac{-\delta_{\rm m2}}{2\Omega_{\rm m}} = \frac{\eta\bar{\omega}_{\rm m}^2}{2\Omega_{\rm E}^2} \quad . \tag{3.35}$$

The parameters $\tilde{\rho}_{\rm s}$ and $\tilde{\rho}_{\rm com}$ are complex amplitudes (not vectors) that can be determined from initial conditions. They are related to the amplitudes of the true normal modes of the system to within a renormalization factor. The magnitude of $\tilde{\rho}_{\rm s}$ should be used to evaluate the average Coulomb coupling parameter $\Omega_{\rm E}$.

The common and separation vectors are no longer exact normal modes to the degree that $\delta_{\rm mag} \neq 0$. The degree of mixing is physically the difference frequency between the uncoupled single ion magnetron modes and the strength of the Coulomb interaction.[†] For

[†]One finds an analogous imperfect mixing of quantum states in the Rabi problem when the Rabi frequency is much greater than the detuning of the coupling from resonance. I have always found these kinds of analogies essential as an atomic physicist for quickly estimating the size of various effects.

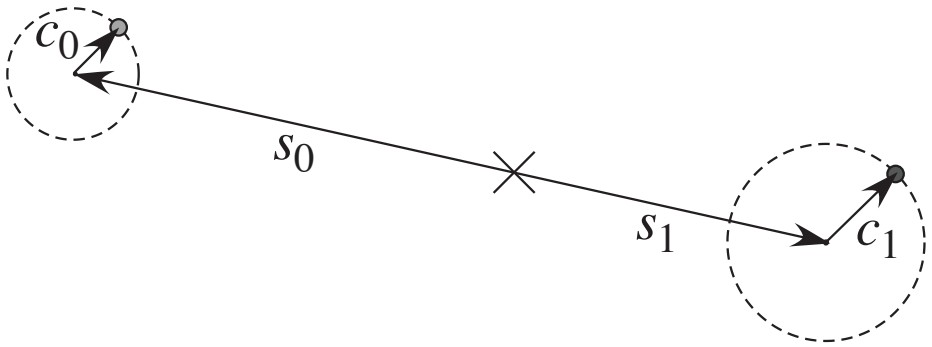

Figure 3-2: The magnetron motion for unequal mass ions with ion 0 on the left and ion 1 on the right . The common-like vectors of length $c_0 = \tilde{\rho}_{\rm com}(1+\delta_{\rm mag})$ and $c_1 = \tilde{\rho}_{\rm com}(1-\delta_{\rm mag})$ rotate clockwise at $\omega_{\rm mc} = \bar{\omega}_{\rm m}$. The separation-like vectors of length $s_0 = \tilde{\rho}_{\rm s}(1-\delta_{\rm mag})/2$ and $s_1 = \tilde{\rho}_{\rm s}(1+\delta_{\rm mag})/2$ also rotate clockwise but with a slightly higher frequency $\omega_{\rm ms} = \bar{\omega}_{\rm m}+\Omega_{\rm m}$. The value of the mode mixing parameter is $\delta_{\rm mag} = 0.20$ in this diagram, which is much larger than a typical experimental value $\delta_{\rm mag} \leq 0.05$.

the example of $^{13}C_2H_2^+$ vs N_2^+, $\delta_{\rm mag}$= 0.027 for an average ion-ion separation of 1 mm. In the limit that the masses are identical (η=0), the frequency difference between the single ion magnetron modes goes to zero, and the common and separation vectors become normal modes again.

Equations 3.34 can in turn be combined with the definitions of $\vec{\rho}_{\rm s}$ and $\vec{\rho}_{\rm com}$ from Eq. 3.6 to yield each ion's magnetron position as a function of time

$$\begin{array}{rclcl} \vec{\rho}_{\rm m0} & = & \vec{\rho}_{\rm com} - \frac{1}{2}\vec{\rho}_{\rm s} & = & \Re\left\{(\hat{x}+\imath\hat{y})\, e^{\imath\bar{\omega}_{\rm m}t}\left[\tilde{\rho}_{\rm com}\,(1-\delta_{\rm mag}) - \frac{1}{2}\tilde{\rho}_{\rm s}\,(1+\delta_{\rm mag})\, e^{\imath\Omega_{\rm m}t}\right]\right\} \\ \vec{\rho}_{\rm m1} & = & \vec{\rho}_{\rm com} + \frac{1}{2}\vec{\rho}_{\rm s} & = & \Re\left\{(\hat{x}+\imath\hat{y})\, e^{\imath\bar{\omega}_{\rm m}t}\left[\tilde{\rho}_{\rm com}\,(1+\delta_{\rm mag}) + \frac{1}{2}\tilde{\rho}_{\rm s}\,(1-\delta_{\rm mag})\, e^{\imath\Omega_{\rm m}t}\right]\right\} \end{array} . \tag{3.36}$$

This is just the result of Ref. [2]^G, Eq. 4.15, but with the time dependence made explicit. The magnetron motion now evolves as in Fig. 3-2 where the imbalance in length scales has been exaggerated to highlight their presence. Each normal mode is dominantly composed of common or separation motion, so we will refer to the common-like mode as simply the common mode and similarly for the separation mode.

The magnetron motion in the special case of $\tilde{\rho}_{\rm com} = 0$ can be physically understood. The heavier ion has a slightly larger centrifugal force than the lighter ion. The larger centrifugal force must be compensated for by a larger velocity to produce a larger inwards Lorentz force. The speed is given by the product of the angular frequency times the orbit radius. However, if the motion is to be stable in time, the ion must orbit the center of the trap at the same frequency as the other ion or else the ions would catch up with one another. The only degree of freedom is then to make the heavier ion's radius slightly larger and the lighter ion's radius slightly smaller. This is exactly what we observe in the above Eqs. 3.36.

The exact form of the imbalance $\delta_{\rm mag}$ can be quickly worked out assuming the form of the modification is

$$\begin{aligned} \vec{\rho}_{\rm m1} &= +\tfrac{1}{2}\,\vec{\rho}_{\rm s}\,(1-\delta_{\rm mag}) \\ \vec{\rho}_{\rm m0} &= -\tfrac{1}{2}\,\vec{\rho}_{\rm s}\,(1+\delta_{\rm mag}) \quad . \end{aligned} \tag{3.37}$$

We can examine the equation of motion for either ion, but let us consider the equation for ion 0 from Eq. 3.22. If we take the rotation frequency about the center of the trap to be $\omega_{\rm ms} = \bar{\omega}_{\rm m} + \Omega_{\rm m}$ then we can expand the various time derivatives to arrive at the equation

$$(\bar{\omega}_{\rm m}^2+2\Omega_{\rm m}\bar{\omega}_{\rm m}+\Omega_{\rm m}^2)(1+\eta)(1+\delta_{\rm mag})\frac{\vec{\rho}_{\rm s}}{2} = \bar{\omega}_{\rm c}(\bar{\omega}_{\rm m}+\Omega_{\rm m})\frac{\vec{\rho}_{\rm s}}{2}(1+\delta_{\rm mag})-\frac{1}{2}\bar{\omega}_{\rm z}^2\frac{\vec{\rho}_{\rm s}}{2}(1+\delta_{\rm mag})-\Omega_{\rm E}^2\,\vec{\rho}_{\rm s} \tag{3.38}$$

As usual, the various terms left to right are the terms due to acceleration, the Lorentz force, the trap electric field, and the ion-ion electric field. We can simplify this expression by observing that $\bar{\omega}_{\rm m}$ satisfies the equation $\bar{\omega}_{\rm m}^2-\bar{\omega}_{\rm c}\bar{\omega}_{\rm m}+\bar{\omega}_{\rm z}^2/2=0$. We will also ignore terms second order in small quantities such as η and $\delta_{\rm mag}$. It is also fair to drop terms of order $\bar{\omega}_{\rm m}\Omega_{\rm m}$ since $\bar{\omega}_{\rm m}\Omega_{\rm m} = 2(\bar{\omega}_{\rm m}/\bar{\omega}_{\rm c})\Omega_{\rm E}^2 \ll \Omega_{\rm E}^2$. Making these substitutions and approximations we can write

$$\eta\bar{\omega}_{\rm m}^2 = \bar{\omega}_{\rm c}\Omega_{\rm m}(1+\delta_{\rm mag}) - 2\Omega_{\rm E}^2 \tag{3.39}$$

where the remaining contributions are from the centrifugal force, the Lorentz force and the ion-ion electric field. We can then substitute the previously calculated value of $\Omega_{\rm m} = 2\Omega_{\rm E}^2/\bar{\omega}_{\rm c}$ to determine $\delta_{\rm mag}$. It is clear that the value of $\Omega_{\rm m}$ is a speed up to cancel the repulsive electric field and the value of $\delta_{\rm mag}$ is chosen to cancel the centrifugal force.

Magnetron Orbits at Second Pass

The normal modes calculated above appear in the initial two-ion proposal and in all subsequent theses. However, there is a problem of self-consistency with the orbits. The initial assumption was that the ion-ion separation was constant so that the Coulomb interaction could be set to a constant value. But our solutions show that the ion-ion separation is modulated in time when the common-like mode $\tilde{\rho}_{\rm com} \neq 0$. The maximum and minimum value of the ion-ion separation occurs when the two normal mode vectors are parallel or antiparallel (see Fig. 3-2). When the common-like mode has zero amplitude, the assumptions and solutions are self-consistent so that the solution for the separation-like mode is correct. This problem was stabbed at in the initial proposal [2]^G, but it was not actually solved.

To find self-consistent orbits when $\tilde{\rho}_{\rm com} \neq 0$, we will proceed using the perturbative route outlined in the previous subsection. The calculation of the separation-like mode is unchanged since it involves the zeroth order motion driving the common mode equation of motion, which does not involve the Coulomb force. To solve for the first order modification

of the common-like mode, we make the ansatz that the separation motion, which is driven by the zeroth order common motion, can be written as a sum of clockwise rotating vectors

$$\vec{\rho}_{\rm s}^{(ansatz)} = \sum_{\rm n=-\infty}^{\infty} \rho_{\rm n} \vec{F}_{\rm n} \tag{3.40}$$

where the real amplitudes $\rho_{\rm n}$ are to be solved for. The n = 0 component represents the zeroth order separation mode motion and is an input rather than a quantity to be solved for. The rotating vectors are defined by

$$\vec{F}_{\rm n} \equiv \Re\left\{(\hat{x} + \imath\hat{y})\, e^{\imath(\omega_{\rm n} t + {\rm n}\phi)}\right\} \tag{3.41}$$

with the frequencies defined as

$$\omega_{\rm n} = \omega_{\rm ms} + {\rm n}\Omega_{\rm m} \quad . \tag{3.42}$$

The rotating vectors satisfy the very useful relation

$$\vec{F}_0 \left(\vec{F}_0 \cdot \vec{F}_{\rm n}\right) = \frac{1}{2}\left(\vec{F}_{\rm n} + \vec{F}_{\rm -n}\right) \quad . \tag{3.43}$$

The denominator of the Coulomb force can be expanded to lowest order in $\rho_{\rm n}/\rho_0$ as

$$\frac{1}{\left(\vec{\rho}_{\rm s}^{(ansatz)} \cdot \vec{\rho}_{\rm s}^{(ansatz)}\right)^{\frac{3}{2}}} \approx \frac{1}{\rho_0^3}\left(1 - \sum_{\rm n=-\infty,\neq 0}^{\infty} 3\vec{F}_0 \cdot \vec{F}_{\rm n} \frac{\rho_{\rm n}}{\rho_0}\right) \tag{3.44}$$

where the sum no longer includes n = 0 since we have explicitly included this term. Substituting this expansion for the Coulomb force in the equation of motion for the separation mode we find

$$\begin{aligned} \sum_{\rm n=-\infty}^{\infty} -\omega_{\rm n}^2 \rho_{\rm n} \vec{F}_{\rm n} \;\; = \;\; & \sum_{\rm n=-\infty}^{\infty} \left[-\bar{\omega}_{\rm c}\omega_{\rm n} + \frac{1}{2}\bar{\omega}_{\rm z}^2 + 2\Omega_{\rm E}^2\right] \rho_{\rm n} \vec{F}_{\rm n} \\ & -3\Omega_{\rm E}^2 \sum_{\rm n=-\infty,\neq 0}^{\infty} \rho_{\rm n}\left[\vec{F}_{\rm n} + \vec{F}_{\rm -n}\right] + 2\eta\bar{\omega}_{\rm m}^2 \tilde{\rho}_{\rm com} \vec{F}_{-1} \end{aligned} \tag{3.45}$$

where here the Coulomb term is evaluated as $\Omega_{\rm E}^2 = q^2/\bar{m}\rho_0^3$. The last term is the drive reexpressed in terms of the rotating vector $\vec{F}_{-1}$ at frequency $\omega_{-1} = \omega_{\rm ms} - \Omega_{\rm m} = \bar{\omega}_{\rm m}$. We can simplify this expression using the fact that the separation frequency satisfies the equation $-\omega_{\rm ms}^2 = \bar{\omega}_{\rm c}\omega_{\rm ms} + \bar{\omega}_{\rm z}^2/2 + 2\Omega_{\rm E}^2$ (actually this defines the value of the separation mode frequency). We can also make the approximations $\omega_{\rm n}^2 \approx \omega_{\rm ms}^2 + 4\omega_{\rm ms}\Omega_{\rm E}^2/\bar{\omega}_{\rm c}$ and $\bar{\omega}_{\rm c} \gg \omega_{\rm ms}$. This leads to the result

$$\sum_{\mathrm{n}=-\infty,\neq 0}^{\infty} \rho_{\mathrm{n}} \left[(2\mathrm{n}+3)\,\vec{F}_{\mathrm{n}} + 3\vec{F}_{-\mathrm{n}} \right] = \frac{2\eta\bar{\omega}_{\mathrm{m}}^2}{\Omega_{\mathrm{E}}^2}\tilde{\rho}_{\mathrm{com}}\vec{F}_{-1} \quad . \tag{3.46}$$

We then require that each rotating vector at a given frequency satisfy the equations of motion independently. This imposes that only terms with $\mathrm{n} = \pm 1$ are nonzero. This is because only these terms have a drive source. Putting all of this together, we find the separation and common mode vectors as a function of time

$$\vec{\rho}_{\mathrm{s}} = \tilde{\rho}_{\mathrm{s}}\vec{F}_0 - 5\delta_{\mathrm{mag}}\vec{F}_{-1} + 3\delta_{\mathrm{mag}}\vec{F}_1 \tag{3.47}$$

$$\vec{\rho}_{\mathrm{com}} = \tilde{\rho}_{\mathrm{com}}\vec{F}_{-1} + \frac{1}{2}\delta_{\mathrm{mag}}\tilde{\rho}_{\mathrm{s}}\vec{F}_0 \quad . \tag{3.48}$$

We can use the definitions of the vectors $\vec{\rho}_{\mathrm{s}}$ and $\vec{\rho}_{\mathrm{com}}$ in Eq. 3.6 to express each ion's magnetron position as a function of time

$$\begin{aligned} \vec{\rho}_{\mathrm{m1}} &= +\frac{1}{2}\tilde{\rho}_{\mathrm{s}}\left(1-\delta_{\mathrm{mag}}\right)\vec{F}_0 + \tilde{\rho}_{\mathrm{com}}\left[\left(1+\frac{5}{2}\delta_{\mathrm{mag}}\right)\vec{F}_{-1} - \frac{3}{2}\delta_{\mathrm{mag}}\vec{F}_{+1}\right] \\ \vec{\rho}_{\mathrm{m0}} &= -\frac{1}{2}\tilde{\rho}_{\mathrm{s}}\left(1+\delta_{\mathrm{mag}}\right)\vec{F}_0 + \tilde{\rho}_{\mathrm{com}}\left[\left(1-\frac{5}{2}\delta_{\mathrm{mag}}\right)\vec{F}_{-1} + \frac{3}{2}\delta_{\mathrm{mag}}\vec{F}_{+1}\right] \quad . \end{aligned} \tag{3.49}$$

The amplitudes $\tilde{\rho}_{\mathrm{s}}$ and $\tilde{\rho}_{\mathrm{com}}$ are here taken to be real constants determined from initial conditions. The phase of the common mode motion relative to the separation mode motion is fixed by the phase ϕ appearing in the definition of $\vec{F}_{-1}$ given by Eq. 3.41. The phase of the separation mode motion is here fixed to zero at $t = 0$, but this is trivial to generalize.

The perturbative results of above should be accurate as long as $\delta_{\mathrm{mag}}\tilde{\rho}_{\mathrm{com}}/\tilde{\rho}_{\mathrm{s}} \ll 1$. In most situations of interest $\tilde{\rho}_{\mathrm{com}}/\tilde{\rho}_{\mathrm{s}} \leq 1$ so that this condition is easily satisfied as long as $\delta_{\mathrm{mag}} \ll 1$. The solid lines of Fig. 3-3 show the results of numerically integrating the equations of motion for the example pair $^{13}\mathrm{C}_2\mathrm{H}_2^+$ vs N_2^+ with the various parameters specified in Sect. 3.1. Also included are the previously predicted circular orbits shown as a small dashed line. The perturbative elliptical orbits we predict are shown as a slightly larger dashed line that is consistently obscured by the solid line of the numerical simulation. In Fig. 3-3, we are observing the magnetron motion in a clockwise rotating frame (centered at the trap center) with frequency ω_{ms} such that there is no average rotation of the ion-ion separation vector $\vec{\rho}_{\mathrm{s}}$. In this rotating frame the lower frequency common mode motion is counterclockwise. The initial position of each ion is indicated by an open circle. In the two lower graphs, the velocity of each ion is computed with each calculation approach shown here as well. The initial velocity of each ion is shown with an open circle. The excellent agreement between our perturbative result and the numerical result in velocity-space (or momentum-space) is as important as the agreement of the position-space results, since we must weight each magnetron position by the inverse speed in order to accurately calculate

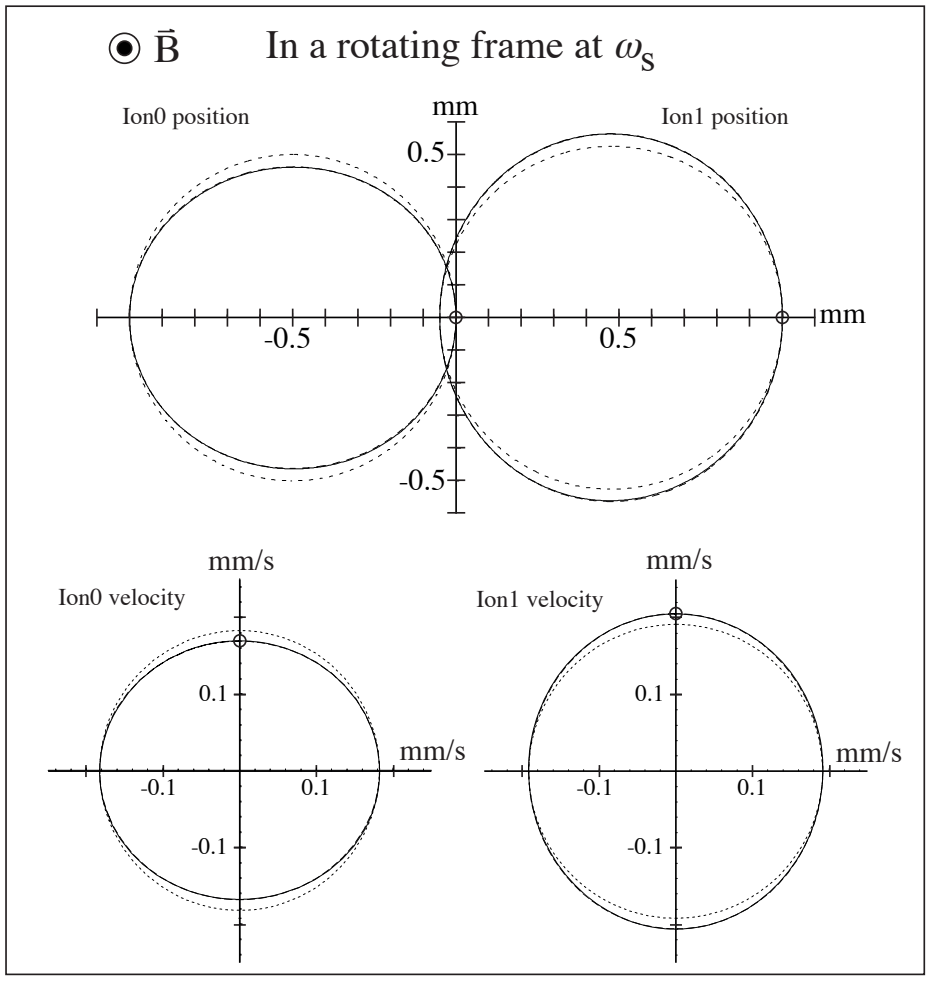

Figure 3-3: Magnetron motion in a frame rotating at the separation frequency $\omega_{\rm ms}$ such that there is no average rotation of the separation vector $\vec{\rho}_{\rm s}$. Both ions move on counter-clockwise orbits in this frame. At $t = 0$ the position of the ions are indicated by small open circles. The solid line is the result of numerically integrating the equations of motion with only an adiabatic assumption to remove motion near the cyclotron frequency. The elliptical orbits predicted after properly linearizing the Coulomb interaction are shown with a longer dashed line that is almost completely obscured by the solid line. For comparison, the circular orbits originally predicted in $[2]^G$ are shown with short dashed lines. The two lower graphs show a comparison of the predicted ion velocities. The perturbation theory result is once again obscured by the numerical simulation results. The agreement between the numerical simulation and the perturbation theory lends confidence that we have properly dealt with the Coulomb interaction even for large common mode amplitudes.

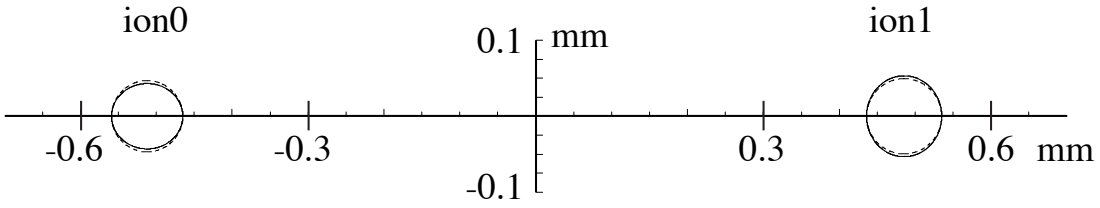

Figure 3-4: Magnetron motion for example pair $^{13}C_2H_2^+$ vs N_2^+ in nearly parked orbits $\rho_{com}/\rho_s = 0.05$ as viewed in a frame rotating at ω_{ms}. For most cyclotron frequency comparisons, the magnetron orbits are close to what is shown here. Refer to the caption of Fig. 3-3 for an explanation of the different curves.

the various time-averaged moments of the magnetron amplitudes.

The excellent agreement between our perturbative result and our numerical simulation indicates that we can accurately predict the coupled magnetron motion in a perfect Penning trap over the entire range of experimental interest. We typically perform our cyclotron frequency comparisons in a nearly ideal parked orbit with $\rho_{com}/\rho_s \leq 0.05$ where the perturbative results should be extremely accurate. An example of the typical nearly-parked orbit configuration is shown in Fig. 3-4.

The numerical results are used as a benchmark since they should be quite accurate. In implementing the numerical simulation, the only approximation is one of adiabaticity to separate motion near the magnetron frequency from motion near the cyclotron frequency. This adiabatic approximation assumes $\Omega_m/\bar{\omega}_m \ll 1$. Since $\Omega_m/\bar{\omega}_m \leq 10^{-4}$, the numerical integration can be considered extremely accurate. The integration is also extremely stable. It typically requires 30 s to integrate the motion for 3600 s or roughly 200 cycles of the beating between the normal magnetron modes. In terms of both the physical stability and numerical accuracy of the integration, after 3600 s we find fractional changes of $\leq 10^{-3}$ and $\leq 10^{-5}$ in the common and separation mode amplitudes respectively. Similarly, the sum of the squares of the magnetron radii $\rho_{m1}^2 + \rho_{m0}^2$ changes from start to finish by only 1 part in 10^{10}.

3.3.3 Systematic Errors Due to Magnetron Radius Imbalance

In the previous sections, we showed that the fractional imbalance of the magnetron radii scales as $\delta_{mag} \sim \rho_s^3$. When combined with the frequency shifts due to trap field imperfections that scale as ρ_m^2 and ρ_m^4, this will lead to systematic errors on the measured trap cyclotron frequency difference that grow rapidly with ion-ion separation as ρ_s^5 and ρ_s^7. This strong dependence on ρ_s sharply limits how large we can make the ion-ion separation and still perform accurate mass comparisons. We calculate here the second and fourth time averaged moments of the magnetron radii from the magnetron orbits of Eq. 3.49. The contribution of the common mode amplitude ρ_{com} to these important moments had not been properly

calculated previously.

The perturbations of the cyclotron frequency arising from B_2, B_4, C_4, and C_6 all scale as even moments of the magnetron radii. The phase of the magnetron beat motion at frequency Ω_m is random with respect to when we perform our cyclotron frequency comparison. The systematic perturbation of the cyclotron frequency ratio is then proportional to the time averaged difference of the even moments of the magnetron radii, which can be calculated from Eq. 3.49:

$$\langle \vec{\rho}_{m1} \cdot \vec{\rho}_{m1} \rangle - \langle \vec{\rho}_{m0} \cdot \vec{\rho}_{m0} \rangle = \delta_{mag} \left(10\tilde{\rho}_{com}^2 - \tilde{\rho}_s^2 \right) \quad , \tag{3.50}$$

$$\left\langle (\vec{\rho}_{m1} \cdot \vec{\rho}_{m1})^2 \right\rangle - \left\langle (\vec{\rho}_{m0} \cdot \vec{\rho}_{m0})^2 \right\rangle = \frac{1}{2}\delta_{mag} \left(40\tilde{\rho}_{com}^4 + 6\tilde{\rho}_{com}^2\tilde{\rho}_s^2 - \tilde{\rho}_s^4 \right) \quad . \tag{3.51}$$

Explicitly writing $\delta_{mag} = \eta\bar{\omega}_m^2/(2\Omega_E^2)$ from Eq. 3.35 and using the frequency shift formulas of Eqs. 2.50, 2.53, 2.56, and 2.59, we find that the trap cyclotron frequency difference $\omega_{ct2} = \omega_{ct1} - \omega_{ct0}$ is systematically shifted by

$$\begin{aligned} \frac{\Delta\omega_{ct2}}{\bar{\omega}_{ct}} &= \frac{\eta\bar{m}\bar{\omega}_m^2}{2q^2} \left(\frac{3C_4\bar{\omega}_m}{d^2\bar{\omega}_c} - \frac{B_2}{2B_0} \right) \rho_s^3 \left(10\tilde{\rho}_{com}^2 - \tilde{\rho}_s^2 \right) \\ &\quad + \left(\frac{-45C_6\bar{\omega}_m}{16d^4\bar{\omega}_c} + \frac{3B_4}{16B_0} \right) \rho_s^3 \left(40\tilde{\rho}_{com}^4 + 6\rho_{com}^2\rho_s^2 - \tilde{\rho}_s^4 \right) \quad . \end{aligned} \tag{3.52}$$

Since we usually operate in the limit $\rho_{com}/\rho_s \ll 1$, we can usually ignore the contribution due to ρ_{com} so that the systematic errors due to C_4 and B_2 scale as ρ_s^5, and the errors due to C_6 and B_4 scale as ρ_s^7. With the measured trap field imperfections in our trap, we cannot perform accurate cyclotron frequency comparisons much beyond $\rho_s = 800$ μm. To extend the range of possible measurement separations, we tune C_4 to cancel the shift of the trap cyclotron frequency difference due to the other imperfections B_2, C_6, and B_4. This so called "fctOpt" tuning of C_4 is described in more detail in Sect. 5.6. Also, note the large scaling with magnetron frequency $\bar{\omega}_m$ and mass $\bar{m}$. By using ions with smaller mass to charge m/q, it should be possible to dramatically reduce systematic errors compared to our present work at $m/q \sim$30 u/e.[‡]

[‡]On a side note, there is a magic ratio $\tilde{\rho}_s/\tilde{\rho}_{com} = \sqrt{10} \approx 3.2$ for which the differences in both the time averaged second and fourth moments of the magnetron radii are zero. The averaged difference in fourth moments has contributions of order δ_{mag}^3 that were dropped from the above expression and so is not exactly zero but is quite close.

It was suggested in the thesis of Frank DiFilippo [43][G] that such a magic cancellation could be exploited to reduce the effect of trap field imperfections. As will be shown later, the presence of a large C_6, which we cannot tune to zero, leads to frequency modulation of the axial modes if the magnetron radii are varying in time. This frequency modulation makes it difficult to extract an accurate axial phase measurement, which is crucial for measuring the cyclotron phase accumulated versus time with our PNP technique. As a result, I do not believe that this is a very practical idea. In addition, I think it is wise to stay as close to the center of the trap as possible for a given ion-ion separation (i.e. make $\tilde{\rho}_{com}$=0) in order to let the multipole expansion

3.3.4 Coupled Magnetron Motion in an Imperfect Trap

Thus far, we have calculated the coupled magnetron motion of two ions in a perfect Penning trap. In a real Penning trap, the electric field is not a pure quadrupole field so that the instantaneous magnetron frequency is a function of the ion's radial position. We cannot presently modify the rather large (at least for our purposes) C_6 in our Penning trap. In addition, we will often introduce a sizeable C_4 for a host of useful purposes including reducing systematic errors on our cyclotron frequency ratio, measuring the swapping motion, cooling the swapping motion, measuring the rms magnetron radius of each ion, and measuring the difference of rms magnetron radii. Since a slightly anharmonic trapping environment is so ubiquitous and useful, we now turn to an examination of its effect on the coupled magnetron motion.

We begin by considering the parked configuration in which the common-like mode has zero amplitude. This is the same limit in which we perform cyclotron frequency comparisons and so is of the most interest. In a perfect trap, the ions are orbiting the trap center with almost identical radii $\rho_{m0}= \rho_s(1+\delta_{mag})/2$ and $\rho_{m0}= \rho_s(1-\delta_{mag})/2$ but on opposite sides of the trap from one another. The small imbalance parameter δ_{mag} is fixed by two frequency scales: the difference in the uncoupled magnetron frequencies $\delta_{m2} = \omega_{m1} - \omega_{m0}$ and the radial Rabi frequency Ω_m. Restating the perfect Penning trap expression for δ_{mag} from Eq. 3.35, we will now use a superscript zero to indicate that it is the zeroth order result:

$$\delta_{mag}^{(0)} = \frac{-\delta_{m2}}{2\Omega_m} \quad . \tag{3.53}$$

In the presence of a C_4 and a C_6 electrostatic imperfection and assuming all other mode amplitudes are zero, we find that the *differential* shift of the magnetron frequencies using Eqs. 2.51 and 2.54 can be written as

$$\Delta\omega_{m2} = \Delta\left(\omega_{m1} - \omega_{m0}\right) = \delta_{mag}^{(1)}\bar{\omega}_m\left(\frac{3C_4}{2}\frac{\rho_s^2}{d^2} - \frac{15C_6}{16}\frac{\rho_s^4}{d^4}\right) \tag{3.54}$$

where $\delta_{mag}^{(1)}$ is the imbalance parameter after including the effect of electrostatic anharmonicities. But the size of the imbalance parameter is just set by the difference in instantaneous magnetron frequencies, so we can write

$$\delta_{mag}^{(1)} = -\frac{\delta_{m2} + \Delta\omega_{m2}}{2\Omega_m} = \delta_{mag}^{(0)} - \delta_{mag}^{(1)}\frac{\bar{\omega}_m}{2\Omega_m}\left(\frac{3C_4}{2}\frac{\rho_s^2}{d^2} - \frac{15C_6}{16}\frac{\rho_s^4}{d^4}\right) \quad . \tag{3.55}$$

Using this selfconsistency relationship, we can solve for the modified imbalance parameter

$$\delta_{mag}^{(1)} = \frac{\delta_{mag}^{(0)}}{1 + \frac{\bar{\omega}_m}{2\Omega_m}\left(\frac{3C_4}{2}\frac{\rho_s^2}{d^2} - \frac{15C_6}{16}\frac{\rho_s^4}{d^4}\right)} \quad . \tag{3.56}$$

of the fields work in your favor.

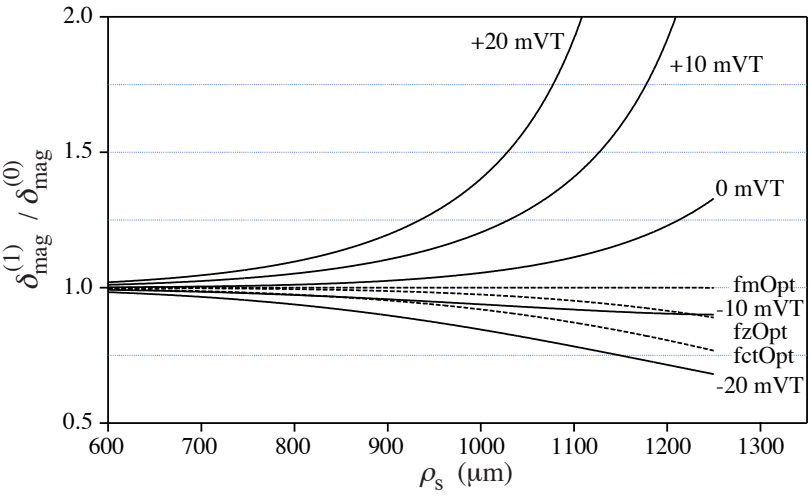

Figure 3-5: Magnetron radius imbalance $\delta^{(1)}_{\rm mag}$ including effect of C_4 and C_6 versus ion-ion separation $\rho_{\rm s}$ (and with $\rho_{\rm com}$=0). The values are expressed as a fraction of the perfect Penning trap value $\delta^{(0)}_{\rm mag}$. The C_6 coefficient is the same for all curves. The results for various values of C_4 are plotted. The solid lines are for constant Guard Ring voltages with the values $-20,\ -10,\ 0,\ +10,\ +20$ mVT corresponding to values of $C_4 = 105,\ 53,\ 0,\ -53,\ -105\ \times 10^{-6}$ respectively. The dashed lines refer to optimized Guard Ring voltages that set the derivative of each mode's frequency versus magnetron radius to zero. The curve labeled fctOpt is the trajectory used when comparing cyclotron frequencies.

The same expression can be obtained from the equations of motion, but this approach captures the physics.

Figure 3-5 shows $\delta^{(1)}_{\rm mag}/\delta^{(0)}_{\rm mag}$ versus ion-ion separation $\rho_{\rm s}$ for several Guard Ring voltage settings. The plot was generated for the example pair $^{13}C_2H_2^+$ vs N_2^+. The solid curves correspond to constant values of C_4. The dashed curves correspond to the optimized Guard Ring trajectories that make the various mode frequencies independent of small changes in $\rho_{\rm m}$ (or equivalently $\rho_{\rm s}$). The accurate comparison of trap cyclotron frequencies is taken along the fctOpt trajectory, for which the size of the magnetron radius imbalance is actually smaller than that for a perfect Penning trap. For $\rho_{\rm s} \leq 950$ μm, the deviation of the imbalance from that of a perfect Penning trap is less than 15% for all Guard Ring tunings except the extreme value of +20 mVT ("T" means that the voltage is expressed with respect to the $V^{\circ}_{\rm gr}$ voltage of Sect. 2.2.1).

3.4 Ion-Ion Axial Perturbations

We will now examine the effect of ion-ion interaction on the axial modes. We will first show that the axial equilibrium positions of the two ions are in the same horizontal plane. This is important since even a slight difference in the average axial position would lead to a differential cyclotron frequency shift in the presence of a linear magnetic field gradient such

as B_1.

The axial modes remain independent of each other as long as the axial frequency difference is much greater than the axial Rabi frequency Ω_z. At mass 30 u, this is the case for mass doublets with a fractional mass difference $2\eta > 10^{-5}$. It is very important that the axial modes remain independent so that we can perform cyclotron phase measurements. In this decoupled regime, the main result of the interaction is a common downward shift of both axial frequencies. There is also a nonsymmetric frequency repulsion of the two modes due to dynamical interaction. This second effect is much smaller than the first since it is of second order in the Coulomb interaction.

Understanding the axial frequency shifts will be important since we must use the measured axial frequencies in the invariance theorem relating the measured trap mode frequencies to the free space cyclotron frequency. We will find that the first order axial frequency shift is exactly cancelled in the invariance relationship by a corresponding shift of the trap cyclotron frequency. The second order frequency shift is small, and will not be of concern.

3.4.1 Axial Equilibrium Position

As the ions move on their collective magnetron orbits, the Coulomb interaction perturbs the axial modes. Of first concern is whether it is energetically favorable for the ions to remain in the same horizontal plane. A simplified model in which ρ_s is held fixed shows that energy is minimized when $z_1 - z_0 = 0$ or when

$$z_1 - z_0 = \pm\rho_s\sqrt{\left(\frac{2\Omega_z}{\omega_z}\right)^{2/3} - 1} \ . \tag{3.57}$$

In all of our work, the axial Rabi frequency is much less than the axial frequency $\omega_z \gg \Omega_z$, so this solution is imaginary and therefore an unphysical solution. Thus, the equilibrium position corresponds to both ions in the same horizontal plane. For the demonstration pair $^{13}C_2H_2^+$ versus N_2^+, the critical value of ion-ion separation is ρ_s= 20 μm. Below this radial separation, the axial equilibrium positions are not in the same horizontal plane.

3.4.2 Axial Frequency Perturbation

With the axial equilibrium position of each ion lying in the same horizontal plane, it is easy to see that if one ion's axial position is displaced a small amount, then the other ion exerts a force on it that opposes the restoring force of the axial electrostatic trap field. This leads to a common reduction of each ion's axial frequency. There is also a second order frequency pulling (or pushing) of the axial frequencies, which is dynamical in nature. As the lower axial frequency ion moves, its modulated Coulomb force drives the higher frequency ion's motion below resonance. The induced motion then acts back resonantly on the lower frequency ion, creating a frequency shift. The higher frequency ion similarly drives the

lower frequency ion but above resonance so that the reaction force picks up a minus sign relative to first case. The exact form of these shifts can be written as

$$\Delta\omega_{z1} = -\frac{\Omega_z}{2} + \frac{\Omega_z^2}{4\delta_{z2}} \tag{3.58}$$

$$\Delta\omega_{z0} = -\frac{\Omega_z}{2} - \frac{\Omega_z^2}{4\delta_{z2}} \tag{3.59}$$

where $\delta_{z2} \equiv \omega_{z1} - \omega_{z0}$ is the frequency difference between the noninteracting axial modes, and the axial Rabi frequency Ω_z is defined by Eq. 3.9. For this perturbative result, we have assumed the typical case of $\delta_{z2} \gg \Omega_z$. The first term represents the common electrostatic repulsion from the equilibrium position. The second term in each equation represent the dynamical frequency repulsion between the modes. The terms looks like the usual Stark shift of two coupled states in quantum mechanics and so is easy to remember when written in this form.

3.5 Ion-Ion Cyclotron Perturbations

Understanding the ion-ion perturbation of the trap cyclotron frequencies, and in particular the trap cyclotron frequency difference, is of utmost importance. The size and our understanding of these errors will ultimately limit the accuracy of our mass ratio comparisons.

The trap cyclotron modes remain independent modes due to the large frequency splitting between the modes ∼kHz compared to the cyclotron Rabi frequency $\Omega_c/2\pi$ ∼50 mHz. The first order effect of the ion-ion interaction will be a common upward shift of the two trap cyclotron frequencies. This is a large $\sim 10^{-9}$ fractional shift, but it is completely symmetric. However, in order to extract the cyclotron frequency ratio from the cyclotron frequency difference, one must know the individual free space cyclotron frequencies with accuracy $\sim 10^{-9}$. We will show that this large shift is exactly cancelled in the invariance relationship by a corresponding shift of the measured axial frequency.

The second order shift is a frequency repulsion between the trap cyclotron modes. It arises from a dynamical interaction between the modes. The effect on the measured mass ratio is typically below 10^{-12} except for extremely good doublets $2\eta < 10^{-4}$ or very small ion-ion separations $\rho_s < 600$ μm.

The finite size of the cyclotron orbits will be shown to give rise to a nonsymmetric frequency shift if $\rho_{c1} \neq \rho_{c0}$. This is predicted to be our leading source of error arising from ion-ion interactions since all of the other shifts are below 10^{-12}. For typical cyclotron amplitudes of 75 μm and a fractional amplitude imbalance of 1%, the shift of the trap cyclotron frequency difference $\Delta\omega_{ct2}/\bar{\omega}_{ct}$ is of order 10^{-12} at an ion-ion separation of 1 mm. We will carry the expansion of the nonlinear perturbation well beyond second order in the cyclotron amplitudes, and show that truncation of the perturbation expansion at lowest

order is accurate to approximately 10%.

Lastly, the magnetic dipole interaction between the two ions is shown to be completely negligible for mass comparisons with fractional accuracies of 10^{-12}.

3.5.1 Monopole Shift

At lowest order, the effect of the ion-ion interaction on the cyclotron motions consists of a common upward frequency shift and a frequency pulling. Imagine that the two guiding centers of the cyclotron motions are stationary and separated by ρ_s. To lowest order, one ion sees the monopole electric field of the other ion. The divergence of the monopole field creates a downward frequency shift. To see this, we remind the reader that cyclotron frequency shifts arise from a net radial force averaged around one cyclotron orbit

$$\vec{F}_{\rm net} = \frac{\hat{\rho}_c}{2\pi}\int_0^{2\pi} \vec{F}\cdot\hat{\rho}_c d\phi \ . \tag{3.60}$$

To calculate this, we can imagine creating a cylindrical pillbox centered on the ion's guiding center with vertical height Δz and radius ρ_c. Gauss's law ensures that the total flux of electric field (generated by the other ion) out of the pillbox is zero. Explicitly writing the electric field flux out of the top and bottom of the box we find

$$\rho_c \Delta z \int_0^{\infty} \vec{E}\cdot\hat{\rho}_c d\phi + \pi\rho_c^2 \frac{q\Delta z}{\rho_s^3} = 0 \ . \tag{3.61}$$

After multiplying through by the charge q, one can solve for the net radial force with respect to the center of the cyclotron motion

$$\vec{F}_{\rm net} = -\vec{\rho}_c \frac{q^2}{\rho_s^3} \ . \tag{3.62}$$

This force could have been more quickly and directly calculated, but I wish to emphasize that this force is related to the force along the axial direction in much the same way as the trap quadrupole electric field. The reason for this emphasis will be made clear shortly. Including this net force, the equation of motion for the cyclotron motion of ion 0, for example, can be written in terms of a new effective axial frequency

$$\ddot{\vec{\rho}}_{c0} = \omega_{c0}\dot{\vec{\rho}}_{c0}\times\hat{z} + \frac{1}{2}\omega_{z0}'^2\vec{\rho}_{c0} \tag{3.63}$$

with the effective axial frequency given by

$$\omega_{z0}' \approx \omega_{z0} - \frac{q^2/(m_0\rho_s^3)}{2\omega_{z0}} = \omega_{z0} - \frac{\Omega_z}{2} \ . \tag{3.64}$$

In the second expression, I have replaced ion 0's mass by the average mass $m_0 \approx \bar{m}$, which introduces a small error of order η. The same result is true for ion 1 after changing ion labels $0 \rightarrow 1$.

The new effective axial frequency ω'_{z0} is just that of the perturbed axial modes from 3.58. If both the perturbed trap cyclotron frequency and the perturbed axial frequency are used to calculate the free space cyclotron frequency via the usual quadrature relationship, then this first order shift is completely cancelled. This cancellation is intimately related to the derivation of the averaged radial force given above.

The perturbation of the trap cyclotron frequency to lowest order in $\Omega_z^2/\bar{\omega}_c$ (and retaining the first mass dependent correction) is given by

$$\Delta\omega_{ct0} = \frac{\Omega_c}{2}\left(1 + \frac{\omega_{z0}^2}{\omega_{c0}^2}\right) \quad . \tag{3.65}$$

This can be derived using Eq. 2.8 and the new effective axial frequency. The same result is true for ion 1 after changing ion labels $0 \rightarrow 1$. The perturbation of the trap cyclotron frequency difference is then

$$\Delta\omega_{ct2} = \Delta\omega_{ct1} - \Delta\omega_{ct0} = -2\eta\frac{\bar{\omega}_z^2}{\bar{\omega}_c^2}\frac{\Omega_c}{2} \quad . \tag{3.66}$$

For the example pair $^{13}C_2H_2^+$ versus N_2^+, this perturbation of the trap cyclotron frequency difference as a fraction of the average free space cyclotron frequency is $\Delta\omega_{ct2}/\bar{\omega}_c = -3.4 \times 10^{-15}$ at $\rho_s = 1$ mm. The ρ_s^{-3} scaling of Ω_c means that $|\Delta\omega_{ct2}/\bar{\omega}_c| \leq 10^{-12}$ for $\rho_s \geq 150$ μm. For our measurements with $\rho_s \geq 500$ μm, the first order shift is extremely symmetric for both trap cyclotron frequencies and has no impact on the measured trap cyclotron frequency difference above 1×10^{-13}.

3.5.2 Frequency Pulling (Pushing)

Each ion's cyclotron motion generates a force that nonresonantly drives the other ion's cyclotron motion. In turn, the induced motion acts back on the original cyclotron motion, giving rise to a resonant force that causes a frequency shift. The force on ion 1 due to the cyclotron motion of ion 0 can be modeled as

$$\vec{F}_1 = \frac{\vec{\rho}_{c1} - \vec{\rho}_{c0} + \rho_s\hat{x}}{|\vec{\rho}_{c1} - \vec{\rho}_{c0} + \rho_s\hat{x}|^3} - \frac{\rho_s\hat{x}}{\rho_s^3} \tag{3.67}$$

where we have removed the dc force on the ion with the second term. This is essentially assuming that the magnetron motion is moving so slowly that we can just consider the vector between the guiding centers of the cyclotron motion $\vec{\rho}_s$ as stationary relative to the fast cyclotron motion. There are two sources of time dependence associated with this force: modulation of the direction of the force (from the numerator) and modulation of the magnitude of the force (from the denominator). If we make the experimentally reasonable assumption that $\rho_{c0},\ \rho_{c1} \ll \rho_s$, then we can expand the denominator to find

$$\vec{F}_1 \approx -2\bar{m}\Omega_E^2\left(x_{c1} - x_{c0}\right)\hat{x} + \bar{m}\Omega_E^2\left(y_{c1} - y_{c0}\right)\hat{y} \quad . \tag{3.68}$$

Assuming circular orbits, the force can be averaged around one orbit of each cyclotron motion to give

$$\vec{F}_1^{avg} \approx -\frac{1}{2}\bar{m}\Omega_{\rm E}^2\,(\,\vec{\rho}_{\rm c1} - \,\vec{\rho}_{\rm c0})\quad . \tag{3.69}$$

There is an equal and opposite averaged force on ion 0 due to ion 1's cyclotron motion $\vec{F}_0^{avg} = -\vec{F}_1^{avg}$. As usual, we will attack the coupled cyclotron motion perturbatively since it is the most intuitive route.

In the equation of motion for ion 1, the portion of the averaged force $-\frac{1}{2}\bar{m}\Omega_{\rm E}^2\,\vec{\rho}_{\rm c1}$ gives rise to a trivial first order frequency shift that is just the monopole shift of the previous Sect. 3.5.1. If we keep terms of higher order in $\rho_{\rm cx}/\rho_{\rm s}$ in the expansion of the force, we find frequency shifts that depend on the amplitude of ion motion. These nonlinear shifts will be discussed from a different perspective in the following Sect. 3.5.3.

In the equation of motion for ion 1 (ion 0), the term in the averaged force proportional to $\vec{\rho}_{\rm c0}$ ($\vec{\rho}_{\rm c1}$) gives rise to a coupling between the two cyclotron motions. If the cyclotron frequencies were identical, then the small coupling would mix the independent cyclotron modes into collective common and difference modes with a frequency splitting between the modes given by the cyclotron Rabi frequency of Eq. 3.10, $\Omega_{\rm c} = \Omega_{\rm E}^2/\bar{\omega}_{\rm c} = 2\pi\,29$ mHz at $\rho_{\rm s} = 1$ mm. If, on the other hand, the frequency difference between the uncoupled modes is much larger than the cyclotron Rabi frequency $\delta_{\rm ct2} \gg \Omega_{\rm c}$, then the modes remain independent and the chief effect is a frequency shift of second order in $\Omega_{\rm c}$.

To perturbatively calculate this frequency pulling, imagine that the zeroth order cyclotron motion of ion 0 at a frequency (to be determined) ω_0 drives ion 1's cyclotron motion nonresonantly. It is assumed that the frequency of motion is very close to the unperturbed trap cyclotron frequency of ion 0 so that $|\omega_0 - \omega_{\rm ct0}| \ll \delta_{\rm ct2}$. Explicitly, we assume ion 0's cyclotron motion is of the form $\vec{\rho}_{\rm c0}^{(0)} = \Re\{\rho_{\rm c0}^{(0)}(\hat{x} + \imath\hat{y})e^{\imath\omega_0 t}\}$, and the response of ion 1's cyclotron motion is of the form $\vec{\rho}_{\rm c0}^{(1)} = \Re\{\rho_{\rm c1}^{(1)}(\hat{x} + \imath\hat{y})e^{\imath\omega_0 t}\}$. It is straightforward to show from the equation of motion for ion 1 that the driven response is

$$\vec{\rho}_{\rm c1}^{(1)} = \frac{\Omega_{\rm E}^2}{4\eta\bar{\omega}_{\rm c}^2}\,\vec{\rho}_{\rm c0}^{(0)} = \frac{\Omega_{\rm c}}{2\delta_{\rm ct2}}\,\vec{\rho}_{\rm c0}^{(0)} \tag{3.70}$$

where the result has been simplified by ignoring corrections of higher order in η and $\bar{\omega}_{\rm m}/\bar{\omega}_{\rm c}$. We can then insert the driven motion of ion 1 into the equation of motion for ion 0 to give

$$(1+\eta)\,\ddot{\vec{\rho}}_{\rm c0}^{(0)} = \bar{\omega}_{\rm c}\dot{\vec{\rho}}_{\rm c0}^{(0)} \times \hat{z} + \frac{1}{2}\bar{\omega}_{\rm z}^2\,\vec{\rho}_{\rm c0}^{(0)} + \frac{\Omega_{\rm E}^2}{2}\,\vec{\rho}_{\rm c0}^{(0)} + \frac{\Omega_{\rm E}^4}{8\bar{\omega}_{\rm c}^2}\,\vec{\rho}_{\rm c0}^{(0)}\quad . \tag{3.71}$$

This equation is easily solved for the shift of ion 0's trap cyclotron frequency with respect to its noninteracting value. The same procedure can be carried out for ion 1, but the symmetry of the equations of motion means that the result can be arrived at by letting $\eta \to -\eta$. We find

$$\Delta\omega_{\rm ct0} = \frac{\Omega_{\rm E}^2}{2\bar{\omega}_{\rm c}} - \frac{\Omega_{\rm E}^4}{8\eta\bar{\omega}_{\rm c}^3} = \frac{\Omega_{\rm c}}{2} - \frac{\Omega_{\rm c}^2}{4\delta_{\rm ct2}} \tag{3.72}$$

$$\Delta\omega_{\rm ct1} = \frac{\Omega_{\rm E}^2}{2\bar{\omega}_{\rm c}} + \frac{\Omega_{\rm E}^4}{8\eta\bar{\omega}_{\rm c}^3} = \frac{\Omega_{\rm c}}{2} + \frac{\Omega_{\rm c}^2}{4\delta_{\rm ct2}} \tag{3.73}$$

The first term is the monopole shift, and the second terms with opposite signs are the dynamical shifts or the frequency pushings. The symmetric monopole shift has a net scaling of $\rho_{\rm s}^{-3}$, and the asymmetric dynamical shift scales as $\rho_{\rm s}^{-6}$. Only the asymmetric part contributes to the shift of the measured trap cyclotron difference frequency

$$\frac{\Delta\omega_{\rm ct2}}{\bar{\omega}_{\rm c}} = \frac{\Delta\left(\omega_{\rm ct1} - \omega_{\rm ct0}\right)}{\bar{\omega}_{\rm c}} = \frac{\Omega_{\rm E}^4}{4\eta\bar{\omega}_{\rm c}^4} = \frac{\Omega_{\rm c}^2}{2\delta_{\rm ct2}\bar{\omega}_{\rm c}} \quad . \tag{3.74}$$

For the example pair $^{13}C_2H_2^+$ vs N_2^+(with $2\eta = 5.8\times10^{-4}$, $\bar{\omega}_{\rm c}/2\pi = 4.67\times10^6$ Hz), the differential shift is 2.9×10^{-14} at $\rho_{\rm s} = 1$ mm. Because the dynamical shift scales as $\rho_{\rm s}^{-6}$, the systematic error reaches 1×10^{-12} at $\rho_{\rm s} = 550$ μm. The frequency pulling shift is not then a concern for our example pair $^{13}C_2H_2^+$ vs N_2^+. But the shift has a net scaling with mass and mass splitting of $\bar{m}^2/\eta$, so that this effect could become significant for a better doublet (η smaller) or a heavier ion ($\bar{m}$ larger).

3.5.3 Nonlinear Coupling: Beyond the Monopole Shift

We find that the finite size of the cyclotron orbits gives rise to a nonsymmetric frequency shift if $\rho_{\rm c1} \neq \rho_{\rm c0}$. This is predicted to be our leading source of error arising from ion-ion interactions (the previously discussed shifts give errors below 1×10^{-12}).

In the limit $\rho_{\rm c}/\rho_{\rm s} \to 0$, the previous discussions accurately describe the cyclotron frequency perturbations. When we compare the trap cyclotron frequencies of two ions, we use typical orbits of radius $\rho_{\rm c} = 75$ μm that are small compared to the typical ion-ion separation $\rho_{\rm s} \geq 600$ μm, but not vanishingly so. In the calculation of this shift, we find a relative minus sign compared to the original discussion in the proposal [2][G]. We feel confident that this reflects a mistake in the previous work. In addition, the new result is found to agree with experiment, whereas the previous expression is ruled out by a 10σ disagreement with experiment.[§]

In Sect. 3.5.1, it was assumed that the time averaged charge distribution of each ion was well described by a monopole field. It was also assumed that each ion sampled the monopole field in the limit of vanishing amplitude. The nonlinear shift of the cyclotron frequency difference will result from removing both of these assumptions. I want to emphasize that this nonlinear shift arises from two distinct physical sources: the higher-order moments of the time averaged charge distribution and the expansion to higher order in the cyclotron

[§]The prediction of the sign flip was made before the experiment was performed, so there is not a chance of experimental pulling of the theory.

radius of the resulting forces about the other ion's cyclotron guiding center.

The electrostatic potential of a uniformly charged ring of radius ρ_{c0} with total charge q centered at the origin and in the plane $z = 0$ is given by

$$\Phi_0 = q \sum_{l=0}^{\infty} \frac{\rho_{c0}^l}{r^{l+1}} P_l(0) P_l(\cos\theta) \tag{3.75}$$

where P_l is the usual Legendre polynomial [44]. This provides an expansion in powers of ρ_{c0}/ρ_s of the effect of the finite charge distribution of ion 0. Each term of this expansion can be written in Cartesian coordinates, and the center of coordinates translated to the guiding center of ion 1. The net radial force averaged around one cyclotron orbit of ion 1 produces a cyclotron frequency shift as described in Sect. 3.5.1. It was found that this averaging can be written in terms of elliptic functions; however, an expansion in powers of ρ_{c1} is of more practical value.

Performing this procedure including the monopole ($l = 0$) and quadrupole ($l = 2$) terms and performing the expansion of the averaged net force to order ρ_c^2, we find the previous result of $[2]^G$ but with the amplitudes interchanged

$$\Delta\omega_{ct0} = \frac{\Omega_c}{2}\left(1 + \frac{9}{8}\left(\frac{\rho_{c0}^2 + 2\rho_{c1}^2}{\rho_s^2}\right)\right) \tag{3.76}$$

$$\Delta\omega_{ct1} = \frac{\Omega_c}{2}\left(1 + \frac{9}{8}\left(\frac{\rho_{c1}^2 + 2\rho_{c0}^2}{\rho_s^2}\right)\right) \quad . \tag{3.77}$$

The effect on the trap cyclotron difference frequency is then

$$\frac{\Delta\omega_{ct2}}{\bar{\omega}_c} = \frac{\Delta\omega_{ct1} - \Delta\omega_{ct0}}{\bar{\omega}_c} = \frac{9\Omega_c}{16\bar{\omega}_c}\left(\frac{\rho_{c0}^2 - \rho_{c1}^2}{\rho_s^2}\right) \quad . \tag{3.78}$$

If we can make the average cyclotron amplitudes exactly equal, then the perturbation of the trap cyclotron frequency difference is zero. If the cyclotron radii are given by $\rho_{c0} = \bar{\rho}_c(1 - \delta_{cyc})$ and $\rho_{c1} = \bar{\rho}_c(1 + \delta_{cyc})$ and the fractional imbalance satisfies $2\delta_{cyc} \ll 1$, then the shift scales as

$$\frac{\Delta\omega_{ct2}}{\bar{\omega}_c} \approx -\delta_{cyc}\frac{9\Omega_c}{4\bar{\omega}_c}\frac{\bar{\rho}_c^2}{\rho_s^2} \quad . \tag{3.79}$$

For the example pair $^{13}C_2H_2^+$ vs N_2^+, the prefactor $(9\Omega_c/4\bar{\omega}_c) = 1.3 \times 10^{-8}$ at $\rho_s = 1$ mm. Further assuming a reasonable value of $\bar{\rho}_c = 75$ μm, the expansion parameter $\bar{\rho}_c^2/\rho_s^2 = 5.6 \times 10^{-3}$. Lastly, taking a reasonable fractional imbalance of the cyclotron orbits $2\delta_{cyc} = -0.01$, we find the differential shift is 3.6×10^{-13} at 1 mm. Because of the ρ_s^{-5} scaling, the shift reaches 1×10^{-12} at $\rho_s = 820$ μm and 1×10^{-11} at $\rho_s = 520$ μm. Clearly, it is imperative that the cyclotron radii be nearly identical. Additionally, the shift has a net scaling of $\bar{m}/B_0$ so that working with lighter ions or at a larger magnetic field would reduce this shift.

Note that in calculating the shift of the measured difference frequency Eqs. 3.78 and 3.79, I have assumed that the frequencies are being measured simultaneously. If one were to alternately measure the cyclotron frequencies, then each ion sees only the monopole charge distribution of the other ion while it is accumulating phase. For alternately measured cyclotron frequencies, the differential perturbation differs by only a sign flip. If one were to average the result of simultaneously and alternately measured cyclotron frequency ratios, then this systematic error could be eliminated even when the average cyclotron amplitudes are not equal.

The large size of the shift due to unbalanced cyclotron radii means that it is important to verify that the result is not significantly changed by truncating the perturbation expansion at the quadrupole order. Having produced the machinery to calculate these shifts, it is easy to extend this to higher multipole order. Including the next two nonzero orders n = 4 and n = 6 in the expansion corresponds to including the hexapole and octapole moments of the charge distribution and expanding the fields about the other ion's guiding center to order ρ_c^6. The result is

$$\frac{\Delta\omega_{ct2}}{\bar{\omega}_c} = \frac{\Delta\omega_{ct1} - \Delta\omega_{ct0}}{\bar{\omega}_c} = \frac{9\Omega_c}{16\bar{\omega}_c}\left(\frac{\rho_{c0}^2 - \rho_{c1}^2}{\rho_s^2} + \frac{25}{12}\frac{\rho_{c0}^4 - \rho_{c1}^4}{\rho_s^4} + \frac{1225}{384}\frac{(\rho_{c0}^2 - \rho_{c1}^2)(\rho_{c0}^4 + \rho_{c4}^2)}{\rho_s^4}\right) . \tag{3.80}$$

Figure 3-6 shows the difference between the nonlinear perturbation expansions carried out to orders n = 4 (hexapole) and n = 12 (dodecapole) compared to the order n = 2 (quadrupole) calculation of Eq. 3.78. This is plotted versus the ratio of the average cyclotron radius of the two ions to the distance between the guiding centers of the cyclotron orbits $\bar{\rho}_c/\rho_s$. Physically, $\bar{\rho}_c/\rho_s = 1/2$ corresponds to the two cyclotron orbits just touching one another. The calculation was performed in the limit $\delta_{cyc} \to 0$ where $\rho_{c0} = \bar{\rho}_c(1 - \delta_{cyc})$ and $\rho_{c1} = \bar{\rho}_c(1 + \delta_{cyc})$ so that only terms linear in δ_{cyc} contribute. For reference, the values of ρ_s are shown for a typical cyclotron radius $\bar{\rho}_c = 75$ μm.

In the region of currently accessible ρ_s between 1500 μm and 500 μm, the good agreement between the hexapole and dodecapole results means that we can treat the dodecapole result as "exact" to better than a percent. One sees that the result at the quadrupole level of Eq. 3.78 differs from the nearly "exact" dodecapole calculation by at most 10% in the region of interest. Additionally, carrying the expansion to the hexapole order makes the result accurate to a percent over the entire experimental range of interest.

Magnetic Dipole Shift

In addition to exerting a Coulomb force on one another, each ion modifies the magnetic field at the other ion's location. It is simple to place an upper limit on the size of this ultimately negligible shift. The magnetic field generated by one ion at the other ion's location can be

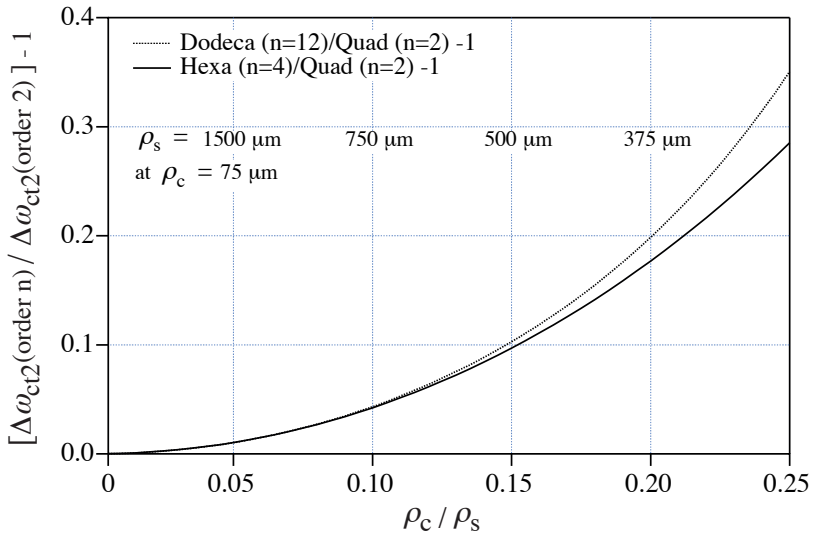

Figure 3-6: Perturbation of the trap cyclotron frequency difference $\Delta\omega_{ct2}$ at order n = 4 (hexapole) and n = 12 (dodecapole) as a fraction of the order n = 2 (quadrupole) result. This is plotted versus the ratio of the average cyclotron orbit radius to the guiding center separation $\bar{\rho}_c/\rho_s$. For connection to experiment, the values of ρ_s are shown for a typical cyclotron radius of $\bar{\rho}_c = 75$ μm. We typically perform measurements between ρ_s= 600 and 1300 μm. The calculation was performed in the limit $\delta_{cyc} \to 0$ where $\rho_{c0} = \bar{\rho}_c(1-\delta_{cyc})$ and $\rho_{c1} = \bar{\rho}_c(1+\delta_{cyc})$.

approximated to first order by a dipole field. The cyclotron motion can be viewed as a tiny current loop giving rise to a dipole moment $\vec{m}$ proportional to the area of the current loop $\pi\rho_c^2$ times the current $I = q\omega_c/2\pi$ divided by the speed of light c

$$\vec{m} = -\frac{q\omega_c\rho_c^2}{2c}\hat{z} \ . \tag{3.81}$$

The magnetic dipole moment of ion 0 $\vec{m}_0$ gives rise to a magnetic field along $\hat{z}$ at ion 1's position a distance ρ_s away

$$B_z = -\frac{\vec{m}_0}{\rho_s^3} \ . \tag{3.82}$$

This extra axial magnetic field gives rise to a fractional cyclotron frequency shift that is given by the ratio of this magnetic field to the uniform magnetic field $B_0\hat{z}$

$$\frac{\Delta\omega_{c1}}{\omega_{c1}} = \frac{1}{2}\frac{q^2/\rho_s}{mc^2}\left(\frac{\rho_{c0}}{\rho_s}\right)^2 = \frac{1}{2}\left(\frac{\Omega_E\rho_{c0}}{c}\right)^2 \tag{3.83}$$

where we have written the shift first as a ratio of energies and secondly as a "relativistic"-like shift involving the ion-ion coupling parameter Ω_E defined previously. The expression was also simplified by assuming $\omega_{c1} = \omega_{c0}$. This shift is proportional to the ratio of the ion-ion Coulomb energy and the rest mass of the ion, whereas the nonlinear Coulomb interaction

shift discussed previously is proportional to the ratio of the Coulomb energy to the kinetic energy of the cyclotron motions. Equivalently, if the kinetic energy and rest mass energy are thought of as terms in the expansion of the total energy, this effect is v_c^2/c^2 smaller than the Coulomb perturbation. With $\rho_s = 500$ μm, $\rho_{c1} = 250$ μm, and ion masses of 1 u, the fractional cyclotron frequency shift of ion 0 is only 4×10^{-16}. This perturbation is well below our level of measurement and hence can be ignored for quite some time to come.

3.6 Effect of Finite Axial Amplitudes

Thus far, the perturbations and mode mixings have been calculated in the limit of vanishing axial amplitudes. This is clearly not true experimentally, since we must excite the axial motion to finite amplitudes for detection purposes. It is important to obtain expressions for how a finite axial amplitude affects the interactions between modes. This is important, for instance, when trying to determine the ion-ion separation from the beat frequency between the common and separation modes by monitoring the frequency modulation of one of the axial modes. Another important instance is in measuring the axial frequencies from the simultaneous axial ringdowns at the end of a simultaneous PNP. This axial frequency is needed to obtain the free space cyclotron frequency of one of the ions; however, we actually want the axial frequency at zero axial amplitude. If left uncorrected, this mistake introduces an error on the measured cyclotron frequency ratio of 5×10^{-12} at small ion-ion separations. We use the results described in this section to apply small corrections to our measurements in both of the scenarios described.

In the following sections, we will calculate corrections to the beat frequency between the magnetron normal modes Ω_m and the first order axial frequency shift $-\Omega_z/2$. This is motivated by the experimental situations described above. We will not calculate the modification of the cyclotron frequency perturbation, which at lowest order is just $+\Omega_c/2$. This is because the axial amplitudes are cooled to their thermal amplitudes when the ions are accumulating phase during a PNP measurement. As a result, the modifications of these already small shifts of the individual cyclotron frequencies are of order $z^2/\rho_s^2 \leq 10^{-3}$. Even more importantly, the shift due to finite axial amplitudes is symmetric and has no effect on the crucial trap cyclotron frequency difference $\omega_{ct2} = \omega_{ct1} - \omega_{ct0}$.

3.6.1 Modified Magnetron Rabi Frequency

The magnetron Rabi frequency Ω_m, which governs the coupled magnetron motion, is modified by finite axial motion with amplitudes z_0 and z_1 by a factor Λ_ρ that goes to unity in the limit $z_0 = z_1 = 0$

$$\Omega_m = \Lambda_\rho \Omega_m^o \quad . \tag{3.84}$$

Figure 3-7 summarizes the results of these calculations. This modified magnetron Rabi

frequency is correct for determining the modifications of the beat frequency between the magnetron common and separation modes. To establish the functional form of Λ_ρ, we observe that $\Omega_{\rm m}$ is proportional to the radial force that one ion exerts on the other ion:

$$\vec{F}_{10} = \frac{q^2\,\vec{\rho}_{\rm s}}{\left(\vec{\rho}_{\rm s}^{\,2} + (z_1(t) - z_0(t))^2\right)^{3/2}} \tag{3.85}$$

where $\vec{F}_{10}$ here signifies the radial force on ion 1 due to ion 0 and the axial amplitudes are written as explicit functions of time. To zeroth order in the coupled magnetron motions, $\rho_{\rm s}$ is independent of time, and so we must simply perform a time average over the fast axial motion near the axial frequencies $\omega_{\rm z}$. To make explicit exactly which terms we wish to time average, we can rewrite the force as:

$$\vec{F}_{10} = \frac{q^2\,\vec{\rho}_{\rm s}}{\rho_{\rm s}^3}\left\langle \frac{1}{\left(1 + \frac{(z_1(t)-z_0(t))^2}{\rho_{\rm s}^2}\right)^{3/2}}\right\rangle = \frac{q^2\,\vec{\rho}_{\rm s}}{\rho_{\rm s}^3}\Lambda_\rho \ . \tag{3.86}$$

The time averaged quantity is just the Λ_ρ we seek.

Taylor Expansion

In principle, this time average can be performed by setting $z_1(t) = z_1\cos(\omega_{\rm z1}t + \phi_1)$ and $z_0(t) = z_0\cos(\omega_{\rm z0}t + \phi_0)$ and integrating, but in practice what one wants is the value averaged over the phases of both axial motions. Thus one can make the simpler substitutions $z_1(t) = z_1\cos(\phi_1)$ and $z_0(t) = z_0\cos(\phi_0)$ and average the phases over 0 to 2π. In many cases, we are interested in the regime z_1,$z_0 \ll \rho_{\rm s}$ so we can perform a Taylor expansion and then perform analytical time averages on each polynomial term to yield

$$\Lambda_\rho = 1 + \sum_{n=1}^{\infty}\beta_{2n}(z_0, z_1, \rho_{\rm s}) \ . \tag{3.87}$$

The values of β_{2n} evaluate to:

$$\beta_2 = -\frac{3}{4}\frac{(z_0^2 + z_1^2)}{\rho_{\rm s}^2} \tag{3.88}$$

$$\beta_4 = +\frac{45}{64}\frac{(z_0^4 + 4z_0^2z_1^2 + z_1^4)}{\rho_{\rm s}^4} \tag{3.89}$$

$$\beta_6 = -\frac{175}{256}\frac{(z_0^6 + 9z_0^4z_1^2 + 9z_0^2z_1^4 + z_1^6)}{\rho_{\rm s}^6} \tag{3.90}$$

$$\beta_8 = +\frac{11025}{16384}\frac{(z_0^8 + 16z_0^6z_1^2 + 32z_0^4z_1^4 + 16z_0^2z_1^6 + z_1^8)}{\rho_{\rm s}^8} \ . \tag{3.91}$$

The Taylor expansion has the advantage of being true for arbitrary combinations of axial amplitudes. The disadvantage is that the expansion must be kept to relatively high order

to be accurate as z/ρ_s approaches 1/2. This is why the expansion coefficients are given to such high order here.

Special Cases

The two special cases of one ion at zero axial amplitude ($z_0 = 0, z_1 \neq 0$) and of both ions at the same amplitude ($z_0 = z_1$) tend to arise often in situations such as PhaseLocking and simultaneous PNPs. The first case of $z_0 = 0$ and $z_1 \neq 0$ can be analytically time averaged giving

$$\Lambda_\rho \mid_{z_0=0} = \frac{1}{2\pi}\int_0^{2\pi} \frac{d\phi}{\left(1 + z_1^2\cos^2(\phi)\right)^{3/2}} = \frac{2}{\pi}\frac{EllipticE\left(z_1^2/\left(1+z_1^2\right)\right)}{\sqrt{1+z_1^2}} \tag{3.92}$$

where we have set $\rho_s = 1$ and $EllipticE$ is the complete elliptic integral of the second kind as defined in Mathematica. The single axial excitation case appears most often when measuring the ion-ion separation using the PhaseLock technique. The current version of LabView has an implementation of the elliptic integrals that could be used to correct the measured beat frequency between the magnetron normal modes for the finite axial amplitude of the ion being measured. Currently, a low order Taylor expansion is used to calculate this correction.

For the second special case of equal axial amplitudes $z_0 = z_1$, no analytic expression was found for Λ_ρ. The phases ϕ_0 and ϕ_1 were numerically averaged over 0 to 2π to obtain Λ_ρ with the results shown in Fig. 3-7.

In both special cases, the calculated Λ_ρ are described to better than 2% for $z/\rho_s \leq 5$ by the average of a Lorentzian and the square root of a Lorentzian:

$$\Lambda_\rho \approx \frac{1}{2}\left(\frac{1}{1+\left(\frac{2}{\Gamma_0}\frac{z}{\rho_s}\right)^2} + \sqrt{\frac{1}{1+\left(\frac{2}{\Gamma_1}\frac{z}{\rho_s}\right)^2}}\right) \tag{3.93}$$

with the fitted parameters for z_0 or z_1=0

$$\Gamma_0 = 1.799 \tag{3.94}$$

$$\Gamma_1 = 2.372 \tag{3.95}$$

and for $z_0 = z_1$

$$\Gamma_0 = 1.156 \tag{3.96}$$

$$\Gamma_1 = 3.438\ . \tag{3.97}$$

These are useful approximations since the time overhead for numerically evaluating the elliptic integral or the numerical integral can potentially be quite high.

The behavior for $z_1/\rho_s \gg 1$ with $z_0 = 0$ is proportional to $1/z_1$ because the time averaged

radial force is dominated by the fraction of time that ion 1 spends near $z = 0$, which for large axial amplitudes is simply inversely proportional to its velocity. The extremely naive prescription of replacing the axial motions with their rms values is correct only to lowest order, and predicts a behavior of $1/z^6$ for $z_1/\rho_s \gg 1$ as shown in Fig. 3-7.

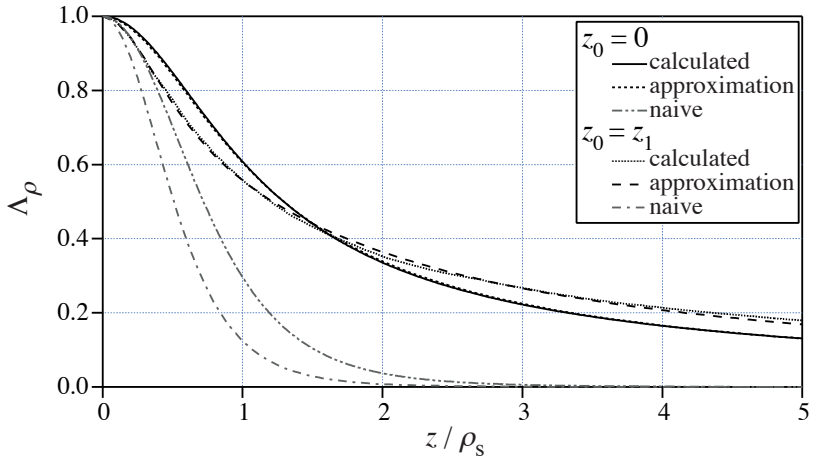

Figure 3-7: Modification of the magnetron Rabi frequency Ω_m versus axial amplitude expressed as a fraction of the ion-ion separation z/ρ_s. The two special cases $z_0 = 0$ and $z_0 = z_1$, which arise in PhaseLock and simultaneous PNPs respectively, are shown. We typically operate with $z \sim 300$ μm so that at ρ_s= 600 and 1200 μm, $z/\rho_s = 0.5$ and 0.25 respectively. When pulsing the axial modes to redistribute the canonical angular momentum between normal modes, $z/\rho_s > 1$. The perturbation results determined semianalytically and numerically are shown along with approximate fits as described in the text. Also shown are the naive (and incorrect) results in which the axial amplitudes are simply replaced by their rms values.

3.6.2 Modified Axial Frequency Shift

The ion-ion interaction creates a common first order downward shift of each ion's axial frequency as discussed in Sect. 3.4.2. The frequency shift is simply half the axial Rabi frequency $-\Omega_z/2$ in the limit $z_0 = z_1 = 0$. With finite axial amplitudes, the symmetry of the axial frequency shift is broken if the axial amplitudes are not the same. The modified axial frequency shift can then be expressed as the axial Rabi frequency Ω_z times separate correction factors for each ion $\Lambda_z^{(0)}$ and $\Lambda_z^{(1)}$ that both go to unity in the limit $z_0 = z_1 = 0$:

$$\Delta\omega_{z0} = \Lambda_z^{(0)}\Omega_z \tag{3.98}$$

$$\Delta\omega_{z1} = \Lambda_z^{(1)}\Omega_z \ . \tag{3.99}$$

We will focus on the axial frequency shift of ion 1 with the understanding that the same results will apply to ion 0 by simply interchanging the ion labels $0 \leftrightarrow 1$. Figure 3-8 summa-

rizes the results of these calculations. It should be stressed that the calculations below are for modifications of the first order axial frequency shift due to ion-ion interactions and not the axial Rabi frequency $\Omega_{\rm z}$. As a result, it is incorrect to think that the modification of the second order axial frequency pulling shift is simply modified by $\Lambda_{\rm z}^2$. Since the modification of the axial frequency pulling is third order in quantities that are usually small, this effect is not calculated.

The axial frequency shift of ion 1 arises from the force acting on ion 1 along $\hat{z}$ that is due to ion 0

$$F_{10} = \frac{q^2\left(z_1(t) - z_0(t)\right)}{\rho_{\rm s}^3} \frac{1}{\left(1 + \frac{(z_1(t)-z_0(t))^2}{\rho_{\rm s}^2}\right)^{3/2}} \quad . \tag{3.100}$$

We wish to find the average force near $\omega_{\rm z1}$, but we must do so carefully since the second factor's magnitude is correlated with the magnitude of the first term.

Taylor Series

In the limit $z_0, z_1 \ll \rho_{\rm s}$, we can make a Taylor expansion of the second factor and perform the substitutions $z_1(t) = z_1\cos(\omega_{\rm z1}t + \phi_1)$ and $z_0(t) = z_0\cos(\omega_{\rm z0}t + \phi_0)$ for *both* the first and second factors. We then keep only the terms near frequency $\omega_{\rm z1}$ that are proportional to $z_1\cos(\omega_{\rm z1}t + \phi_1)$. This is the same approach used to calculate frequency shifts arising from trap anharmonicities described in Sect. 2.2.2. The result can be written as a sum

$$\Delta\omega_{\rm z1} = \Omega_{\rm z}\left(1 + \sum_{n=1}^{\infty}\beta_{2n}^{(1)}(z_0, z_1, \rho_{\rm s})\right) \quad . \tag{3.101}$$

The values $\beta_{2n}^{(1)}$ evaluate to:

$$\beta_2^{(1)} = -\frac{9}{8}\frac{(2z_0^2 + z_1^2)}{\rho_{\rm s}^2} \tag{3.102}$$

$$\beta_4^{(1)} = +\frac{75}{64}\frac{(3z_0^4 + 6z_0^2z_1^2 + z_1^4)}{\rho_{\rm s}^4} \tag{3.103}$$

$$\beta_6^{(1)} = -\frac{1225}{1024}\frac{(4z_0^6 + 18z_0^4z_1^2 + 12z_0^2z_1^4 + z_1^6)}{\rho_{\rm s}^6} \tag{3.104}$$

$$\beta_8^{(1)} = +\frac{19845}{16384}\frac{(5z_0^8 + 40z_0^6z_1^2 + 60z_0^4z_1^4 + 20z_0^2z_1^6 + z_1^8)}{\rho_{\rm s}^8} \quad . \tag{3.105}$$

These expansions are not (and were not expected to be) symmetric with respect to the ion indices 0 and 1, as was the case in the previous section in which the radial force was modified. Once again, the Taylor expansion has the advantage of being true for any arbitrary combination of axial amplitudes. But the expansion badly diverges as $z/\rho_{\rm s}$ approaches 1/2 unless very high order terms are retained.

Special Cases

Let us further examine the two special cases of $z_0 = 0$ and $z_0 = z_1$. The averaging can be performed without the Taylor expansion by observing that the time dependence of the force can be written as a Fourier series, and a mixing step can isolate the coefficient of the force at frequency ω_{z1} up to a factor of 1/2. Choosing units such that $\rho_s = 1$, we can write

$$\Lambda_z^{(1)} = \lim_{T\to\infty} \frac{1}{T} \int_0^T \frac{2\cos(\omega_{z1}t + \phi_1)\left(z_1\cos(\omega_{z1}t + \phi_1) - z_0\cos(\omega_{z0}t + \phi_0)\right)}{\left(1 + \left(z_1\cos(\omega_{z1}t + \phi_1) - z_0\cos(\omega_{z0}t + \phi_0)\right)^2\right)^{3/2}} dt \quad . \tag{3.106}$$

In practice, the time average can be evaluated by replacing the time dependent factors with independent phases and integrating over each phase as described in the preceding Sect. 3.6.1. The special case $z_0 = 0$ can be expressed in terms of the complete elliptic integral E and the elliptic integral of the first kind K as defined in Mathematica:

$$\Lambda_z^{(1)}\,|_{z_0=0} = \left(\frac{4}{\pi}\right) \frac{EllipticK\left(z_1^2/\left(1+z_1^2\right)\right) - EllipticE\left(z_1^2/\left(1+z_1^2\right)\right)}{z_1^2\sqrt{1+z_1^2}} \quad . \tag{3.107}$$

The second special case $z_0 = z_1$ is of much greater interest since this is the situation that arises when simultaneously measuring the axial frequencies of the two ions at the end of a PNP sequence. When the usual quadrature relation is used to obtain the free space cyclotron frequency, the ion-ion axial frequency shift measured at zero axial amplitudes is exactly cancelled by the corresponding shift of the trap cyclotron frequency. Because we measure the axial frequencies at finite axial amplitudes, we must use the results calculated here to determine the frequencies that would have been measured in the limit of zero axial amplitudes. At small ion-ion separations of ρ_s=600 μm and typical axial amplitudes of $z_0 = z_1 = 350$ μm, this shift causes an error on the measured cyclotron frequency ratio of 5×10^{-12} for the example pair $^{13}C_2H_2^+$ vs N_2^+. In all our data analysis, we make a correction for this perturbation that needs to only be accurate to 20% to null the perturbation of the ratio to 1×10^{-12}.

No analytical expression was found for the important special case $z_0 = z_1$, but the integral was evaluated numerically with the results shown in Fig. 3-8. The functional forms in each case are well approximated to $\leq 2\%$ for $z_1 \leq 10\rho_s$ by Lorentzians

$$\Lambda_z^{(1)} \approx \frac{1}{1 + \left(\frac{2}{\Gamma_0}\frac{z}{\rho_s}\right)^2} \tag{3.108}$$

with the fitted parameters for z_0 or z_1=0

$$\Gamma_0 = 1.769 \tag{3.109}$$

and for $z_0 = z_1$

$$\Gamma_0 = 1.089 \ . \tag{3.110}$$

Figure 3-8 includes the approximation functions for comparison.

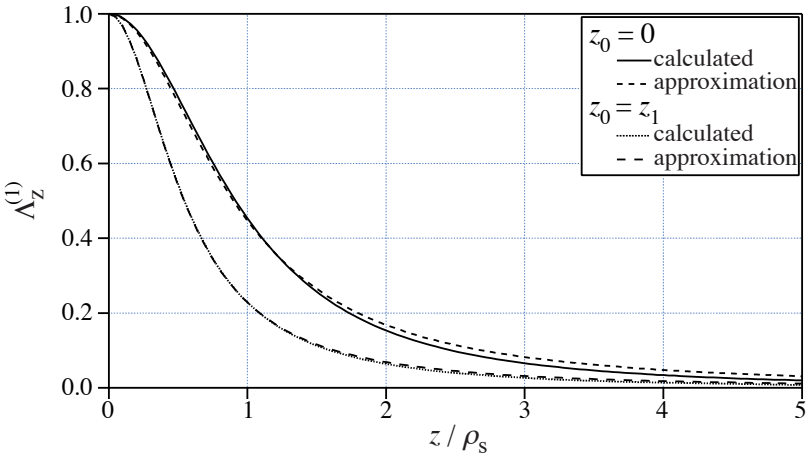

Figure 3-8: Modification of the common axial frequency shift versus axial amplitude expressed as a fraction of the ion-ion separation z/ρ_s. The two special cases $z_0 = 0$ and $z_0 = z_1$, which arise in PhaseLock and simultaneous PNPs respectively, are shown. The perturbation results determined semianalytically and numerically are shown along with approximate fits as described in the text. We typically operate with $z \sim 300$ μm so that at ρ_s= 600 and 1200 μm, $z/\rho_s = 0.5$ and 0.25 respectively. When pulsing the axial modes to redistribute the canonical angular momentum between normal modes, $z/\rho_s > 1$.

Chapter 4

Measurement and Control of Magnetron Motion

In this chapter we turn to our experiment. We will describe how we load a pair of ions into our trap and then subsequently observe and control the collective magnetron motion. The results of our observations lend much support to the validity of our theoretical model of the magnetron modes. The parameters we can measure and in some instances compare with theory include: the relative phase between the instantaneous magnetron motions, the ion-ion separation $\rho_{\rm s}$, the common mode amplitude $\rho_{\rm com}$, the rms magnetron radius of each ion $\sqrt{\langle\rho_{\rm m1}^2\rangle}$ and $\sqrt{\langle\rho_{\rm m0}^2\rangle}$, and the difference of the rms magnetron radii $\sqrt{\langle\rho_{\rm m1}^2\rangle}-\sqrt{\langle\rho_{\rm m0}^2\rangle}$. These measurements are crucial for understanding and controlling the various ion-ion and trap field imperfection shifts of the cyclotron frequency ratio. For instance, all of the predicted systematic shifts scale as high powers of the ion-ion separation $\rho_{\rm s}$, so it is important to know its value very accurately. The measured values of $\sqrt{\langle\rho_{\rm m1}^2\rangle}-\sqrt{\langle\rho_{\rm m0}^2\rangle}$ versus $\rho_{\rm s}$ are in good agreement with theory, which is important for accurately estimating uncertainties arising from trap field imperfections.

The ultimate aim of control is to park the ions on a common magnetron orbit but on opposite sides of the trap. We also want to be able to control the radius of the common magnetron orbit or equivalently $\rho_{\rm s}$. We have developed tools to accomplish these goals. The techniques 2MagPulses and MNZ represent substantial experimental work. They work by removing the canonical angular momentum from the common magnetron mode. In the end, these two techniques were supplanted by more effective methods.

Conservation of energy and canonical angular momentum would seem to prohibit control of the ion-ion separation $\rho_{\rm s}$. The key technique for controlling $\rho_{\rm s}$ is to violate conservation of energy. Violation of energy conservation can be accomplished by exciting the axial motions of the ions in the presence of azimuthally symmetric electrostatic anharmonicities, a fact that we discovered somewhat serendipitously. This allows us to change the total energy contained in the coupled magnetron modes and hence $\rho_{\rm s}$. This technique violates

conservation of energy, but it does not violate conservation of canonical angular momentum. Hence, we only redistribute the canonical angular momentum between the two collective separation and common magnetron modes. In practice, this is quite useful, since it allows us to easily reset the ions to the same ion-ion separation.

Operationally, if the ions are too close to one another then the ion-ion interaction causes the axial modes to be extremely anharmonic. In this regime, we cannot use the powerful technique of coupling the collective modes that is described next. A few good random whacks to the axial mode of one of the ions is usually good enough to move the ions far enough apart that the axial modes are once again harmonic (i.e., the axial frequency chirps with axial amplitude by less than a linewidth).

We can fine tune the magnetron orbits by modulating the axial amplitude of one of the ions with a fixed phase relative to the beating of the collective magnetron modes. In order for this to work, it is necessary to introduce azimuthally symmetric anharmonicities. We will show that the axial amplitude modulation creates a resonant coupling between the common and separation modes. The axial amplitude modulation is created by a "speedbump" in axial frequency space. The "speedbump" is simply a continuous axial drive just below or just above the axial resonance. With this very simple technique, we can move some or all of the canonical angular momentum from one collective mode to the other.

Using the collective magnetron coupling technique, we can move all of the canonical angular momentum to the separation mode so that the common mode amplitude is zero. This is exactly the parked orbit configuration that we desire. To increase the ion-ion separation, we inject angular momentum into the common mode with a resonant dipole drive, and then transfer this angular momentum into the separation mode with our coupling technique. To move the ions closer together, we remove angular momentum from the system by simultaneously applying short sideband couplings between each magnetron mode and its damped axial mode. These techniques allow us to measure the cyclotron frequency ratio versus systematically varied ion-ion separation. By observing how much the answer changes, we can strongly constrain the size of possible systematic errors (Sect. 5.7.

Why is it so important to obtain the parked magnetron orbit? After all, the theory of the coupled magnetron motion in a perfect Penning trap predicts that if the common mode amplitude $\rho_{\rm com}$ is not zero, the ions will swap magnetron amplitudes on time scales of the beat frequency $\Omega_{\rm m}$ and thus average away differential shifts due to trap field imperfections. There are four answers all of which are related to the fact that we do not have a perfect Penning trap. First, each ion's axial frequency chirps as the magnetron radius varies. This results in increased measurement phase noise that is prohibitive for making precise cyclotron frequency comparisons. Second, in an imperfect trap, the instantaneous magnetron frequency of each ion depends on each ion's magnetron radius. The resulting modification of the coupled magnetron orbits is understood in the parked configuration limit $\rho_{\rm com} \ll \rho_{\rm s}$, but not so in the limit $\rho_{\rm com} \sim \rho_{\rm s}$. If the difference in rms magnetron

radii of the two ions is significantly modified, then our estimates of uncertainties will be incorrect. Third, the technique described in the next chapter—applying a substantial C_4 to compensate for the differential shifts of the trap cyclotron frequencies arising from B_2, C_6, and B_4 (Sect. 5.6)—will not work very well when $\rho_{\rm com} \sim \rho_{\rm s}$. Lastly, we would like to explore as little of the trap volume as possible for a given ion-ion separation. This lets the multipole expansion of the trap field imperfections work in our favor.

With this overview, let us begin by examining how we produce the two ions in the Penning trap.

4.1 Loading a Single Ion

4.1.1 Ionization

In order to place two ions in a trap, one must first place a single ion in the trap. In ICR slang, we refer to this process as making. The process begins by first emptying the trap by tipping the electrostatic axial confinement potential so that any ions in the trap strike the Lower Endcap and stick or are neutralized. With an empty trap, we restore the axial confinement and then introduce a small puff of neutral gas (typically $\sim$ 100 cc$\times$mTorr) into our vacuum system. There is a straight path from the room temperature part of the apparatus to the top of the Penning trap at 4 K, allowing some of the gas to enter the trap through a small hole (diameter 500 μm) in the Upper Endcap (see Fig. 2-2). A field emission point (FEP) generates an electron beam, $\sim$ 5 nA at $\sim$ keV, that enters the trap from an identical hole in the Lower Endcap and ionizes some of the neutral gas. A typical sequence is to open the valve between the small volume of gas and the insert at t=0 and then close the valve after 1 s. The FEP is then fired in the approximate interval t = 5 to 6 s. The delay between injecting the gas and turning on the FEP was chosen based on a mapping of the number of ions made versus the delay time between the events with the point of maximum number chosen. The maximum is chosen so that as little neutral gas as possible can be used. We ascribe this large delay time to the extremely low conductance of the path that the gas must take to the trap. The amount of neutral gas and the electron beam current are adjusted to make a single ion every few attempts. It should be noted that we typically find that the ion is created with a magnetron radius of $<$ 100 μm, and the cyclotron motion is even smaller.

4.1.2 SmartCool

Most often, the axial frequency of a newly ionized atom or molecule is initially shifted up by 50 to 200 Hz as a result of an extremely large axial amplitude. The large axial amplitude after ionization is consistent with the assumptions that the ion is equally likely to be ionized anywhere along the trap axis and that where it is ionized sets its initial axial amplitude. The large axial amplitude then shifts the axial frequency with a sign consistent with the

measured trap anharmonicity C_6. The large axial excitation can take many minutes to damp because the ion is far from the center frequency of the coil that provides the damping of the axial motion. To speed up the cooling process, the trapping voltage is adjusted to bring the ion's perturbed axial frequency into resonance with the coil. However, a small reduction in the axial amplitude causes the axial frequency to chirp out of resonance with the high-Q coil.

A discrete feedback scheme called SmartCool was developed to more rapidly reduce this axial motion. The computer begins by stepping the trapping voltage to produce axial frequency changes in steps of 50 Hz and listening to the axial signal for 0.5 s at each setting. When a peak is detected, the computer changes the trap voltage to bring the detected axial motion into resonance with the coil in a single update. The computer repeats this process until the axial amplitude drops below a threshold set by the user. This system was a vast improvement over the previous technique (DumbCool!) of manually scanning the trapping voltage by hand and monitoring the detected signal on an oscilloscope. SmartCool allows cooling of an ion in 30 s compared to minutes previously and would greatly increase the speed with which alternate cyclotron frequency measurements could be performed, were we to revert to that simpler technique.

4.1.3 Killing with One Ion

Having created a single ion of interest (the good ion) and having cooled its axial motion, we proceed to killing (i.e., getting rid of) other ions that we do not want in the trap (the bad ions). This is accomplished by applying broadband (Normal kill) or targeted narrowband (Fragment kill) rf noise on the Lower Endcap (LEC) that excites the axial motion of the ions we do not want. We then ensure that the good ion's axial motion is small by sweeping the trap voltage over a few Hz for ~ 10 s about the trap voltage setting that makes the good ion's axial motion resonant with the detector that provides damping. The axial equilibrium position of the trap is then adiabatically Dipped toward the LEC by applying a dc voltage to the LEC of $\sim 85\%$ of the Ring voltage. The ions in large axial orbits strike the LEC and stick or neutralize. A small voltage ± 0.5 V from the computer can be added to the Ring to fine tune how closely the equilibrium position is Dipped toward the LEC. After several kills of increasing Dip strength, only the good ion is left in the trap. On a good day, we would typically perform an initial shallow Dip, followed by two Fragment and two Normal kills. We consistently found that the good ion was more likely to be killed by a broadband Normal kill. This is probably as a result of inadequate axial cooling before the Dip.

4.1.4 Improvements to Making

In addition to the SmartCool system described above, several other improvements were made to the making scheme. The first was an intelligent system for automatically setting the amount of gas used in a make. The second improvement was to ensure that the voltage

applied to the FEP returned to ground quickly. Apparently in all previous work, the FEP control circuit was hardwired to maintain the high voltage for 3 s after it was nominally turned off. In addition, it was found that the FEP continued to float at a keV for the duration of a long lunch (over an hour). There should be two time scales for the decay of the voltage—an initial discharge of the capacitance driven by field emission and a slower discharge driven by the finite resistance of the dielectric. The measured capacitance of the FEP and several meters of high voltage coaxial cable was 700 pF. Using this capacitance and a measured current of 5 nA at 1 kV, the time constant associated with field emission is $\sim$ 2 minutes. The effective resistance to ground was estimated to be $\sim$ 1000 GΩ based on the measured variation of measured offset current with probe resistance. The RC constant of 13 min is somewhat smaller than the hour time scale we observed. To fix these problems, we eliminated the 3 s hold logic and installed a new high voltage relay that pulls the FEP to ground 45 ms after the FEP is nominally turned off. In summary, the voltage on the FEP can now be controlled with a time constant of 10 ms and with a fixed delay of 45 ms before the FEP is pulled to ground.

4.2 Loading Two Ions

4.2.1 Making without Parking

In order to make a pair of ions, we use the single ion techniques described above to create one of the pair first, say ion 0. After using sideband couplings to the axial mode to cool the magnetron and cyclotron modes, we drive the magnetron motion of ion 0 to a radius of 1 mm. We then inject the neutral gas needed to produce the other ion and fire the FEP to create ion 1 near the center of the trap. In a perfectly harmonic trap, the separation between the ions is now a constant of the motion, and the ions start to orbit the center of charge located 500 μm from the trap center, and we could proceed to make cyclotron frequency comparisons. In an anharmonic Penning trap, the variation of the axial frequency with instantaneous magnetron radius introduces too much phase noise into our measurements. This simple loading technique was demonstrated in the original work of Ref. [2]^G.

4.2.2 Killing with Two Ions

We can robustly kill bad ions even with both good ions in the trap. This allows us to introduce arbitrary pairs of ions into the trap. For example, we made the pair $^{29}Si^+$ vs $^{28}SiH^+$ by first making the $^{29}Si^+$ from SiH_4 neutral gas and killing all of the bad ions. We then produced the $^{28}SiH^+$ ion from the same SiH_4 neutral gas. The single ion killing techniques were then used to kill all of the other bad ions that are produced in similar quantities to the good ion $^{28}SiH^+$. For instance, we removed bad ions such as $^{28}Si^+$, $^{28}SiH_2{}^+$, $^{28}SiH_3{}^+$, and $^{28}SiH_4{}^+$.

When possible, we make the ion with the larger number of possible fragments (or types of bad ions) first. We can then eliminate all of the bad ions using the single ion killing techniques discussed previously. We then proceed to make the more complex ion. For example, we would first make the more complex $^{13}C_2H_2^+$ ion from $^{13}C_2H_2$ gas and then use the usual killing techniques to obtain a single ion. We would then make the simpler ion N_2^+ from N_2 gas. If we are lucky, the dominant species after impact ionization is N_2^+. By properly choosing the make parameters (i.e., electron current and amount of neutral gas), we can most often make a single N_2^+ ion with no bad ions.

Most often we are not lucky, and we create several to many bad ions as described in the opening example of $^{29}Si^+$ vs $^{28}SiH^+$.* We found that we could use the usual single ion killing techniques on the pair of ions if we very carefully cooled the axial motions of both ions before performing the dip toward the Lower Endcap. The axial signals of the good ions might appear very anharmonic after a kill, which was usually indicative of the presence of bad ions. If the signals did not become harmonic after several kills, then the axial frequencies may have been chirping with amplitude due to the ions being very close to one another ($\rho_s < 600$ μm). To move the two good ions radially apart from one another, the axial mode of one of the ions was driven very hard. This technique is described in Sect. 4.2.5.† If the axial signals appeared more harmonic, this was indicative that the bad ions were gone, and we had simply needed to move the ions apart from one another. We would then stop killing and try to fine tune the magnetron orbits into a parked configuration as described in Sect. 4.4.1. If the axial signals did not become more harmonic, we would continue the killing process.

Toward the end of our experimental work, we could typically create a pair of ions, clean the trap of bad ions, and park the ions on a common magnetron orbit in about 1 to 3 hours of work.‡

4.2.3 2MagPulses

In order to park the ions on opposite sides of the trap, we wish to drive the center of charge to the center of the trap. To accomplish this, we sandwich the creation of ion 1 between two magnetron drives (or pulses) with relative phases chosen so that they destructively interfere. The key is that the second magnetron drive is performed at half the amplitude of the first

*The presence of bad ions after a make is a real problem for the 2MagPulse and MNZ techniques described below and is one of their significant drawbacks.

†In order to be able to move the ions apart from one another without exerting a torque on the system, all of the canonical angular momentum must be in the magnetron modes to start with. As described in Sect. 4.2.1, the first ion is driven to a magnetron radius of ~ 800 μm just before making the second ion. This ensures that there is enough canonical angular momentum in the system to allow the ions to be moved ~ 1 mm apart from one another using the axial pulsing technique.

‡The actual making and killing takes 30 to 120 minutes. It should go more quickly, but since we only need to make a new pair every few weeks, there is overhead associated with remembering how to make and overcoming silly mistakes such as forgetting to open the insert valve that allows the neutral gas to be injected into the UHV system.

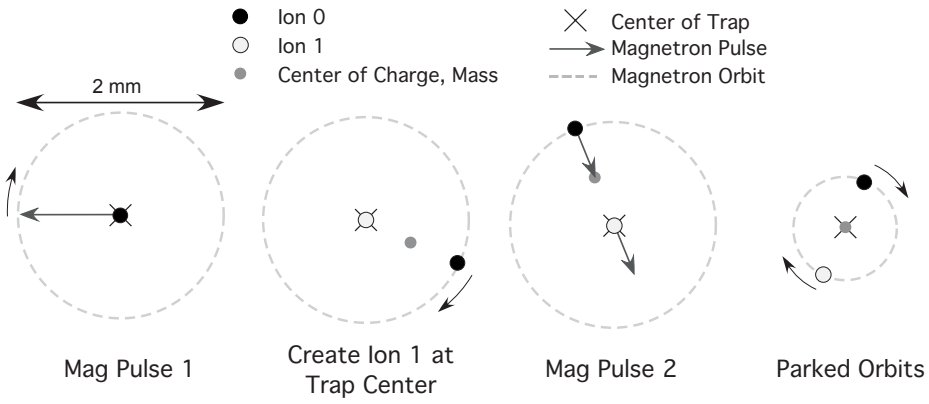

Figure 4-1: The measured magnetron radius of a single ion after two magnetron drives 0.5 s apart versus the phase of the second magnetron drive. For parking two ions on a common orbit, the second pulse's amplitude will be reduced to half of the first pulse's amplitude and the phase will be chosen such that the two pulses destructively interfere.

pulse so that ion 0 is driven halfway back to a radius of 500 μm and the other ion halfway out to a radius of 500 μm. The usual rf dipole field used for driving the magnetron motion of a single ion acts identically on the magnetron motion of each of the two ions because of the frequency degeneracy of the modes. Thus, our dipole drive can be described as acting on the center of charge of the ions.

To find the correct phase of the second magnetron pulse, we perform the sequence without injecting the neutral gas needed to create ion 1 and with the second pulse at the same amplitude as the first. By observing the magnitude of the remaining magnetron motion versus the phase of the second magnetron pulse, we can choose the proper phase needed to cause destructive interference of the two pulses. Figure 4-2 is an example of such a measurement. The phase resulting in destructive interference of the two drives can easily be determined to a few degrees. The maximum time between the pulses is set primarily by the time scale on which the ions become aware of each other, i.e., the period of the beat motion $2\pi/\Omega_{\mathrm{m}} \sim 20$ s. With the improvements to the time response of the FEP discussed above, we can easily produce an ion 1 within 200 ms, setting a soft lower limit on the time interval between pulses.

The 2MagPulse technique works well when the second ion is created with very small axial amplitude. When the second ion is created at large amplitudes, the electrostatic anharmonicity of the trap shifts the instantaneous magnetron frequency of the ion by an amount proportional to z^2 or z^4. This shift breaks the frequency degeneracy of the magnetron modes, resulting in independent magnetron motions. The second ion accumulates a phase advance or phase lag in its magnetron motion with respect to the first ion until the ions are very close to one another or until the axial amplitude damps and the magnetron modes strongly mix. This effect makes this technique very difficult, with often many days

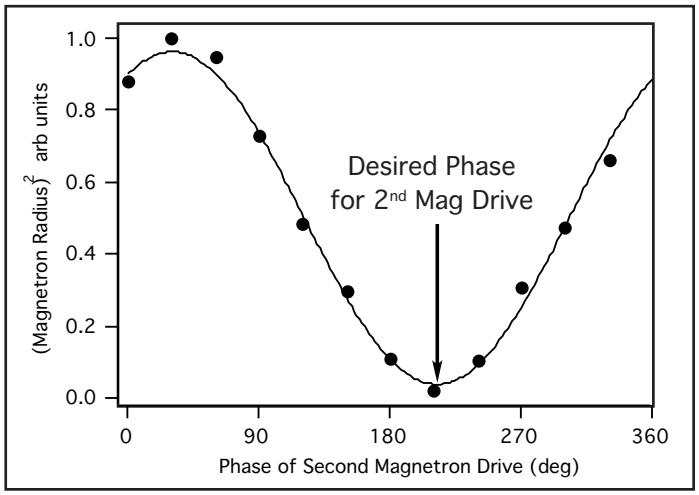

Figure 4-2: The measured magnetron radius of a single ion after two magnetron drives 0.5 s apart versus the phase of the second magnetron drive. For parking two ions on a common orbit, the second pulse's amplitude will be reduced to half of the first pulse's amplitude and the phase will be chosen such that the two pulses destructively interfere.

of ion making necessary to make a pair of parked ions.

One possible solution to the problem of large axial amplitudes is to quickly measure the amplitude and phase of ion 1's axial motion and then apply a correction pulse to drive its axial amplitude to zero. Because the axial frequency of the inner ion 1 would chirp by ~ 50 Hz during this process, a broadband pulse of comparable frequency width would have to be applied that would deleteriously drive the axial motion of the outer ion 0. Essentially, one ion's axial amplitude would be reduced while the other ion's axial amplitude would be increased by a comparable amount. A more subtly tailored drive pulse might be used to avoid this, but most likely the technique would collapse under the weight of its complexity.

Adiabatic compression of the axial motion is another possible solution. If the second ion is initially created in a very weak trap with an axial frequency much less than the final axial frequency $\omega_{\mathrm{zi}} \ll \omega_{\mathrm{zf}}$, then adiabatically ramping the trap voltage over time scales $\gg 2\pi/\omega_{\mathrm{zi}}$ would lead to compression of the axial amplitude. This is easiest to understand using a simple quantum argument. Adiabatic means that the quantum state does not change, so that the axial harmonic oscillator quantum number remains constant throughout the process. This means that after compression, the energy has been increased by $\omega_{\mathrm{zf}}/\omega_{\mathrm{zi}}$. But the ratio of classical expressions for the energies is just $(\omega_{\mathrm{zf}}^2 z_{\mathrm{f}}^2)/(\omega_{\mathrm{zi}}^2 z_{\mathrm{i}}^2)$. Equating the expressions shows that

$$\frac{z_{\mathrm{f}}}{z_{\mathrm{i}}} = \sqrt{\frac{\omega_{\mathrm{zi}}}{\omega_{\mathrm{zf}}}} = \left(\frac{V_{\mathrm{ri}}}{V_{\mathrm{rf}}}\right)^{1/4} \tag{4.1}$$

where the last expression results from the axial frequency dependence on the Ring voltage.

If one assumes that ions are created with uniform probability along the trap axis, then the number of ions that fall below a critical axial amplitude threshold for the 2MagPulse sequence to work is only increasing like the fourth root of the ratio of trap voltages. This dependence is much too weak for this technique to be of significant value.

4.2.4 Measure aNd Zero (MNZ)

In principle, the problem of the magnetron motions decoupling and recoupling when the ions are close to one another would be solved if the axial motion of ion 1 could be cooled before the second magnetron pulse of the 2MagPulse sequence is applied. The technique Measure aNd Zero (MNZ) was developed to accomplish precisely this. A MNZ sequence starts in the same way as the 2MagPulse sequence—driving the first and only ion in the trap, say ion 0, to a magnetron radius of 1 mm. The Guard Ring voltage $V_{\rm gr}$ is then mistuned by approximately $\widetilde{V}_{\rm gr} \approx 0.75$ V (or as a fraction of the Ring voltage $\widetilde{V}_{\rm gr}/V_{\rm r} \approx 0.047$) to create a large magnetron frequency variation with $\rho_{\rm m}^2$. For scale, this mistuning shifts the magnetron frequency at $\rho_{\rm m}$=1 mm by $\Delta f_{\rm m0} = 750$mHz. The other ion is then created in the center of the trap with < 100 μm magnetron radius. Because the large anharmonicity breaks the frequency degeneracy of the magnetron modes, the inner and outer ions are not coupled, and we are then free to leisurely cool the axial motion of ion 1 to zero using the SmartCool routine described above. The discrete feedback scheme SmartCool is particularly useful because it can be set to look in a large frequency range of several 100 Hz for the axial motion of ion 1.

In the process of cooling the axial motion of the inner ion, we lose all phase information about the magnetron motion of the outer ion, so we must measure its phase. To do this, first $V_{\rm gr}$ is reset to its tuned setting so that the axial modes are harmonic once again, and then a $\sim \pi/20$-pulse is applied between ion 1's magnetron and axial modes, creating ~ 300 μm axial motion. This reduces the magnetron amplitude by less than 1%. The phase of the axial motion is measured (M of MNZ) for 2 s and then used to determine the phase of the correction magnetron pulse needed to zero (Z of MNZ) the common mode motion. The half-amplitude correction pulse is applied approximately 3 s after the start of the partial π-pulse, before the ions have time to significantly swap magnetron amplitudes.

The condition for magnetron mode decoupling is that the frequency difference must be much greater than the radial Rabi frequency $\Delta f_{\rm m} \gg \Omega_{\rm m}/2\pi$. This condition is well satisfied for the above scenario for which $\Delta f_{\rm m0} = 750$ mHz and $\Omega_{\rm m}/2\pi = 50$ mHz. The outer ion's magnetron motion creates a rotating electric field at the inner ion's location that nonresonantly drives the inner ion's magnetron motion. The result is modulation of its magnetron motion with peak amplitude $\rho_{\rm m1}\Omega_{\rm m}/(2\pi\Delta f_{\rm m0}) \approx 70$ μm and with frequency $\Delta f_{\rm m0} \approx 750$ mHz.

The phase of the measured axial motion is related to the desired phase of the correction pulse by a fixed phase offset if all the time intervals in the sequence are held constant.

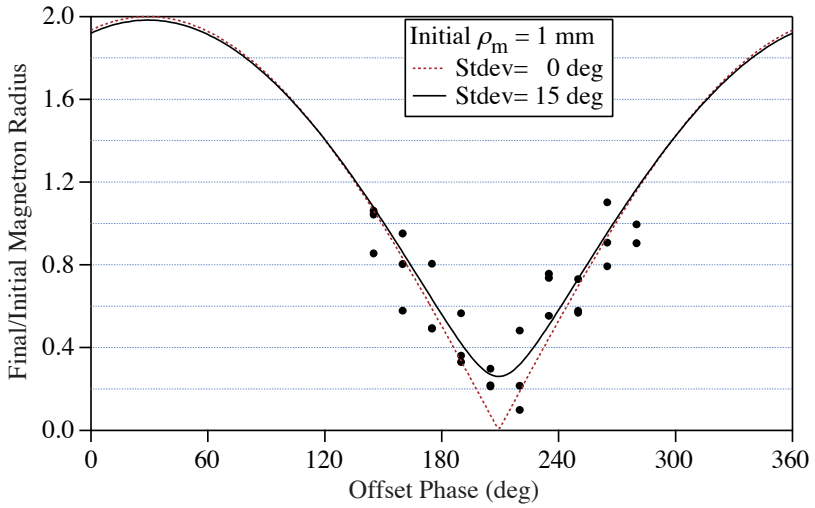

Figure 4-3: Testing Measure and Zero (MNZ) technique with a single ion. The ion is initially driven to a magnetron radius of 1 mm, and then a partial π-pulse between the magnetron and axial modes is used to determine the phase of the drive necessary to zero the magnetron amplitude. The offset phase relating the measured axial phase and the correct magnetron drive phase is purposely scanned to show the dependence. The expected RMS magnetron radius after the correction pulse is given by the dashed curve for the case of zero measurement noise. The solid curve is the convolution of the dashed curve with the observed Gaussian distributed phase measurement noise of 15°.

This offset phase is determined in a manner similar to that for the 2MagPulses sequence. With a single ion in the trap, a magnetron drive is applied at $t = 0$ with the same phase each trial. Several seconds later, the partial π-pulse is applied, and the phase of the axial motion is measured for ≈ 2 s. A correction pulse with the same amplitude of the first pulse is applied ≈ 3 s after the partial π-pulse and with a phase that is varied each trial *independent* of the measured axial phase. The remaining magnetron amplitude is then plotted versus the phase of the second magnetron pulse to determine which value causes destructive interference of the two magnetron pulses. The average measured axial phase differs from this optimum magnetron pulse phase by a fixed offset. This phase offset can be determined to a few degrees by taking the difference of the average measured phase and the optimum magnetron pulse phase.

The system can be tested using a single ion by applying a magnetron pulse of random phase, and allowing the system to predict the desired phase of the correction pulse using the measured axial phase and the phase offset. Figure 4-3 shows such a case in which we also varied the phase offset about the correct value. With a typical 15° standard deviation of the measured axial phase due to detection noise, the expected rms final amplitude of the magnetron motion is $\sim 25\%$ of the initial amplitude, which is in good agreement with the experimentally measured value as shown in Fig. 4-3. The same fractional reduction of the common mode amplitude should occur. So, for the case of ion 0 initially driven to

1 mm, the final state should be described by a separation distance of $\rho_s = 1$ mm and a common amplitude of $\rho_{com} = 125$ μm. Also note that there is a phase error below which "you have done no harm." When the offset phase is mistuned ±60°, there is no reduction as one expects.

Actually testing the system with two ions is quite difficult since we suffer from low statistics. This is in part because we rarely desire to kick a pair of well parked ions out of the trap and try again. Despite the low statistics, there is a clear reduction of the common mode amplitude as evidenced by a reduction of the amplitude of axial frequency modulation. Unfortunately, a more quantitative statement is not presently possible.

There are several subtleties to implementing this sequence. Carefully accounting for the phases and details given here is critical to making the MNZ technique a practical one. The first is the requirement of maintaining the same relative phases of both magnetron pulses, the magnetron-axial coupling and the mixer. This is accomplished by taking advantage of a special "Burst" mode available on the SRS DS345 and Agilent 3025 synthesizers. The desired frequencies and number of cycles to be generated by each synthesizer can be programmed via GPIB in advance of the sequence and then triggered via digital inputs on the rear. The digital triggers are generated using the usual DIO32HS card from National Instruments that is also used for the more common sequences such as PNP, Axial Pulse, etc. The phase of the output when the digital trigger arrives can be programmed via GPIB, and this is how the phase of the second magnetron pulse is set. While the computer's signal processing algorithm can determine the correct phase in less than 100 ms, the actual adjustment of the phase on the synthesizers can take 700 ms for the SRS DS345 synthesizer and 200 ms for the Agilent 3025 Synthesizers. As a result, an Agilent is used for the second magnetron pulse. In addition, Agilents are used for the mixer and magnetron-axial coupling since the SRS synthesizers cannot be set to a large enough number of cycles.

Another technical detail is the fact that the measured signal is actually the response of the Q=45000 self-resonant transformer (the coil) to the axial motion of the ion. The ion's motion drives the coil, which is itself an harmonic oscillator. There is a 180° phase difference of the coil's response to the drive between when the ion is infinitely below or above the center frequency of the self-resonant coil. The actual phase response is given by an arctangent

$$\phi_{coil} = \phi_{ion} - \arctan(\delta^*) \tag{4.2}$$

where $\delta^* = (f_z - f_{coil})/f_{HWHM}$ is the detuning of the ion's axial frequency with respect to the coil center frequency divided by the coil's HWHM. Figure 4-4 is a trivial demonstration of this effect performed by comparing the phase of the observed coil response with respect to an rf drive applied to the LEC that capacitively couples to the coil through stray trap capacitance. When the drive is below resonance ($\delta^* < 0$), the coil response leads the drive, while the reverse happens when the drive is above resonance. In MNZ, if the offset phase is

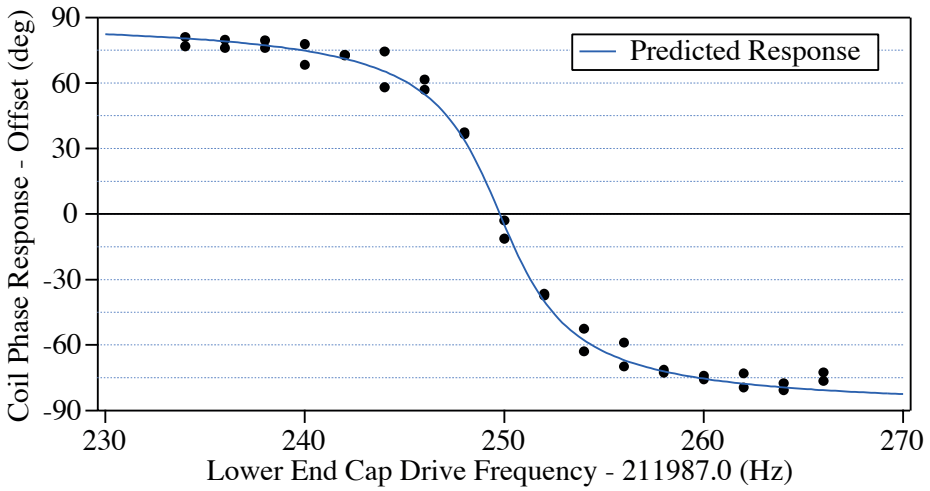

Figure 4-4: Coil phase response relative to the phase of the rf drive on the Lower Endcap. An rf drive applied to the LEC couples through the stray trap capacitance to the coil, causing a detected response that leads or lags the phase of the rf drive, depending on whether the drive is below or above the coil's resonance. This must be accounted for in the MNZ sequence in order to avoid a systematic error in the phase of the correction magnetron pulse caused by drifts of the coil's center frequency.

measured at the coil center, then a drift of the coil center frequency of only 1 Hz produces a 20° error in the phase of the correction pulse. This results in a maximum reduction of the common mode amplitude to 37% of its initial value. To deal with this, the MNZ system is designed to automatically calculate an adjustment to the measured phase based on the measured axial-coil detuning.

Another detail is that as the inner ion's axial motion is being cooled, its magnetron frequency might chirp through resonance with the outer ion's magnetron motion, causing momentary coupling. This is not a problem for the magnetron frequency shifts generated by the mistuning of V_{gr}, since the shifts proportional to $C_4 z^2$ and $C_4 \rho_{\mathrm{m}}^2$ have opposite signs. On the other hand, the magnetron frequency shift proportional to $C_6 z^4$ is fixed in sign and a crossing of the inner and outer magnetron frequencies can occur for a given sign of C_4. For the mistuning of V_{gr} typically used, this crossing would occur for axial amplitudes larger than the axial trap size, and so this is not a concern. However, there is no harm in choosing the sign of the V_{gr} mistuning to ensure that this magnetron frequency crossing cannot occur at any axial amplitude.

4.2.5 Axial Pulsing for Coarse Parking

The MNZ technique described above definitely improves our ability to load a pair of ions onto parked orbits, although it is difficult to precisely quantify due to low statistics. As will be discussed in a following section, techniques were discovered that allow us to fine

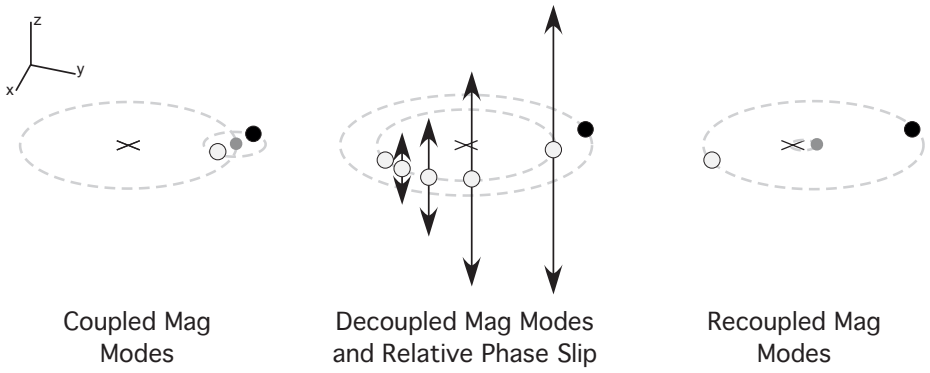

Figure 4-5: Cartoon Sequence of Magnetron Modes Decoupling and Recoupling. The magnetron modes are initially strongly coupled into a separation and common mode shown here with $\rho_{\rm com} \gg \rho_{\rm s}$. The white ion is driven to a large axial amplitude that in the presence of anharmonicities leads to decoupling into independent magnetron modes. The white ion gains phase relative to the black ion over the several seconds during which the axial motion damps. When the magnetron frequency shift becomes comparable to the radial Rabi frequency, the motions recouple as shown here with $\rho_{\rm s} \gg \rho_{\rm com}$.

tune the parking and so it has become less critical to park the ions during the make. In fact, in much of the final work, the original technique of simply placing the first ion on a 1 mm orbit and making the other ion in the center of the trap without any correction was used. In place of the precision tools of 2MagPulses and MNZ, we found that a hammer worked nicely to coarsely park the ions. The "hammer" turns out to be the bane of the other two techniques—large axial amplitudes. We found that if the ions were too close to one another (as indicated by large axial frequency chirping with axial amplitude due to the strong ion-ion interaction), then we could whack one of the axial modes so that the axial amplitude was a few mm. The axial frequency chirps several Hz due to the large axial amplitude and trap electrostatic anharmonicities, but remains close enough to the center frequency of the coil so that the motion would damp in several seconds. During this time, however, the trap anharmonicity also causes the magnetron frequency of that ion to shift by amounts proportional to $C_4 z^2$ and $C_6 z^4$. As described above, these shifts are large enough to decouple the magnetron motions, so that one ion can gain or lose phase in its magnetron motion with respect to the other ion depending on the signs of the anharmonicities. Figure 4-5 is a cartoon sequence of such an event. It was found that several repetitions of this blind whacking was sufficient to reduce the common mode amplitude and move the ions far enough apart for our fine tuning method to take over (Sect. 4.4.1).

The total phase lag or gain acquired by the axially excited ion can be approximated as the integral of the instantaneous magnetron frequency shift during the time period for which the ions are decoupled. The integral can be cut off when the instantaneous frequency shift becomes comparable to the magnetron Rabi frequency $2\pi\Delta f_{\rm m} = x\Omega_{\rm m}$ and the ions

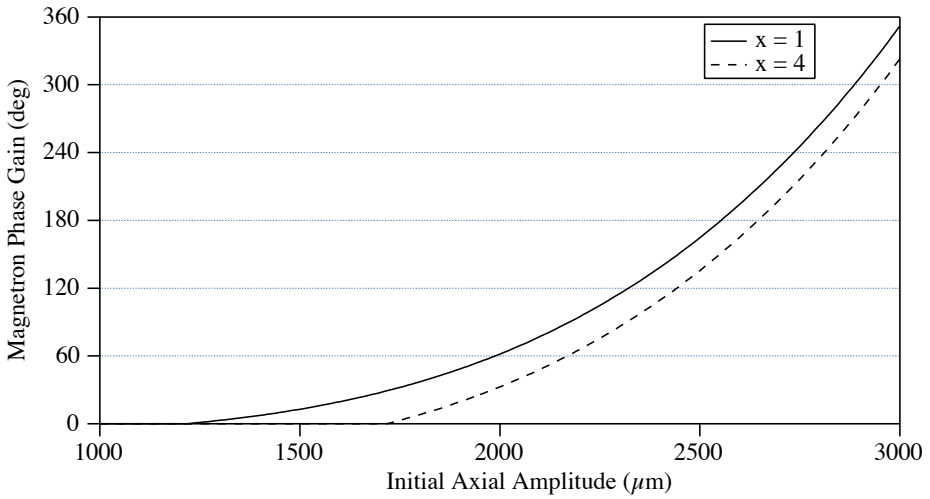

Figure 4-6: Estimated Magnetron Phase Gain versus Initial Axial Amplitude. The ion gains or loses phase with respect to the other ion due to an axially-dependent frequency shift of the magnetron mode. Typically, the axial motion would be excited to ~ 2700 μm corresponding to a phase shift near 180°. The phase is calculated for two cutoff values x where $2\pi\Delta f_{\rm m} = x\Omega_{\rm m}$ and using typical values for the axial damping time $\tau = 1$ s, the anharmonicities $C_4 = 0$, $C_6 = 8.3{\times}10^{-4}$, and for the magnetron Rabi frequency $\Omega_{\rm m}|_{\rho_{\rm s}=1\ {\rm mm}}$.

recouple. The exact choice of the cutoff factor $x > 1$ changes the calculated shift in detail, but not in its gross result, as shown in Fig. 4-6. Typically, when the ions appeared to be close to each other (as signified by their axial modes appearing extremely anharmonic at axial amplitudes of only a few 100 μm), the axial amplitude of one of the ions would be pulsed to ~ 2700 μm corresponding to nearly a 180° phase change, as depicted in Fig. 4-6.

We typically needed to use this hammer 2-5 times before the ions were sufficiently far enough apart from one another and the axial signals appeared harmonic and stable in time. We achieved similar results with dipping the pair close to the Lower Endcap, and believe that this is a result of a similar type of decoupling of the magnetron modes, although we have not attempted to carefully model this mechanism. There is some evidence that dipping slightly changes the total canonical angular momentum in the magnetron modes, but this observation is based on very low statistics.

4.3 Measurement of Magnetron Motion

The entire method of simultaneously comparing the cyclotron frequencies of two ions in a Penning trap depends on the correctness of the theoretically predicted mixing of the magnetron modes. This theory relies on approximations such as the linearization of the Coulomb interaction and ignoring various small terms at various stages of the calculations. These approximations seem quite "good" and "reasonable," but the question must be asked: "Do

the ions actually orbit in a manner described by our theory?" Since experimental validation of the theory is deemed so crucial to achieving accurate mass comparisons, much effort was expended in this cause.

What theoretical predictions might we test with experiment? The most obvious prediction to test is the mixing of the magnetron modes. Do the mixed magnetron modes actually beat against one another? One might also wish to see if the frequency with which the magnetron modes beat against one another scales like $1/\rho_s^3$ as predicted. Lastly, one would like to verify the predicted degree to which the modes do not completely mix. The answers to these various questions will be discussed in the following sections, but in summary the experimentally observed behavior is very well described by our two-ion theory described in Chap. 3.

Lastly, having experimentally confirmed the theory, we can rely on theoretical expressions for extracting parameters of interest such as the ion-ion separation ρ_s and the rms magnetron radius of each ion $\sqrt{\langle\rho_m^2\rangle}$. These parameters are crucial to mapping the systematic errors associated with trap imperfections and ion-ion interactions, both of which scale with large powers of the ion-ion separation.

4.3.1 Measuring the Relative Magnetron Phase

We can measure the relative phase between each ion's instantaneous magnetron motion as measured with respect to the center of the trap. If the ion-ion separation is not constant, then we expect the relative phase between the two magnetron motions to fluctuate in time. In the extreme case that the ions are not interacting, then we will expect the relative magnetron phase to vary by 2π over time scales of the inverse frequency difference between the two instantaneous magnetron frequencies, which is typically of order ~ 10 min.

To measure the relative magnetron phase, we perform simultaneous partial π-pulses between each ion's magnetron and axial modes. Each shot reduces the magnetron amplitude of each ion symmetrically and by only about 0.5% so that the measurements are only very slightly destructive. When the ions are in a parked orbit with the center of charge at the center of the trap, the measured difference of the two phases should be constant in time and equal to 180°. Figure 4-7 on the following page is an example of a series of such measurements. From a linear fit to the data, a limit on the relative frequency of rotation of the two magnetron vectors can be set at 5 ± 20 μHz. This is to be compared to the expected frequency difference of 1.4 mHz for the case of two completely noninteracting ions, which in Fig. 4-7 is represented by the dashed line. This is a direct and powerful piece of evidence that the ions are strongly coupled to one another and that the ion-ion separation is constant in time.

The standard deviation of 21° is consistent with typical measurement phase noise. However, one can also use this to set an upper limit on the ratio of the common and separation amplitudes. If one assumes that $\rho_s \gg \rho_{com}$, then it is easiest to view the motion in a frame

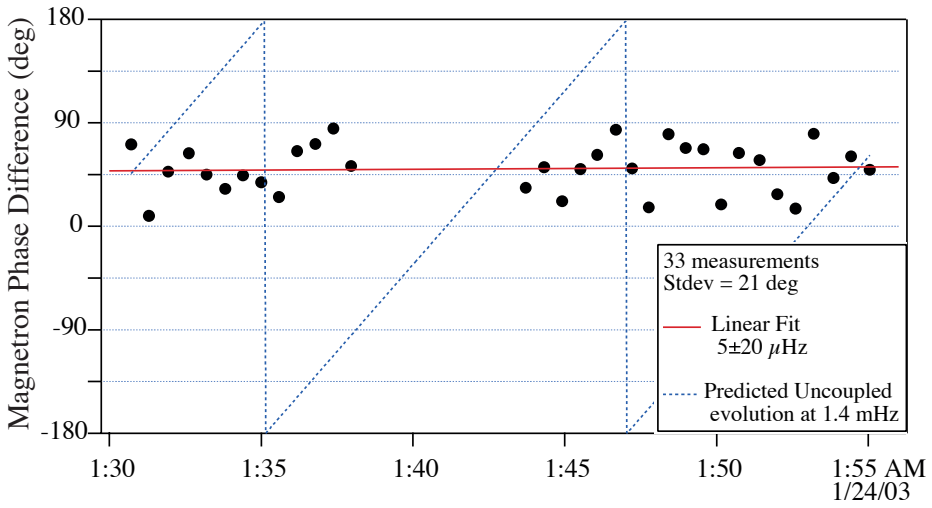

Figure 4-7: Measured Phase Difference between Magnetron Motion of CD_2^+ and CH_4^+ vs time. The relative phase of the motions is constant in time with a fitted drift 5 ± 20 μHz that is much less (by a factor > 70) than the uncoupled magnetron frequency difference of 1400 μHz. The expected evolution for uncoupled motion is superimposed for emphasis. The 21° standard deviation of the phase sets an upper limit on the ratio $(\rho_{\rm com}/\rho_{\rm s}) \leq 0.13$. The phase difference is not 180° for reasons discussed in the text.

rotating with the separation mode. Simple geometrical arguments then show that

$$\sqrt{\langle \delta\phi^2 \rangle} \approx 2 \left(\frac{\rho_{\rm com}/\sqrt{2}}{\rho_{\rm s}/2} \right) = 2\sqrt{2} \left(\frac{\rho_{\rm com}}{\rho_{\rm s}} \right) \tag{4.3}$$

where the ratio of the amplitudes is the small angle approximation to the arctangent, the leading factor of 2 comes from the fact that both ions are moving together, the $\sqrt{2}$ arises from the time average around one orbit, and the remaining factor of 2 expresses that the average magnetron radius is just half the separation distance $\rho_{\rm m} = \rho_{\rm s}/2$. Using the measured standard deviation of the difference phase 21°$= 0.37$ rad yields an upper limit on the ratio of normal mode amplitudes $(\rho_{\rm com}/\rho_{\rm s}) \leq 0.13$.

The measured phase difference in Fig. 4-7 does not equal 180° as it should in our model of the ions moving on a shared magnetron orbit but on opposite sides of the trap. This is true even after correcting for phase shifts associated with the frequency dependent phase response of the coil, the phase of the coupling drives, and the differential phase accumulated in the axial mode during the π-pulse. Ultimately, the discrepancy was traced to a mistake in the measurement of the relative phase offset between the sideband coupling synthesizers. A subsequent set of data in which the phase offsets were properly measured showed a phase difference of 172°, which is much closer to the expected 180°.

4.3.2 Measuring the Ion-Ion Separation ρ_s

As described in Sect. 3.3, the frequency with which the common and separation modes beat against one another is an extremely sensitive probe of the ion-ion separation because of the $1/\rho_s^3$ dependence of the beat period. We observe this beating by introducing a small electrostatic anharmonicity (C_4) set by the voltage on the Guard Ring electrode in addition to the fixed small anharmonicity C_6. This causes variation of each ion's axial frequency proportional to the second and fourth power of each ion's magnetron radius. Writing each ion's magnetron vector in terms of the normal modes $\vec{\rho}_{com}$ and $\vec{\rho}_s$ and assuming to first order that the masses are degenerate, then we can write

$$\frac{\Delta\omega_z}{\omega_z} = -\frac{3\ C_4}{2}\frac{\left(\tilde{L} \pm \vec{\rho}_s \cdot \vec{\rho}_{com}\right)}{d^2} + \frac{45\ C_6}{16}\frac{\left(\tilde{L}^2 \pm 2\tilde{L}\,\vec{\rho}_s \cdot \vec{\rho}_{com} + (\vec{\rho}_s \cdot \vec{\rho}_{com})^2\right)}{d^4} \tag{4.4}$$

with the + for ion 1 and the − for ion 0. The pseudo-angular momentum $\tilde{L} = \rho_{com}^2 + \frac{1}{4}\rho_s^2$ is approximately constant in time because of conservation of canonical angular momentum. It is useful to analyze this in terms of the frequency components of the modulation, so setting an overall arbitrary phase to zero we can substitute

$$\vec{\rho}_s \cdot \vec{\rho}_{com} = \rho_s \rho_{com} \cos\Omega_m t \tag{4.5}$$

to find

$$\frac{\Delta\omega_z}{\omega_z} = -\frac{3\ C_4}{2}\frac{\tilde{L}}{d^2} + \frac{45\ C_6}{16}\frac{\left(\tilde{L}^2 + \frac{1}{2}\rho_s^2\rho_{com}^2\right)}{d^4} \tag{4.6}$$

$$\pm\cos\Omega_m t \quad \frac{\rho_s\rho_{com}}{d^2}\left(\frac{3\ C_4}{2} + \frac{45\ C_6}{8}\frac{\tilde{L}}{d^2}\right) \tag{4.7}$$

$$+\cos 2\Omega_m t \quad \frac{45\ C_6}{16}\frac{\left(\tilde{L}^2 + \frac{1}{2}\rho_s^2\rho_{com}^2\right)}{d^4} \tag{4.8}$$

again with + for ion 1 and − for ion 0. Measuring the frequency with which the axial frequency of either ion is modulated directly determines the beat frequency Ω_m and hence the separation ρ_s from

$$\rho_s = \left(\frac{2q}{m\omega_c\Omega_m}\right)^{\frac{1}{3}} = \left(\frac{2c}{\Omega_m B_0}\right)^{\frac{1}{3}} \quad . \tag{4.9}$$

In addition, once the separation magnitude ρ_s is known, the amplitude of the frequency modulation of either ion determines the size of ρ_{com}. In the oft-encountered limit $\rho_{com} \ll \rho_s/2$, we find $\tilde{L} \approx \rho_s^2/4$ and

$$\frac{1}{\rho_{\rm com}} \approx \frac{\omega_{\rm z}}{\Delta\omega_{\rm z}}|_{\Omega_{\rm m}} \frac{\rho_{\rm s}}{d^2}\left(\frac{3\ C_4}{2} + \frac{45\ C_6}{32}\frac{\rho_{\rm s}^2}{d^2}\right) \quad . \tag{4.10}$$

The quantity $(\Delta\omega_{\rm z}/\omega_{\rm z})|_{\Omega_{\rm m}}$ signifies the amplitude of the axial frequency modulation at the beat frequency $\Omega_{\rm m}$, as a fraction of the total axial frequency.

We have observed frequency modulation of the axial motions using two independent techniques. The first technique will be referred to as the resolved sideband technique and is a frequency domain observation of this modulation. This technique works best when $\Omega_{\rm m}/2\pi > 0.20$ Hz or $\rho_{\rm s} < 650$ μm. For most of our work, $\Omega_{\rm m}/2\pi < 0.20$ Hz, and a time domain technique we call PhaseLock is used to monitor the instantaneous axial frequency as a function of time.

Resolved Sideband Technique

When several beat periods occur within the damping time of the axial mode, we are in the resolved sideband limit. Since our beat frequencies are ~ 19 s at $\rho_{\rm s}$=1 mm, this limit is best achieved at smaller separations or for damping times much longer than the typical resonant damping times of 1 s. Figure 4-8 is an example in which we tune the trap voltage such that ion 0's axial frequency is below the detector and ion 1's axial frequency is above the detector. Because the ions are symmetrically detuned from resonance, the damping times are each increased to $\tau = \tau^\circ\left(1+\delta^{*2}\right) = 150$ s where δ^* is the ion-detector detuning in units of HWHM of the detector resonance and τ° is the axial damping time when the ion is resonant with the detector ($\delta^* = 0$). The ion-ion separation is initially estimated to be at $\rho_{\rm s}$=550 μm, giving an expected beat period $T_{\rm b}$= 3.1 s. Initially, the common mode amplitude was close to zero, and then a 200 μm magnetron drive was applied to set $\rho_{\rm com}$=200 μm. The axial motion of each ion was then excited to 350 μm, and the resulting signal was monitored for 32 s. The power spectrum of the detected signal reveals that each ion signal has symmetric sidebands spaced $\sim 1/T_{\rm b}$ from the center frequency. We identify these as the $J_{\pm1}$ sidebands of our frequency modulated signals. There is more information contained in these signals, since we also expect that the difference frequency is modulated while the sum frequency is not. To see this, for signal to noise reasons we begin by taking a Fourier transform of our data (not a power spectrum!) and setting to zero the regions of frequency space far from our ion signals. The inverse Fourier transform is then taken, and the resulting filtered time data is squared. Squaring multiplies the time signal of the two ions, creating signals at the sum and difference frequencies. The prefiltering eliminates an extra background due to the detector noise profile. Looking near the sum frequency, we see a single unmodulated peak, while near the difference frequency we see a frequency modulated signal with the sidebands larger than the fundamental. This confirms the prediction that the two axial modes are frequency modulated out of phase with one another.

A beat period of $T_{\rm b}$= 3.6 s is predicted from half the frequency difference between the

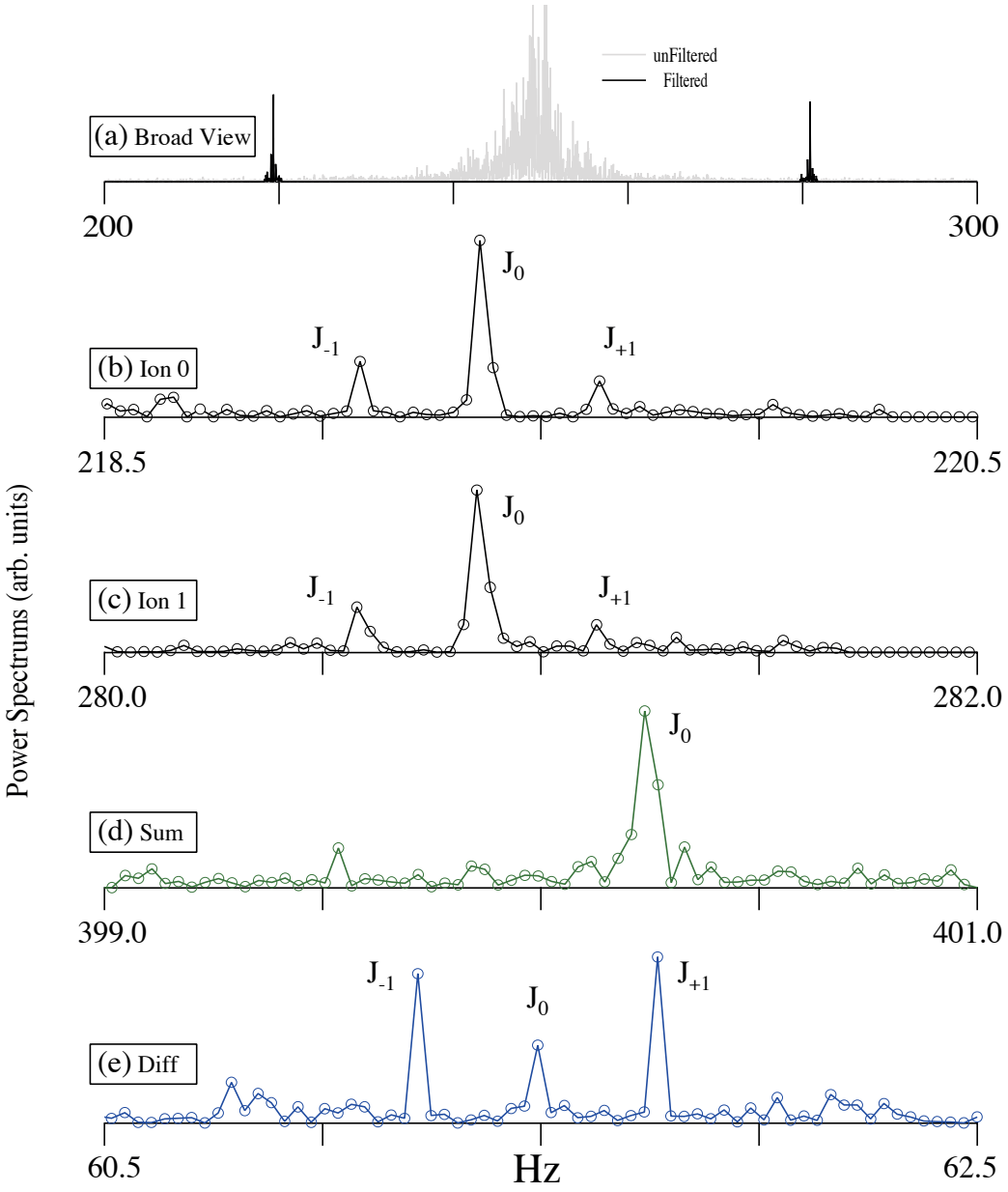

Figure 4-8: Modulation of the axial frequencies at the magnetron beat frequency in the resolved sideband limit. (a) Broad power spectrum showing symmetric detuning of ions and with respect to the detector. After a filtering stage, only the black region remains in the time domain data. (b, c) The power spectrum of each ion with clearly resolved $J_{\pm 1}$ sidebands. After squaring the time data to beat one signal against the other, the power spectrum near (d) the sum frequency (shifted by a fixed amount for technical reasons) shows a single peak indicating no modulation. (e) The power spectrum near the difference frequency shows strong FM modulation. This demonstrates that the axial frequency modulation of the two ions is out of phase as is expected (see text).

upper and lower sidebands. This beat period corresponds to an ion-ion separation of ρ_s= 580 μm. This is in good agreement with our initially predicted value of ρ_s= 550 μm or a beat period of 3.1 s. From the amplitude ratio of the sidebands to the fundamental we predict a modulation index of 1.7, or given the sideband spacing, a 0.92 HzPP frequency modulation amplitude. Using ρ_{com}= 200 μm, ρ_s= 580 μm, and the known values of C_4 and C_6, the predicted peak-to-peak frequency modulation is 0.74 HzPP, in good agreement with our observation.

The resolved sideband technique was not extensively used because of an additional advantage of the PhaseLock technique to be discussed below. In addition, we have shown one of the better detected signals. The shot-to-shot reproducibility was a little lacking. It might be interesting in the future to use the passive shorting of noise currents in the detector by the ion to detect this modulation at the thermal axial amplitudes. For instance, one could listen to the detected signal for several 100 s, break the data into chunks of 32 s, and take an average of the power spectrums of the filtered time data. Using the filtering-squaring technique to just look at the difference frequency would have the advantage of eliminating trap voltage drifts during the data acquisition. This would provide a nice comparison with the ion-ion separations measured at finite axial amplitudes using PhaseLock.

Frequency Modulation in Time Domain

With two ions in the trap, we can use the PhaseLock system described in Sect. 2.3.3 to continuously monitor the instantaneous axial frequency of one of the ions, as shown in Fig. 4-9. A power spectrum of the measured instantaneous axial frequency (Fig. 4-10) shows a clear peak that we identify as the beat frequency between the new normal-mode magnetron motions. This frequency modulation is not an artifact of the PhaseLock feedback loop, since we do not observe this behavior with a single ion in the trap, and the size of the observed frequency modulation depends on the Guard Ring voltage.

Figure 4-10 shows the high signal to noise with which we can measure the modulation frequency. We can measure the modulation frequency to a few percent, yielding three times the relative precision for the ion-ion separation ρ_s since $\Omega_m \propto \rho_s^3$. The second power spectrum is of the detected axial amplitude squared and shows a clear peak that is a result of the finite gain of the PhaseLock feedback loop. The important consequences of this axial *amplitude* modulation will be discussed in Sect. 4.4.1.

Figure 4-11 is an example in which $\rho_{com} \sim \rho_s/2$ and the Guard Ring voltage has been tuned to near fzOpt. Under these conditions we observe a strong harmonic of the beat frequency. We find that we can enhance or suppress either the fundamental or harmonic by simply varying the Guard Ring voltage (and hence C_4). But Eq. 4.8 predicts that the strength of the harmonic should not be affected by C_4. A careful examination of the magnetron orbits in an anharmonic trap might account for this behavior. When $\rho_{com} \ll \rho_s/2$, we do not observe such an harmonic.

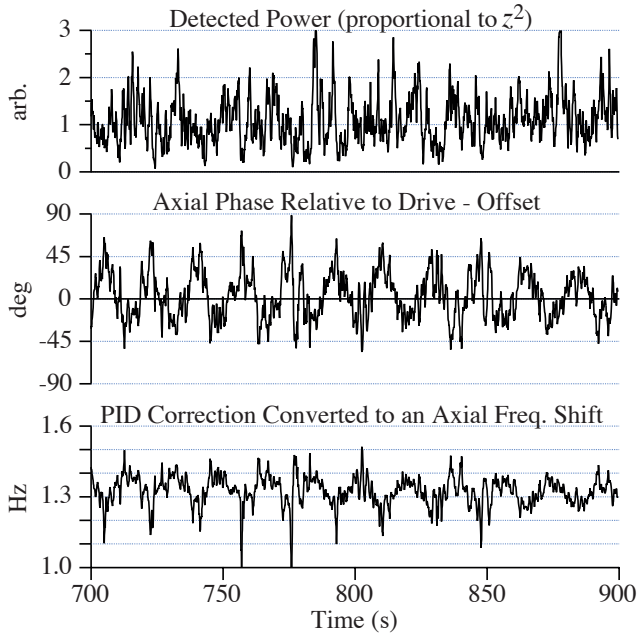

Figure 4-9: Example PhaseLock signals for measuring the instantaneous axial frequency versus time. The large amplitude of frequency modulation and the finite gain of the feedback loop leads to large excursions of the phase from the set point of zero. This in turn leads to a modulation of the power that can almost be detected by eye and is obvious in the lower power spectrum of Fig. 4-10.

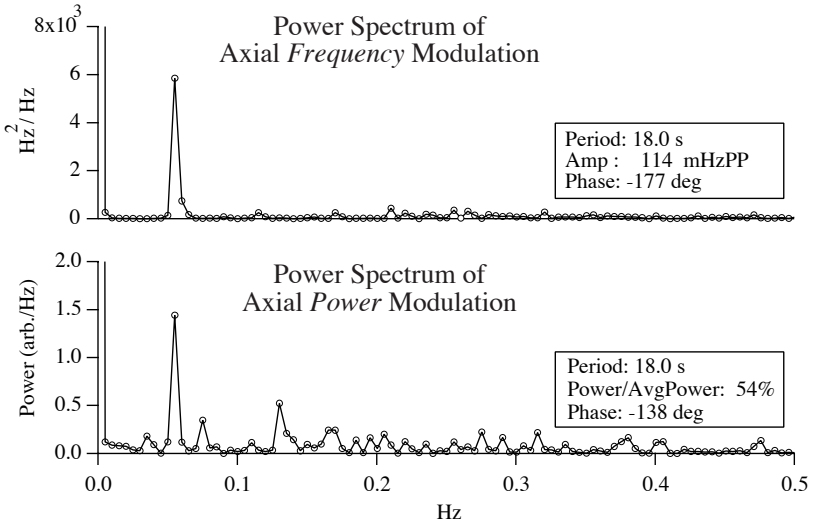

Figure 4-10: Example Power Spectrums of the detected axial frequency modulation and axial power modulation (i.e., modulation of z^2). The axial frequency versus time was determined from the PID feedback signal in PhaseLock. The axial power or z^2 versus time was determined from the detected axial power in PhaseLock. The beat frequency between the separation and common magnetron modes is determined by a fit to the peak. The axial power is also modulated at the beat frequency due to the finite gain of the feedback loop.

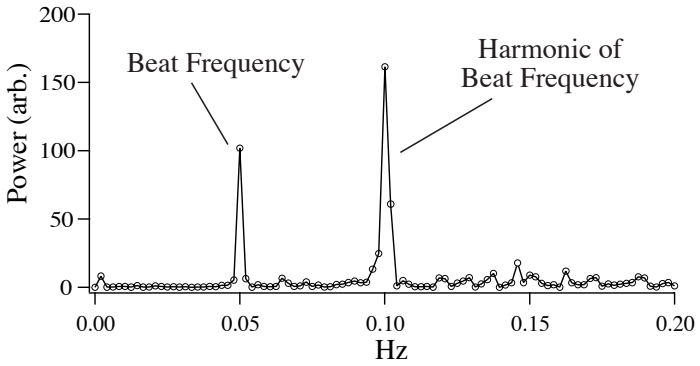

Figure 4-11: Generation of Harmonic with $\rho_{\rm com} \sim \rho_{\rm s}/2$ and Guard Ring voltage $V_{\rm gr}$ tuned near fzOpt.

Systematic Errors on $\rho_{\rm s}$

The ion-ion separation $\rho_{\rm s}$ can be inferred from the frequency modulation of the axial mode over most of the range of interest with an accuracy of $\leq 4\%$. The accuracy is limited by uncertainties on the systematic perturbations of the measured beat frequency. The systematic perturbations arise from the finite axial amplitude of $z \approx 250$ μm needed to perform the measurement of the beat frequency, and from the impact of the trap electrostatic anharmonicities C_4 and C_6 on the magnetron dynamics. The perturbations are typically $\leq 20\%$ of the beat frequency and thus give an error of $\leq 7\%$ on the ion-ion separation $\rho_{\rm s}$. Lastly, using our knowledge of the anharmonicities and axial amplitudes, we can conservatively correct for these perturbations to better than 50%. The perturbation arising from a finite axial amplitude ($z_0 = 0$, $z_1 \neq 0$) is discussed in Sect. 3.6.1 and is the dominant perturbation for $\rho_{\rm s} < 1000$ μm. The effect of magnetic field inhomogeneity can be ignored because the magnetic field is better represented as uniform than the electrostatic field is as a pure quadrupole potential.

The perturbation of the beat frequency $\Omega_{\rm m}$ due to electrostatic anharmonicities dominates for $\rho_{\rm s} > 1100$ μm. To calculate these shifts to lowest order, we can assume that the ions are of equal mass and write down the equations of motion for the sum and difference mode as in Eq. 3.24, but with the extra forces due to electrostatic anharmonicities included. All single particle magnetron motions $\vec{\rho}_{\rm m0}$ and $\vec{\rho}_{\rm m1}$ are then expressed in terms of the normal mode sum and difference motions $\vec{\rho}_{\rm s}$ and $\vec{\rho}_{\rm com}$. The frequency shift of each mode can be calculated following the prescription of Sect. 2.2.2, in which the zeroth order magnetron motions are used to calculate the average radial force around one orbit. This averaged force gives rise to a frequency shift of the normal modes. The perturbation of the beat frequency is the difference between the perturbations of the difference and sum modes

$$
\begin{aligned}
\Delta\Omega_{\rm m} &= \Delta\left(\omega_{\rm ms}-\omega_{\rm mc}\right) \\
&= -\omega_{\rm m}\frac{3C_4}{2}\frac{\rho_{\rm com}^2-\frac{1}{4}\rho_{\rm s}^2}{d^2} \\
&\quad +\omega_{\rm m}\frac{15C_6}{8}\frac{\left(\rho_{\rm com}^2-\frac{1}{4}\rho_{\rm s}^2\right)}{d^2}\left(\frac{2\left(\rho_{\rm com}^2-\frac{1}{4}\rho_{\rm s}^2\right)+3\left(z_1^2+z_0^2\right)-3\left(\rho_{\rm c1}^2+\rho_{\rm c0}^2\right)}{d^2}\right) \quad .^{\S}
\end{aligned}
$$

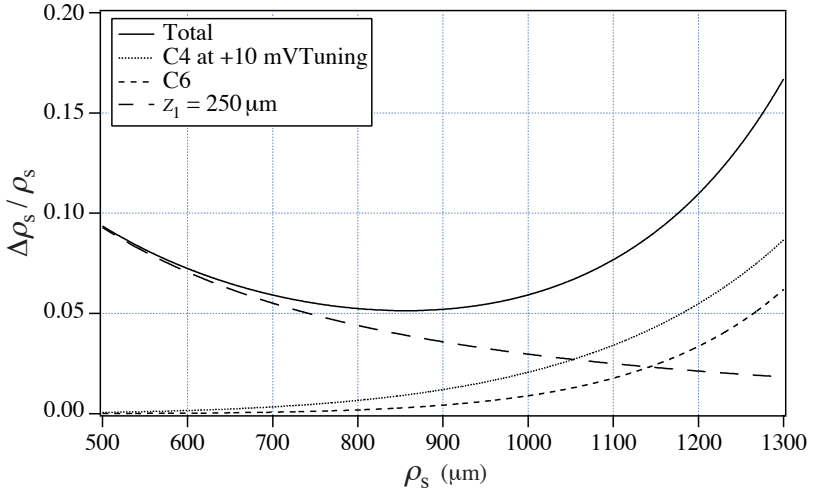

Figure 4-12: Fractional systematic error $\Delta\rho_{\rm s}/\rho_{\rm s}$ on measurement of ion-ion separation $\rho_{\rm s}$ from measurement of the beat frequency between the magnetron normal modes. The three sources of perturbation are the finite axial amplitude of one of the ions for detection purposes and the electrostatic anharmonicities C_4 and C_6. The size and sign of the perturbation due to C_4 can be varied by changing the voltage on the Guard Ring electrodes, and the worst case is shown in which all three sources add. We correct for the error caused by these perturbations, leaving a net error of less than 50% of the total shown.

Figure 4-12 shows the predicted systematic errors on $\rho_{\rm s}$ using the measured anharmonicities of Table 2.1 for a trap tuned for mass 28 u ions, a typical $V_{\rm gr}$ corresponding to 10 mVTuning and axial amplitudes $z_1 = 250$ μm, $z_0 = 0$. The sign and magnitude of

[§] Although not of interest here, the perturbation of the sum of the two normal mode magnetron frequencies is given by

$$
\begin{aligned}
\Delta\left(\omega_{\rm ms}+\omega_{\rm mc}\right) &= -\omega_{\rm m}\frac{3C_4}{2}\frac{3\left(\rho_{\rm com}^2+\frac{1}{4}\rho_{\rm s}^2\right)-2\left(z_1^2+z_0^2\right)+2\left(\rho_{\rm c1}^2+\rho_{\rm c0}^2\right)}{d^2} \\
&\quad +\omega_{\rm m}\frac{15C_6}{8}\left(\frac{4\rho_{\rm com}^4+3\rho_{\rm com}^2\rho_{\rm s}^2+\frac{1}{4}\rho_{\rm s}^4}{d^4}+\frac{9\left(\rho_{\rm com}^2+\frac{1}{4}\rho_{\rm s}^2\right)\left(\rho_{\rm c1}^2+\rho_{\rm c0}^2-z_1^2-z_0^2\right)}{d^4}\right. \\
&\qquad \left.+\frac{3\left(\rho_{\rm c1}^4+\rho_{\rm c0}^4-4\rho_{\rm c1}^2z_1^2-4\rho_{\rm c0}^2z_0^2+z_1^4+z_0^4\right)}{d^4}\right) \quad .
\end{aligned}
$$

the perturbation due to C_4 can be varied by changing $V_{\rm gr}$, and a worst case example was chosen in which all three perturbations add. Using our knowledge of the anharmonicities and axial amplitudes, we correct for these perturbations with uncertainties less than 50%, yielding a final uncertainty on $\rho_{\rm s}$ of $\leq 4\%$ for most of the range of interest. This correction is actually performed immediately on the results of the fitting routines in the PhaseLock software, allowing the user a more definite knowledge of $\rho_{\rm s}$.

Experimentally, we find the measured beat frequency and ion-ion separation is less sensitive to variations of the Guard Ring tuning as a result of our corrections. For example, we measure "raw" beat periods of 21.7 and 29.6 s at the same ion-ion separation but for Guard Ring tunings differing by 37.1 mV. After iteratively applying our corrections to obtain more and more accurate estimates of the ion-ion separation $\rho_{\rm s}$, we predict unperturbed beat periods of 25.2 and 25.6 s respectively or identical separations of 1110 μm to within significant digits. Although this was a randomly chosen example from experimental data, this agreement is better than we usually observe. Our typical quoted final uncertainty on $\rho_{\rm s}$ of $\sim 4\%$ seems slightly conservative but perhaps by only a factor of 2.

4.3.3 Measuring the RMS Magnetron Radius $\sqrt{\langle \rho_{\rm m}^2 \rangle}$

The root-mean-square magnetron radius of each ion can be determined from the derivative of the axial frequency with respect to C_4. The precision of the measurement is typically a few percent. Specifically, we measure the variation of the dc axial frequency (i.e., the axial frequency averaged over several periods of $\Omega_{\rm m}$) with respect to variation of the Guard Ring voltage $V_{\rm gr}$, which is related to a variation of C_4 by Eq. 2.34 and our knowledge of the Guard Ring's geometric coefficient D_4. Using Eq. 2.52, we can relate a change in the dc axial frequency to a change in C_4 by

$$\frac{\delta \langle f_{\rm z} \rangle}{\delta C_4} = -f_{\rm z} \frac{3}{2} \frac{\langle \rho_{\rm m}^2 \rangle}{d^2} \quad . \tag{4.11}$$

The time averaging is performed using PhaseLock to continuously measure the instantaneous axial frequency over several beat periods. For a fixed amount of angular momentum in the magnetron modes, it is simple to show that the rms magnetron radius $\sqrt{\langle \rho_{\rm m}^2 \rangle}$ of each ion is independent of how the angular momentum is distributed between the common and separation modes. In addition, the rms radius of each ion should be the same up to the finite mass difference correction $\delta_{\rm mag}$.

To calibrate out two small effects, we do not actually rely on Eq. 4.11 to measure the rms magnetron radius. First, we perform the axial frequency measurement at a finite axial amplitude of ~ 250 μm. The presence of a C_6 can then provide a quadratic dependence on magnetron radius since it also has an axial frequency shift that scales as $z^2 \rho_{\rm m}^2$. Second, when we change the Guard Ring voltage $V_{\rm gr}$, we not only change C_4, but we also slightly change C_2. This contributes an offset to the derivative $\delta \langle f_{\rm z} \rangle / \delta V_{\rm gr}$ that does not depend on

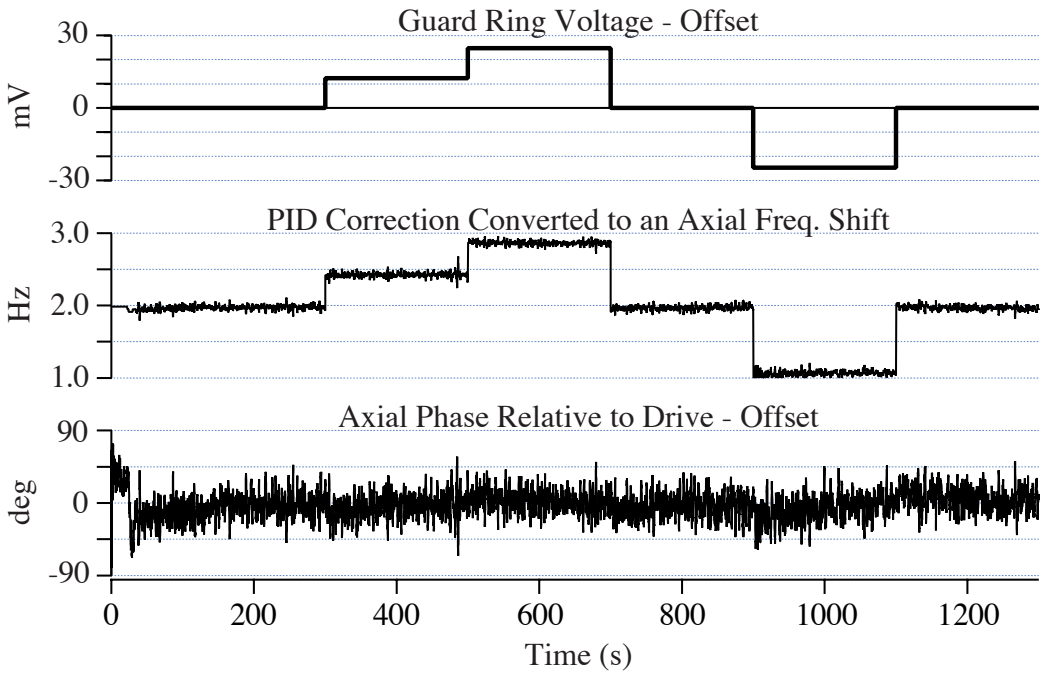

Figure 4-13: Variation of Axial Frequency with Guard Ring voltage for a single ion with $\rho_{\rm m}$= 700 μm.

magnetron radius.

To account for these two effects, we perform an independent calibration with a single ion in the trap by measuring its axial frequency variation $\delta\langle f_{\rm z}\rangle/\delta V_{\rm gr}$ versus $\rho_{\rm m}$. Figure 4-13 is an example in which the ion is cooled to zero magnetron radius and then driven to $\rho_{\rm m}$= 700 μm.[¶] The axial frequency is then measured versus the Guard Ring voltage $V_{\rm gr}$. As shown in Fig. 4-13, the axial frequency variation is a few Hz full scale. To maintain lock at each of the jumps in $V_{\rm gr}$, a coarse estimate of $\delta\langle f_{\rm z}\rangle/\delta V_{\rm gr}$ is used to apply an initial correction voltage to the Ring at each jump. The feedback system is allowed to relax to its set point for $\sim$ 100 s before measuring the axial frequency change. The average error signal over the measurement interval is used to provide an additional single-shot correction to the measured axial frequency. This process is then repeated for different values of $\rho_{\rm m}$, and the measured values of $\delta\langle f_{\rm z}\rangle/\delta V_{\rm gr}$ are plotted versus $\rho_{\rm m}$ as shown in Fig. 4-14. With two ions in the trap, the ions are normally between $\rho_{\rm m} \approx \rho_{\rm s}/2$ =300 and 600 μm.
The data are well described by a parabola with a vertical offset

$$\frac{\delta\langle f_{\rm z}\rangle}{\delta V_{\rm gr}} = a + c\rho_{\rm m}^2 \tag{4.12}$$

[¶]The magnetron drive calibration used in this discussion results from a cross calibration with the cyclotron drive calibration. The cyclotron drive strength in turn was calibrated to $\sim$ 3% by measuring the relativistic shift of the cyclotron frequency versus cyclotron amplitude for ions with very large cyclotron frequencies. This will be discussed in more detail shortly.

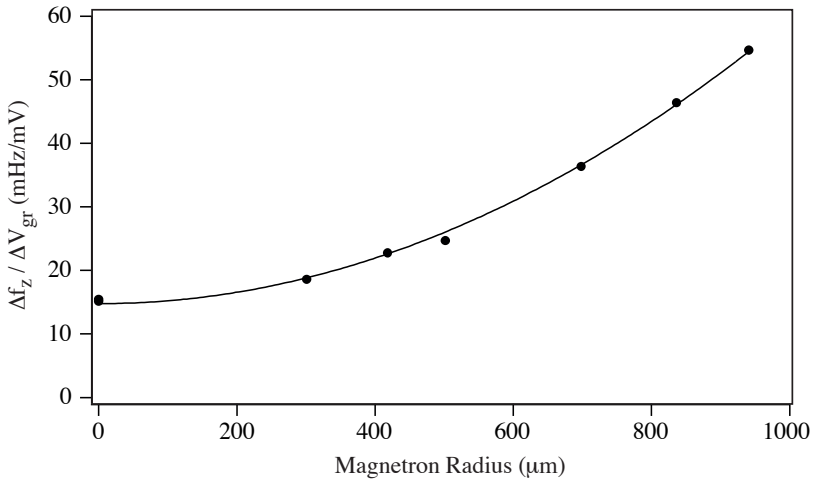

Figure 4-14: Calibration of $\Delta f_z/\Delta V_{gr}$ versus magnetron radius using a single ion in the trap.

with typical values at mass 28 u for the offset $a = 15$ mHz/mV and curvature $c = 0.46$ mHz/$\left(\text{mV} \times (100\mu\text{m})^2\right)$ with typical precisions on these quantities of $\sim 1\%$. It is important to know the offset with good relative precision because it is responsible for the majority of the axial frequency shift at small magnetron radii. For instance, at ρ_s= 700 μm and ρ_{com}=0, the curvature term accounts for only 1/4 of the total axial frequency shift versus V_{gr}. This limits our accuracy at small ρ_s to $\sim 4\%$. As shown in the next Sect. 4.3.4, the shot-to-shot noise in the measurement of the rms radius $\sqrt{\langle\rho_m^2\rangle}$ of each ion is typically several percent.

4.3.4 Comparing ρ_s and $\sqrt{\langle\rho_m^2\rangle}$

The measured ion-ion separation ρ_s should equal the twice the rms magnetron radius $\sqrt{\langle\rho_m^2\rangle}$ when $\rho_s \gg \rho_{com}$. Figure 4-15 shows this agreement for 50 measurements of ion 0 ($^{13}C_2H_2^+$) and 36 measurements of ion 1 (N_2^+). For these measurements, it is expected that $\rho_{com}/\rho_s \leq 0.10$, and the two quantities should be equal to order $(\rho_{com}/\rho_s)^2 \leq 0.01$. The nice linear dependence indicates that we are correctly interpreting the axial frequency modulation as arising from the beating of the magnetron normal modes.

The deviation of the slope from unity is believed to be indicative of an error in the magnetron drive calibration that enters into the rms radius measurements. A similar comparison using CD_2^+ and CH_4^+, using the same drive calibration technique as in the first comparison, predicts different values of the geometric coefficients D_4 and B_2. Geometric coefficients ought not to change with trap voltage V_r or m/q, and so we conclude that our calibration is incorrect. If the measured slope of $2 \times \sqrt{\langle\rho_m^2\rangle}$ versus ρ_s is used to rescale the drive calibration, we find that D_4 and B_2 are constant to within errors over the range of m/q = 16 to 33 u/e. We currently trust this new method for calibrating our drive strengths and believe it is accurate to $\sim 5\%$.

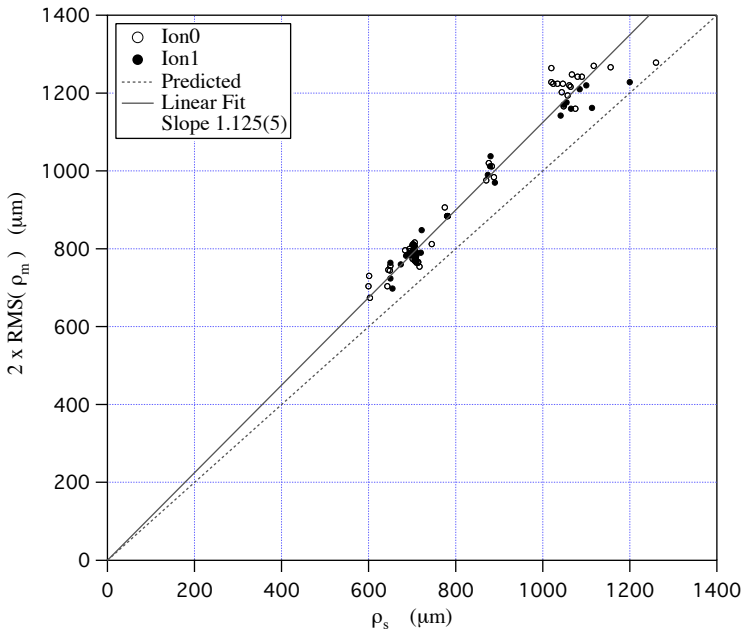

Figure 4-15: Plot of $2 \times \sqrt{\langle \rho_{\rm m}^2 \rangle}$ versus $\rho_{\rm s}$. The self-consistency between the measurements indicates that we are properly interpreting the data. In each case, the measurements were performed with $\rho_{\rm com}/\rho_{\rm s} \leq 0.1$ so that the expected slope should be 1 to better than 0.01. The discrepancy is assigned to a 12% error in our magnetron drive calibration.

4.3.5 Radial Drive Calibrations

The magnetron drive calibration, believed to be in error above, results from a chain of measurements ultimately relating to a cyclotron drive calibration based on the measured relativistic shift of the cyclotron frequency versus cyclotron amplitude for Ne^{++} and Ne^{+++}.[‖] A typical cyclotron calibration is $\rho_{\rm c}^{\rm cal} = 25.7\ \mu{\rm m}/({\rm ms} \times {\rm Vpp})$ so that if one applies a cyclotron drive of nominally 200 mVpp from the synthesizer for 20 ms the final cyclotron radius is $\rho_{\rm c}$= 103 μm.

However, the transfer functions of the cryoelectronics, the amplifiers, and the synthesizer voltage calibration are frequency dependent. As a result, the calibrations for ions of different m/q are not the same. We do expect that the ratio of the coefficients relating the quadrupole coupling field (used to generate a cyclotron to axial π-pulse) and dipole driving field for a given voltage on the Guard Ring electrode is fixed by the trap geometry and is independent of frequency in our quasi-electrostatic regime. Because the axial-cyclotron coupling differs from the cyclotron drive frequency by just the axial frequency and $\omega_{\rm c} \gg \omega_{\rm z}$, we can calibrate out the frequency dependence of our system by measuring the Rabi frequency at a nominal synthesizer voltage.

Using this method to calibrate out any frequency dependencies, we found that the two

[‖]See Simon Rainville's thesis [1][G] for a more complete discussion of the topic of this section.

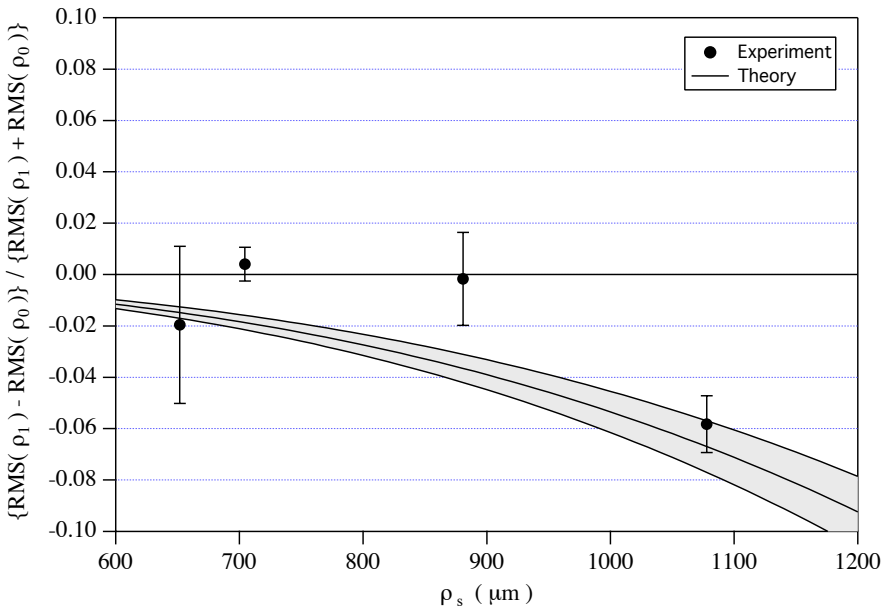

Figure 4-16: The measured fractional imbalance $\delta_{\rm mag}$ in the rms magnetron radii versus $\rho_{\rm s}$ as determined from measurements of the axial frequency variation with Guard Ring voltage. Included is the theoretical prediction with 15% uncertainty bands resulting from 5% uncertainty on $\rho_{\rm s}$.

independent cyclotron drive strength calibrations for Ne^{++} and Ne^{+++} agreed to 3%, and this is the quoted error on our relativistic cyclotron calibration. The calibration was then scaled to other m/q such as 28 u/e using the same procedure of comparing Rabi frequencies. The magnetron drive calibration was then obtained by comparing the size of axial excitation after alternating cyclotron and magnetron PNPs.

The measured geometrical coefficients D_4 and B_2 appear to vary linearly over the range of $m/q = 16$ to 33 u/e at which they are measured. The values change by about $\sim 50\%$ over this range. The variation is experimentally significant since it represents $\sim 5\sigma$ deviation away from simply constant values. We have no explanation for why this is so. If instead we rely on the determination of $\rho_{\rm s}$ as inferred from the frequency modulation of the axial mode, then the comparison of $\rho_{\rm s}$ versus $2 \times \sqrt{\langle \rho_{\rm m}^2 \rangle}$ is a way to calibrate the magnetron drive strength and in turn the cyclotron drive strength at each m/q independently. When this is performed, the values of the geometrical coefficients D_4 and B_2 are constant to within errors at all measured mass to charge ratios $m/q = 16$ to 33 u/e. For this reason, we presently rely on the measured slope of $2 \times \sqrt{\langle \rho_{\rm m}^2 \rangle}$ versus $\rho_{\rm s}$ to calibrate our radial drive strengths.

4.3.6 Measuring the Magnetron Radius Imbalance $\delta_{\rm mag}$

For an accurate comparison of cyclotron frequencies, it is critical that the ions have very similar rms magnetron radii so that the effect of trap field imperfections will be common

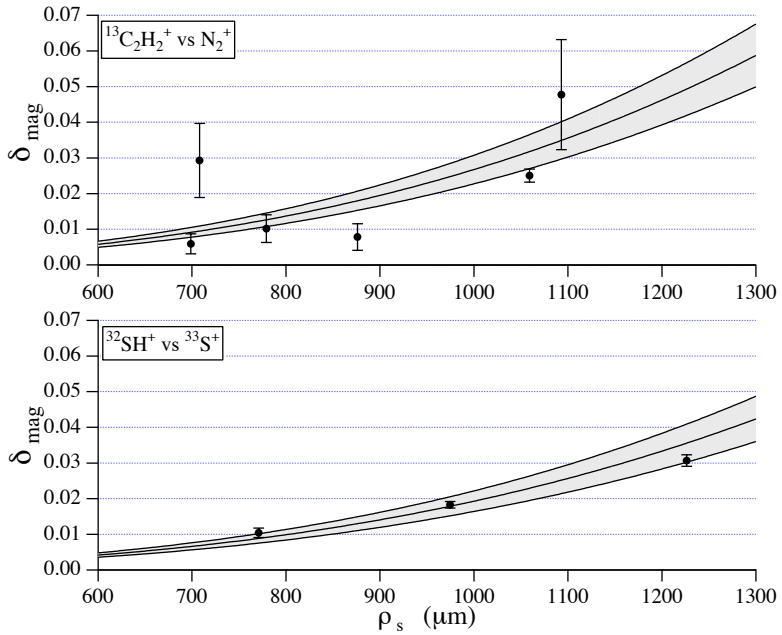

Figure 4-17: Measured fractional imbalance $\delta_{\rm mag}$ in the rms magnetron radii versus $\rho_{\rm s}$. The measured $\delta_{\rm mag}$ is determined from the variation of the cyclotron frequency ratio R with Guard Ring voltage and using Eq. 4.15. The predicted values are included with 15% uncertainty bands resulting from 5% uncertainty on $\rho_{\rm s}$.

to both cyclotron modes and will cancel when the ratio of frequencies is taken. For ions with slightly different masses, the fractional difference in the rms magnetron radii can be calculated from the parameterization of the magnetron amplitudes as

$$\vec{\rho}_{\rm m0} = -\frac{\vec{\rho}_{\rm s}}{2}\,(1+\delta_{\rm mag}) \tag{4.13}$$

$$\vec{\rho}_{\rm m1} = \frac{\vec{\rho}_{\rm s}}{2}\,(1-\delta_{\rm mag}) \quad . \tag{4.14}$$

where we have taken $\rho_{\rm com} = 0$ and the usual convention $m_0 > m_1$. The predicted value of $\delta_{\rm mag}$ from Eq. 3.35 is $\delta_{\rm mag} = \eta\bar{\omega}_{\rm m}^2/(2\Omega_{\rm E}^2)$ (also see Sect. 3.3.2.) Binning the rms magnetron data of Fig. 4-15 by ion type and $\rho_{\rm s}$, we can determine the fractional difference in the rms magnetron radii versus $\rho_{\rm s}$ with the results shown in Fig. 4-16. The data are noisy, and the agreement with theory is only good at the largest ion-ion separation. The good news of course is that the measured imbalances have the predicted sign and are not larger in magnitude than what is predicted by our theory.

A more precise way to observe this magnetron radius imbalance is to measure the trap cyclotron frequency difference $\omega_{\rm ct2}$ versus C_4 at a fixed $\rho_{\rm s}$. As can be shown from Eq. 2.50, the cyclotron frequency difference varies with magnetron radius by an amount $\Delta\omega_{\rm ct2} = 3\bar{\omega}_{\rm m}C_4(\rho_{\rm m1}^2 - \rho_{\rm m0}^2)/d^2$.

Over the several days to weeks it takes to perform this measurement, the average magnetic field and trap voltage changes from day to day. To eliminate these small effects, it is best to actually compare the variation of the cyclotron frequency ratio with C_4, $\delta R/\delta C_4$. The variation of the ratio R is dominated by the fractional variation of the trap cyclotron frequency difference versus C_4, with other contributions such as axial frequency variation with C_4 being negligible. Using the expression of 2.2.4 for the variation of the cyclotron frequency with C_4 and defining the mass ratio as $R = m_0/m_1$, it is straightforward to show that

$$\delta_{\rm mag} = \frac{1}{3}\frac{d^2}{\rho_{\rm s}^2}\frac{\omega_{\rm c}}{\omega_{\rm m}}\left(\frac{\delta R}{\delta C_4}\right) \quad . \tag{4.15}$$

The variation of C_4 is simply related to the variation of the Guard Ring voltage $V_{\rm gr}$ using Eq. 2.34.

Figure 4-17 shows the computed values of $\delta_{\rm mag}$ from measurements of $\delta R/\delta C_4$ (and using Eq. 4.15) for the pairs $^{13}C_2H_2^+$ vs N_2^+ and $^{32}SH^+$ vs $^{33}S^+$. The predicted values of $\delta_{\rm mag}$ are included along with 15% uncertainty bands due to a 5% uncertainty on $\rho_{\rm s}$. The good agreement between prediction and experiment means that we can accurately predict the size of the systematic errors associated with trap electrostatic anharmonicities and magnetic field inhomogeneities.

4.4 Control of Magnetron Motion

In the preceding section we have demonstrated the ability to carefully measure the dynamics of the coupled magnetron motions for two ions in the Penning trap. We now turn our attention to *controlling* the magnetron motion. This will include the ability to both increase and decrease the ion-ion separation $\rho_{\rm s}$ and reduce the size of $\rho_{\rm com}$. An important part of this control, already discussed in Sect. 4.2.5, is the ability to move the ions apart from one another by creating a large axial excitation of one of the ions. Having done this, the control technique discussed below can be used to fine tune the parking of the ions. Along the way, we will show that we can also measure the common mode amplitude $\rho_{\rm com}$ from the amplitude of the axial frequency modulation arising from the magnetron mode beating.

4.4.1 Coupling the Collective Magnetron Modes $\rho_{\rm com}$ and $\rho_{\rm s}$

We have serendipitously discovered a technique to resonantly and reversibly couple the common mode and the separation mode to one another. The mathematical form of the coupling is quite similar to that of a standard classical Rabi problem such as our resonant coupling of the axial and cyclotron modes. The main difference is that the coupling rates are proportional to the canonical angular momentum in each mode, so that the coupling shuts itself off as either mode amplitude goes to zero.

To understand this coupling of the mixed modes, it is important to clearly understand the separation of time scales of the various couplings in our two-ion system. On time scales short compared to the swapping motion $\Delta t \ll 2\pi/\Omega_{\rm m}$, the magnetron motions appear to be independent of one another, and one should describe the motion in terms of the single particle amplitudes $\vec{\rho}_{\rm m0}$ and $\vec{\rho}_{\rm m1}$. On time scales comparable to the swapping motion $\Delta t \sim 2\pi/\Omega_{\rm m}$, the dc Coulomb force between the ions completely mixes the magnetron modes, and one should think in terms of the collective common and separation modes $\vec{\rho}_{\rm com}$ and $\vec{\rho}_{\rm s}$. For time scales much larger than the swapping motion $\Delta t \gg 2\pi/\Omega_{\rm m}$, one should think of the collective mode amplitudes as slowly varying in time. To intuit the behavior of our coupled two-ion system, it is important to know which time scale is relevant.

To accomplish this coupling, a fixed-frequency axial drive is applied just above or below resonance with one of the ions. When electrostatic anharmonicity is present, the detuning of the axial mode from the drive is modulated at the beat frequency between the normal modes. In practice, the PhaseLock system is used to hold the average detuning constant, but the finite gain of the feedback loop means that the frequency modulation is not completely suppressed. The axial *frequency* modulation in turn produces axial *amplitude* modulation. The axial *amplitude* modulation combined with the electrostatic anharmonicity generates a *frequency* modulation of the instantaneous *magnetron frequency*. One can picture this as creating a phase advance or lag of the ion's motion with respect to the other ion as measured from the center of the trap. This phase advance or lag is modulated at the beat frequency between the modes. If it occurs when the ions are at the same magnetron radius $\rho_{\rm m0} = \rho_{\rm m1}$, this will lead to the ion either catching up or losing ground with respect to the other ion. By controlling the magnitude of C_4 and the sign of the magnetron frequency modulation by placing the drive above or below resonance, we can control the coupling rate and whether canonical angular momentum is transferred from the common to the separation mode or the reverse.

Before giving a detailed explanation of this mechanism, let us discuss how we observe that this coupling is occurring. This will also show that we can accurately determine the common mode amplitude from the amplitude of the observed axial frequency modulation. We will then turn to a qualitative discussion of the coupling mechanism followed by a more quantitative explanation. In order to follow the discussion below, see the preceding Sect. 4.3.2.

Observation

We observe the coupling of the mixed magnetron modes via three signals. We can observe changes in the ion-ion separation (1) by monitoring the magnetron beat frequency $\Omega_{\rm m}$, and (2) by monitoring the dc axial frequency (i.e., the instantaneous axial frequency averaged over several cycles of $\Omega_{\rm m}$). We can observe changes in $\rho_{\rm com}$ (3) by observing the size of the axial frequency modulation at $\Omega_{\rm m}$. Figure 4-18 shows the power spectrum of the

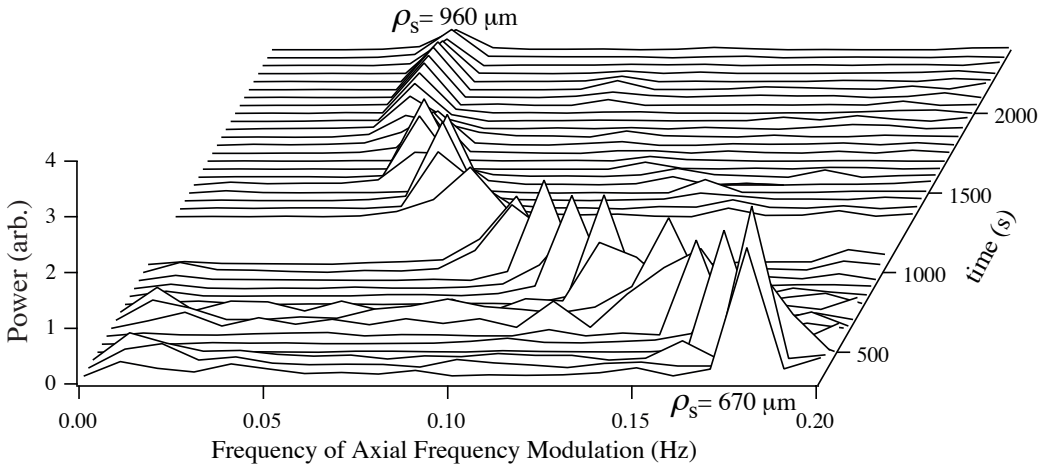

Figure 4-18: Power spectrum of instantaneous axial frequency as measured in PhaseLock versus time.

instantaneous axial frequency of one of the ions versus time as measured in PhaseLock. The frequency of the peaks determine Ω_m, which in turn tells us ρ_s. We see that Ω_m decreases from 0.18 Hz to 0.06 Hz over about 30 minutes. Converting this to an ion-ion separation, this means that ρ_s increased from 670 μm to 960 μm. The size of the axial frequency modulation decreases with time, indicating that ρ_{com} is decreasing. Also note the exponential decay of the coupling rate. We would normally increase the coupling rate by making C_4 larger in order to reach the limit $\rho_s \gg \rho_{com}$ more quickly.

As shown in Sect. 3.4, the axial frequency of each ion is shifted down by the Coulomb interaction an amount given by the axial Rabi frequency $\Omega_z/2$, which is inversely proportional to ρ_s^3. The dc component of the power spectrum, which yields the slow variation of the dc axial frequency, is not shown in Fig. 4-18 for purposes of display, but varies in a manner indicative of ρ_s increasing.

The three signals of normal mode coupling are displayed together in Fig. 4-19 for another data set: the measured period and amplitude of the axial frequency modulation, and the dc axial frequency with a large offset subtracted. All three variations exhibit exponential decays with time constants here of 850 s. The amplitude decay time constant is twice as large simply because it is the amplitude squared that should be fit to an exponential for comparison.

If one plots the dc axial frequency versus the beat frequency (see Fig. 4-20), the common dependence of the axial and radial Rabi frequencies on ρ_s^3 results in a straight line whose slope should just be the ratio $-\Omega_z/(2\Omega_m) = -\omega_c/(4\omega_z) = -5.50$. The measured slope is -3.3(1). However, the nonzero C_4 and C_6 lead to an additional variation of the dc axial frequency as the ion-ion separation changes. The axial frequency shift due to C_4 is proportional to the rms magnetron radius of the ion, so that if this coupling conserves

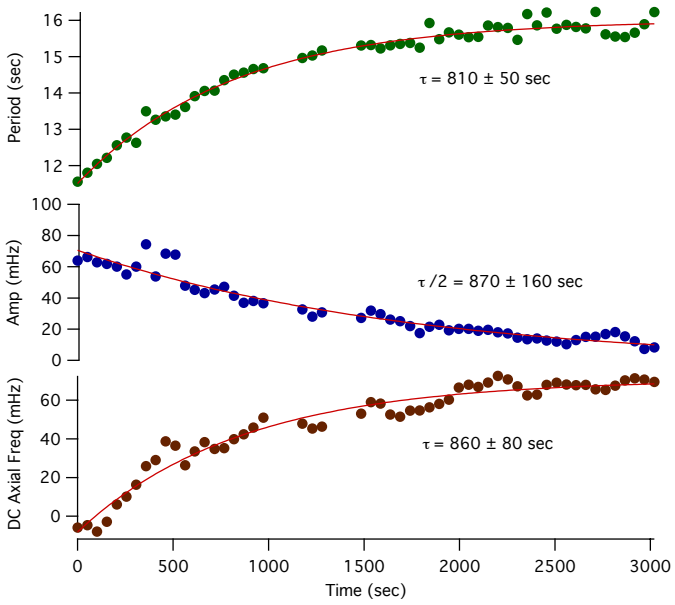

Figure 4-19: Example of Magnetron Mode Coupling and the variation of the beat frequency (or period shown here), the amplitude of the frequency modulation, and the dc value of the axial frequency. The behavior is indicative of the ion-ion separation increasing and the common mode amplitude decreasing in a manner consistent with conservation of canonical angular momentum.

canonical angular momentum, only the frequency shift due to C_6 will change in time. On the other hand, if canonical angular momentum is not conserved, then the frequency shift due to C_4 also varies. One can subtract from the observed dc axial frequency variation the contribution due to anharmonicities using these two models and an estimate of the total canonical angular momentum in the system based on extrapolating the measured Ω_m to $t = \infty$. One finds that the corrected slope is -5.8(1) assuming conservation of canonical angular momentum and -0.6(1) assuming canonical angular momentum is not conserved. Clearly, it appears that the total canonical angular momentum in the system is being conserved.

Having established that the canonical angular momentum is being conserved, we can use the estimated value of $\rho_s^\circ = 952$ μm at $t = \infty$ (when presumably ρ_{com}=0) to predict the size of the common motion ρ_{com} for a measured value of ρ_s using the relation

$$\rho_{com}^2 + \frac{\rho_s^2}{4} = \frac{\rho_s^{\circ 2}}{4} \quad . \tag{4.16}$$

The common mode amplitude can also be estimated from the size of the axial frequency modulation combined with our knowledge of ρ_s, C_4, C_6, and the response of our feedback system. Figure 4-21 compares these calculations and shows the excellent agreement. The estimate of ρ_{com} from the amplitude of axial frequency modulation is only 25% larger than

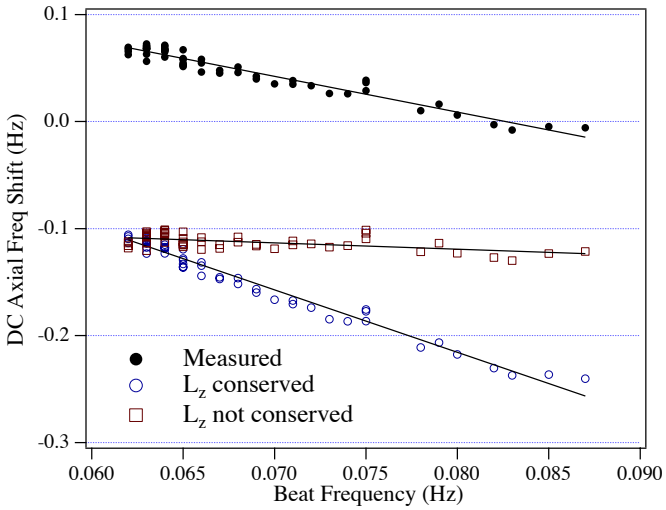

Figure 4-20: Measured dc axial frequency (with large offset) versus the measured radial Rabi frequency Ω_m from Fig. 4-19. The measured dc axial frequency values must be corrected for the trap electrostatic anharmonicities. The measured values with no corrections applied are shown in the top set of data. The correction differs depending on whether one assumes the mode coupling conserves canonical angular momentum (lowest set of data) or not (middle set of data). We can surmise that canonical angular momentum is conserved because of the good agreement between the measured slope of -5.8(1) of the lowest set of data with the predicted slope $-\Omega_z/(2\Omega_m) = -\omega_c/(4\omega_z) = -5.50$.

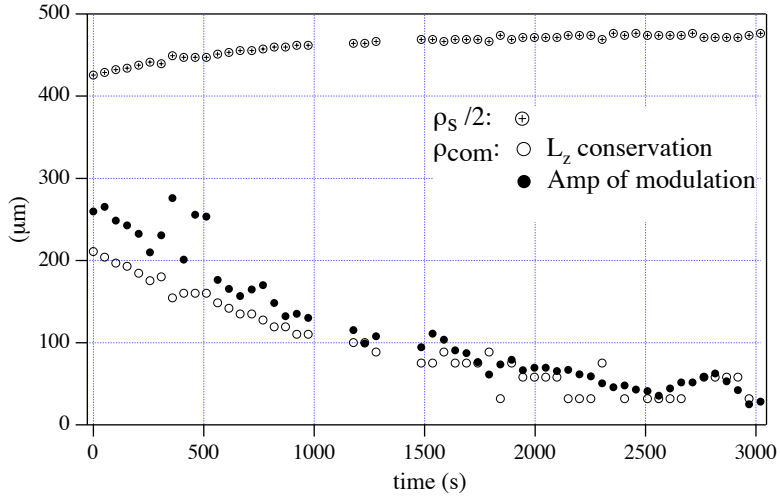

Figure 4-21: The common mode amplitude ρ_{com} and half the ion-ion separation $\rho_s/2$ calculated from Fig. 4-19 versus time. The ion-ion separation ρ_s is calculated from the measured beat frequency Ω_m. The common mode amplitude is calculated from the ρ_s data assuming conservation of canonical angular momentum and that $\rho_{com} = 0$ at $t = \infty$. This is compared to the value calculated from the amplitude of the axial frequency modulation and knowledge of the trap anharmonicities.

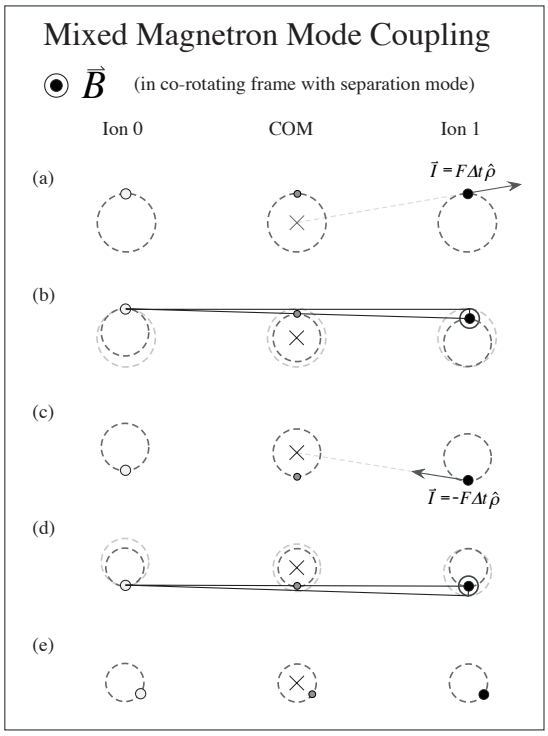

Figure 4-22: Transferring the canonical angular momentum from the common mode to the separation mode in the limit $\rho_{\rm s} \gg \rho_{\rm com}$.

that from conservation of canonical angular momentum, with the agreement becoming better at smaller $\rho_{\rm com}$. One hypothesis for this small discrepancy is that the finite mass difference between the ions results in the distance between the ions being modulated in time. This produces a modulation at $\Omega_{\rm m}$ of the first order axial frequency shift due to ion-ion interaction with amplitude of order $12\Omega_{\rm z}\delta_{\rm mag}\rho_{\rm com}/\rho_{\rm s} \sim 2\pi\ 65$ mHz $\times\rho_{\rm com}/\rho_{\rm s}$, which is about the right fraction of the observed amplitude of axial frequency modulation shown in Fig. 4-19 that was the data source for Fig. 4-21.

Qualitative Explanation

The coupling of the common $\rho_{\rm com}$ and separation $\rho_{\rm s}$ magnetron modes is a subtle business. Let us begin by examining how such a coupling might be achieved in the limit $\rho_{\rm s} \gg \rho_{\rm com}$ as shown in Fig. 4-22. The figure shows a series of sequential cartoons representing the magnetron motion of each ion as seen by an observer in a frame rotating clockwise at the frequency of the separation mode $\omega_{\rm ms} \approx \omega_{\rm mc} + \Omega_{\rm m}$. This frame is chosen so that the difference vector between the ions $\vec{\rho}_{\rm s}$ is stationary. The common motion appears as counterclockwise orbits at $\Omega_{\rm m}$ and is represented by the dashed circles. The position of the common mode is shown with respect to the trap center, which is indicated by a cross. In (a), a radially directed force modeled as an impulse is applied to ion 1 when it is at the top of

its common orbit. For an impulsive force, ion 1 does not know about ion 0 and the response of its radial motion can be thought of as that for uncoupled motion. (b) The momentum of this impulse is taken up by the cyclotron motion of ion 1, and the guiding center of this cyclotron motion defines the new magnetron position of ion 1 (see Sect. 2.1.3 for a discussion of what it means to push on the radial motion of an ion.) Since the cyclotron motion moves clockwise, this means that the new magnetron vector of ion 1 $\vec{\rho}_{\mathrm{m1}}$ moves closer to the center of the previous common orbit. For reference, the previous common orbit is shown in grey. The magnetron motion will now evolve as coupled motion, and we must reproject onto this mixed basis. Since the magnetron motion carries so little momentum, this projection is just given by calculating the instantaneous common vector $\vec{\rho}_{\mathrm{com}}$ and separation vector $\vec{\rho}_{\mathrm{s}}$ given by the defining equations

$$\vec{\rho}_{\mathrm{com}} = \frac{1}{2}\left(\vec{\rho}_{\mathrm{m1}} + \vec{\rho}_{\mathrm{m0}}\right) \tag{4.17}$$

$$\vec{\rho}_{\mathrm{s}} = \vec{\rho}_{\mathrm{m1}} - \vec{\rho}_{\mathrm{m0}} \ . \tag{4.18}$$

Graphically, one sees that the center of charge or common mode position is moved closer to the center of the trap while the separation between the ions increases only at second order. (c) The ions then move on their new common motion and a radially directed force of opposite sign to the first is applied when ion 1 reaches the bottom of its common motion. We can ignore the cyclotron motion generated by the previous impulse because the effect on the cyclotron motion will add randomly to zero. The same reasoning as in (b) is used to determine the new common and separation modes resulting from this impulse. The final result in (e) is a reduction of ρ_{com} and an increase in ρ_{s} at second order. Reversing the sign of the forces in the sequence would result in ρ_{com} increasing and ρ_{s} decreasing.

Figure 4-23 shows a similar sequence in the limit $\rho_{\mathrm{com}} \gg \rho_{\mathrm{s}}$. This is shown in a frame rotating at the common mode frequency ω_{mc} so that the position of the common vector $\vec{\rho}_{\mathrm{com}}$ is stationary while the radial vector between the ions rotates clockwise at Ω_{m}. Following the same arguments of above, one sees that radially directed forces can increase the separation between the ions and decrease the size of the common motion at second order. As above, reversing the sign of the forces in the sequence would result in ρ_{com} increasing and ρ_{s} decreasing. Since these forces are directed parallel or antiparallel to $\hat{\rho}$, they cannot change the total canonical angular momentum of the system.

How we generate these forces is the subtle business, and we will first talk our way through the explanation and take up a more rigorous approach later. The normal mode coupling is created by applying a fixed frequency axial drive just below or above the axial frequency of one of the ions. The other ion's axial mode is not affected by this drive because it is far from resonance. The relative detuning between the axial frequency and the drive is modulated by its radial motion in the presence of electrostatic anharmonicities. The two

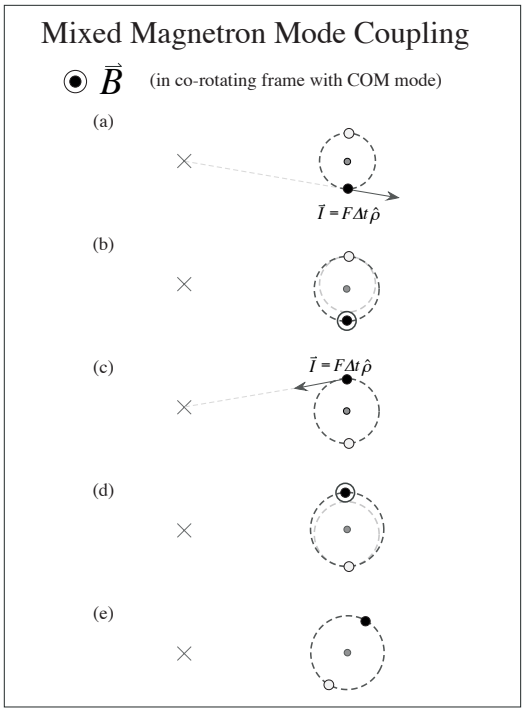

Figure 4-23: Transferring the canonical angular momentum from common mode to the separation mode in the limit $\rho_{\rm s} \ll \rho_{\rm com}$.

extremes of the drive detuning occur when the ion is closest and furthest from the center of the trap. The frequency modulation is converted into axial amplitude modulation by making the average ion-drive detuning approximately $\pm\gamma/2$, i.e. one HWHM of the axial resonance.

The frequency of the axial amplitude modulation is at the beat frequency, but the relative phase of the amplitude modulation lags the phase of the axial frequency modulation because of the finite response time of the axial mode, which is quantified by its energy damping time τ. The phase lag ϕ_{lag} of the axial amplitude modulation with respect to the axial frequency modulation can be estimated by

$$\phi_{lag} \approx -2\tau\Omega_{\rm m} \quad . \tag{4.19}$$

In the limit $|\tau\Omega_{\rm m}| \ll 1$, the axial amplitude around one beat cycle appears as in Fig. 4-24 (a) with the amplitude extremes occurring when the ion is closest or furthest from the trap center. Whether the maximum axial amplitude is reached when the ion is closest or furthest from the trap center is determined by where the axial mode is shifted toward resonance with the fixed frequency drive, which in turn is set by the sign of the average detuning and the sign of the trap anharmonicities. When the phase lag is $\pi/2$, the axial amplitude around one beat cycle appears as in Fig. 4-24 (b) with the amplitude extremes occurring in between the

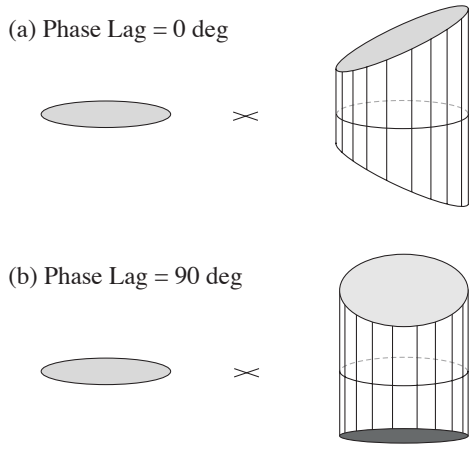

Figure 4-24: Phase of amplitude modulation with respect to common motion. The frame is rotating at $\omega_{\rm ms}$ so that the ions execute counterclockwise circular motion at $\Omega_{\rm m}$. The modulation of the relative detuning between the axial mode of the right ion and a fixed frequency axial drive causes its axial amplitude to be modulated. Figure (a) shows the relative phase of the amplitude modulation with respect to the common motion when the ion's amplitude adjusts itself immediately to a change in the detuning. Figure (b) shows the special case when the ion's axial amplitude response lags the detuning by exactly $t = 2\pi/(4\Omega_{\rm m})$. Because of C_4, the square of the amplitude directly translates into the size of the excess radial force that causes the mixed magnetron modes to couple.

extremes of the radial orbit. For $\tau = 1\ s$, this corresponds to a beat period of $2\pi/\Omega_{\rm m} = 8$ s, which occurs for an ion-ion separation of $\rho_{\rm s} = 760$ μm. The configuration (b) is necessary to drive the mode coupling, but since in general the axial amplitude modulation can be written as a linear superposition of (a) and (b), the coupling rate is decreased but is still nonzero as long as $\phi_{lag} \neq 0$.

Figure 4-10 experimentally demonstrates the modulation of z^2 by showing the power spectrum of the detected axial amplitude squared. One sees that the axial power modulation is at the same frequency as the axial frequency modulation, as shown just above it in the power spectrum of the detected instantaneous axial frequency. Additionally, the relative phase of the two modulations is -39°, while the predicted phase lag from Eq. 4.19 is -40° for the observed beat period of 18 s and τ= 1.0 s.

The electrostatic trap anharmonicity characterized by C_4 generates a radial force proportional to the square of the axial amplitude. The average axial amplitude during one beat cycle creates a constant radial force that produces a small mixing of the common and separation modes that will be ignored for now. The resonant coupling is actually driven by the modulation of the radial force about the average value. In the ideal case of Fig. 4-24 (b) $\phi_{lag} = \pi/2$, the radial force is a sinusoidally modulated version of the desired impulsive forces in Figs. 4-23 and 4-22 that create the coupling of the magnetron collective modes.

The phase of the radially directed force determines whether the coupling causes $\rho_{\rm s}$ to

increase or decrease. The phase is set by the phase of the amplitude modulation and the sign of the radial force's dependence on z. Assuming the trap anharmonicity is characterized by C_4 only, then both the radial force and the amplitude modulation (through the frequency modulation) are proportional to C_4 so that the coupling rate depends on C_4^2. This prediction agrees with the observed behavior that the direction of coupling is independent of the sign of C_4. An overall sign of the amplitude modulation can be changed by placing the fixed frequency axial drive above or below resonance, and this is exactly what we observe experimentally. When the drive is below the axial resonance, we observe $\rho_{\rm s}$ increase, and the opposite is true when the drive is above the axial resonance.

As the coupling proceeds, the average value of the axial frequency drifts due to changes in the dc anharmonic shifts, changes in the Coulomb force between the ions, and variation of the trapping voltage. We use the PhaseLock technique discussed above to lock to the side of the axial resonance. This maintains the average drive detuning at a fixed value. This also allows us to monitor the coupling to determine when the common mode is reduced to a small value and to determine the final ion-ion separation. The feedback loop in PhaseLock suppresses the axial frequency modulation that drives the coupling mechanism, but the finite gain of the feedback loop allows sufficient axial frequency modulation to occur.

Quantitative Explanation

It remains to be shown that our model of the mode coupling explains the sign and rate of the mode coupling. To do this, we now turn to a more quantitative discussion. To maintain the symmetry of the equations of motion, we will use a more symmetric definition of the mode amplitudes, which we will differentiate with a prime, given by

$$\vec{\rho}_{\rm com'} = \vec{\rho}_{\rm m1} + \vec{\rho}_{\rm m0} \tag{4.20}$$

$$\vec{\rho}_{\rm s'} = \vec{\rho}_{\rm m1} - \vec{\rho}_{\rm m0} \ . \tag{4.21}$$

For simplicity, we will further assume that the ion masses are degenerate but that we can still independently drive the axial modes. We will also assume for simplicity that the trap anharmonicity is completely specified by C_4 alone (i.e., C_6=0). Each ion experiences a radial force, which after averaging over the fast axial motion near $\omega_{\rm z}$ is given by

$$\vec{F}_i = \frac{3C_4 m\omega_{\rm z}^2}{2}\frac{z_{\rm i}^2}{d^2}\,\vec{\rho}_{\rm mi} \tag{4.22}$$

where $i = 0, 1$ denotes the ion, and $z_{\rm i}$ is the axial amplitude of ion i. For definiteness, we will assume that only ion 1 is being driven and set $z_0 = 0$. The equations of motion can be written as

$$\ddot{\vec{\rho}}_{com'} = \omega_{\rm c}\dot{\vec{\rho}}_{com'} \times \hat{z} + \frac{1}{2}\omega_{\rm z}^2 \left(1 + \frac{3C_4 z_1^2}{2d^2}\right) \vec{\rho}_{\rm com'} + \frac{3C_4\omega_{\rm z}^2 z_1^2}{4d^2}\,\vec{\rho}_{\rm s'} \tag{4.23}$$

$$\ddot{\vec{\rho}}_{s'} = \omega_{\rm c}\dot{\vec{\rho}}_{s'} \times \hat{z} + \frac{1}{2}\omega_{\rm z}^2 \left(1 + \frac{4\Omega_{\rm E}^2}{\omega_{\rm z}^2} + \frac{3C_4 z_1^2}{2d^2}\right) \vec{\rho}_{\rm s'} + \frac{3C_4\omega_{\rm z}^2 z_1^2}{4d^2}\,\vec{\rho}_{\rm com'} \quad . \tag{4.24}$$

Ignoring the last term in each equation, which gives rise to the mode coupling, we see that each mode is shifted in frequency by the same amount, so the beat frequency is unaffected

$$\omega_{\rm mc} \approx \frac{\omega_{\rm z}^2}{2\omega_{\rm c}} \left(1 + \frac{3C_4 z_1^2}{2d^2}\right) \tag{4.25}$$

$$\omega_{\rm ms} \approx \frac{\omega_{\rm z}^2}{2\omega_{\rm c}} \left(1 + \frac{4\Omega_{\rm E}}{\omega_{\rm z}^2} + \frac{3C_4 z_1^2}{2d^2}\right) \quad . \tag{4.26}$$

For scale, this common shift of the normal mode frequencies is typically ≤ 2 mHz.

Turning to the coupling terms, if z_1^2 is constant in time, then the coupling terms do not resonantly drive the normal modes. On the other hand, if z_1^2 is modulated at the difference frequency between the normal modes, then the radial motion can mix with the axial motion to create frequency components of the forces that are resonant with the normal modes. The axial amplitude modulation due to its radial motion can be written in a general form as

$$z_1^2 \approx z_{\rm dc}^2 \left\{1 + \beta\left[\vec{\rho}_{\rm s'} \cdot \vec{\rho}_{\rm com'} \cos\phi_{lag} + (\vec{\rho}_{\rm s'} \times \vec{\rho}_{\rm com'}) \cdot \hat{z} \sin\phi_{lag}\right]\right\} \tag{4.27}$$

where $z_{\rm dc}^2$ is the average squared amplitude, β specifies the modulation depth, and ϕ_{lag} specifies the phase lag between the axial frequency modulation and the resulting axial amplitude modulation as discussed previously. We have dropped terms that will generate time dependencies at twice the beat frequency, since these cannot generate any resonant forces at first order. The effect of the dc term will be discussed in Sect. 4.4.1. We must now determine which terms produce resonant forces, and of these, which terms exert torques. We begin by writing the normal mode motions as

$$\vec{\rho}_{\rm com'} = \rho_{\rm com'} \left(\hat{x}\cos c + \hat{y}\sin c\right) \tag{4.28}$$

$$\vec{\rho}_{\rm s'} = \rho_{\rm s'} \left(\hat{x}\cos s + \hat{y}\sin s\right) \tag{4.29}$$

where we assume the phase factors c and s evolve near the normal mode frequencies and the amplitudes $\rho_{\rm com'}$ and $\rho_{\rm s'}$ are slowly varying functions of time. Using these substitutions, we can examine the form of the coupling forces that are proportional to $\cos\phi_{lag}$

$$(\vec{\rho}_{\rm s'} \cdot \vec{\rho}_{\rm com'})\,\vec{\rho}_{\rm s'} = \frac{1}{2}\rho_{\rm s'}^2\,\vec{\rho}_{\rm com'} + \frac{1}{2}\rho_{\rm s'}^2\rho_{\rm com'}\left[\hat{x}\cos(2s - c) + \hat{y}\sin(2s - c)\right] \tag{4.30}$$

$$(\vec{\rho}_{s'} \cdot \vec{\rho}_{com'})\, \vec{\rho}_{com'} = \frac{1}{2}\rho_{com'}^2\, \vec{\rho}_{s'} + \frac{1}{2}\rho_{com'}^2 \rho_{s'} \left[\hat{x}\cos(2c-s) + \hat{y}\sin(2c-s)\right] \quad . \tag{4.31}$$

The first terms of these equations are resonant and give rise to frequency shifts of the normal modes, while the second terms generate nonresonant forces that slightly mix the normal modes. In any case, there are no resonant coupling forces here.

The coupling forces proportional to $\sin\phi_{lag}$ can be shown to be of the form

$$[\hat{z} \cdot (\vec{\rho}_{s'} \times \vec{\rho}_{com'})]\, \vec{\rho}_{s'} = \frac{1}{2}\rho_{s'}^2\, \vec{\rho}_{com'} \times \hat{z} + \frac{1}{2}\rho_{s'}^2 \rho_{com'} \left[-\hat{x}\sin(2s-c) + \hat{y}\cos(2s-c)\right] \tag{4.32}$$

$$[\hat{z} \cdot (\vec{\rho}_{s'} \times \vec{\rho}_{com'})]\, \vec{\rho}_{com'} = -\frac{1}{2}\rho_{com'}^2\, \vec{\rho}_{s'} \times \hat{z} + \frac{1}{2}\rho_{com'}^2 \rho_{s'} \left[\hat{x}\sin(2c-s) - \hat{y}\cos(2c-s)\right] \quad . \tag{4.33}$$

The first terms in each equation create resonant forces that exert torques on the normal modes, but with opposite signs. The second terms generate nonresonant mixing of the normal modes. Rewriting Eqs. 4.23 and 4.24 and including only the resonant interactions that exert torques, we arrive at the relevant equations of motion

$$\ddot{\vec{\rho}}_{com'} = \omega_c \dot{\vec{\rho}}_{com'} \times \hat{z} + \frac{1}{2}\omega_z^2\, \vec{\rho}_{com'} + \frac{3C_4\omega_z^2 z_{dc}^2 \rho_{s'}^2 \beta \sin\phi_{lag}}{8d^2}\, \vec{\rho}_{com'} \times \hat{z} \tag{4.34}$$

$$\ddot{\vec{\rho}}_{s'} = \omega_c \dot{\vec{\rho}}_{s'} \times \hat{z} + \frac{1}{2}\omega_z^2 \left(1 + \frac{4\Omega_E^2}{\omega_z^2}\right) \vec{\rho}_{s'} - \frac{3C_4\omega_z^2 z_{dc}^2 \beta \rho_{com'}^2 \sin\phi_{lag}}{8d^2}\, \vec{\rho}_{s'} \times \hat{z} \quad . \tag{4.35}$$

Making the adiabatic approximation that the amplitudes vary slowly in time compared to the normal mode frequencies, one can reduce the equations of motion to first order differential equations for slowly varying mode amplitudes. Since we are chiefly concerned with the variation of the magnitude of the mode amplitudes with time, we can further reduce these equations of motion to equations governing the squares of the mode amplitudes

$$\dot{\tilde{L}}_s = -\frac{1}{\tau_c}\frac{\tilde{L}_s \tilde{L}_{com}}{\tilde{L}_{tot}} \tag{4.36}$$

$$\dot{\tilde{L}}_{com} = \frac{1}{\tau_c}\frac{\tilde{L}_s \tilde{L}_{com}}{\tilde{L}_{tot}} \tag{4.37}$$

where

$$\tilde{L}_s = \rho_{s'}^2 \tag{4.38}$$

$$\tilde{L}_{com} = \rho^2_{\mathrm{com}'} \tag{4.39}$$

$$\tilde{L}_{tot} = \tilde{L}_s + \tilde{L}_{com} \tag{4.40}$$

$$\frac{1}{\tau_c} = \frac{3\omega_{\mathrm{m}} C_4}{4} \frac{z^2_{\mathrm{dc}}}{d^2} \tilde{L}_{tot} \beta \sin\phi_{lag} \quad . \tag{4.41}$$

The functions $\tilde{L}_s$ and $\tilde{L}_{com}$ are just proportional to the canonical angular momentum in each magnetron mode up to corrections of order $\eta\omega_{\mathrm{m}}/\omega_{\mathrm{c}}$. From the equations, one immediately sees that this coupling preserves the total canonical angular momentum L_{z} at the same order since

$$\dot{L}_{\mathrm{z}} \approx \frac{m\omega_{\mathrm{c}}}{4}\left(\dot{\tilde{L}}_s + \dot{\tilde{L}}_{com}\right) = \frac{m\omega_{\mathrm{c}}}{4}\dot{\tilde{L}}_{\mathrm{tot}} = 0 \quad . \tag{4.42}$$

The time constant τ_c sets the time scale for exponential decay or growth in the limit that one mode amplitude is much greater than the other. This limit is just the regime in which we spend most of our time coupling the modes to reduce the common mode amplitude. For example, if $\rho_{s'} \gg \rho_{\mathrm{com}'}$ then $\tilde{L}_{tot} \approx \tilde{L}_s$ and Eqs. 4.36 and 4.37 reduce to equations for exponential growth (decay) of the common motion. Growth or decay occur depending on the sign of the axial amplitude modulation parameter β. General solutions for Eqs. 4.36 and 4.37 can be written with the initial conditions $\tilde{L}_s = \tilde{L}^\circ_s$ and $\tilde{L}_{com} = \tilde{L}^\circ_{com}$ at $t = 0$,

$$\tilde{L}_s(t) = \frac{e^{t/\tau_c}\tilde{L}_{tot}}{e^{t/\tau_c} + \frac{\tilde{L}^\circ_{com}}{\tilde{L}^\circ_s}} \tag{4.43}$$

$$\tilde{L}_{com}(t) = \frac{e^{-t/\tau_c}\tilde{L}_{tot}}{e^{-t/\tau_c} + \frac{\tilde{L}^\circ_s}{\tilde{L}^\circ_{com}}} \quad . \tag{4.44}$$

The remaining problem is to specify the form of the axial amplitude modulation parameter β, which is defined by Eq. 4.27. If we use PhaseLock to fix the average drive-axial detuning and assume small fluctuations about this point, then we can use the known Lorentzian frequency response of the axial mode to convert a change in the drive detuning expressed in HWHM of the axial resonance $\Delta\delta_i = \Delta(\omega_{\mathrm{d}} - \omega_{\mathrm{z}})/(\gamma/2)$ to a fractional change in the square of the axial amplitude $\Delta(z^2)/(z^2_{\mathrm{dc}})$:

$$\frac{\Delta(z^2)}{z^2_{\mathrm{dc}}} = \frac{-2\delta_i}{1+\delta_i^2}\Delta\delta_i \tag{4.45}$$

where δ_i is the average drive-axial detuning in units of $\gamma/2$ and z^2_{dc} is the squared amplitude at this detuning. The variation of the drive-axial detuning is set by the axial frequency shift resulting from radial motion in the presence of C_4 as given by Eq. 4.8 (recall that we

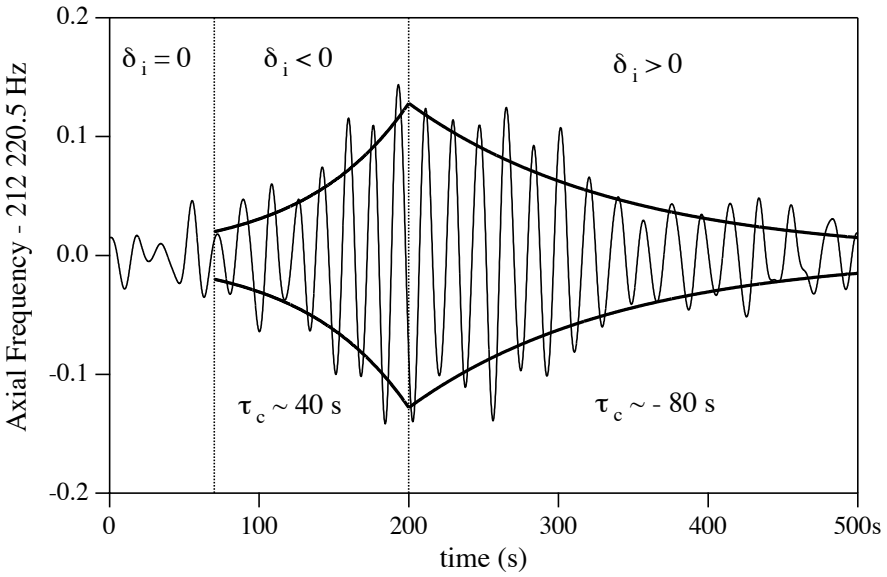

Figure 4-25: Control of the mode coupling by varying the drive detuning. The difference in the fitted damping times τ_c is most likely caused by an uncertainty in the position of $\delta_i = 0$ when the data was taken. This is actual data with the higher frequency components filtered out to make the oscillations more obvious.

have assumed C_6=0 for simplicity and that $\rho_{\mathrm{com}'} = 2\rho_{\mathrm{com}}$), so that we can write

$$\Delta\delta_i = -\frac{3\omega_{\mathrm{z}} C_4}{2G\gamma}\frac{\rho_{\mathrm{s}'}\rho_{\mathrm{com}'}}{d^2} \tag{4.46}$$

where the axial frequency modulation is reduced by the gain factor $G \sim 3$ of the feedback loop in PhaseLock that opposes the axial frequency modulation. Using the identification

$$\beta\rho_{\mathrm{s}'}\rho_{\mathrm{com}'} = \frac{\Delta(z^2)}{z_{\mathrm{dc}}^2} \tag{4.47}$$

we solve for the parameter β

$$\beta = -3\frac{\omega_{\mathrm{z}}}{\gamma}\frac{C_4}{Gd^2}\frac{\delta_i}{1+\delta_i^2} \quad . \tag{4.48}$$

Substituting the above expression for β in Eq. 4.41 for the coupling time τ_c, we find

$$\frac{1}{\tau_c} = \frac{9}{2}\frac{\omega_{\mathrm{m}}\omega_{\mathrm{z}}C_4^2}{\gamma G}\frac{z_{\mathrm{dc}}^2\tilde{L}_{tot}^2}{d^4}\frac{\delta_i}{1+\delta_i^2}\sin\left(2\tau\Omega_{\mathrm{m}}\right) \tag{4.49}$$

where ϕ_{lag} has been approximated by Eq. 4.19 and the other parameters have been defined above. Note that the sign of τ_c is equal to the sign of the average drive-axial detuning δ_i, since all other quantities are either positive or squared.

Experimentally, we observe that the behavior of the coupling (i.e., whether ρ_{s} increases

or decreases) does not depend on the sign of C_4. Since τ_c from Eq. 4.49 depends on C_4^2, the sign of τ_c also does not depend on the sign of C_4. Hence, our model predicts the observed behavior that the direction of angular momentum transfer does not depend on the sign of C_4.

Secondly, when the drive-axial detuning $\delta_i < 0$ ($\delta_i > 0$), the common mode amplitude exponentially decreases (increases) for $\rho_{\rm s} \gg \rho_{\rm com}$ exactly as observed. An experimental example of this behavior is shown in Fig. 4-25. Initially, the common amplitude is small. By making the drive-axial detuning negative starting at $t = 70$ s, the common mode amplitude (as evidenced by the axial frequency modulation) is increased. At $t = 200$ s, the detuning is made positive, and the common mode amplitude decreases. The observed value of τ_c is of the same magnitude as that predicted using Eq. 4.49. For instance, Eq. 4.49 predicts $\tau_c = 450$ s for a typical set of parameters $C_4 = 5.3 \times 10^{-6}$ (or 10 mVTuning), δ_i = -1, $\tilde{L}_{tot} = (1.1\text{ mm})^2$, $z_{\rm dc} = 0.3$ mm, $d = 5.49$ mm, $\tau = 1/\gamma = 1$ s, $2\pi/\Omega_{\rm m} = 25$ s, $\omega_{\rm z}/2\pi = 212$ kHz, $\omega_{\rm m}/2\pi = 4.9$ kHz, $G = 3.5$. When we are interested in reducing $\rho_{\rm com'}$ more quickly, we make the size of the anharmonicity twice as large so that the quadratic dependence on C_4 gives an estimate of the damping time $\tau_c \sim 100$ s in agreement with Fig. 4-25. At large separations the contribution of C_6 to the axial frequency modulation is significant, and a detailed comparison of theory and experiment would need to include this contribution. It should also be noted that $\Omega_{\rm m}$ is also a function of $\rho_{\rm s'}$, so that our solution will only be accurate over time scales during which $\Omega_{\rm m}$ does not change significantly, which is true for the limit $\rho_{\rm s'} \gg \rho_{\rm com'}$ where we most often work.

Numerical simulations were performed to verify that no significant physics was dropped from the above explanation of the magnetron mode coupling. The simulations included the coupled magnetron motion and driven axial motion in the presence of the anharmonic forces generated in the axial and radial direction by the trap anharmonicity specified by C_4. Figure 4-26 shows a comparison between the numerical simulation (modulated line) and the semi-analytic expression 4.49 (smooth line) for similar parameters as in the preceding paragraph. The simulation starts with one ion at zero magnetron radius and the other at 0.8 mm radius. With the drive below resonance, we see that the distance between the ions increases with time while the common mode decreases. The fitted time constant τ_c to the numerical simulation is 280 s compared to a predicted value of 190 s from our model. The discrepancy is most likely related to the fact that in the simulation, the radial Rabi frequency $\Omega_{\rm m}$ decreases as $\rho_{\rm s}$ increases, as in our actual experiment. In contrast, the predicted value of τ_c assumes a constant value of $\Omega_{\rm m}$ which is evaluated at $t = 0$. When $\Omega_{\rm m}$ is fixed in the simulation, the fitted value agrees to 10% with our model.

Limitations on setting $\rho_{\rm com} = 0$

The modulation of the normal mode amplitudes in the numerical simulation shown in Fig. 4-26 indicate that the common and separation modes are not the normal modes of the system.

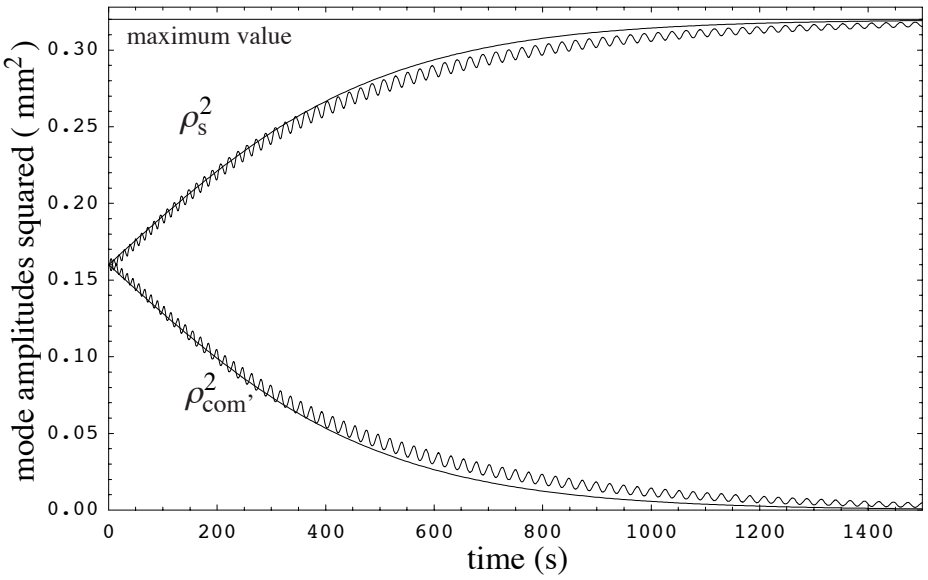

Figure 4-26: Semi-analytic (smooth line) and numerical simulation (modulated line) of the transfer of the canonical angular momentum from the common mode to the separation mode.

This is despite the fact that the simulation was performed with completely degenerate mass particles. The reason for this is that the symmetry between the ions is broken by the average finite axial amplitude of one of the ions given by $z_{\rm dc}$ in the previous section. This average axial amplitude in the presence of C_4 produces a shift of that ion's instantaneous magnetron frequency. This small frequency splitting between the modes means that the single particle magnetron motions are not completely mixed by the Coulomb interaction between the ions.

The coupling of the two imperfectly mixed modes shuts itself off when the amplitude of the common-like mode is zero. If the axial amplitude or the anharmonicity is suddenly reduced to zero, the normal modes of motion cannot follow and one is left with a nonzero common amplitude. Adiabatic following of the modes occurs when the condition is met that the time scale over which the normal modes are changed is much longer than the beat period between the normal modes $\sim 2\pi/\Omega_{\rm m}$. Figure 4-27 shows a numerical simulation of such a process for two equal mass ions. Initially, ion 1's axial motion is driven and the common and separation modes are coupled, leading to a reduction of the ringing of each ion's magnetron amplitude. If the drive is shut off instantaneously as in the upper graph, the normal modes must be reprojected onto a new basis. This projection results in ringing of the magnetron amplitudes. If the drive is shut off over many cycles of $\Omega_{\rm m}$, as shown in the lower graph, then the normal modes are adiabatically transformed and no ringing occurs. Since in most of our experimental work we would instantaneously shut off our axial drives or set C_4=0, this means that the ratio of the common-like mode to separation mode was typically reduced to only about $\rho_{\rm s}/\rho_{\rm com} \approx 0.05$. This could be improved by just changing

parameters more slowly, but since the time scale of the beat period is typically 10 to 40 s, this would be painful in practice.

Tuning $\delta_{\rm mag}$ to zero

It is paramount for precise cyclotron frequency comparisons that both ions have identical rms magnetron radii. For ions of identical mass $\eta = 0$, the rms magnetron radii are identical. For ions with slightly different masses $\eta \neq 0$, the rms magnetron radii differ by a fractional amount $\delta_{\rm mag}$ because of the slight frequency difference of the uncoupled magnetron modes. It would be extremely useful for reducing systematic errors if we could tune the uncoupled magnetron frequency difference to zero so that the rms magnetron radii would then be identical.

One possibility for tuning the instantaneous magnetron frequency difference is to excite the axial motion of one of the ions to a small constant amplitude and adjust C_4 to shift the magnetron frequency of the ion into exact resonance with the other ion. This would make the measurement of the cyclotron frequency difference much less sensitive to the radial dependence of the magnetic field inhomogeneities such as B_2 and B_4 as well as the electrostatic anharmonicity such as C_6 and C_4. However, the finite axial amplitude coupled with B_2 and B_4 would shift that ion's cyclotron frequency. This systematic error could be eliminated by the following. Say that the difference in the rms magnetron radii $\delta_{\rm mag}$ could be set to zero using $C_4 = C_4^\circ$ and by exciting ion 1's axial amplitude to $z_1 = z^\circ$. Then, $\delta_{\rm mag}$ could also be set to zero using $C_4 = -C_4^\circ$ and exciting ion 0's axial amplitude to $z_0 = z^\circ$. By taking the average of the measured cyclotron frequency difference in each configuration, the effect of finite axial amplitude would be eliminated. Alternatively, one could simply plot the measured cyclotron difference frequency versus the absolute value of C_4 for each configuration and where the values cross would determine the unperturbed cyclotron frequency difference. This technique does not require critical knowledge of the average radial position of each ion, since the magnetron frequency shift is independent of $\rho_{\rm m}$. A quick calculation shows that this could be reasonably achieved for a mass doublet $\eta = 4 \times 10^{-4}$ with $z = 300$ μm and $C_4 = 1.1 \times 10^{-4}$ (or 20 mVTuning).

4.4.2 Varying the Ion-Ion Separation $\rho_{\rm s}$

Changing the ion-ion separation $\rho_{\rm s}$ is a matter of changing the total canonical angular momentum in the system. *Reducing* the ion-ion separation is accomplished by performing partial π-pulses between each ion's instantaneous magnetron mode and its damped axial mode. The amount of magnetron motion coupled into the axial mode is set by the criterion that the axial motion not be made too large lest the magnetron modes decouple and the ions move close to one another. Typically, we keep $z \leq 300$ μm, giving a typical time scale for these pulses of ~ 50 ms (for $t_\pi \approx 800$ ms). The coupling is unaffected even if the axial frequencies are varying a little in time due to swapping. This is because the modes do not

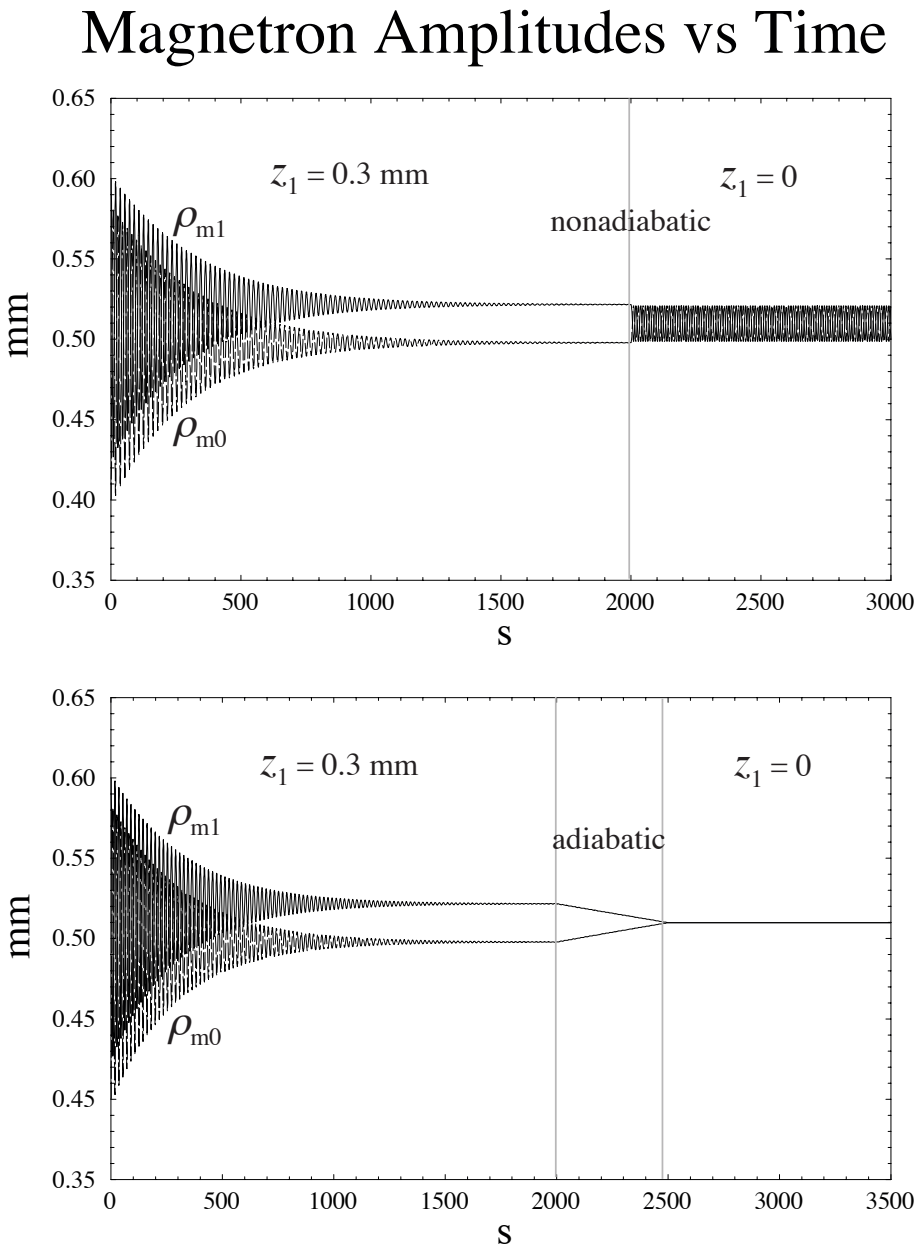

Figure 4-27: Numerically simulated individual magnetron amplitudes ρ_{m0} and ρ_{m1} versus time for equal mass ions with mode coupling occurring until the oscillations disappear. The frequency degeneracy of the magnetron modes is broken by the finite axial amplitude of ion 1 combined with the nonzero C_4 that drives the normal mode coupling. In steady state, the ions are at slightly different radii. If the drive exciting the axial motion is turned off instantaneously, as in the upper graph, then the normal modes project onto those of degenerate masses, leading to a ringing of the magnetron amplitudes. If the drive is turned off adiabatically, as in the lower graph (here it is extremely adiabatic), the normal modes adiabatically follow and there is no ringing at the end.

have enough time to sense that the couplings are not perfectly resonant (as can be seen from the Rabi formula along with the small angle approximation). Because each fractional π-pulse changes the magnetron amplitude by $\leq 1\%$, we usually run 10 or 20 in a row. If we start with $\rho_{\rm com} = 0$, we typically find that $\rho_{\rm com} = 0$ even after reducing $\rho_{\rm s}$ by several 100 μm using 30 to 40 partial π-pulses.** For scale, we can typically move from $\rho_{\rm s}$= 1200 μm to $\rho_{\rm s}$= 700 μm in about 30 minutes.

Increasing the ion-ion separation $\rho_{\rm s}$ means that we must inject angular momentum into the system. To do this, we start by transferring all of the angular momentum in the common mode into the separation mode using the mode coupling technique discussed in the previous section. We can then inject angular momentum into the common mode by applying a dipole drive at the magnetron frequency that acts symmetrically on both modes. We then transfer this angular momentum into the separation mode. If we wish to move to a specific ion-ion separation, we can simply use conservation of canonical angular momentum to predict how much angular momentum we need to inject into the common mode. For large changes in the ion-ion separation, we must proceed via several iterations of this process. This is because the PhaseLock feedback loop that we use to perform the angular momentum transfer cannot follow the axial frequency modulation caused by swapping if the common amplitude is made too large. This typically means we create common amplitudes $\rho_{\rm com} \leq 300$ μm. Using this drive and couple technique, we can move from $\rho_{\rm s}$= 700 μm to $\rho_{\rm s}$= 1200 μm in about 45 minutes.

**See Sect. 4.3.1 and Fig. 4-7 for use of these simultaneous couplings to observe the relative magnetron motion of the two ions.

Chapter 5

Simultaneous Cyclotron Frequency Comparisons

5.1 Obtaining the Cyclotron Frequency Ratio

We want to determine the cyclotron frequency ratio from quantities that can be precisely and accurately measured. If a quantity cannot be precisely or accurately measured then we would like our result to depend only weakly on it. When making *alternating* cyclotron frequency comparisons with one ion in the trap at a time, we need to measure five quantities to determine the cyclotron frequency ratio (in order of decreasing precision): the trap cyclotron frequencies ω_{ct1} and ω_{ct0}, the axial frequencies ω_{z1} and ω_{z0}, and the trap tilt angle θ_{t}.*

When making simultaneous cyclotron frequency comparisons with two ions in the same trap, we need to measure only three quantities (in order of decreasing precision): the difference in trap cyclotron frequencies $\omega_{\mathrm{ct2}} = \omega_{\mathrm{ct1}}$-$\omega_{\mathrm{ct0}}$, the trap cyclotron frequency of either ion $\omega_{\mathrm{ct0,1}}$, and the axial frequency of the same ion $\omega_{\mathrm{z0,1}}$.

To start, we define the mass ratio

$$R \equiv \frac{m_1}{m_0} = \frac{\omega_{\mathrm{c0}}}{\omega_{\mathrm{c1}}} \quad . \tag{5.1}$$

Note that following our convention that $m_0 > m_1$, the mass ratio always satisfies $R < 1$. We can then write down the invariance theorem for each ion separately

$$\omega_{\mathrm{c0}}^2 = \omega_{\mathrm{ct0}}^2 + \omega_{\mathrm{z0}}^2 + \omega_{\mathrm{m0}}^2 \tag{5.2}$$

$$\omega_{\mathrm{c1}}^2 = \omega_{\mathrm{ct1}}^2 + \omega_{\mathrm{z1}}^2 + \omega_{\mathrm{m1}}^2 \quad , \tag{5.3}$$

*We do not have to measure the magnetron frequencies ω_{m1} and ω_{m0}, since we can calculate them by combining the other two mode frequencies ω_{ctx} and ω_{zx} with a small correction given by the trap tilt angle.

where the frequencies are those one would measure in a perfect Penning trap with only a single ion. Because the ions are in the same trap, they experience the same magnetic field B_0, trap voltage V_r, and trap size d. We can reexpress the free space cyclotron frequency and axial frequency of ion 0 in terms of ion 1's frequencies and the ratio

$$\omega_{c0}^2 = R^2 \omega_{c1}^2 \tag{5.4}$$

$$\omega_{z0}^2 = R \omega_{z1}^2 \quad . \tag{5.5}$$

Since the magnetron frequencies are almost identical, we can approximate that $\omega_{m0}^2 = \omega_{m1}^2$. This produces no loss of accuracy on our final expression for R above 1×10^{-12} for our example pair $^{13}C_2H_2^+$ vs N_2^+.[†] Making these substitutions and subtracting the two invariance relationships, one finds a quadratic equation for R. The physical of the two solutions can be written as

$$R = \frac{1}{2}\left(\frac{\omega_{z1}}{\omega_{c1}}\right)^2 + \sqrt{\left(1 - \frac{1}{2}\left(\frac{\omega_{z1}}{\omega_{c1}}\right)^2\right)^2 + \frac{\omega_{ct2}\left(\omega_{ct2} - 2\omega_{ct1}\right)}{\omega_{c1}^2}} \quad , \tag{5.6}$$

with the usual definition of the trap cyclotron frequency difference

$$\omega_{ct2} \equiv \omega_{ct1} - \omega_{ct0} \quad . \tag{5.7}$$

The free space cyclotron frequency ω_{c1} is obtained using[‡]

$$\omega_{c1} \approx \sqrt{\omega_{ct1}^2 + \omega_{z1}^2 + \left(\frac{\omega_{z1}^2}{2\omega_{ct1}}\right)^2} \quad . \tag{5.8}$$

Of course, a similar expression for R can be obtained involving the mode frequencies of ion 0 and the trap cyclotron difference frequency still defined as $\omega_{ct2} = \omega_{ct1}$ - ω_{ct0}

$$R = \left(\frac{1}{2}\left(\frac{\omega_{z0}}{\omega_{c0}}\right)^2 + \sqrt{\left(1 - \frac{1}{2}\left(\frac{\omega_{z0}}{\omega_{c0}}\right)^2\right)^2 + \frac{\omega_{ct2}\left(\omega_{ct2} + 2\omega_{ct0}\right)}{\omega_{c0}^2}}\right)^{-1} \quad . \tag{5.9}$$

[†]As nicely described in Simon Rainville's thesis [1][G] section 4.3.1, the fractional error on the ratio due to this approximation scales as $\Delta R/R \approx -\eta\left(\bar{\omega}_z/\bar{\omega}_{ct}\right)^6/4$. Additionally, the approximate calculation of the free space cyclotron frequency of Eq. 5.8 introduces an error on the ratio $\Delta R/R \approx \eta\left(\bar{\omega}_z/\bar{\omega}_{ct}\right)^6/2$. The net scaling of these errors for a fixed axial frequency is $\sim \eta\bar{m}^3$. For the same mass doublet as our example pair $^{13}C_2H_2^+$ vs N_2^+, the fractional error on the ratio approaches 1×10^{-11} around $\bar{m}/q \approx 60$ u/e. This is not a truly fundamental problem since it is trivial to include small corrections for the errors introduced by our approximations.

[‡]See the previous footnote.

5.2 Reduced Sensitivity to Noise and Errors

Using Eq. 5.6, we can calculate the mass ratio R from the trap cyclotron frequency difference $\omega_{\rm ct2}$ and the individual mode frequencies $\omega_{\rm ct1}$ and $\omega_{\rm z1}$ (or $\omega_{\rm ct0}$ and $\omega_{\rm z0}$). But exactly how accurately must we measure these quantities? This is where the real payoff of the two-ion technique occurs. By differentiating Eq. 5.6 with respect to each parameter, we find in decreasing order of importance

$$\left.\frac{\Delta R}{R}\right|_{\Delta\omega_{\rm ct2}} \approx -\frac{\Delta\omega_{\rm ct2}}{\bar{\omega}_{\rm c}} \tag{5.10}$$

$$\left.\frac{\Delta R}{R}\right|_{\Delta\omega_{\rm ct1}} \approx -2\eta\frac{\Delta\omega_{\rm ct1}}{\bar{\omega}_{\rm c}} \tag{5.11}$$

$$\left.\frac{\Delta R}{R}\right|_{\Delta\omega_{\rm z1}} \approx -2\eta\left(\frac{\bar{\omega}_{\rm z}}{\bar{\omega}_{\rm c}}\right)^2\frac{\Delta\omega_{\rm z1}}{\bar{\omega}_{\rm z}}\ . \tag{5.12}$$

In these expressions we have ignored corrections of order η^2 and $(\bar{\omega}_{\rm z}/\bar{\omega}_{\rm c})^2$. The small errors in the parameters can be either random variation from noise sources (such as the magnetic field or trap voltage noise or from detection noise) or from systematic errors associated with how we measure the quantities. In either case, we win big since typically $2\eta \leq 10^{-3}$. A slightly more detailed discussion for the expert will be given in the following sections.

To compare the cyclotron frequencies of our example pair $^{13}C_2H_2^+$ vs N_2^+ to a fractional accuracy 1×10^{-12}, we must measure the

- trap cyclotron difference frequency to $\Delta\omega_{\rm ct2}/2\pi = 4.7$ μHz or $\Delta\omega_{\rm ct2}/\bar{\omega}_{\rm ct} = 1\times10^{-12}$
- trap cyclotron frequency of ion 1 to $\Delta\omega_{\rm ct1}/2\pi = 8.1$ mHz or $\Delta\omega_{\rm ct1}/\bar{\omega}_{\rm c} = 1.7\times10^{-9}$
- the axial frequency of ion 1 to $\Delta\omega_{\rm z1}/2\pi = 0.18$ Hz or $\Delta\omega_{\rm z1}/\omega_{\rm z1} = 8.4\times10^{-7}$.

These are extremely relaxed requirements, and are easily met by the current apparatus. We require that the magnetic field be stable to only 2×10^{-9} instead of the previous draconian requirement of 1×10^{-12}. Additionally, the trap voltage must be stable to only 2×10^{-6} (or about 30 μV) instead of the difficult requirement of 1×10^{-9} (or about 20 nV). I want to jump up and down to impress upon the reader that this is a gigantic experimental win.

To emphasize the experimental gain made by simultaneously comparing ions of similar mass in the same trap, let us look at the requirements for alternating comparisons. To compare the cyclotron frequencies of our example pair $^{13}C_2H_2^+$ vs N_2^+ to a fractional accuracy 1×10^{-12}, then we would have to measure the

- trap cyclotron frequency of ion 0 to $\Delta\omega_{\rm ct0}/2\pi = 3.3$ μHz or $\Delta\omega_{\rm ct0}/\bar{\omega}_{\rm c} = 1\times10^{-12}/\sqrt{2}$
- trap cyclotron frequency of ion 1 to $\Delta\omega_{\rm ct1}/2\pi = 3.3$ μHz or $\Delta\omega_{\rm ct1}/\bar{\omega}_{\rm c} = 1\times10^{-12}/\sqrt{2}$

- the axial frequency of ion 0 to $\Delta\omega_{z0}/2\pi = 73$ μHz or $\Delta\omega_{z0}/\omega_{z0} = 3.4 \times 10^{-10}$
- the axial frequency of ion 1 to $\Delta\omega_{z1}/2\pi = 73$ μHz or $\Delta\omega_{z1}/\omega_{z1} = 3.4 \times 10^{-10}$.

For alternating comparisons to achieve a precision of 10^{-12}, the axial frequencies must be measured as precisely as the cyclotron frequencies were in all of our previous work comparing masses at 1×10^{-10}. This is a real warning flag. If we wish to achieve mass ratio precisions of 1×10^{-12} with the alternating technique, then we are moving further and further from the elegantly simple *gedanken* experiment of ions in a uniform magnetic field. Despite its apparent increased complexity, the two-ion technique returns us closer to the ideal experiment, since the only quantity that must be measured to high precision is the difference of trap cyclotron frequencies.

5.2.1 Impact on Detection Noise and Systematic Errors

In addition to significantly reducing our sensitivity to magnetic field noise and trap voltage noise, the two-ion technique also has several other benefits. First, it greatly reduces the effect of detection noise associated with measuring the axial frequency. For instance, in a single 8 s measurement of the axial frequency, we can measure the axial frequency to ~ 20 mHz. This is precise enough for a determination of the mass ratio to 1×10^{-12} using our new technique of simultaneous cyclotron frequency comparisons. With the alternating technique we would have to average about 80000 such measurements to achieve the necessary 73 μHz precision. The axial frequency measurements alone would take 7 days!

Second, the two-ion technique greatly relaxes the requirements on systematic errors associated with measuring the axial frequency. To a large extent, one obtains the common mode rejection of systematic errors arising from trap electrostatic anharmonicities C_4 and C_6 for the alternating technique as well. But with the alternating technique one must worry about the symmetry of the axial amplitudes, whereas this is not required to reap the benefits of common mode rejection of systematics in the two-ion technique. Also, there are small systematic errors that are inherently not symmetric, for example, the frequency pulling associated with the axial detector and the ion-ion axial interaction at second order. The effect of axial frequency pulling is small enough for the two-ion technique that it does not matter, but for the alternating technique it would have to be carefully measured and controlled.

Lastly, the two-ion technique allows us to optimize the trapping environment to minimize the systematic errors on the real quantity of interest—the trap cyclotron frequency difference ω_{ct2}. In a few sections we will discuss how we need to introduce a significant C_4 to cancel the differential shift of the two cyclotron frequencies at a given magnetron radius.* While this minimizes the systematic error on ω_{ct2}, it introduces large systematic errors on both axial

*The C_4 is chosen to balance the differential shifts of the trap cyclotron frequencies at a given magnetron radius due to magnetic field inhomogeneities and higher order electrostatic anharmonicities B_2, C_6, and B_4.

frequencies $\omega_{z0,1}$ and both trap cyclotron frequencies $\omega_{ct0,1}$. With the two-ion technique, we can largely neglect these errors because of the insensitivity of the calculated ratio to these parameters.

5.2.2 Residual Noise from Magnetic Field, Trap Voltage, and Trap Size

Our measurement of the ratio R is *completely* insensitive to magnetic field and trap voltage noise (and trap size noise). But this statement is only true if we measure the values of ω_{ct1} and ω_{z1} averaged over the period of time it takes to measure ω_{ct2}. However, this is not what we do.

We measure ω_{ct1} several 100 s before or after measuring ω_{ct2}. We typically need to use a cyclotron phase evolution time $T_{evol} \sim 400$ s in a single PNP sequence to obtain the necessary precision on ω_{ct2}. Over this time scale, magnetic field noise would introduce several 2π uncertainty in the accumulated phase of either ion's cyclotron motion so that ω_{ct0} and ω_{ct1} cannot be unambiguously be determined. Instead, we use a shorter PNP measurement $T_{evol} \sim 10$ s before or after the measurement of ω_{ct2} to unambiguously measure ω_{ct0} and ω_{ct1}. As a result, we are still slightly sensitive to magnetic field variation between the two measurements. However, the effect of magnetic field noise on the measured ratio R is down by $2\eta \leq 10^{-3}$ compared to the single ion technique. This $> 1000\times$ reduction of the impact of magnetic field noise pushes this noise source well below other sources of noise.

We measure the axial frequency ω_{z1} averaged over ~ 8 s at the end of the PNP measurement of the trap cyclotron difference frequency ω_{ct2}. We are slightly sensitive to random variation of the trap voltage V_r or of the trap size d between the two separate measurements. But as with the magnetic field noise, we are now less sensitive to this source of noise by a factor $2\eta \leq 10^{-3}$ because of the common effect of the noise sources on the two ions.[†]

5.3 Simultaneous Axial Detection

The key to making simultaneous cyclotron frequency comparisons is being able to detect the phase of each ion's axial motion. As a reminder to the reader, we use the Pulse aNd Phase technique of Sect. 2.1.5 to measure the phase accumulated by the cyclotron motion versus time. To perform the phase measurement, we map the cyclotron phase onto the phase of the axial motion that we then detect. Figure 5-1 shows an example power spectrum of 8 s of the image currents induced in the Endcaps of the Penning trap by a single N_2^+ and a single CO^+. The ions are on a common magnetron orbit of approximately 1 mm diameter, but on opposite sides of the trap. They are simultaneously oscillating along the axial direction with amplitudes $z_0 = z_1 \sim 350$ μm. The trap voltage is adjusted to place

[†]In principle, one could continuously measure the axial frequency while the two cyclotron modes are accumulating phase for the measurements of ω_{ct2} and ω_{ct1}. This could be done with small axial excitations or by observing the shorting of the Johnson noise of the coil by the axial modes. However, the reduction of noise on the ratio R is negligible compared to other sources of noise, so this is not of current interest.

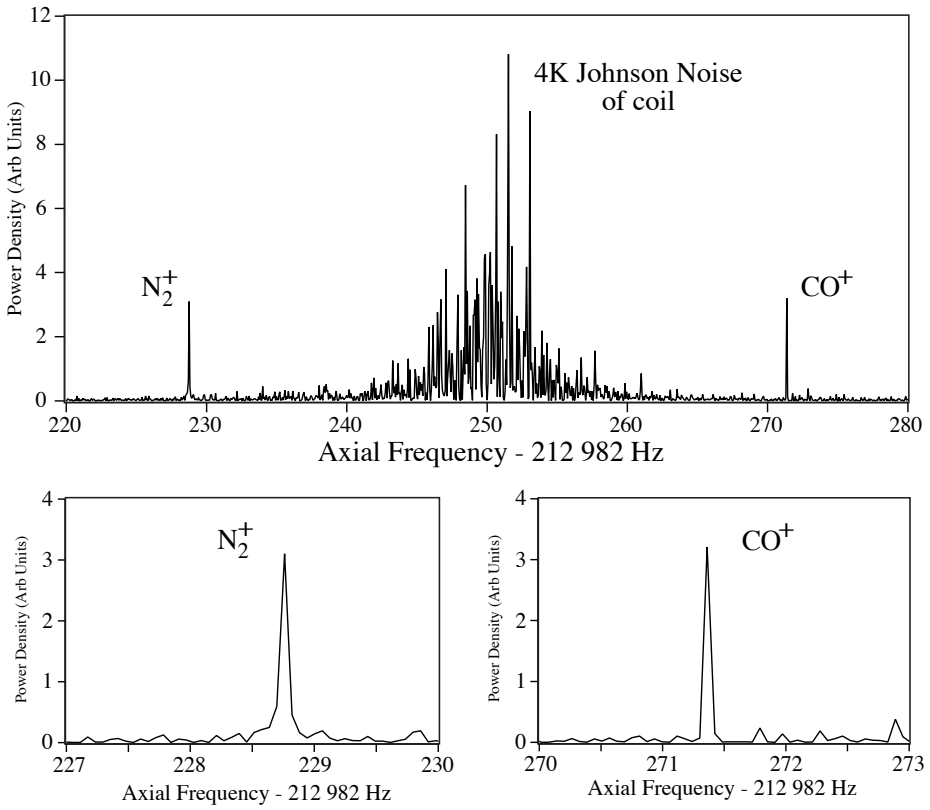

Figure 5-1: Power spectrum of 8 s of simultaneously detected image currents induced by the axial motion of a single N_2^+ and CO^+. From the time domain signals, we can determine each ion's axial phase, frequency, and amplitude to $\pm 20°$, ± 20 mHz, and $\pm 10\%$ respectively. The large noise profile is the 4 K Johnson noise of the self-resonant detection circuit called the coil. Despite detecting the signals in the wings of the detector's resonance, there is no real loss of signal to noise. This is because the Johnson noise still dominates the uniform dc SQUID noise floor even at these large detunings.

the axial signals symmetrically about the center frequency of the self-resonant detection circuit (the coil). From the time domain signals, we can determine each ion's axial phase, frequency, and relative amplitude to about $\pm 20°$, ± 20 mHz, and $\pm 10\%$ respectively.[‡] The phase estimation directly translates into the ability to determine the phase of each ion's cyclotron motion to $\pm 20°$.

We can typically determine the critical difference phase between the cyclotron motions with precision between $\pm 20°$ and $\pm 30°$ depending on the trap tuning and ion-ion separation. If we assume all frequency noise is eliminated, then a measurement noise of $\Delta\phi_2$ on the cyclotron difference phase means that we can determine the mass ratio with a fractional uncertainty $\Delta R/R$ given by

[‡]We use the Laplace transform Maximum Likelihood Estimate signal processing scheme described in Vassant Natarajan's thesis [45]^G.

$$\frac{\Delta R}{R} = \frac{\Delta\phi_2}{360}\frac{1}{T_{\rm evol}\bar{f}_{\rm ct}} \tag{5.13}$$

where $T_{\rm evol}$ is the time the cyclotron motions are allowed to accumulate phase in the PNP measurement and $\bar{f}_{\rm ct}$ is the average cyclotron frequency. For the example pair $^{13}C_2H_2^+$ vs N_2^+ and taking $\Delta\phi_2 = \pm 25°$, we find $\Delta R/R = 1 \times 10^{-11}$ for $T_{\rm evol} = 25$ minutes and $\Delta R/R = 1 \times 10^{-12}$ for $T_{\rm evol} = 4.1$ hours. This sets the absolute best that we can possibly do with the current phase noise. We believe the measurement phase noise is limited solely by the Johnson noise of the 4 K detector.

One way to increase the detection signal to noise is to increase the signal. This corresponds to using larger axial amplitudes. When working with a single ion in the trap, we use axial amplitudes approximately twice as large as those we use when working with two ions in the trap. Using smaller amplitudes is important for not perturbing the coupled magnetron motion, as discussed in Sect. 4.2.5. This also reduces the ion-ion perturbation of the cyclotron frequency ratio, as described in 3.5.3 (since larger axial amplitudes require that we use larger cyclotron amplitudes). For a single ion of $m/q \sim 28$ u/e tuned to resonance with the coil and $z \approx 700$ μm, we can measure the axial phase, frequency, and relative amplitude to $\pm 8°$, ± 10 mHz, and $\pm 10\%$ respectively. Thus, the requirement of small axial amplitudes increases the measurement noise by about a factor of 2.

5.3.1 Detection Bandwidth

Direct Detection

The large noise profile in Fig. 5-1 is that of the 4 K Johnson noise of the coil and reflects the frequency profile of the coil's resonance. The Johnson noise can be modeled as a current noise source with uniform spectral density in parallel with the ion, the latter acting as a slowly damped current source. Since the ion signal has an extremely small bandwidth compared to the coil's resonance, we are only concerned with the local noise density near the ion's axial resonance. Hence, we can accurately approximate the detection noise as uniform and with the value at the center of the axial resonance. Thus, at the dc SQUID, both the detected Johnson noise $i^2_{\rm jsquid}$ of interest and the induced ion current $i^2_{\rm isquid}$ fall off with the detuning from resonance with the coil in the same manner

$$i^2_{\rm isquid} = \frac{i^{\circ 2}_{\rm isquid}}{1 + \delta^{*\,2}} \tag{5.14}$$

$$i^2_{\rm jsquid} = \frac{i^{\circ 2}_{\rm jsquid}}{1 + \delta^{*\,2}} \quad , \tag{5.15}$$

where i° is the detected current when the axial mode is resonant with the coil. Thus, we only expect a significant loss of signal to noise when the detected Johnson noise level becomes comparable to the uniform noise floor of the dc SQUID. With the present detection circuit,

this occurs at ion-coil detunings of ±27 Hz. If the trap voltage is tuned so that the axial signals of the two ions are symmetrically located on either side of the resonance, then we can simultaneously detect mass doublets with fractional mass difference $2\eta \leq 5.0 \times 10^{-4}$ without significant loss of signal to noise. As will be discussed below, the use of a single sideband mixer before sampling the data would increase the effective detection range by $\sqrt{2}$ to ±38 Hz or doublets with a fractional mass difference of $2\eta \leq 7.1 \times 10^{-4}$.[§]

Axial Sideband Detection

In the original work with two ions in a single Penning trap [2][G], the axial motion of the two ions was detected by modulating the Ring voltage to create FM sidebands on each ion's axial motion. The trap voltage was tuned so that the axial modes were symmetric about the center frequency of the coil. The modulation frequency was then chosen so that a first order sideband from each ion was near to resonance with the coil. We were able to do this as well; however, we found that the signals were often flaky. We also had some suspicion that the Ring modulation was affecting the magnetron motion of the ions. I now believe that the flakiness was caused by pulsing the axial motions to too large an amplitude. In the future, perhaps choosing the modulation frequency so that the sidebands are still far from resonance might help. I am fairly optimistic that with the experience gained, the use of FM modulation can be used to increase the range of doublets whose axial motions we can simultaneously detect.

The biggest concern with using sidebands is that even in the best case scenario in which all of the axial motion is contained in the first upper and lower sidebands, the effective instantaneous amplitude at each frequency component is down by $\sqrt{2}$. If one listens for the entire damping time, then the same energy is extracted from the ion and so there should be no reduction in parameter estimation. But, in an anharmonic trap, the factor of two longer damping time leads to a greater impact of frequency chirping on the estimation of the phase at $t = 0$. Empirically, working with a single ion in the trap, we have found an increase in the phase noise of about 50%.

To accurately measure the difference phase, one could choose the modulation frequency so that ion 0's first upper and ion 1's first lower FM sidebands exactly overlap close to resonance with the coil. This would give a factor of 2 boost in the instantaneous amplitude of the detected signal. One might even imagine then producing a π phase slip in one of the axial modes to read out the other quadrature of the difference phase. This might be accomplished by introducing a large "AC Stark shift" of one of the two axial modes by a far

[§]Using feedback to artificially increase or decrease the Q of the transformer does not significantly increase or decrease the critical detuning at which the (possibly subthermal or superthermal) Johnson noise of the transformer becomes comparable to the dc SQUID background. To see this, one must know that feedback causes the peak Johnson noise to scale as $(Q_0/Q_m)^2$, while the FWHM of the Lorentzian detector response scales as (Q_m/Q_0) where Q_0 is the Quality factor with no feedback and Q_m is the modified Quality factor with feedback applied.

from resonance sideband coupling to its cyclotron mode. Knowledge of the Rabi frequency can be combined with the coupling's detuning to determine exactly how long the "π-phase slip" drive would need to be applied.

Alternating Detection

It is not absolutely necessary that the axial frequencies be simultaneously detected. One could encode the cyclotron phase information in its amplitude, as is done in the SOF technique described in Vassant Natarajan's thesis [45]^G, and in Ref. [46]^G. The amplitudes could then be sequentially read out. It might also be possible to simply measure one axial phase and then the other by changing the trap voltage between the measurements. Because of the anharmonicity of the axial mode, it would probably be best to perform the π-pulse for each ion only when its axial motion is ready to be detected immediately. The requirement on the stability of the magnetic field becomes greater, since the shortest evolution time possible is then the time needed to measure the axial phase, which is typically between 4 and 8 s. One could use an external magnetometer to correct for fast variation of the magnetic field during this 4 to 8 s, since such fast variation tends to arise external to the magnet.

Improvements for Direct Detection

The ability to measure ion signals in the wings of the coil resonance is new. In previous work, the peak Johnson noise and rf SQUID technical noise were of comparable magnitude, and it was important that the signals be detected on resonance. A 10× quieter (in power) dc SQUID has replaced the previous rf SQUID.[¶] In addition, we were able to increase the coupling of the coil to the dc SQUID by a factor of 25 without reducing the Q of the self-resonant coil. The net result is that the SQUID noise floor was reduced by approximately ×250 relative to the Johnson noise.

Figure 5-2 shows an averaged power spectrum of the noise from our axial detector. The average was calculated by taking 100 s of time data and dividing it into 50 independent chunks of 2 s from which 50 independent power spectrums were calculated and then averaged together. The noise spectrum is well described by the expected Lorentzian (associated with the coil's 4 K Johnson noise) on top of a uniform noise floor (associated with the dc SQUID's technical noise). The ratio of the fitted peak power to the noise floor power is 120 ± 10. However, the signal from the SQUID was mixed down with a standard mixer before sampling with the computer. The contribution of the negative frequency components effectively doubles the observed noise floor in the digitized data. The true noise floor is then

[¶]Michael P. Bradley and James V. Porto deserve all the credit for upgrading from the rf to the dc SQUID. Not only is it a quieter detector, but based on reading previous theses and working with the rf SQUID myself, but the dc SQUID is also much less flaky once in working condition.

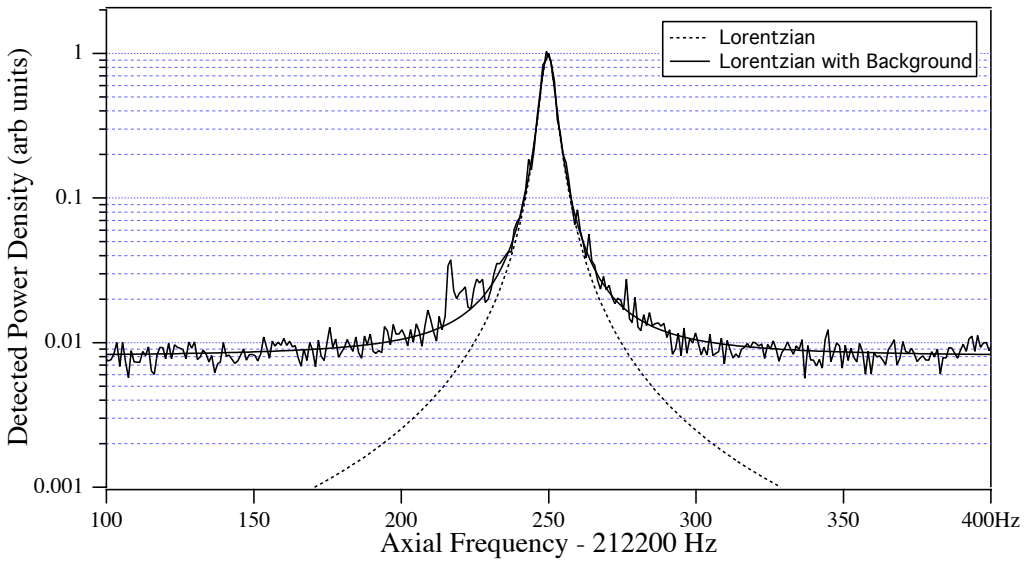

Figure 5-2: Average power spectrum of the noise from our axial detector.

240 ± 20 below the peak Johnson noise.[‖] This agrees well with the previous observation that the peak Johnson noise and rf SQUID technical noise were of comparable magnitude[**] and the fact that we expect a reduction of $\times 250$.

The use of a single sideband mixer would remove the contribution of the negative frequency components.[††] This would increase the range of axial frequencies that could be simultaneously detected by $\sqrt{2}$. The single side band mixer uses a negative interference to cancel the negative frequency components. However, this tends to work only in the neighborhood of a particular frequency. The large axial separation of even good doublets means that two independent mixers would have to be used. But this slightly breaks the common path of the two signals before digitizing, and I would only do this if I needed results fast. Instead, I would suggest that the signal be directly sampled without mixing and then that the SSB stage occur in software. Alternatively and perhaps more easily, the SQUID signal could be mixed down in two parallel steps—with a cosine-quadrature and sine-quadrature version of the local oscillator. Each intermediate frequency signal could then be low pass filtered and digitally sampled independently. The interferometric cancellation of the negative frequency components could then be performed in software at each ion's axial frequency independently. The local oscillator phase shifter could be made simply and robustly. Any gain imbalance could be corrected in-software.[‡‡]

[‖] I verified that the measured noise floor is well above the contribution from amplifiers and lowpass filters after the SQUID. However, I cannot find direct evidence of this in the log books, so I would encourage that this be easily confirmed in the future.

[**] The quoted ratio of peak Johnson noise to rf SQUID noise was measured with a single sideband mixer.

[††] Early in my graduate career, I built such a device, and it should still be in good working condition. In addition, the previous single sideband mixer still exists although it may be less reliable.

[‡‡] An IC chip may exist that would do all of this, given the advancement of cellphone technology.

5.3.2 Feedback on Axial Detector

Since we can now precisely measure the thermal Johnson noise with the dc SQUID, it might be possible to use feedback to reduce its impact on our measurements. We attempted to implement this and showed that feedback could indeed reduce the effective temperature of the Johnson noise by as much as a factor of 8, from 4 K to an effective temperature of 0.5 K. Since the feedback loop also reduces the size of the effective Johnson noise we are detecting, the maximum possible temperature reduction goes like the square root of the peak Johnson noise to the noise floor, which for our detector gives a reduction of $\sqrt{240} = 16$. The lowest temperature we could possibly cool to is then $\sim$ 0.25 K. If the ion's axial temperature were to come to equilibrium with the subthermal electronic mode of the coil, then this would reduce the PNP-to-PNP fluctuation of the cyclotron amplitudes by a factor of 4. However, we could not show that this negative feedback resulted in a reduction of the ion's axial temperature, and this remains an open and possibly very fruitful avenue of pursuit especially in light of the recent demonstration of ion cooling demonstrated by D'Urso, *et al.* in the group of Gabrielse [3].

We did show a factor of 2 improvement in phase estimation when using the feedback. The improvement is believed to result from lengthening the damping time of the ion while maintaining the instantaneous signal to noise ratio fixed. In the time domain, we have simply increased the time over which we average the signal. In the frequency domain, we have reduced the bandwidth of the detected signal. The improvement in parameter estimation was greatest for ions with short damping times such as Ne^{++} or Ne^{+++}, for which the parameter estimation was poor without feedback. For longer damping times, the chirping of the axial frequency (due to anharmonicities combined with damping) leads to greater uncertainty in the phase of the axial motion at $t = 0$. We wish to know the phase of the axial motion at $t = 0$ since this encodes the phase of the cyclotron motion. Our approach to improved phase estimation is discussed in much more detail in Simon Rainville's thesis [1]^G.

5.4 Simultaneous PNPs

As shown in Sect. 5.2, we expect simultaneous cyclotron frequency comparisons to be 2η less sensitive to magnetic and trap voltage noise than the previous technique of alternately comparing the frequencies. We have developed the ability to park the ions on a common magnetron orbit on opposite sides of the trap, and the ability to precisely measure the phase of the axial motions. We are now in position to perform simultaneous cyclotron frequency comparisons by performing PNP measurements on both ions simultaneously. Figure 5-3 shows the measured phases (modulo 2π) of ion 1 versus ion 0 after letting both cyclotron modes accumulate phase for $T_{\rm evol} = 200$ s. While the individual phases vary over the full 360° range of the graph, they clearly vary together. The range of variation corresponds

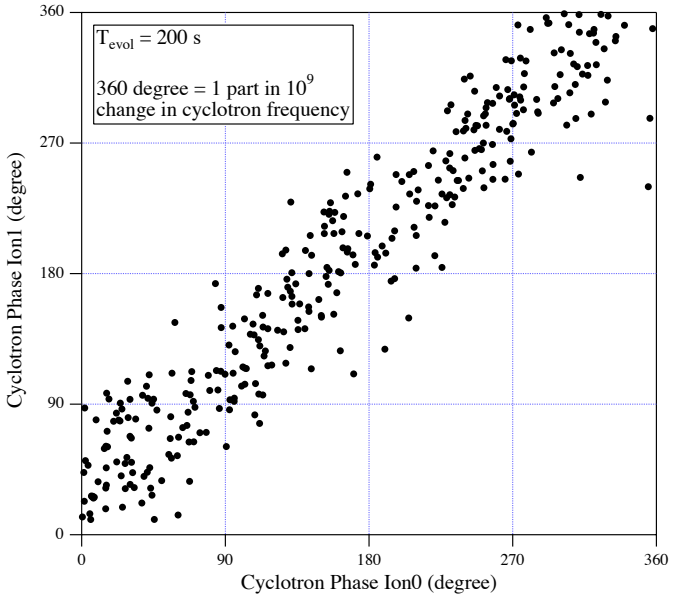

Figure 5-3: The cyclotron phase of ion 1 vs ion 0 at the end of a PNP with $T_{\rm evol} = 200$ s. The strong correlation indicates the common effect of the magnetic field and trap voltage noise on the trap cyclotron frequency of both ions. In this data, ion 1 is a $^{13}C_2H_2^+$ and ion 0 is a N_2^+.

to changes in each individual cyclotron frequency by at least 1 part in 10^9, although the actual variation is larger than this because we actually lose track of several 2π. The obvious correlation of the individual phases is a clear indication that we have truly achieved common mode rejection of the magnetic field noise when the important difference phase is calculated.

The limitation on how precisely we can measure the mass ratio is how precisely we can measure the trap cyclotron frequency difference $\omega_{\rm ct2} \equiv \omega_{\rm ct1} - \omega_{\rm ct0}$. Figure 5-4 shows the measured $\omega_{\rm ct2}$ versus time for the example pair $^{13}C_2H_2^+$ vs N_2^+. The vertical arrow indicates how much the points would have to move to change the mass ratio R by 1 part in 10^9. The longest evolution time was $T_{\rm evol} = 200$ s. In terms of determining the mass ratio R, the data points are distributed with a standard deviation of 9×10^{-11}. In only 3 minutes we obtain the same precision as 5 hours of data taking at night with the alternating technique! In addition, we can take data even when the subway is running so that we can accumulate much more data. In this example, there are a total of 371 points taken over 3.3 days. The data were taken under complete computer control with human intervention approximately every 15 hours*. From these data, the mass ratio R could be determined with a *precision* of 5×10^{-12}. Since the measured phase noise at the longest evolution times is still dominated by the phase measurement noise, a longer evolution time of $T_{\rm evol} \sim 600\ s$ would allow a precision of 3×10^{-12} in the same time interval. With no further improvements, we could

*We were actually able to leave the lab for most of this time.

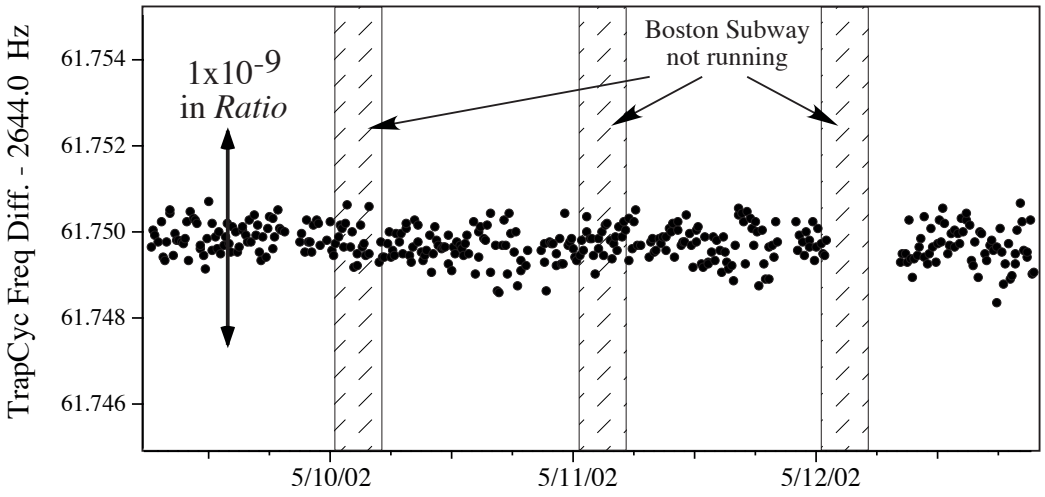

Figure 5-4: The trap cyclotron frequency difference $\omega_{ct2}/2\pi$ vs time. In this data, ion 1 is a $^{13}C_2H_2^+$ and ion 0 is a N_2^+.

average down to a precision of $\sim 10^{-12}$ in only one week.

We had to work extremely hard to get to the point of being able to produce data such as that shown in Fig. 5-4. But having arrived, it is clear that the two-ion technique works spectacularly well at rejecting magnetic field noise. There is not much more to say on the subject of common mode rejection of magnetic field noise other than hooray! I will briefly turn to a discussion of the new limitations on our precision. But first we will examine the systematic errors we confront, and how we have dealt with them. Simon Rainville's thesis [1]^G contains a much more complete accounting of the systematic error budget than is given here.

5.5 Ion-Ion Nonlinear Coupling

The expected systematic errors associated with ion-ion interactions are thoroughly discussed in Sect. 3.5. The major expected systematic error above a few parts in 10^{12} arises from a possible systematic imbalance in the cyclotron amplitudes of the two ions while they are accumulating cyclotron phase.

5.5.1 Observation of Nonlinear Cyc-Cyc Frequency Perturbation

As explained in Sect. 3.5.3, there is a shift of the trap cyclotron frequency difference ω_{ct2} that results from the combined monopole and quadrupole charge distribution experienced by one ion due to the other ion's time averaged cyclotron motion. We predicted that higher order terms in the expansion of the charge distribution were not required to accurately predict the size of the shift that depends on the cyclotron amplitudes. Restating the result of Eq. 3.79, we have

$$\frac{\Delta\omega_{ct2}}{\bar{\omega}_c} \approx -\delta_{cyc}\frac{9\Omega_c}{4\bar{\omega}_c}\frac{\bar{\rho}_c^2}{\rho_s^2} \tag{5.16}$$

with the cyclotron amplitudes given by $\rho_{c0} = \bar{\rho}_c(1+\delta_{cyc})$ and $\rho_{c1} = \bar{\rho}_c(1-\delta_{cyc})$.

We can test this prediction by purposefully changing δ_{cyc} by a known amount and measuring how much the trap cyclotron frequency difference ω_{ct2} changes. By changing the voltages on the cyclotron drive synthesizers, we alternated between $\delta_{cyc} = +0.1$ and $\delta_{cyc} = -0.1$ and measured ω_{ct2} for each setting.* As an example, we will consider such a test for the example pair $^{13}C_2H_2^+$ vs N_2^+ $[1]^G$. At an ion-ion separation $\rho_s = 700$ μm and $\bar{\rho}_c = 66$ μm, we observed a change of $\Delta\omega_{ct2}/\bar{\omega}_{ct} = -1.00(17)\times 10^{-11}$. This is in excellent agreement with the theoretical prediction of Eq. 5.16, $\Delta\omega_{ct2}/\bar{\omega}_{ct} = -0.80(19)\times 10^{-11}$. The uncertainty arises mainly from a 5% uncertainty on ρ_s. Since δ_{cyc} is not vanishingly small, there is a contribution from a term of order δ_{cyc}^2 that increases the predicted shift by a fractional amount $\delta_{cyc}/2 \sim 0.05$. Also, including the next higher order term in the multipole expansion of the field increases the predicted shift by another 5% (see Fig. 3-6). The predicted value including higher order effects is then $\Delta\omega_{ct2}/\bar{\omega}_{ct} = -0.88(21)\times 10^{-11}$. Theory and experiment therefore have a ratio 0.88(25), which is consistent with unity. This provides confidence that we have correctly treated the nonlinear ion-ion interactions. This is important because this interaction is expected to be the dominant ion-ion systematic error in determining the mass ratio R.

For this test, it was necessary to make the perturbation from the nonlinear interaction much greater than that from trap field imperfections such as B_2, C_4, etc. Since the nonlinear interaction of Eq. 5.16 scales as $1/\rho_s^5$, this was accomplished by moving the ions to an ion-ion separation of approximately $\rho_s = 700$ μm. For our example pair $^{13}C_2H_2^+$ vs N_2^+, the predicted effect of nonlinear interaction was approximately 10× larger than that from trap imperfections. The contribution of trap field imperfections was subtracted before comparison with theory in the result discussed above.

See Sect. 3.5.3 for a suggestion of how to eliminate this source of systematic error by averaging the cyclotron frequency ratios determined from both simultaneous and alternate cyclotron frequency comparisons.

5.5.2 Measuring the Drive Synthesizer Imbalance

Since the cyclotron modes are not damped during the phase evolution period of the PNP measurement, the task is to apply initial drives that are as symmetric as possible. The largest possible source of cyclotron amplitude imbalance is expected to arise from a differential voltage calibration of the two synthesizers supplying the two drive signals. In addition, the two independent drive signals are combined using a Mini-Circuits signal com-

*When we took accurate cyclotron frequency ratio data to determine the mass ratio, the value of δ_{cyc} was at least 10× smaller than this purposeful imbalance.

biner that could have an imbalance of the input ports. We have measured the beating of the two combined drives against one another on a scope. From the amplitude modulation depth of the observed trace as the two signals beat against one another, we can infer that the drive amplitudes are the same to $\leq 0.5\%$. This is an upper limit and not a lower limit since the cyclotron drive amplifier is observed to produce significant harmonics that would artificially decrease the measured amplitude modulation depth.

5.5.3 Swapping Drive Synthesizer Roles

The most likely source of cyclotron amplitude imbalance is an asymmetry in the cyclotron drive synthesizers or in combining the two independently generated drives. We can test for this source of cyclotron drive imbalance by swapping the roles of the two synthesizers (which also swaps the signal combiners) and comparing the measured cyclotron frequency ratio. Specifically, the cyclotron frequency ratio R_a is measured with the synthesizer labeled HP1 (HP2) providing the resonant cyclotron drive for ion 0 (ion 1). The cyclotron frequency ratio R_b is measured with the synthesizer labeled HP2 (HP1) providing the resonant cyclotron drive for ion 0 (ion 1). We can then ask by how much the measured ratio changed R_a/R_b - 1. We found for the example pair $^{13}C_2H_2^+$ vs N_2^+ that at a small ion-ion separation of $\rho_s \sim 700$ μm, the ratio changed by $-6(13)\times10^{-12}$. But this ought to be twice the systematic error. So we can place a limit of $-3(7) \times 10^{-12}$ on the nonlinear interaction at the ion-ion separation of $\rho_s = 700$ μm.

The imbalance of the drive synthesizers could be removed as a source of systematic error by randomly swapping the roles of the two cyclotron drive synthesizers throughout a sequence of PNP measurements. Any systematic drive imbalance would average to zero. This has not been done because the role swapping breaks the phase coherence of the measurement scheme. The breaking of phase coherence could be overcome by directly measuring the relative phase between each cyclotron drive and its associated coupling drive. The phase comparison could be performed during the axial ringdown so that no time is lost. In addition, the high signal to noise of the relative phase measurement means that the role swapping would introduce only a negligible increase in the total measurement phase noise $\leq 0.1°$. Even if this is performed, it will still pay to make the output of the two drive synthesizers as balanced as possible so that the averaging process does not introduce any significant frequency noise into the cyclotron frequency comparison.

We will now justify why we ignore other small sources of cyclotron amplitude imbalance. If the cyclotron driving forces applied to the two ions are identical, then the small fractional mass difference will make the cyclotron radii the same to $2\eta \leq 10^{-3}$. Since the ions are on the same parked magnetron orbit to a few percent, spatial variation of the local effective cyclotron drive strength is of fractional order $\delta_{\rm mag}\rho_{\rm m}^3/d^3 \leq 5 \times 10^{-4}$ assuming the $C_1^1Y_1^1$ and $C_3^1Y_3^1$ geometric coefficients of the split guard rings are comparable. What about the frequency difference between the drives? We choose drive strengths such that the typical

cyclotron drive time is $\sim$ 20 ms. If one of the cyclotron drives is exactly resonant and the other is detuned by ≤ 1 Hz from resonance, then the fractional amplitude difference is $(t_{\rm d}\delta^2/2)^2/3 \leq 1.3 \times 10^{-3}$. The wavelength of the cyclotron drive is 60 m compared to the trap size of $d = 5.49$ mm so that the description of the drive is well within the electrostatic limit and there is no chance of a cavity resonance. For lack of any better choice of scale, we can place a limit of $\omega_{\rm ct2}/\bar{\omega}_{\rm ct} \sim 2\eta \leq 10^{-3}$ on any such geometrical differences associated with the different wavelengths. We can conclude that if identical amplitude voltages at each trap cyclotron frequency are applied to the split Guard Rings, then the fractional difference in cyclotron radii will be $\leq 3 \times 10^{-3}$.

How precisely identical can we make the cyclotron drive voltages applied to the split Guard Rings? The transfer functions between the synthesizers and the Guard Ring electrodes involve resistive-capacitive dividers that will give at most a fractional shift of order $\delta\omega_{\rm ct2}/\bar{\omega}_{\rm ct} \sim 2\eta \leq 10^{-3}$. Transformers in the cryogenic filters give rise to a $Q \sim 2$ resonance in the transfer function centered at about 4.5 MHz. This actually serves to make the transfer function even more flat since the center frequency of the low-Q resonance is very close to the trap cyclotron frequencies of the ions used. We do not expect nor have we observed any other resonance or sharp frequency dependence in the net transfer function between the split Guard Rings and the synthesizers supplying the drive signals. The above experimental considerations confirm that the main source of concern is any asymmetry in the cyclotron drive synthesizers or signal combiners.

5.5.4 Varying Average Cyclotron Radius $\bar{\rho}_{\rm c}$

In addition to swapping the roles of the two drives, we can vary the cyclotron drive time so that the average cyclotron radius $\bar{\rho}_{\rm c}$ is changed. If there is an imbalance in the drive strengths or transfer functions, then we expect the systematic error to vary as the square of the average cyclotron amplitude $\bar{\rho}_{\rm c}^2$. By comparing the change in the measured ratio, we can extract a cyclotron imbalance of $\delta_{\rm cyc} = -0.028(20)$ for the example pair $^{13}C_2H_2^+$ vs N_2^+. This is a weak constraint because we found that at small ion-ion separations where the effect is of greatest concern, we can only change $\bar{\rho}_{\rm c}$ by about a factor of 2. The range of $\bar{\rho}_{\rm c}$ experimentally accessible is limited by signal to noise at the low end and increased cyclotron frequency noise at the high end. The high end limit is due to a linear growth in the shot-to-shot frequency noise arising from shot-to-shot variation of the cyclotron amplitudes coupled with trap field imperfections, ion-ion interactions and special relativity. The amplitude fluctuations are caused by the initial thermally-distributed amplitudes of the cyclotron motions just before the cyclotron drive is applied.

5.6 Controlling the Impact of Trap Field Imperfections

The perturbations of the measured cyclotron frequency ratio due to ion-ion interactions fall off rapidly as ρ_s^{-5} and ρ_s^{-6}. Thus there is large motivation to make ρ_s as large as possible. On the other hand, the fractional imbalance in the rms magnetron radii δ_{mag} grows as ρ_s^3. The cyclotron frequency of each ion is perturbed as ρ_m^2 due to B_2 and C_4 and ρ_m^4 due to C_6 and B_4. Since the average magnetron radius $\bar{\rho}_m = \rho_s/2$, this means that the differential effects of trap imperfections scale as ρ_s^5 and ρ_s^7 (see Sect. 3.3.3). As a result, we must carefully control the trap fields to avoid large systematic errors. On the positive side, the only quantity we need to know precisely is ω_{ct2}, so we can focus on tuning the trap to avoid perturbing this quantity without having to worry significantly about resulting perturbations of the other two quantities of interest ω_{ct1} and ω_{z1} (or equivalently ω_{ct0} and ω_{z0}).

When working with a single ion, we used zero magnetron amplitudes and small cyclotron amplitudes so that the errors caused by higher order terms in the multipole expansion in powers of r/d were insignificant. The chief goal was then to minimize the magnitudes of C_4 and B_2. The magnitude of C_4 was minimized by careful choice of the Guard Ring voltage, and the magnitude of B_2 was minimized by a superconducting shim built into the magnet. The goal was to set both of these parameters to zero. Imagine that one were to make a plot for a single ion of the variation of the trap cyclotron frequency versus magnetron radius or Δf_{ct} versus ρ_m. The goal was then to make the plot completely flat, with the contributions from C_6 and B_4 only causing the plot to depart from zero well outside of the region of experimental interest. In this sense, the goal was to make the plot globally zero within the region of interest.

When working with two ions in the trap, we will have to settle for local flatness of Δf_{ct} versus ρ_m about the magnetron radius of interest. This is chiefly because we do not have shim electrodes with which to tune C_6 to zero. For a pair of ions parked on a common magnetron orbit on opposite sides of the trap, we will introduce a C_4 that causes the plot of Δf_{ct} versus ρ_m to have a minimum or maximum at the average magnetron radius of the two ions $\bar{\rho}_m$. This also makes the measurement completely independent of the size of the magnetron imbalance δ_{mag}, so that even if the anharmonicities slightly modify δ_{mag} (see Sect. 3.3.4), our answer is not affected. This optimal value of C_4 is precisely the fctOpt defined in Sect. 2.2.5.

If we could calculate and produce exactly the optimal C_4 at a given ion-ion separation, then the net effect of all trap field imperfections on ω_{ct2} is zero up to order δ_{mag}^3. But in fact, we cannot precisely determine the optimal C_4 or fctOpt. This is because of the uncertainties on the measured parameters D_4, V_{gr}°, B_2, C_6, B_4, and ρ_s. For instance, imagine that we make a small error in our estimate of ρ_s. Then when the trap is tuned to the calculated fctOpt, the local extremum in the plot of Δf_{ct}versus ρ_m is at a slightly different position from $\rho_s/2$. This introduces a differential error on ω_{ct2} that scales as the curvature of the function Δf_{ct} evaluated at the local extremum times the fractional magnetron imbalance

parameter $\delta_{\rm mag}$. For a polynomial of the form $\alpha\rho_{\rm m}^2 + \beta\rho_{\rm m}^4$, the curvature of the extremum grows as $\rho_{\rm m}^2$. In addition, the fractional imbalance $\delta_{\rm mag}$ grows as $\rho_{\rm s}^3$. As a result, one calculates uncertainties—not systematic errors—that grow as $\rho_{\rm s}^5$ and higher. This optimal tuning procedure is preferrable to simply applying systematic corrections after taking the data. Such corrections would require precise knowledge of the actual magnetron radius imbalance, which is predicted to be slightly perturbed in an imperfect Penning trap.

5.7 Ratio versus Ion-Ion Separation (R vs $\rho_{\rm s}$)

The acid test of our understanding of the systematic errors is to measure the cyclotron frequency ratio R versus $\rho_{\rm s}$ to see if we can account for any observed variation. This will truly be a culmination of all of our work.* To accomplish this, we use the techniques described in Sect. 4.4.2 for moving the ions closer together or further apart and approximately zeroing the common mode magnetron motion. We then measure the cyclotron frequency ratio at several values of C_4 at and around the fctOpt value discussed in the preceding section. From the variation of the ratio R with C_4, we can extract the value of $\delta_{\rm mag}$. We find good agreement with theory, as is described in Fig. 4-17.

Finally, we fit a straight line to a plot of R vs C_4 at a constant $\rho_{\rm s}$. From the fit we extract a value of R at the fctOpt value of C_4. Repeating this procedure for several ion-ion separations yields Figures 5-5 and 5-6 for the ion pairs $^{33}S^+$ vs $^{32}SH^+$, $^{29}Si^+$ vs $^{28}SiH^+$, and $^{13}C_2H_2^+$ vs N_2^+. The data sets are shown in the reverse order in which they were taken, with the first pair representing a month of data taking on $^{13}C_2H_2^+$ vs N_2^+ as we learned lots of experimental ropes. The following two data sets took approximately 2 weeks each, and I believe the increased quality of the data sets reflects the experience gained in working with the first pair.

The ratios have a large offset subtracted for display purposes. Each grid mark corresponds to a fractional change of 1×10^{-11} in the ratio. The final quoted ratio is indicated by the horizontal solid line. The final quoted error on the ratio is indicated by the horizontal dashed lines above and below the average. The two regions centered about the average are by how much we might have expected the ratio to vary with $\rho_{\rm s}$. The hatched area represents uncertainties associated with ion-ion interactions, which grow quickly at short distances. The darker band represents uncertainties arising from knowledge of the trap field imperfections, which grow quickly at large ion-ion separation $\rho_{\rm s}$. The observed variation of the ratio is much smaller than the trap imperfection bands predict. This is a strong indication that we have been overly conservative in estimating how well we know the trap

*These graphs feel somewhat like children because of all of the work that it took to get them. The concepts for analyzing these graphs were developed by myself and Simon Rainville, and we both jointly took the data. That being said, in the division of labor for our thesis it was Simon Rainville who carried through the final analysis for the plots of the measured cyclotron frequency ratio R versus ion-ion separation $\rho_{\rm s}$. I have taken them directly from his thesis [1]^G, and one should see Simon's thesis for a careful accounting of the various sources of error and corrections.

fields, ion-ion separation, etc.

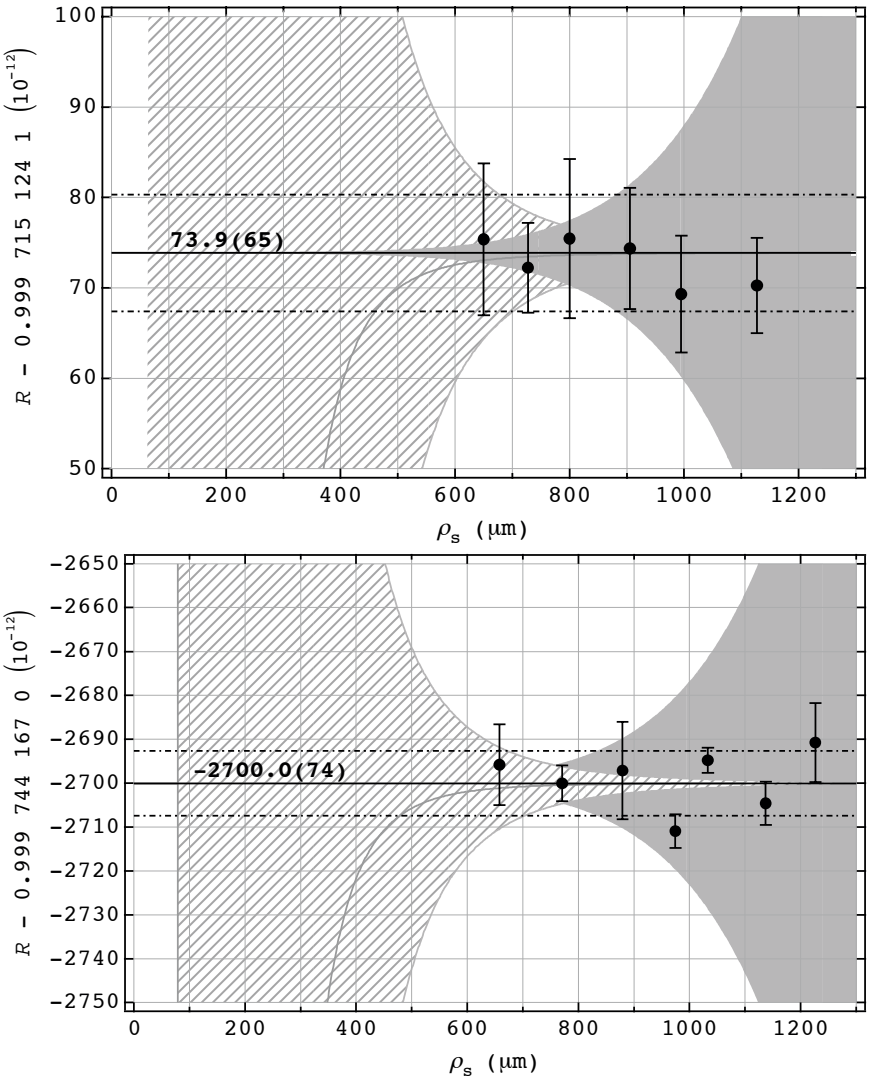

Figure 5-5: Measured ratios $R = m[^{29}\mathrm{Si}^+]/m[^{28}\mathrm{SiH}^+]$ (top) and $R = m[^{33}\mathrm{S}^+]/m[^{32}\mathrm{SH}^+]$ (bottom) versus the ion-ion separation. The final quoted ratio R and uncertainty of 7×10^{-12} is represented by the solid and dashed lines respectively. These comparisons will be used to test the relation $E = mc^2$ by "weighing" the γ-rays emitted in the neutron capture process relating the two isotopes of S and Si.

We have chosen to remain conservative. We essentially calculate our uncertainty on the systematic errors as the quadrature sum of where the ion-ion and trap field imperfection bands cross. Adding in quadrature a statistical uncertainty of comparable magnitude to the two systematic uncertainties gives fractional uncertainties on each ratio of 7×10^{-12}. This is a full order of magnitude more accurate than was ever achieved in our laboratory. The fact that the final errors on the ratio overlap with almost all of the measured values, is once again an indication that we are being conservative with this error assignment. Further

studies of systematics may reveal that we are limited by statistics and not by systematics, and that we can reach accuracies of $\sim 10^{-12}$ by simply integrating.

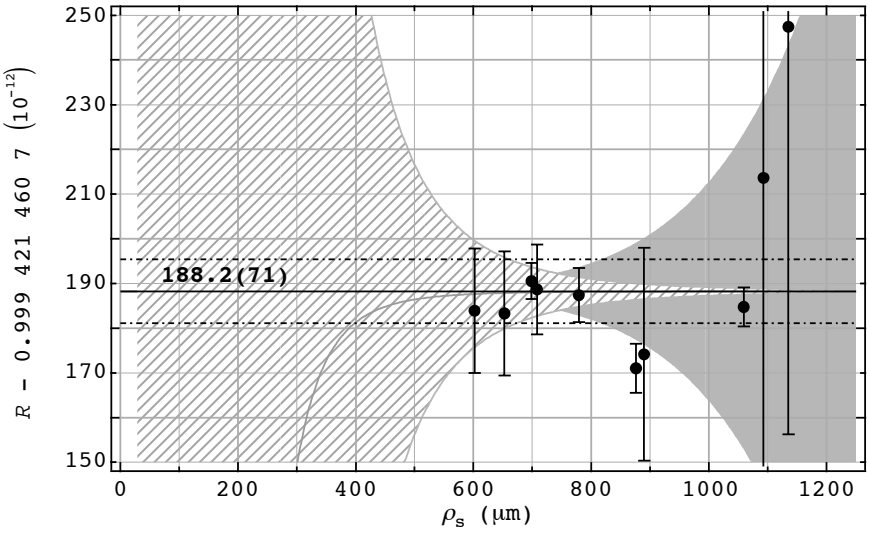

Figure 5-6: Measured ratio $R = m[^{13}C_2H_2^+]/m[N_2^+]$ versus the ion-ion separation. The final quoted ratio R and uncertainty of 7×10^{-12} is represented by the solid and dashed lines respectively.

Chapter 6

Polarization Forces

6.1 Experiment

The cyclotron frequency ratio of CO^+ versus N_2^+ is observed to vary by as much as 1 part in 10^9. The variation actually occurs in discrete jumps between approximately three values. With the two-ion technique, we can easily resolve these jumps with a series of single measurements, each of several 100 s duration. Figure 6-1 shows an example. One sees that the value can be quite stable for many hours only to jump from one measurement to the next. Several hours later, the ratio just as suddenly returns to the previous value. This is a very reproducible behavior that we have observed over approximately two years of intermittent measurement.

The source of these jumps was a complete mystery when first observed. Such behavior had not been observed when alternately trapping ions to compare their cyclotron frequencies. Since we first applied the two-ion technique to comparing CO^+ versus N_2^+, we naturally assumed that the jumps must be the result of a problem with the new technique. This belief motivated the development of much of the measurement and control techniques that have proved so crucial for precisely and accurately comparing cyclotron frequencies. We now understand these jumps as resulting from an induced dipole charge distribution in the CO^+ molecule. Before discussing this explanation in the following sections, we will first examine some of the other possible sources of the jumps and some interesting pieces of the puzzle that led to our current understanding.

6.1.1 Possible Sources Ruled Out

To be more specific, the jumps in the measured cyclotron frequency ratio result from jumps in the measured trap cyclotron frequency difference $\omega_{ct2} = \omega_{ct1} - \omega_{ct0}$. For scale, the jumps in the difference frequency are of order 5 mHz. The measured ratio is shown in Fig. 6-1 for convenience and for a more practical purpose. The possibility of the cyclotron frequency jumps occurring as a result of a large change in the magnetic field or the trap voltage is ruled

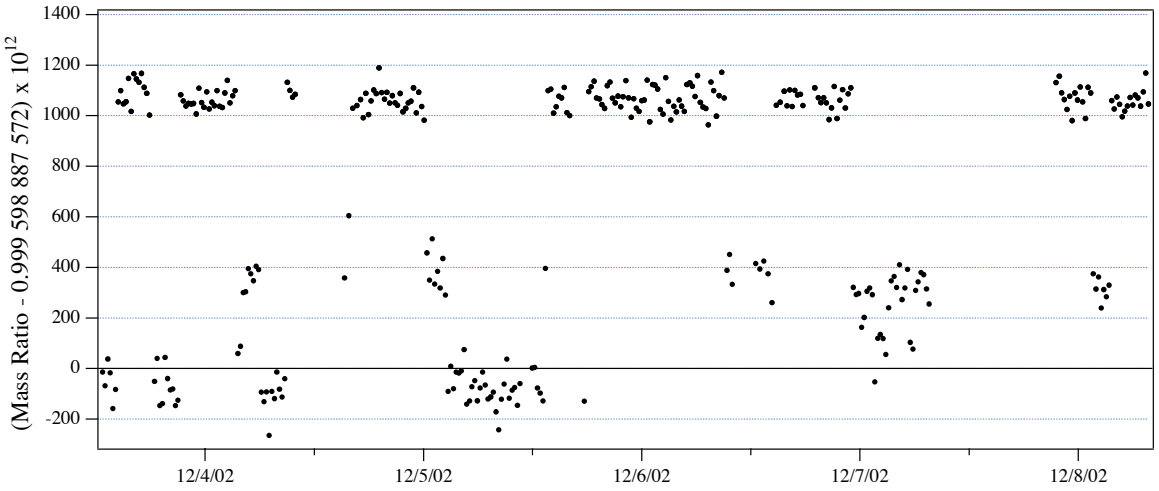

Figure 6-1: Measured cyclotron frequency ratio of N_2^+/CO^+ versus time. The discrete jumps in the ratio can be tracked to jumps in the measured trap cyclotron frequency difference ω_{ct2}.

out by the fact that the jumps occur in the measured ratio, since the ratio is completely insensitive to all but unreasonably large changes. In addition, this might perhaps lead to a single discrepant measurement, but not a series of discrepant values. For scale, the magnetic field would have to change by more than 1 part in 10^6 to change the difference frequency by the observed 5 mHz. This would correspond to changing each cyclotron frequency by about 5 Hz. For such a large change of field, the sideband couplings used to form a cyclotron to axial π-pulse would no longer be resonant, and we would not even be able to take data! Similarly, the trap voltage would have to change by more than 1 part in 10^4. This would correspond to an axial frequency change of $\geq$ 20 Hz, which would be completely obvious since we can measure the axial frequencies to 20 mHz in only 8 s.

One source of cyclotron frequency shifts is the trap field imperfections. If the cyclotron frequency is measured on a millimeter magnetron orbit, the cyclotron frequency is different from that at the center of the trap by $\sim$ 1 part in 10^9. One might imagine that the predicted magnetron coupling of Sect. 3.3 is not accurate in an imperfect Penning trap. One could hypothesize that the magnetron motions are bistable, with the stable configuration consisting of one ion at the trap center and the other ion on a large magnetron orbit. A tristable theory might also include a stable orbit with both ions at the same magnetron radius. When the ions switch between these stable orbits, the cyclotron frequency ratio changes because of the change in the differential perturbation due to the field imperfections. After developing our techniques for monitoring the ion positions, we were able to rule out such an hypothesis by observing the ion-ion separation ρ_s and the rms radius of each ion before and after individual jumps. We saw no changes at the few percent level. Based on knowledge of the size of the trap field imperfections, it is impossible that the jumps result

from a rearrangement of the magnetron orbits.

The observed behavior also is not consistent with the jumps resulting from an ion-ion interaction. First, the ion-ion separation was not observed to vary across the jumps. Second, as we varied the ion-ion separation ρ_s, the magnitude of the observed jumps did not change. This second observation torpedoes almost any hypothetical perturbation one could imagine. For instance, one might imagine that a slow drift in the various mode frequencies causes a drift through a resonance for some high-harmonic interaction between the modes. Even if this were the case, the resonant interaction would depend on the strength of the electric field between the ions and so ought to depend on the ion-ion separation.

Another hypothesis was that the jumps might result from a locking-up of the relative phase of the two cyclotron motions. Such an interaction might be independent of the ion-ion separation ρ_s, since the only requirement might be the existence of regions of stability, with only a weak requirement on the depth of these regions of stability. To test this, we varied the initial relative phase of the two cyclotron drives in the PNP measurement from 0 to 2π. We observed that the final relative phase also smoothly varied from 0 to 2π with no clumping of the values to indicate a locking-up of the cyclotron motions. In addition, by measuring the accumulated phase versus phase evolution time, we firmly established that the jumps correspond to jumps in the trap cyclotron frequency difference and not just a jump in the relative phase of the cyclotron motions.

We performed alternate measurements of the cyclotron frequencies with the idea that this might reduce any nonlinear interaction that could be responsible for the jumps. To accomplish this, we used an external magnetometer to apply corrections for short term changes in the external magnetic field. The jumps were still observed to occur. This further restricts the types of ion-ion interactions that could be giving rise to the jumps.

Experimental artifacts were also a possibility. For example, if a near-resonant cyclotron drive were to intermittently leak onto the split Guard Rings, then this might pull the cyclotron motion. However, since there is no damping of the cyclotron modes while they are accumulating phase, a drive leak would lead to ringing of the cyclotron amplitude. We did not observe the measured cyclotron amplitude to depend on phase evolution time, thus ruling out this possibility.

Another possibility was an intermittent leak of an axial-cyclotron sideband coupling onto the split Guard Ring electrodes. If the rf leak were small, then the effective coupling to the axial mode could result in an "ac Stark shift" of the measured cyclotron frequency. This did not seem very likely, since the jump sizes tend to be constant. To rule this out, however, we removed any signals at the sideband coupling frequencies while the ions accumulated phase.* This was accomplished by setting one synthesizer to the average of the

*It is probably a very good idea to generate the sideband couplings by amplitude modulating a signal at the average of the two frequencies. We did not do this in everyday operation just to simplify control of the experiment. It would be relatively straightforward to perform this by relying on our advanced degree of automation and control to handle the added complexity for the operator.

two sideband coupling frequencies. Another synthesizer was then set to half the difference of the coupling frequencies. The second synthesizer was then used to amplitude modulate the average frequency signal to generate the two resonant frequencies needed. By using a "burst" mode on the amplitude modulation synthesizer, we could shut off the amplitude modulation while the ions were accumulating phase. The amplitude modulation would then be turned on just for the π-pulse at the end of the phase evolution. As a result, there was no synthesizer or any otherwise generated signals at the sideband coupling frequencies during the cyclotron frequency comparison. The jumps were still observed to occur, thus ruling out the sideband-leak hypothesis.

The data acquisition system was built from scratch and so might have had an unknown bug in the acquisition or analysis aspect of it. Another source of the jumps might be a drift of a synthesizer frequency due to a bad phaselocked loop or an extremely poor master frequency reference to which all the synthesizers are phaselocked. To test this, a separate frequency reference was used for the two cyclotron drive synthesizers while all the other synthesizers remained in the normal configuration. The two cyclotron drive synthesizers were then used as fake cyclotron modes. To generate the fake axial signals for a fake PNP phase measurement, the sideband coupling drives were mixed with the cyclotron drives during the fake axial ringdown. This test included everything except the cryofilters, the ions, and the axial detector. Otherwise, it reproduced a PNP measurement. The measured frequency difference between the two cyclotron drive synthesizers was measured to be extremely stable in time, as one would expect. The sum of the frequencies was observed to drift over many hours by several part in 10^{12}, which is consistent with a reasonable drift between the two stable frequency references. No jumps were observed in this dummy experiment, lending much confidence to the measurement chain and new data acquisition system.

Despite many hours contriving means to generate a differential cyclotron frequency shift (some reasonable and some highly improbable), we could find no evidence that the two-ion technique or experimental artifacts were responsible for the observed variation of the cyclotron frequency ratio. There are other tests that could be mentioned, but instead let us turn to the pieces of the puzzle that pushed us toward enlightenment.

6.1.2 Key Pieces of the Puzzle

There were two key observations that broke open the enigma of the jumps in the cyclotron frequency ratio. First, we were able to observe the cyclotron frequency of each ion independently. See Fig. 6-2 for an example. The signal to noise is not high, but it is clear that the CO^+ molecule alone exhibits jumps in its cyclotron frequency consistent with the observed jumps in the ratio. We never observed the cyclotron frequency of the N_2^+ molecule change in a way that was not common to both ions. Such common shifts can be ascribed to a magnetic field change.

In order to measure the individual cyclotron frequencies such as in Fig. 6-2, we need the

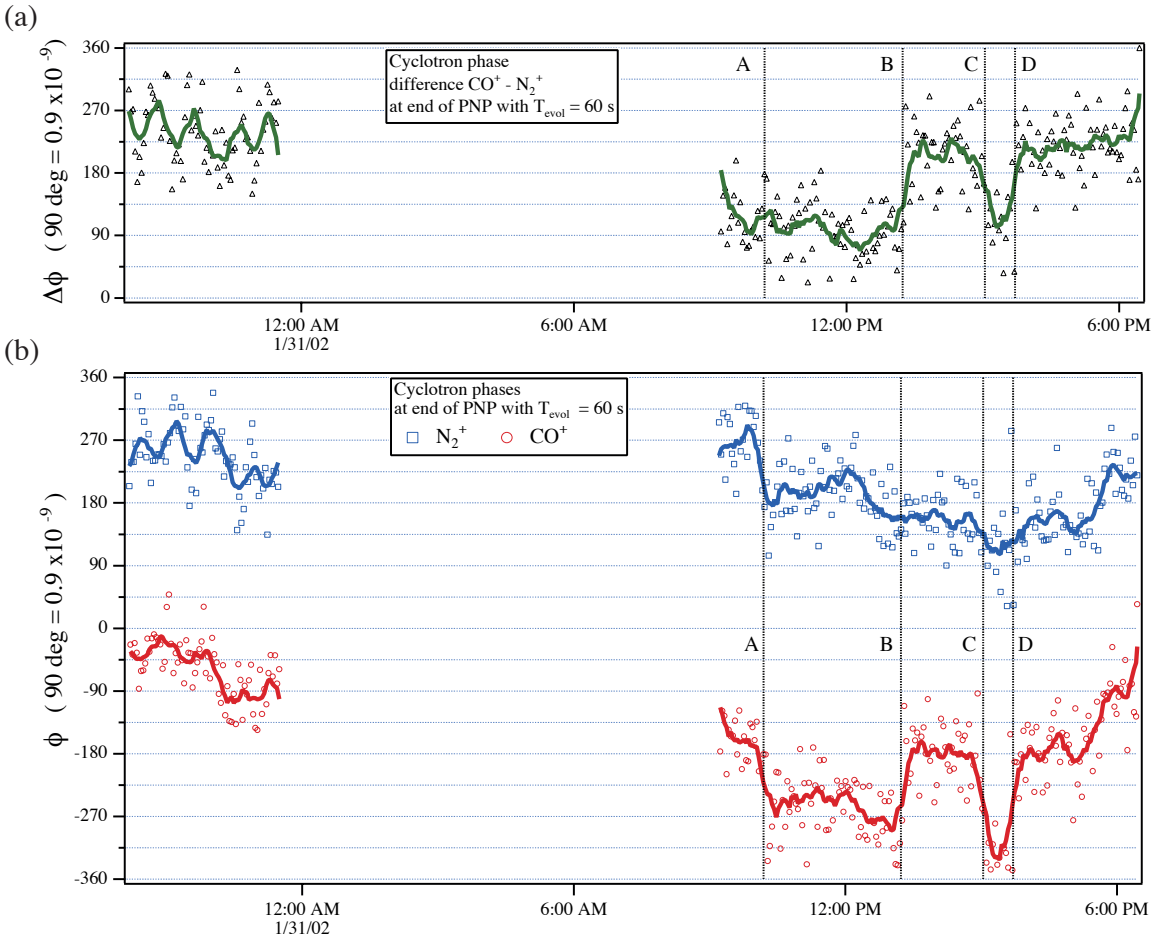

Figure 6-2: Trap cyclotron (a) difference phase and (b) both individual phases for the ion pair CO^+ and N_2^+. The phases were measured after accumulating phase for $T_{\rm evol}$= 60 s. A change of 90° corresponds to a fractional change in the cyclotron frequency of 0.9×10^{-9}. In (a), the cyclotron difference frequency is observed to change at B, C, and D. Examination of the individual phases in (b) shows that it is the cyclotron frequency of the CO^+ ion that changes at points B, C, and D. At these same points, the cyclotron frequency of the N_2^+ ion does not change. At points where the frequency of N_2^+ changes (such as point A), the frequency of the CO^+ ion changes by the same amount. Thus, any variation of the N_2^+ cyclotron frequency can be ascribed to magnetic field variation.

magnetic field to be stable to much better than 1 part in 10^9. The quietest time to take data is at night when the subway is not running. During this period, the typical short time frequency noise is of order $\sim 2.5 \times 10^{-10}$, which is quiet enough to resolve the jumps. But the average time between the cyclotron frequency jumps would make it difficult to catch one or several during this small five hour window. To increase the size of the observation window, we used an external magnetometer to monitor external magnetic field variations and apply a correction to the measured phases based on correlation measurements. The data of Fig. 6-2 have had this correction applied.[†]

The second key observation was motivated by the first result. We compared the cyclotron frequencies of $^{13}C_2H_2^+$ vs N_2^+, which is a fairly similar mass ratio to CO^+ vs N_2^+. This comparison was discussed in the previous chapters. A particular example is shown in Fig. 5-4. In all of the data with $^{13}C_2H_2^+$ vs N_2^+ we never observed sudden jumps in the trap cyclotron frequency difference.

6.1.3 Eureka! CO^+ is the Culprit

The question must be posed: What differentiates the CO^+ molecule from the N_2^+ and $^{13}C_2H_2^+$ molecules? If the mass of the CO^+ molecule is actually changing, then this corresponds to a change of $\sim$ 28 eV. It is difficult to imagine a long-lived excited state of the CO^+ molecule with this kind of energy. Even if such a state did exist, where does the energy to excite it come from? This energy corresponds to a temperature of approximately 3×10^5 K—far from either room temperature or the 4 K trap environment. Another possible source of energy is the external degrees of motion. The largest energy reservoir in the external degrees of freedom is the cyclotron motion. The energy stored in the CO^+ cyclotron motion is approximately 2 eV/(100 μm)^2. For a typical cyclotron radius of $\rho_c = 75$ μm, the kinetic energy is only 1 eV. Based on these considerations, it is completely improbable that these jumps result from an actual mass change of the CO^+ molecule.

The CO^+ molecule differs from the N_2^+ and $^{13}C_2H_2^+$ molecules in that it does not have the same high degree of symmetry about its center of mass. This means that the CO^+ molecule can have an electric dipole moment in its body frame.[‡] A literature search revealed theoretical estimates of the body-frame dipole moment $\mu \sim 1\ ea_\circ$ with respect to its center of mass. This is a relatively large value. We believe that this electric dipole moment is responsible for the observed cyclotron frequency jumps, because it gives the molecule a polarizability that depends on its internal quantum state.

We will show that an electrically polarizable ion will have its cyclotron frequency shifted by a fractional amount (in SI)

[†]The particular data of Fig. 6-2 were taken by alternately measuring the cyclotron frequencies of the two ions. Based on the measured scatter of the difference phase, the precision on the cyclotron frequency ratio is approximately $1.0 \times 10^{-10}/\sqrt{\text{hour}}$.

[‡]We chose to compare $^{13}C_2H_2^+$ to N_2^+ because of the high symmetry and the fact that it was a similar doublet pair.

$$\frac{\Delta\omega_c}{\omega_c} = -\frac{\alpha B^2}{m} \quad . \tag{6.1}$$

where α is the dc polarizability of the ion. This is a systematic error and is bad in its own right. But the systematic error is constant and would not result in the cyclotron frequency jumps we observe. However, the value of the polarizability depends on the internal quantum state of the molecule, which we will denote with a single label λ. For instance, the label λ specifies a unique electronic, vibrational, rotational state. We should then rewrite the cyclotron frequency shift (in SI) as

$$\frac{\Delta\omega_c^\lambda}{\omega_c} = -\frac{\alpha_\lambda B^2}{m} \quad . \tag{6.2}$$

The size and sign of the systematic error now depends on the quantum state λ of the molecule. Absorption or emission of blackbody radiation moves the ion between internal quantum states. We observe these transitions as jumps in the measured cyclotron frequency. In the case of the CO^+ molecule, the ion predominantly spends its time in the four lowest energy rotational states (when we count each M state.) Since two of these states have the same polarizability, this leads to three distinct values of the polarizability and hence the three cyclotron frequency values that we measure. Like all good physics explanations, we will show that this elegantly explains nearly all of the observed behavior. First, let us explain how this shift arises.

6.2 Origin of Polarization Forces

6.2.1 Lagrangian Derivation

In the instantaneous rest frame of an object moving with velocity $\vec{v}$ in a uniform and time independent magnetic field $\vec{B}$, the object experiences a motional electric field $\vec{E}_m = \vec{v}\times\vec{B}$. If the object is electrically polarizable with scalar polarizability α, then there is a polarization energy

$$V_p = -\frac{1}{2}\alpha\vec{E}_m^2 \quad . \tag{6.3}$$

The Lagrangian L for such a polarizable object is just the kinetic energy minus the potential energy

$$L = \frac{1}{2}m\vec{v}^2 + \frac{1}{2}\alpha\left(\vec{v}\times\vec{B}\right)^2 \tag{6.4}$$

where the motional electric field has been explicitly written. If we make the simplification that the magnetic field points along $\hat{z}$, then the Lagrangian can be separated into the velocity in the x-y plane $\dot{\vec{\rho}}$ and the axial velocity $\dot{z}$

$$L = \frac{1}{2} m_\rho \dot{\vec{\rho}}^2 + \frac{1}{2} m \dot{z}^2 \quad , \tag{6.5}$$

where the new effective mass in the radial direction is given by

$$m_\rho = m \left(1 + \frac{\alpha B^2}{m} \right) \quad . \tag{6.6}$$

The Lagrangian is that for a free particle with a different mass in the x-y plane than along $\hat{z}$.

In the case of an object such as an ion with net charge q, the Lagrangian is only modified by the usual term $q\vec{v} \cdot \vec{A}$ where $\vec{A}$ is the usual magnetic vector potential. This term has no mass dependence so that we can solve for the motion in the x-y plane using the effective mass m_ρ. The cyclotron frequency of the polarizable ion is inversely proportional to the radial effective mass

$$\omega_c = \frac{qB}{m_\rho} \quad . \tag{6.7}$$

Explicitly writing this as a fractional frequency shift with respect to the cyclotron frequency of a nonpolarizable ion of the same mass to charge gives (in SI units)

$$\frac{\Delta\omega_c}{\omega_c} = -\frac{\alpha B^2}{m} \quad . \tag{6.8}$$

The polarizability α in this expression is the dc polarizability. While the electric field in the ion's instantaneous rest frame is constant in magnitude, the direction of the electric field is rotating at the cyclotron frequency. Since the cyclotron frequency is much lower than the internal frequency scales of the ion, it is correct to use the dc polarizability. It is only in instances where $\omega_c \sim E_{int}/\hbar$ that it is incorrect to use the dc polarizability.

6.2.2 Perturbative Derivation

We can also understand this cyclotron frequency shift if we model the polarizable ion as a pair of massless opposite charges e attached to either end of a spring with a third charge q (and mass m) at the center of the spring. As long as any induced dipole is much smaller than the cyclotron orbit, then we can use perturbation theory and assume to zeroth order that the particle motion is circular motion near the unperturbed cyclotron frequency. If we really "zoom in" on the circular cyclotron motion, then locally the particle looks as though it is moving in a straight line. The two opposite charges are pulled in opposite directions perpendicular to the ion motion by the magnetic field. The equilibrium separation distance l_{eq} is determined by balancing the magnetic force and the restoring force due to the spring. This charge separation is an induced dipole moment with respect to the center of mass of the ion $d_{ind} = el_{eq}$. We can relate this induced dipole to the polarizability by setting

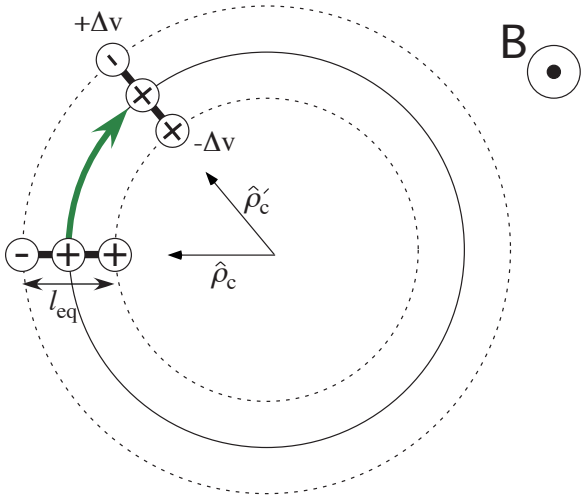

Figure 6-3: Cyclotron motion of a single ion induces a dipole moment (not to scale of course) along the radial cyclotron vector. The induced dipole adiabatically follows the radial cyclotron vector causing the negative tip of the dipole to move slightly faster than the positive tip giving rise to a nonzero Lorentz force. This gives rise to a cyclotron frequency shift since the size of the induced dipole is proportional to the average velocity, and hence, the cyclotron radius.

$el_{eq} = \alpha E_m$. The motional electric field E_m observed in the ion's instantaneous rest frame is given by $E_m = vB$ where v is the ion's speed perpendicular to the magnetic field.

Now, if we zoom back out, we see that the motion is actually circular and that the induced dipole adiabatically follows the radial vector pointing from the center of cyclotron motion to the center of mass. This means that one end of the induced dipole is moving slightly faster than the other end of the induced dipole. This gives rise to a nonzero and radially directed Lorentz force

$$\vec{F_p} = -e\omega(\rho_c + l_{eq}/2)B\hat{\rho}_c + e\omega(\rho_c - l_{eq}/2)B\hat{\rho}_c = el_{eq}\omega B\hat{\rho}_c \tag{6.9}$$

where ρ_c is the radius of the cyclotron orbit and $\hat{\rho}_c$ is the unit vector pointing from the guiding center of the cyclotron motion to the ion's position. Adding this extra force to the equations of motion and assuming circular motion gives the characteristic equation for the frequency ω

$$-m\omega^2 = -\omega qB + \frac{el_{eq}\omega B}{\rho_c} \quad . \tag{6.10}$$

If we now use $el_{eq} = \alpha vB$ and $v = \omega\rho_c$, we find

$$\omega = qB\left(\frac{1}{m + \alpha B^2}\right) \quad , \tag{6.11}$$

which is just the previous result. The cyclotron frequency is shifted because first, the motion

in the magnetic field separates opposite charges to form a dipole. Second, a nonzero radial force is generated because the two ends of the dipole moment move at slightly different speeds. The differential speed is a result of the induced dipole adiabatically following the radial vector of the cyclotron motion.

One can also express the fractional cyclotron frequency shift as a ratio of length scales. If the opposite charges that we use to model our the induced-dipole moment, are taken to be equal in magnitude to the net charge of the ion, then the magnitude of the fractional cyclotron frequency shift is given by the ratio of the induced dipole's length divided by the cyclotron radius. This can be understood by translating the dipole moment along the radial direction so that the net charge located at the center of mass is exactly canceled by the end of the dipole moment with equal and opposite charge. The center of charge of the molecule then appears to be orbiting at a slightly different cyclotron radius than the center of mass.

For an induced dipole moment of 1 $ea_\circ$, a cyclotron radius of ρ_c= 100 μm, and a net charge of e, the ratio of length scales is $\sim 0.5 \times 10^{-10}\,\mathrm{m}/1 \times 10^{-4}\,\mathrm{m} \sim 5 \times 10^{-7}$. In the case of the CO^+ molecule for which we observe cyclotron frequency shifts of order 10^{-9}, we can immediately predict that the induced electric dipole moment is of order 1/500 $ea_\circ$, in agreement with the more carefully calculated values below.

6.2.3 New Effective Mass? A Microscopic Model

What exactly does this new effective mass represent? We can construct a microscopic model of the polarization force by considering a particle moving along $\hat{x}$ in the presence of a uniform magnetic field $B\hat{z}$. The polarizability of the particle can be modelled as two equal and opposite charges q connected by a spring with force constant k. If the ion moves with velocity $\dot{x}\hat{x}$, then the magnetic field exerts a force that wants to stretch the spring along the $\hat{y}$ direction. The equation governing the stretching along $\hat{y}$ is

$$m\ddot{Y} = -kY + q\dot{x}B \tag{6.12}$$

where Y represents the relative coordinate between the two opposite charges. From this equation, the equilibrium separation of the charges Y_{eq} is simply

$$Y_{\mathrm{eq}} = \frac{q\dot{x}B}{k} \quad . \tag{6.13}$$

If the speed $\dot{x}$ is constant and the charges have reached their equilibrium separation, there is no net force on the center of mass of the particle. On the other hand, if the speed changes then $\ddot{x} \neq 0$, and the equilibrium separation Y_{eq} changes as well. As the charges move to the new equilibrium separation, they generate a Lorentz force $\vec{F}_p$ that opposes the acceleration along $\hat{x}$

$$\vec{F}_p = q\dot{Y}_{\mathrm{eq}}\hat{y} \times B\hat{z} = -\hat{x}\ddot{x}\frac{q^2B^2}{k} \tag{6.14}$$

where we have simply differentiated the previous expression for $Y_{\rm eq}$ and substituted. Of course, we would like to link this to a polarizability. Taking as a defining relationship for the polarizability $\mu = \alpha E$, we can write

$$\mu = qY_{\rm eq} = \alpha \dot{x} B \quad . \tag{6.15}$$

We have substituted the effective motional electric field $\dot{x}B$ that the particle experiences in its rest frame. We see ,then, that the polarizability is just $\alpha = q^2/k$ and the polarization force is

$$\vec{F}_p = -\hat{x}\ddot{x}\alpha B^2 \quad , \tag{6.16}$$

which is consistent with the previous results. It is trivial to extend this to a two dimensional oscillator in the $x - y$ plane and show that there is a new effective mass for motion in the plane perpendicular to the magnetic field. In the case of our cyclotron motion, the particle is accelerating as it moves on its circular path, thus giving rise to a radial force opposing this acceleration.

Also note that there was an assumption of adiabaticity in this derivation. If the particle is accelerated too quickly, the oscillator would not adiabatically move to the new equilibrium position. Instead, the oscillator would bounce or ring, giving rise to oscillations in the polarization force (although the time averaged force would still agree with our result.) The condition of adiabaticity for a quantum system is that the accelerating potential not be so large as to excite the system from one state to another.

In summary, as a polarizable particle accelerates perpendicular to a magnetic field, the increased Lorentz forces pulling in opposite directions on the two ends of the dipole moment cause the dipole moment to stretch or increase. To reach the new equilibrium position, the ends of the dipole actually move perpendicular to both the magnetic field and the direction of acceleration.[§] The motion of the charges as they move to the new equilibrium position generates a Lorentz force that opposes the acceleration. If a constant velocity is then maintained, the charges do not move, and there is no additional force on the particle. It is only as the particle accelerates (or decelerates) that a nonzero force is generated. Since the magnitude of the force is proportional to the acceleration and either opposes or enhances the acceleration (depending on the sign of the polarizability), this looks like an effective change in the particle's mass.

[§]If one does not like the idea that the length of the induced dipole is changing, then imagine that charge flows from one side of the particle to the other. This electrical current causes the reaction force.

6.3 Polarization Forces and CO^+

6.3.1 Polarizability of CO^+

In order to understand our spectrum of measured cyclotron frequency values for the CO^+ molecule, we need to examine its quantum guts. Before diving in, I would like to point out that this is completely new for this experiment. In all previous work, the ions were treated as charged point particles with small corrections for ionization and binding energies to obtain the masses of the neutral atoms. It is a testament to the exquisite sensitivity of the two-ion technique that we must now concern ourselves with the detailed internal structure of what we are measuring.

Molecular ions have not been as extensively studied as neutral molecules. Some of the first pioneering work on molecular ions was done on the CO^+ molecule. The rotational spectrum was measured in [47], and several theoretical predictions of its electric dipole moment have since been performed [48], [49], [50].

CO^+ at zero magnetic field

The three significant modes of excitation in order of decreasing energy are the electronic, vibrational, and rotational modes. For the CO^+ molecule, the ground electronic state is a $X^2\Sigma^+$ state (see [51] Chapter 7 and footnote).¶ The energy separation between the minimums of the two lowest electronic states $X^2\Sigma^+$ and $A^2\Pi$ corresponds to an effective temperature of $\sim 30\,000$ K. As a result, it is not very likely that our trapped ion spends any time outside of the ground electronic state $X^2\Sigma^+$.

For a fixed electronic configuration, the internuclear motion can be expanded about the potential minimum. The two quantized normal modes of motion are then a rigid rotor with angular momentum $\vec{N}$ and a vibrational mode along the internuclear axis with harmonic oscillator quantum number ν. Corrections to these basic modes result from effects such as the vibration being slightly anharmonic and centrifugal stretching of the internuclear distance. To include these effects, the energy can be expanded as (see [51] Chapter 1)

¶Molecular spectroscopy has a language of its own, so here is a quick overview. In the Born-Oppenheimer approximation, one fixes the internuclear separation and calculates a stationary electronic configuration. By varying the internuclear distance and recalculating the equilibrium electronic state, one obtains an effective potential versus nuclear separation. This procedure works because the electrons can rearrange themselves about the nuclei on time scales much shorter than the time scales associated with movement of the much heavier nuclei.

Let us decode the "$X^2\Sigma^+$" designation of the ground electronic state. The projection Λ of the electronic orbital angular momentum $\vec{L}$ onto the internuclear axis is denoted by Σ, Π, Δ, meaning 0, 1, 2. The plus sign indicates the positive parity of the electronic state under a mirror reflection through the plane perpendicular to the internuclear axis. The electronic spin multiplicity $2S+1$ is denoted by the 2. Lastly, the leading X, A, B, C are analogous to the atomic principle quantum number and indicate the states in which one of the electrons have been promoted to a higher energy atomic orbital. By convention the "X" is always used in place of "A" to denote the total ground electronic state.

$$E_{\nu N} = \omega_e(\nu+\frac{1}{2}) - \omega_e x_e(\nu+\frac{1}{2})^2 + \omega_e y_e(\nu+\frac{1}{2})^3 + \omega_e z_e(\nu+\frac{1}{2})^4 + B_\nu N(N+1) - D_e N^2(N+1)^2 + H_e N^3(N+1)^3 \quad , \tag{6.17}$$

with

$$B_\nu = B_e - \alpha_e(\nu+\frac{1}{2}) + \gamma_e(\nu+\frac{1}{2})^2 \quad . \tag{6.18}$$

The subscript 'e' refers to the value of the parameter evaluated at the equilibrium distance r_e, which is the position of the minimum in the internuclear potential. Table 6.1 summarizes the spectroscopic constants appearing in the above expansion.

The first excited vibrational level has an effective temperature of 3 100 K so that the ion spends almost all of its time in $X^2\Sigma^+$, $\nu = 0$. The ground $N = 0$ and first excited rotational state $N = 1$ are split by approximately $2 \times B_e \approx 120$ GHz, corresponding to approximately 5.5 K—quite close to the 4 K of the trap electrodes that surround the ion. As a result, we expect the ion to spend the majority of its time in the lowest two rotational states, $N = 0$ and $N = 1$.

CO^+ is known to follow Hunds coupling case b, for which a spin-rotation coupling exists $\gamma_o \vec{N} \cdot \vec{S}$. The spin-rotation coupling constant γ_o is given in Table 6.1. In brief, this interaction arises because the molecular rotation causes a small mixing of $X^2\Sigma^+$ with the $A^2\Pi$ electronic state, for which an electronic spin-orbit interaction exists (see [51] Chapter 7: Molecules with Electronic Angular Momentum). The spin-rotation coupling means that we must work in the total $\vec{J} = \vec{N} + \vec{S}$ basis with good quantum numbers J, M_J, N, and S. Since both C and O have zero nuclear spin, there is no hyperfine structure.

CO^+ in Paschen-Back Regime

Because the ion's velocity is relatively small, $v/c \sim 10^{-5}$, the magnetic field in the ion's rest frame is just the 8.5 T field of the lab frame. The unpaired electron's magnetic moment couples strongly to this field giving rise to an interaction energy $\mu_B B \approx 120$ GHz. Because this energy is much larger than the spin-rotation coupling $\gamma_o \vec{N} \cdot \vec{S} \sim 0.5$ GHz, we expect a decoupling of $\vec{N}$ and $\vec{S}$. The good quantum numbers are now N, M_N, S, and M_S (see Fig. 6-5). The result is that the spin up and down states separate into two independent manifolds.

The spin-rotation interaction can be written as

$$\vec{N} \cdot \vec{S} = N_z S_z + \frac{1}{2}(N_+ S_- + N_- S_+) \quad , \tag{6.19}$$

where $N_\pm$ and $S_\pm$ are the standard raising and lowering operators. These operators only connect states of constant N, so that the accidental near degeneracy of the $N = 2$, $M_S =$

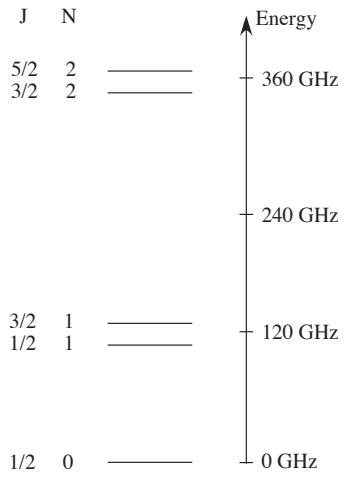

Figure 6-4: Lowest Rotational Energy Levels of CO^+ for the ground electronic and vibrational state $X^2\Sigma^+$, $\nu = 0$. The fine structure splitting is exaggerated since it is only ~ 0.5 GHz.

Table 6.1: CO^+ molecular constants. Values denoted with * are theoretical predictions.

Vibrational Properties	[52]	
ω_e	2214.2	cm^{-1}
$\omega_e x_e$	15.16	cm^{-1}
$\omega_e y_e$	-0.000	cm^{-1}
Rotational Properties	[47],[52]	
B_e	59.275	GHz
B_0	58.983	GHz
α_e	0.567	GHz
γ_e	0	GHz
D_e	0.190×10^{-3}	GHz
γ_o	0.27296	GHz
Other Properties	[52], [48]	
r_e	1.1151	Å
μ	1.015	$ea_\circ{}^*$

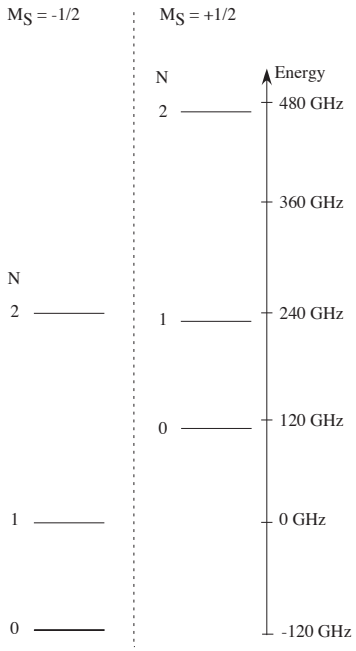

Figure 6-5: Paschen-Back Regime Lowest Rotational Energy Levels of CO^+ for the ground electronic and vibrational state $X^2\Sigma^+$, $\nu = 0$ in a magnetic field of 8.5 Tesla. The near degeneracy between $N = 2$, $M_S = +1/2$ and $N = 1$, $M_S = -1/2$ is accidental and of no consequence.

$-1/2$ and $N = 1$, $M_S = +1/2$ states does not give rise to any mixing of the spin manifolds.

DC Polarizability of CO^+ in Paschen-Back Regime

Calculating the dc polarizability of CO^+ in the Paschen-Back Regime can be done using standard second order perturbation theory. Taking the magnetic field and quantization axis along $\hat{z}$, the motional electric field rotates in the $x - y$ plane. The rotation of the motional electric field in the ion's rest frame is at the trap cyclotron frequency, which is much less than the frequency splitting between rotational states $\omega_{\rm ct} \ll |\omega_{NM_N} - \omega_{N'M'_N}|$. As a result, the molecule responds as though a static electric field were being applied. In addition, there is no difference in the magnitude of the x and y dipole matrix elements. We can simply calculate the polarizability by taking the motional electric field to lie along $\hat{x}$. We can write the polarizability in spherical coordinates as

$$\alpha_{N,M_N} = -2\mu^2 \sum_{N',M'_N} \frac{|\langle N', M'_N| \sin\theta\cos\phi |N, M_N\rangle|^2}{E_{N',M'_N} - E_{N,M_N}} \tag{6.20}$$

where μ is the molecular dipole moment with respect to the center of mass, and θ, ϕ are the usual spherical coordinates defined with respect to the $\hat{z}$ direction. The sum is implicitly taken over states with $M'_S = M_S$ since only these matrix elements are nonzero. The usual

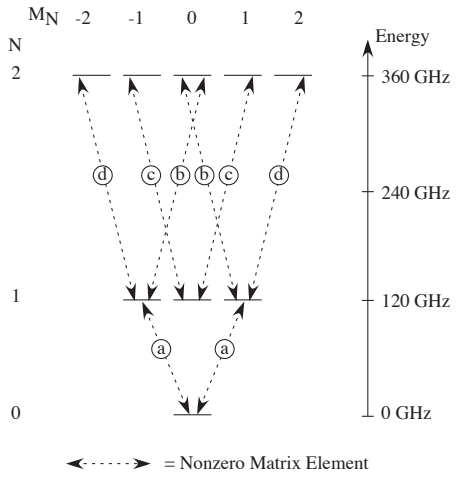

Figure 6-6: Nonzero matrix elements for the magnetic field and quantization axis along $\hat{z}$ and the electric field along $\hat{x}$. The lines are dashed to emphasize that this is a dc interaction and not a resonant interaction.

Table 6.2: Second Order Perturbation Parameters for interactions specified in Fig. 6-6.

Transition	$\lvert\langle m\rvert \sin\theta\cos\phi \lvert n\rangle\rvert^2$	$\lvert E_m - E_n\rvert$ (GHz)
a	$\frac{1}{6}$	118.0
b	$\frac{1}{30}$	235.9
c	$\frac{1}{10}$	235.9
d	$\frac{1}{5}$	235.9

dipole selection rules apply so that only matrix elements between states with $\Delta N = \pm 1$ and $\Delta M_N = \pm 1$ are nonzero. Figure 6-6 graphically shows the nonzero matrix elements.

Thinking of this in terms of level repulsion, it is clear that the polarizability of the $M_N = 0$ states for $N = 0$ and $N = 1$ will be positive, since there are no lower levels that "push their energies up." In contrast, we expect the magnitude of the polarizability to be smaller for most other states, since these levels are repelled by levels from both above and below and have larger energy denominators. Table 6.2 gives calculated values for the matrix elements labeled in Fig. 6-6.

The calculated polarizability for each state is listed in Table 6.3. To calculate these polarizabilities, we assumed the body-frame dipole moment is $\mu = 1\ ea_\circ$. This will be shown to be an accurate estimate. This choice also allows easy rescaling by μ^2 once a more accurate value is obtained. Also given are the fractional cyclotron frequency shifts for each state. To go from the polarizabilities to the frequency shifts, we use the experimentally measured magnetic field of 8.5295 T. Lastly, the induced dipole for a 100 μm cyclotron radius is given in Table 6.3 in atomic units of $ea_\circ$. The fact that $\mu_{\text{ind}} \ll \mu$ indicates that

Table 6.3: Calculated Polarizabilities, Cyclotron Frequency Shifts and Lifetimes assuming $\mu = 1ea_\circ$ and for a magnetic field of 8.5294 T. For comparison, the polarizabilities of H, Na, and H^- are 0.67, 24.1, and 30.5 $Å^3$, respectively [53], [54], [55].

N	M_N	α(SI) C m^2/ V $\times 10^{-38}$	α(CGS) $(Å)^3$	$\Delta\omega_c/\omega_c$ $\times 10^{-9}$	$\mu_{ind} = \alpha E_{mot}$ $ea_\circ/(100\ \mu m)$
0	0	61.29	5508	-0.959	0.0018
1	0	18.40	1653	-0.288	0.0005
1	± 1	-9.184	-825	0.144	-0.0003

our perturbative treatment is justified. Our current description must be modified when the induced dipole becomes comparable to the body-frame dipole moment $\mu_{ind} \sim \mu$. For CO^+, this occurs when the cyclotron orbit is approximately $\rho_c \sim 100$ cm, as occurs in large mass spectrometers.

6.3.2 Comparison with Experiment

The theoretical cyclotron frequency shifts calculated in the previous section assuming $\mu = 1\ ea_\circ$ and given in Table 6.3 are in excellent agreement with the spectrum of measured cyclotron frequency ratios. To see this, we histogram the measured cyclotron frequency ratios N_2^+/CO^+ from Fig. 6-1. Figure 6-7 shows the result. The cyclotron frequency ratio measured previously using the alternating technique is subtracted from the x-coordinate. The solid line indicates a first-pass fit to the data using our model, and will be discussed in detail in the following section. From left to right, we interpret the measured peaks as indicating that the ion was in the rotational state $(N, M_N) = (1\ ,\ \pm 1)\ ,\ (1\ ,\ 0)$, or $(0\ ,\ 0)$.

To test these assignments, the spectrum can be fit with three independent Gaussians. The values of the three centroids are labeled R_{N,M_N}, i.e., R_{00}, R_{10}, and $R_{1\pm1}$. We can predict the ratio of intervals given below without any knowledge of the dipole moment μ:

$$\frac{R_{1\pm1} - R_{00}}{R_{10} - R_{00}} = 1.64 \quad \text{(Theory)} \tag{6.21}$$

$$= 1.60(9) \quad \text{(Experiment)}\ . \tag{6.22}$$

The theory and experiment agree to 3(5)%. This is strong evidence that the spectrum of measured ratios arises from variation of the polarization force shift as the molecule changes rotational state.

We can also compare the lifetimes of the observed states to the theoretical predictions shown in Table 6.4. The spontaneous decay times are given to show the importance of including stimulated emission and absorption driven by the 4.2 K blackbody radiation. In order to measure the lifetime of a state, we must actually see a jump to another state. We

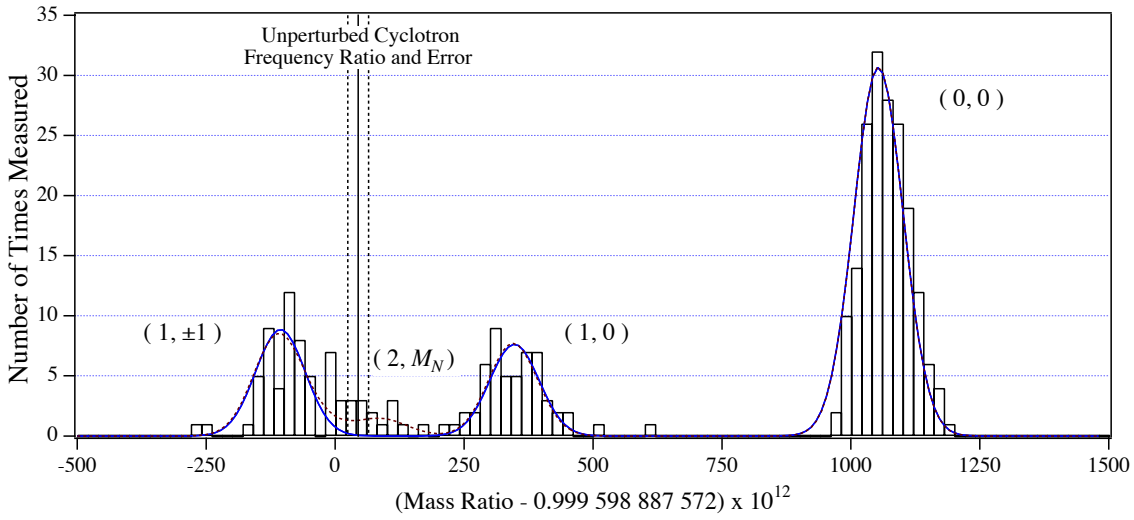

Figure 6-7: Histogram of measured cyclotron frequency ratios of N_2^+/CO^+. The spectrum of measured values is well described by theory. The zero of the graph is chosen to be the previously measured cyclotron frequency ratio for this pair using the alternating technique.

Table 6.4: Lifetimes and fractional occupation times. All lifetimes are given in hours. The normalized Boltzmann weights predict what fraction of the total time is spent in each state. To determine the fraction of time spent in a given rotational state summed over M_N, one must multiply by the multiplicity $(2N+1)$.

N	τ spont.	τ at 4.2 K	τ observed	Normalized Boltzmann Weight	Fractional Dwell Time
0	∞	6.1	7(3)	0.54	0.46
1	5.6	2.3	4(2)	0.14	—
2	0.19	0.04	—	0.01	—

do not have to see the ion enter the state, since the probability of making a transition to another state at a given moment in time is completely uncorrelated with how long the ion has been in the state. This measurement is somewhat difficult to perform for the excited states, but for the ground state we can identify 6 clear excitation events. The average time for the excitation to occur is 7(3) hours compared to a predicted thermal excitation rate of 6.1 hours for $\mu = 1\ ea_\circ$. For the (0, ±1) state, we can discern a total of 4 jumps out of the state, with an average transition time of 4(2) hours. This is to be compared to the calculated 2.3 hour lifetime at 4.2 K. These are coarse comparisons, but clearly the observed lifetimes are consistent with theory.[‖]

[‖]In a more detailed analysis of lifetimes, it might be necessary to include suppression or enhancement of emission and absorption resulting from the presence of the Penning trap electrodes. Such effects are routinely observed with electrons in Penning traps with cyclotron frequencies of order the rotational splitting of the CO^+ molecule.

We observe that the CO^+ molecule spends roughly half of its time in the ground state. We can compare this to the expectation from the normalized Boltzmann weight, which describes the average state occupation of a system in thermodynamic equilibrium. Of course, we do not have the usual ensemble, but instead a single molecule. In this case, the Boltzmann weights describe the time averaged occupation of each state. The predicted fraction of time spent in the ground state is 0.54, in excellent agreement with the observed value of 0.46.

In our spectrum, we cannot differentiate state (0,1) from state (0,-1). As a result, we expect the (0,±1) peak to have twice the number of counts as the (0,1) peak. We actually observe fairly equal amplitudes. This is not too much of a concern since the number of actual transitions is fairly low. We assume that the expected imbalance would be made manifest by simply taking more data.

When the ion is in the rotational state N=1, we observe apparent transitions between states of constant N, but different M_N. This violates the usual electric dipole selection rules (specifically parity). We believe that the explanation lies in the 2.6 minute lifetime of the N= 2 states. This is about half of the time needed to perform a single cyclotron frequency comparison ($T_{\rm evol} \sim 5$ minutes). In addition, if the ion is in the $N = 1$ state, then the transition rate to the $N = 2$ state $\Gamma(1 \rightarrow 2)$ is calculated to be almost the same as the transition rate to the ground state $\Gamma(1 \rightarrow 0)$. Specifically, we find that $\Gamma(1 \rightarrow 2)/\Gamma(1 \rightarrow 0) = 0.7$. The apparent violation of parity is simply the result of a pair of transitions to and back from the $N = 2$ state that we do not clearly resolve in our measurements.

The normalized Boltzmann weights predict that the CO^+ molecule should spend approximately 5% of its time in the $N = 2$ rotational state. In the data set shown, there are a total of 305 measurements, so approximately 15 of the measurements should have occurred while the ion was in the $N = 2$ state. The polarizability of the $N = 2$ states are 393, 196, $-394 \times 10^{-24}\mathrm{cm}^3$ (CGS) for $(N, M_N) = (2, 0)$, $(2, \pm 1)$, and $(2, \pm 2)$, respectively. Again, we have assumed that the dipole moment is $\mu = 1\ ea_\circ$. The calculated fractional perturbation of the cyclotron frequency is $-68,\ -34,\ 69\ \times 10^{-12}$, with the values listed in the same order as above. When the contributions of the $N = 2$ rotational states are included in a simultaneous fit to the entire spectrum of measured ratios (to be described in the following section), we see excellent agreement, as shown by the dashed line in Fig. 6-7. The solid line indicates a simultaneous fit to all three peaks, ignoring the contribution from $N = 2$. The small background of points between the (1 ±1) and (1, 0) peaks is consistent with arising from time spent in the $N = 2$ rotational state. Assuming errors of $\sqrt{\mathrm{N}}$ for each bin, the reduced chi-square for the fit is $\chi^2_\nu = 0.77$, indicating that our model accurately describes the data. To illustrate the quality of the model, the residuals from the fit along with the expected $\sqrt{\mathrm{N}}$ error interval are shown in Fig. 6-8. The contribution of the $N = 2$ states to the spectrum is a small correction and is not critical for understanding the gross structure. To emphasize this point, if a simultaneous fit is performed that ignores the $N = 2$

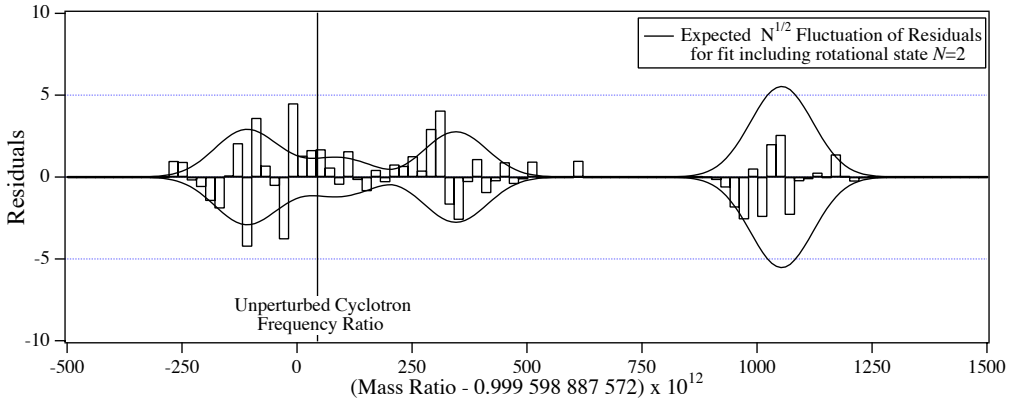

Figure 6-8: Residuals from fit to spectrum of measured ratios. The curves represent the expected $\sqrt{\mathrm{N}}$ variation of the residuals.

contributions, the reduced chi-square $\chi^2_\nu = 1.1$ is still quite good.

In summary, the spectrum of measured ratios is well described by the model of polarization forces that depend on the quantum state of the molecule. We see good agreement of the predicted magnitudes of the shifts relative to the previously measured mass ratio, which we take to be an unperturbed value as will be explained shortly. The relative sizes of the intervals between the peaks can be accurately predicted independently of knowledge of the actual dipole moment. The lifetimes and fractional dwell times in each state are also consistent with theory.

Having gained the confidence that we understand the spectrum of ratios, we can proceed to extract a measurement of the electric dipole moment μ and the unperturbed mass ratio.

6.3.3 Extraction of Dipole Moment μ and Mass Ratio CO^+/N_2^+

From the observed spectrum of mass ratios, we can extract the electric dipole moment μ of the CO^+ molecule along with the unperturbed mass ratio CO^+/N_2^+. We will find that the uncertainty on the electric dipole moment ultimately limits the accuracy with which we can determine the unperturbed mass ratio. Of all the rotational states, we can resolve and measure the $N = 0$ state the best. As a result, we can quote a final uncertainty of 7×10^{-12} on its cyclotron frequency ratio with N_2^+ in a magnetic field of 8.5294 T. To extract the unperturbed mass ratio with similar accuracy, we need to correct for the $\sim 10^{-9}$ perturbation of the cyclotron frequency when CO^+ is in its ground rotational state. Since the size of the cyclotron frequency shift scales as the square of the electric dipole moment, we need to determine μ to $\sim 0.5\%$ to determine the mass ratio with an accuracy of 1×10^{-11}. Experimentally, we will extract the value of the electric dipole moment to be $\mu = 1.025(15)\ ea_\circ$. This is a fractional accuracy of 1.5%. When we include the extra information given by the measured values of the $N = 1$ states, which perturb the cyclotron

frequency much less, we can determine the mass ratio of CO^+/N_2^+ with a fractional accuracy of 2×10^{-11}.

To extract the unperturbed mass ratio and the electric dipole moment, we fit a sum of Gaussians to the observed spectrum of measured cyclotron frequency ratios:

$$G(R) = \sum_{\lambda=(N,M_N)} A_\lambda e^{-\frac{\left(R-(\mu^2\Delta_\lambda+R_\circ)\right)^2}{2\sigma^2}} \tag{6.23}$$

where the independent parameter is R and the fitted parameters are the electric dipole moment μ in units of $ea_\circ$, the unperturbed cyclotron frequency ratio $R_\circ$, a single standard deviation σ characterizing the shot-to-shot measurement noise, and amplitudes A_λ. The parameters Δ_λ are fixed to the calculated perturbations of the ratio, which are determined from the polarization model with the dipole assumed to be 1 $ea_\circ$. This is what fixes the units of the fitted dipole moment. In addition, if the spectrum has a large offset subtracted and has then been multiplied by a large number, as is the case in Fig. 6-7, then we must multiply by the same large number. For instance, from Table 6.3, we find $\Delta_{(0,0)} = 959$, $\Delta_{(1,0)} = 288$, and $\Delta_{(1,\pm1)} = -144$ where the sign is flipped with respect to the table because we wish to know the effect on the mass ratio CO^+/N_2^+, which is inversely proportional to the cyclotron frequency of the CO^+. Lastly, the sum does not count states with the same value of Δ_λ more than once, i.e., a single term is used to fit the identical contributions from (0, 1) and (0, -1).

If we include the three distinguishable contributions to the spectrum from (0, 0), (0, 1), and (0, -1), we find μ= 1.025(2) $ea_\circ$ and $R_\circ = 45(4)$. The result of this fit is shown as the solid line in Fig. 6-7. The value of the unperturbed ratio given here must be multiplied by 10^{-12}, and the offset of 0.999 598 887 572 must then be added back in. Making the bin size larger and smaller by a factor of 2 and shifting the bin centers by 1/2 bin cause the value of the ratio to vary between 50 and 34 or a full range of 1.5×10^{-11}. The fitted dipole moment varies by a full range of 0.5%. Performing a weighted fit with the errors determined from the number of points in each bin N as $\sqrt{\mathrm{N}}$, we find an excellent reduced chi-square of $\chi^2_\nu = 1.1$. The fitted values of the ratio and dipole moment are 58(7) and 1.020(4) $ea_\circ$ respectively. For all of these different analyses, the fitted ratio varies by 2.5×10^{-11} full range, while the dipole moment varies by 1% full range.

We can also perform independent fits to the data, including only two of the three peaks in each fit. The three possible pairs are {(0,0), (1,0)}, {(0,0), (1,$\pm$1)}, and {(1,0), (1,$\pm$1)}. The fitted ratios are 21(14), 50(7), and 49(24) respectively. This is a total variation of 3×10^{-11}. The fitted dipole moments are 1.040(8), 1.026(4), and 0.993(50). The last fit is significantly less precise because the interval between the peaks is small and both peaks have fewer counts than the ground state peak.

Lastly, we can include contributions to the fit from the next excited rotational state $N = 2$. The values of the polarizabilities and cyclotron frequency shifts are given in the

text of the previous section. To maintain the stability of the fit, we do not fit the amplitudes A_λ for the $N = 2$ states. Instead, we assume that each state contributes a fixed fraction of the total number of 305 measurements. The fraction is determined by the normalized Boltzmann weight at 4.2 K. An unweighted fit gives the dashed line in Fig. 6-7. The values of the ratio and dipole moment are 41(4) and 1.028(2) $ea_\circ$. A weighted fit gives an excellent reduced chi-square of $\chi^2_\nu = 0.77$. The residuals of the fit along with the expected distribution of the residuals are shown in Fig. 6-8. The fitted ratio and dipole moment are 51(7) and 1.024(4) $ea_\circ$.

The good agreement between the fits including and excluding the $N = 2$ contributions is a result of the $N = 2$ contribution being small and the fixing of the standard deviation σ of each contribution to be the same for each peak. Fixing the Gaussian width to a common value acts as a filter so that the answer is not significantly pulled by the small background from the $N = 2$ states.

Comparing all of the various fits, the value of the dipole moment varies from 1.040(8) to 1.020(4) $ea_\circ$. There is a smaller value at 0.993(50), but the 5% error is large, making it consistent with the other values. We choose to be conservative and quote a final value of 1.025(15) $ea_\circ$ that spans all of the precisely fitted values. In addition, an independent data set consisting of several days of data gives a dipole moment of 1.022(6) $ea_\circ$, in good agreement with our final value. The quoted value and error were settled upon before extracting this second value, from the other data set so in some sense this can be thought of as a blind test. To our knowledge, this is the first time ever that the molecular dipole moment of an ion has been measured at this level of accuracy. This result can be compared to theoretical predictions of the dipole moment of CO^+ in its ground state 1.015 [48], 1.09(4) [49], and 1.0(2) [50] $ea_\circ$. The first prediction is the most recent and perhaps should be considered most carefully, since increases in computational speed have rapidly advanced the ability to accurately calculate molecular properties. We see that the most recent theoretical prediction differs from our measured value by only $2\sigma/3$ or about 1%.

The fitted ratio varies over the range of 58 to 34 (a variation of 2.4 $\times 10^{-11}$) depending on how we perform the fitting. Some of the fits are less than optimal, and it is conservative to choose the final value and error to span the entire range. However, this is exactly what we will do. For a final value of the mass ratio R= M[CO^+]/M[N_2^+], we will choose 45(15). Including the offset, the ratio is R= 0.999 598 887 617(15). The quoted uncertainty is a fractional error of 1.5×10^{-11}, making this one of the most precisely and accurately known mass ratios.

For scale, this final quoted ratio and the uncertainty interval are indicated on Fig. 6-7 with a vertical solid line and two dashed lines. The offset was chosen to be our previous most accurate value for the ratio R= M[CO^+]/M[N_2^+]. The uncertainty σ on the ratio was 77×10^{-12}. The new value is in excellent agreement, lying only 0.4 $\sigma_{previous}$ away from the previous value.

The systematic errors associated with the two-ion technique measurements have been only briefly discussed in this thesis, but are covered in wonderful detail in Simon Rainville's thesis [1]^G. The data set shown is the only one for which we feel confident that we truly understand the systematic errors. The pair are at an ion-ion separation of ρ_s= 715 μm in this data set. At this separation, the ion-ion interactions and trap field imperfections contribute approximately equal uncertainty on the systematic error for the ratio. The uncertainties combined in quadrature are $\approx 5 \times 10^{-12}$. This is smaller than the final uncertainty quoted above, so we are not too concerned about the systematic errors on the ratio.

The precision on the ratio unperturbed by polarization force shifts is limited by knowledge of the dipole moment of the CO^+ molecule. The cyclotron frequency ratio when the CO^+ is in its ground rotational state can be measured much more precisely to 1063(4) with respect to the previous offset. This is a precision of 4×10^{-12}. We can add in quadrature to this the uncertainty from the systematic error arising from ion-ion interactions and trap field imperfections. This gives a final value of R= 0.999 598 888 635(7) - $959 \times \mu^2 \times 10^{-12}$ where the dipole moment must be expressed in $ea_\circ$. If the dipole moment were perfectly known, this would be a final uncertainty of 7×10^{-12}, demonstrating the power of the two-ion technique. For the errors to be equal, the dipole moment would have to be determined to 0.4%, while we have determined it to 1.5%.

6.4 Applications of Polarization Force

6.4.1 Impact on Previous MIT Mass Comparisons

The polarization shifts are observed so clearly because of the long periods of time that we hold onto a specific CO^+ molecule. This gives the ion many hours to reach its lowest rotational levels, where the shifts become large enough to easily discern. In the previous technique of alternately trapping ions, a particular CO^+ molecule was held in the trap for approximately 10 to 20 minutes after ionization. This did not give the ion time to reach the lowest rotational states, since it is presumably left in a high vibrational-rotational state following the electron impact ionization.

While vibrational states typically decay on time scales of ms, the decay would scramble the rotational state of the molecule and hence the size and sign of the shift. For molecules such as CO^+ with relatively large moments of inertia, the ion can remain in a high rotational state for several minutes before decaying to the lowest few states, at which point the decay rate drops dramatically. During the 10 to 30 minutes necessary between making the ion and completing measurements of the ion's cyclotron frequency, such a molecule would not reach the ground state very often. In contrast, molecules such as $^{28}SiH^+$ with much smaller moments of inertia will radiate very quickly to the ground state, possibly even before we complete our measurements. But the larger energy spacing between the rotational levels also decreases the size of the cyclotron frequency shifts due to the reduction in the polarizability.

Except for ions with exceptionally large electric dipole moments, such as HF^+, the cyclotron frequency is not systematically perturbed above 10^{-10}.

For a simple diatomic molecule, it has been shown that the polarizability averaged over the rotational states at constant N is zero except for the case $N = 0$ [51]. If from measurement to measurement (or ionization to ionization) the value of M_N is randomized, then this will appear as a source of noise that averages to zero and so there is no systematic error. In fact, one way to deal with this new source of systematic error would be to continually excite the ion into a high vibrational state. The rotational state would then be randomized as the vibrational states decay with typical time scales $\ll 1$ s.

Even if the ion had reached the ground state in previous work, the sudden jump in the measured cyclotron frequency would have been ascribed to magnetic field variation. Alternatively, the perennially favorite catch-all of "bad ions" would be invoked to justify removing the one or two discrepant points from the data set. In fact, the technique of Robust statistics implemented by Frank DiFillipo [43]^G is exactly appropriate for eliminating these largely discrepant values.

We still believe that the previous results are trustworthy, and the excellent agreement of the CO^+/N_2^+ mass ratios from the new and the previous measurements supports this belief. One might look for this effect in the previous data as an increased scatter of the cyclotron frequency values for the CO^+ data compared to the N_2^+ data.

6.4.2 Other and Future Experiments

The polarization force shift of the cyclotron frequency is a general phenomenon affecting all cyclotron frequency comparisons of nonelementary particles. Table 6.5 lists the predicted cyclotron frequency shifts for other species. These estimates are for order-of-magnitude inspection, since they were performed ignoring fine and hyperfine structure that might change the results in detail.

The most immediately significant of these shifts is for H^-, since it played an integral role in the proton/antiproton mass to charge comparison briefly discussed in Sect. 1.3. The unaccounted-for polarization shift, calculated in the magnetic field of 5.9 T used in the experiment, is a systematic error with magnitude comparable to the quoted error on the comparison. If the correction is applied, we find that the ratio of the mass to charge of the proton to antiproton differs from one by $-1.6(9) \times 10^{-10}$ [11].** Clearly, any future improvement of this baryonic test of CPT will have to carefully account for polarization shifts.

The measured shifts are interesting in their own right. Our observations can be described as a QND (Quantum-Non-Demolition) measurement of the rotational state of a single molecular ion. In the future, it might be possible to do spectroscopy by applying

**I do not believe that this is indicative of a real violation of CPT, since 2σ discrepancies are quite common in precision measurements.

Table 6.5: Estimated systematic shifts of cyclotron frequencies due to polarization force for various species. The references provide the information used to calculate the polarizabilities. The shifts are evaluated for an 8.5 T magnetic field. The value indicated with * is evaluated in a 5.9 T field. For further comparison, the fractional mass shifts in an 8.5 T for neutral H and Na atoms are 3 and 5 $\times 10^{-12}$ respectively.

Species	$\frac{\Delta\omega_{ct}}{\omega_{ct}} \times 10^{12}$	Ref.
H^-	-150	[55]
H^-	-70	*
HD^+	-100	[56]
SiH^+	-8	[57]
SH^+	-40	[58]
SD^+	-60	[58]
SH^-	-2	[58]
SD^-	-10	[58]
OH^+	-90	[59]
OD^+	-90	[59]

radiation and detecting when the ion changes state via a cyclotron frequency shift. This was considered very early after gaining an understanding of these jumps. This may or may not pan out, since the readout time for a single event is several 100 s. Future significant improvements in signal to noise or careful selection of a species with exceptionally large shifts might make this more feasible.

Chapter 7

Conclusion and Future

7.1 Summary of Accomplishments

We can now compare the masses of single ions with a fractional accuracy of $\sim 7 \times 10^{-12}$, with the key advance being the simultaneous confinement and control of two ions in a Penning trap. This allowed us to perform simultaneous cyclotron frequency comparisons to eliminate the effect of magnetic field noise. The accuracy achieved is an order of magnitude improvement over our previous capabilities. To place this accomplishment in historical context, this experiment's first demonstration comparison of CO^+ vs N_2^+ was performed in 1989 $[40]^G$ with a relative precision of 4×10^{-10}. The precision was limited by magnetic field noise. Several technical improvements and optimization of the ion making process allowed mass comparisons at 1×10^{-10} by 1993 $[46]^G$, $[15]^G$. The present work represents a jump in precision and accuracy that is most comparable in nature to that attained in 1989.

It is clear that we can reach a statistical precision of $\sim 2 \times 10^{-12}$ with several days of measurement. We believe that we have conservatively estimated the systematic errors, as is evidenced by the measurement of the mass ratio versus ion-ion separation. Further studies of systematic errors may reveal that we have already developed and implemented the techniques needed to achieve the holy grail of this experiment—cyclotron frequency comparisons with accuracies of 10^{-12}.

Along the way, we discovered that our measurements are sensitive to induced charge distributions within the ions. This was completely unexpected, although in hindsight it seems obvious. We can nondestructively measure the quantum state of a single CO^+ molecule by measuring its cyclotron frequency relative to a reference such as a single N_2^+ molecule. We can observe the CO^+ molecule absorb and emit microwave photons from the blackbody background of the 4 K trap. By carefully observing and modelling the spectrum of measured cyclotron frequency ratios, we have extracted the CO^+ electric dipole moment to 2% and the mass ratio of CO^+/N_2^+ to 2×10^{-11}. Such a direct determination of the electric dipole moment of a molecular ion has never been performed before because of the difficulty of applying electric fields without driving the ions from the detection region. The uncertainty

on the mass ratio of CO^+/N_2^+ is completely limited by uncertainty on the measured dipole moment.

While we can accurately compare cyclotron frequencies of single ions, the true limitation in the short term is going to be understanding and correcting for polarization shifts of the measured cyclotron frequency ratio needed to determine the mass ratio. For most molecular hydrides A-H, the cyclotron frequency shifts are much smaller than observed in CO^+ because of the larger spacing of the rotational levels. In addition, the CO^+ molecule has a rather large dipole moment. Nevertheless, these shifts will still be of order 10^{-11} and will have to be carefully calculated. It will be very important to no longer treat the ions as charged point particles. A careful understanding of molecular polarizabilities and of the fraction of time spent in each molecular state will be critical to generally achieve mass comparisons with accuracies below 10^{-11}.

Lastly, I am thrilled to have been involved with the ICR experiment during a period of such fruitfulness, and to have had the chance to work with such excellent colleagues. We have been able to make significant contributions to science, including: new determinations of the fine structure constant α and the molar Planck constant $N_A h$, a direct test of $E = mc^2$ by weighing γ-rays, the discovery of polarization force shifts of cyclotron frequency measurements, and a unique determination of the electric dipole moment of a molecular ion. In addition, we were able to implement an elegant technique that has advanced the state of the art of single-ion mass metrology by at least an order of magnitude. As a result, I am left with a deep sense of satisfaction.

In conclusion, I will briefly discuss the prospects for and issues associated with comparing $^3He^+$ to $^3H^+$. I will then outline several avenues of research that are worthy of pursuit for confirming and improving systematic errors. The thesis will conclude with a brief discussion of an alternative approach to performing simultaneous cyclotron frequency comparisons–two ions in two separate Penning traps.

7.2 Neutrino Mass: $^3He^+$ versus $^3H^+$

My only regret is not having determined the mass ratio of $^3He/^3H$ for helping to determine the electron neutrino mass. However, I believe that we have demonstrated most of the experimental techniques needed for the comparison. Our ability to create and measure a single pair of ions for weeks will be crucial. In previous work, it was found that the vacuum was quickly spoiled by the introduction of ^3He gas, which possesses a substantial vapor pressure even at 4.2 K.

The axial modes of $^3He^+$ and $^3H^+$ are nearly degenerate and will lock up into collective sum and difference modes. It still might be possible to extract cyclotron phase information from the collective axial modes. The pair $^3He^+$ vs $^3H^+$ is a fantastic doublet with a fractional mass difference $2\eta = 6.6 \times 10^{-6}$. If the center frequency of the detector is kept at 200 kHz,

the axial frequency difference is only 0.66 Hz, which is much smaller than the axial Rabi frequency of $\Omega_z/2\pi$= 5.8 Hz at ρ_s=1000 μm. In this regime, the two axial modes will lock up into a sum and difference mode. If the cyclotron-axial Rabi frequency can be made much larger than the axial Rabi frequency Ω_z, then the axial motion at the end of a PNP measurement will encode the sum and difference of the cyclotron phases just before the π-pulse. The *ratio* of the axial sum and difference *amplitudes* encodes the desired phase difference of the cyclotron motions. The *phase* of each normal mode is related to the sum of the two cyclotron phases.

The axial sum mode will couple strongly to our detector and will damp at four times the single ion damping rate. On the other hand, we cannot directly detect the axial difference motion because it induces no net image current between the endcaps. However, the sum mode's amplitude and phase can be measured and then allowed to completely damp. We can then map the axial difference mode onto the axial sum mode via a π-phase slip of one of the individual axial motions. This can be accomplished most simply by applying a 2π-pulse drive between one of the axial modes and its cyclotron mode. The amplitude and phase of the difference mode are mapped onto the sum mode, and can then be directly detected. Once again, it is key that the axial-cyclotron Rabi frequency be much greater than the axial Rabi frequency.

The systematic errors are extremely favorable for comparing $^3He^+$ and $^3H^+$. The systematic errors arising from imbalance of the rms magnetron radii coupled with trap field imperfections will be well below 10^{-12}. This is the result of the scaling of the magnetron imbalance parameter $\delta_{mag} \propto \eta\bar{m}\bar{\omega}_m^2 \propto \eta\bar{m}^3$. In the second step, we have assumed that the trap voltage is tuned to keep the axial modes near resonance with our fixed frequency detector. This results in $\bar{\omega}_m \propto \bar{m}$. Compared to the example pair $^{13}C_2H_2^+$ vs N_2^+, the magnetron radii imbalance δ_{mag} will be $\sim 10^5$ times smaller. In addition, the cyclotron-cyclotron pulling and nonlinear interactions (assuming a systematic imbalance of the cyclotron orbit size δ_{cyc}= 0.01) are below 10^{-12} for ion-ion separations greater than 500 μm. Thus, the systematic errors at $\bar{m}$= 3 u look even more favorable than our current work at $\bar{m}$=30 u.

Unfortunately, in this locked axial frequency regime, our methods for measuring the ion-ion separation and controlling the relative motion of the two ions will not work. One can imagine decoupling the axial modes by applying a continuous sideband coupling between the axial and cyclotron modes of the ion whose axial mode is not being measured. If this does not work, it might be necessary to independently compare $^3He^+$ and $^3H^+$ to the intermediate ion HD^+. The fractional mass difference for these comparisons ($^3He^+/HD^+$ and $^3H^+/HD^+$) is rather large at $2\eta = 2.0\times10^{-3}$. This leads to an axial frequency difference of $\sim$ 200 Hz. As discussed in Sect. 5.3.1, simultaneous axial detection could be achieved by modulating the Ring voltage to create FM sidebands on the axial motions that lie near the center frequency of the detector. Alternatively, a scheme of alternately reading out the cyclotron phases could be used. The systematic errors on these cyclotron frequency

comparisons are not quite as good as for the direct comparison, but an accuracy of better than 10^{-12} should still be easily achieved. In addition, most of the systematic errors will be common to each comparison. As a result, the systematics will almost completely cancel when the ratio of the two measurements is taken to extract the desired ratio $^3He^+/^3H^+$.

One of the most pressing questions is whether there is enough signal to noise to perform accurate axial phase measurements. The ion-ion Coulomb force introduces a length scale into the problem that does not change with mass to charge. As a result, the possible axial amplitudes will be limited to approximately the same size we use now at $\bar{m}$= 30 u. However, the total energy available for detection will be down in proportion to the trap voltage, which is tuned to bring the axial modes into resonance with the fixed frequency detector. As a result, there is 10 times less energy available to detect. It might be necessary to wind a higher frequency detector to remedy this. A self-resonant transformer with a center frequency of $\sim$ 600 kHz would provide the same trap voltage, and hence, the same energy for detection at a given axial amplitude. We have experimentally checked that the dc SQUID will detect gross signals in this frequency range despite being substantially outside of its feedback range. In addition, a higher axial frequency would have several other benefits. The axial damping time would be similar to current values so that the mode coupling technique used to control the relative motion of the two ions would behave exactly as it does now. Also, the thermal amplitude of the cyclotron mode would be reduced by $\sqrt{3}$, which would reduce the relativistic cyclotron frequency noise by the same amount.

Assuming no significant loss in axial signal to noise due to a higher frequency detector, the precision of the comparison will be better, since the cyclotron frequency is 10 times higher than our current values. The systematic errors due to trap field imperfections on comparisons such as $^3He^+/HD^+$ will be larger due to the larger magnetron frequency by a factor of 100 relative to the same comparison with axial frequencies of 200 kHz. Nevertheless, these systematic errors are still a factor of 10 smaller compared to our present work at $\bar{m}$=30 u. And, as before, the systematic errors on the mass ratio of $^3He^+/^3H^+$, as determined from comparisons to the intermediate ion HD^+, will be approximately 100 times smaller because of the common nature of many of the systematic errors.

I am quite optimistic that the mass ratio of $^3He^+/^3H^+$ can be easily determined to 1×10^{-11} and probably to a few times 10^{-12} using the two-ion technique. Some of the issues discussed above will have to be patiently examined, but I do not believe they represent serious impediments.

7.3 Future Improvements

Understanding the polarizability of molecular ions will be the single most important task in the immediate future of the experiment. It would be very beneficial to collaborate with a good molecular theorist who would be willing to calculate the spectrum of polarization

force shifts for arbitrary molecular ions. Since my expertise lies in accurately comparing cyclotron frequencies, I will concentrate on that subject here.

7.3.1 Technical Improvements

There are two technical improvements that would contribute significantly to improving our mass comparisons. The first improvement would be a robust feedback technique to cool the ions below the thermal limit of the 4.2 K axial detection circuit. In the past, this was considered to be of most importance for light ions, where special relativity turns shot-to-shot cyclotron amplitude fluctuations into large shot-to-shot cyclotron frequency fluctuations. With two ions in the trap, the nonlinear interaction between the cyclotron modes efficiently turns cyclotron amplitude fluctuations into cyclotron frequency noise. For the example pair CO^+ vs N_2^+, the shot-to-shot noise in the cyclotron frequency difference approaches 1×10^{-10} for $\rho_s \sim 500$ μm. This makes it very difficult to precisely measure the systematic errors due to ion-ion interactions at the small separations where they ought to be the largest. Reducing the amplitude fluctuations would allow us to more precisely constrain the size of the ion-ion systematic errors.

The second technical improvement would be a new set of electrostatic shims to tune the trap's C_6 component. It will be difficult to accomplish this while maintaining orthogonality to the C_2 and C_4 terms of the field. However, the C_6 coefficient would not need to be adjusted very often, so this might not be a grave concern.

In addition to reducing the electrostatic anharmonicity, it should also be possible to reduce the magnetic field inhomogeneity. The newly automated technique for measuring the B_2 coefficient should allow B_2 to be more accurately shimmed to zero with the existing magnetic shim coils. A reduction of both B_2 and C_6 would allow the mass ratio to be accurately determined at larger ion-ion separations.

Nulling the B_2 inhomogeneity is less important than nulling C_6, since the effect of B_2 on the ratio can be nulled at all ion-ion separations by a proper choice of the C_4 coefficient. On the other hand, adding C_6 shims without adding new sources of noise seems doable, but it is not trivial.

7.3.2 Tuning the Magnetron Radius Imbalance δ_{mag}

An appealing way to deal with the effect of trap field inhomogeneities is to engineer the magnetron orbits. All of the major errors on the cyclotron frequency ratio arising from trap field imperfections result from the imbalance in the rms magnetron radii of the two ions. If the instantaneous magnetron frequencies of the two ions can be made identical, then the rms magnetron radii will also be identical. Tuning the difference in magnetron radii to zero simultaneously reduces the effect of all of the important trap field imperfections B_2, B_4, C_4, and C_6. In Sect. 4.4.1, a method was discussed for tuning the magnetron radius imbalance parameter δ_{mag} to zero. This was based on exciting a small axial motion

in one ion and tuning C_4 to create an axial-amplitude-dependent frequency shift of the instantaneous magnetron frequency of the ion. This is probably difficult to do precisely, and also introduces concerns about the effect of finite axial amplitudes while the cyclotron motions accumulate phase.

A more elegant way to tune $\delta_{\rm mag}$ to zero would be to apply a far-off-resonance sideband coupling between each ion's magnetron mode and its axial mode. This technique holds the prospect of reducing the size of $\delta_{\rm mag}$ by about an order of magnitude. The strength Ω and detuning δ of the sideband coupling would be chosen to ac Stark shift the magnetron frequencies into precise resonance with one another. For a given coupling and detuning, the frequency shift of the magnetron mode is $\Omega^2/(4\delta)$. The magnetron-axial Rabi frequency Ω can be measured to 5%. The detuning of the coupling δ can be made large enough that the fractional error due to uncertainty on the axial or magnetron frequencies is less than 1% and can be ignored. Thus, the fractional uncertainty on the Stark frequency shift is 10%. On the other hand, the difference in instantaneous magnetron frequencies is calculable to much better than 1%. Thus, the size of the magnetron frequency difference, and hence $\delta_{\rm mag}$, can potentially be reduced by a factor of 10. This simultaneously reduces the effect of B_2, B_4, C_4, and C_6 by a factor of 10! In addition, this tuning is completely independent of the ion-ion separation.

To avoid an axial amplitude imbalance while the cyclotron modes accumulate phase, both magnetron modes should be Stark shifted simultaneously by half the total frequency shift needed. Alternatively, the ion that is Stark shifted should be alternated from one cyclotron frequency measurement to the next. Although the sideband coupling is not resonant, it will induce an axial motion of order $a_{ind} \approx (\Omega/(2\delta))\sqrt{\omega_{\rm c}/\omega_{\rm z}}\rho_{\rm m}$ at a frequency of $\omega_{\rm z}+\delta$. Consider the case in which only a single coupling is applied below resonance with ion 0. Taking $\rho_{\rm s} = 1$ mm and $\rho_{\rm m} = \rho_{\rm s}/2$, this gives $a_{ind} \approx 2400 \times (\Omega/(2\delta))$ μm for the example pair $^{13}C_2H_2^+$ vs N_2^+. A soft upper limit on the detuning δ is set by the spacing between the axial frequencies of the ions, which is 61 Hz. To null the frequency difference between the magnetron modes, one must apply a differential Stark shift of 2.9 mHz. Including the effect of the coupling on ion 1, one finds that $\Omega/2\pi \approx \sqrt{8 \times 61 \text{ Hz} \times 2.9 \times 10^{-3} \text{ Hz}} \approx 1.2$ Hz. The resulting induced axial motions are $a_0 = 2 \times a_1 = 24$ μm, with both axial responses occurring at $\approx \omega_{\rm z0} - 2\pi\, 61$ Hz. The fractional difference in the squared axial amplitudes will lead to a differential shift of the cyclotron frequencies due to magnetic field inhomogeneity given by $\Delta\omega_{\rm ct2}/\bar{\omega}_{\rm c} = (1/2)(a_1^2 - a_0^2)B_2/B_0$. For the present magnetic field inhomogeneity of $B_2/B_0 = 6.1 \times 10^{-9}/\text{mm}^2$, the differential shift is only $\Delta\omega_{\rm ct2}/\bar{\omega}_{\rm c} \approx 1.3 \times 10^{-12}$. By going to a more symmetric mode coupling or by alternating which ion is receiving the dominant Stark shift, this systematic error can be reduced well below this value and will not be a concern.

The other concern of such a coupling is that it will lead to a damping of the magnetron modes. In the example above, the induced axial response is at $\omega_{\rm z0} - 2\pi$ 61 Hz. If the trap

voltage is tuned so that the axial modes lie symmetrically about the center frequency of the detector, this means that the effective damping time of axial motion at the frequency of the induced motion is ~ 22 minutes. But the fraction of the magnetron mode's action in the axial mode is down by $(\Omega/2\delta)^2 \sim 10^{-4}$. Hence, the damping of the magnetron mode has a time constant of 150 days, which is of no concern to us. Of more concern might be the amount of the magnetron mode's action left in the axial modes if the coupling is instantaneously turned off just before the π-pulse to read out the cyclotron phase. On average, the magnetron mode would lose $\sim (\Omega/2\delta)^2 \sim 10^{-4}$ of its action each time this happened. Still, one could perform 1000 such instantaneous shutoffs before changing the ion-ion separation by 5%. This can be further reduced if the coupling is ramped down over several periods of the detuning. For our example, 10 periods is only 160 ms, which is easily realizable. As a result, damping of the magnetron motions is not a real concern for our example pair.

Tuning the magnetron imbalance $\delta_{\rm mag}$ seems like a very promising route for reducing the systematic errors associated with trap field imperfections by a factor of 10. Used in combination with the technique of tuning the trap to local flatness of $\Delta f_{\rm ct}$ vs $\rho_{\rm m}$, the contribution of trap field imperfections could be suppressed well below 10^{-12} for ion-ion separations with correspondingly small ion-ion systematic errors.

We did not attempt to apply this technique because we found that if the magnetron-axial sideband coupling was left on continuously for more than 5 to 10 minutes, the center frequency of the detection circuit would drift. We attribute this to dissipation of power in the cryogenic magnetron-drive filters. These filters could be trivially modified to avoid this heating. Such a modification is also easier to implement than shims for the C_6 electrostatic imperfection.

7.3.3 Self-Consistency Checks and Scalings

A strong advantage of using molecules is that it allows a large number of self-consistency checks. For instance, we can measure both $^{13}C_2H_2^+/N_2^+$ and $^{13}CH^+/\ N^+$ to determine the same mass ratio ^{13}CH/N. The factor of 2 difference in the mass to charge actually changes the size of several systematics by quite a bit. First, the nonlinear cyclotron-cyclotron interaction is proportional to the average mass $\bar{m}$, so this effect should be twice as small for the lighter pair. Second, any imbalance in the cyclotron drive strengths or transfer functions will change when working at a different cyclotron frequency. Third, the cyclotron-cyclotron frequency pulling is proportional to $\bar{m}^2$ so that this effect will be four times smaller.

The effect of trap field imperfections changes by an even greater amount with m/q, because of the scaling of the magnetron imbalance parameter $\delta_{\rm mag}$. The net scaling of $\delta_{\rm mag}$ is $\bar{m}\bar{\omega}_{\rm m}^2 \propto \bar{m}V_{\rm r}^2$. Since the Ring voltage is always adjusted to bring the ion into resonance with the fixed frequency axial detector, the Ring voltage scales as $V_{\rm r} \propto \bar{m}$. As a result, $\delta_{\rm mag} \propto \bar{m}^3$. If the size of the trap field coefficients B_2, B_4, C_4, and C_6 do not change

significantly with trap voltage, the impact of all the trap field imperfections on the cyclotron frequency ratio will change by a factor of 8. In addition, the impact of the electrostatic imperfections C_4 and C_6 on the ratio scale as $\bar{\omega}_m/\bar{\omega}_c \propto \bar{m}^2$. As a result, the impact of electrostatic imperfections is reduced by a total factor of 32 when working with the lighter pair. In summary, measuring the same mass ratio at different average mass allows one to dramatically change the size of most systematic errors, thus providing a powerful check of systematic errors.

7.4 Double-Trap

Another method for eliminating the impact of magnetic field noise on the measured ratio of cyclotron frequencies is to use two axially adjacent Penning traps to perform simultaneous cyclotron frequency comparisons with one ion in each trap. The systematic error due to the difference in the magnetic field at the two trap centers can be canceled by alternately swapping the ions between the traps and measuring the ratio in each configuration. In this scenario, one is most sensitive to a varying linear magnetic field gradient between the alternating measurements. We have developed a coil configuration that can potentially shield such fluctuations by more than three orders of magnitude [20]^G. In the ideal measurement sequence, the ions would actually be swapped back and forth several times during the phase evolution period of a single PNP measurement in order to reduce the impact of a varying linear magnetic field gradient.

We will discuss some of the advantages of the double-trap scheme compared to our single-trap scheme. Not heating the magnetron and axial modes when swapping the ions between traps is crucial if we want to perform multiple swaps during the phase evolution period, and so will be discussed. Progress toward building the double-trap will be outlined along with possible technical problems and configurations. Lastly, disadvantages of the double-trap technique and then a weighing against our single-trap technique will be given. The comparison of the two techniques comes at the end since it is helpful to first see what is actually involved in implementing the double-trap technique.

7.4.1 Advantages

The double-trap scheme has several advantages over our two-ions-in-one-trap or single-trap technique. The biggest advantage is that it relaxes the constraint on the fractional mass difference $\Delta m/m$ of the ions being compared. Using ions with fractional mass difference $< 10^{-3}$ is currently very important for obtaining high accuracy in our single-trap technique. In addition, different charge states can be used to form good doublets in the double-trap technique. For instance, we could compare Ne^+/Ar^{++} or $Cs^{+++}/CO_2{}^+$. In this sense, the double-trap would be a much more general mass spectrometer. On the other hand, the constraint is not relaxed as much as one might at first think—a point that will be returned

to in Sect. 7.4.4.

The systematic errors appear to be smaller in the double-trap technique. First, one does not have to worry about ion-ion interactions. Second, the impact of the even azimuthally symmetric trap field imperfections are reduced. This is because one can work near the center of the traps (i.e., $\rho_m = 0$), where the multipole expansion of the field works in your favor. Roughly, the leading order systematic errors due to B_2 and C_4 on the cyclotron frequency ratio are down by $(\rho_m/\rho_c)^2 \sim (500\ \mu m/150\ \mu m)^2 \sim 10$ with respect to our single-trap technique. Even more importantly, the systematic errors due to C_6 and B_4, which we cannot shim, are down by $(\rho_m/\rho_c)^4 \sim 100$. Of course, this gain assumes that the magnetic field inhomogeneity is the same in both traps as what we now have in our single trap, which might not be easily accomplished with the present magnetic field shims alone.

Further, one can use larger cyclotron orbits in order to optimize the signal to noise in the axial mode. With twice the axial signal as used in the single-trap technique, we can typically obtain a shot-to-shot phase measurement noise of $\pm 8^\circ$ (compared to $\pm 20^\circ$ in the single-trap technique).

7.4.2 Swapping without Heating

We now turn to a discussion of how to swap ions between traps. Using techniques discussed below, it should be possible to swap the ions between the traps without increasing their axial or magnetron amplitudes. This might allow the ions to be swapped several times between the traps during a single phase evolution period. Performing multiple swaps would greatly reduce the impact of fluctuating magnetic gradients.

Swapping the ions between traps *cannot* be achieved by simple adiabatic variation of the trap voltages, since the paths of the two ions cross. This makes our swapping very different than the simple translation of ions between Penning traps that has been demonstrated in several other experiments [10], [6].

The swapping can be accomplished by very quickly bringing the Middle Endcap voltage (or Outer Endcaps) toward (away from) the Ring voltage. Each ion will accelerate toward the middle Endcap and pass through into the opposite trap if the voltage change is large enough. The Middle (or Outer) Endcap can then be restored to its previous value in order to gently catch the ion.

One wishes to toss the ion from one trap to the other much like one might play catch with an egg. Here we are not worried about breaking the ion, but about leaving the ion with a large axial excitation after being caught by the other trap. In order to do this, it is best to begin by not throwing the "egg" very hard. This can be accomplished by first adiabatically lowering the Ring voltage. Adiabatic here is understood to be with respect to the instantaneous axial frequency, meaning that the time scale for lowering the Ring voltage must be $\gg 1/f_z \sim 5\ \mu s$. One can then apply a smaller voltage change to the middle or outer endcaps in order to swap the ions.

The small voltage change on the endcaps should be done *almost* adiabatically. The swapping pulse on the endcaps should be designed both to adiabatically move the axial equilibrium position close to the Middle Endcap and to nonadiabatically produce a very small amount of kinetic energy so that it can clear any remaining potential energy barrier near the Middle Endcap. Because there is no dissipation, a time reversed sequence beginning when the ions are halfway between the traps will catch the ions in opposite traps with no axial excitation.

Simon Rainville and James V. Porto have performed numerical simulations showing that it is possible to swap the ions between traps using ms voltage pulses with RC rise and fall characteristics. Given an RC time constant, one varies the pulse amplitude and duration in order to swap the ions without exciting their axial modes. Using pulse shapes with RC profiles is important, because experimentally, a square input pulse will be distorted by various frequency filters in the VBox and the cryogenic electronics. The actual fine tuning of the pulse amplitude and duration would be performed empirically with ions in the trap. The ms time scale of the pulses is also important, because the frequency components are then far from the center frequency of our detector, allowing us to filter out noise that might affect our detection signal to noise. Rainville and Porto have also shown that it might be possible to perform the swapping with very short voltage pulses of order 25 μs, which would be advantageous for eliminating errors on the measured axial frequency for multiple swaps during a single PNP.

Given the presently measured trap tilt of $\sim 1^\circ \sim 0.02$ rad and a separation between the trap centers of ~ 2.5 cm, the ions should just pass through the 500 μm diameter holes in the Center Endcap, since $(2.5\,\mathrm{cm}/2)\sin(0.02\text{ rad}) \sim 250$ μm. Thus, it might be necessary to increase the hole size. But the Middle and Outer Endcaps should all be increased by the same amount in order to maintain symmetry about the plane $z = 0$.

At the end of a swap, the ions will have magnetron orbits of order 500 μm given the present trap tilt. This prediction assumes that during the swap, the radial motion is purely cyclotron motion and the guiding center will simply travel along a magnetic field line. In order to swap the ions between traps without creating significant magnetron motion, it is important that the trap equilibrium positions (i.e., the ion locations when $\rho_c{=}\rho_m{=}0$) be connected by a magnetic field line. This can be achieved by orienting the split Guard Rings in the separate traps at 90° with respect to one another. By biasing a pair of Guard Rings on one side of the trap, the equilibrium position in the upper trap can be translated in the horizontal plane along $\hat{x}$, while the equilibrium position in the lower trap can be translated along $\hat{y}$. By properly biasing the two pairs of Guard Rings, it should be possible to avoid heating of the magnetron orbit when swapping the ions. The magntiude of the differential bias voltages required is comparable to the Ring voltage given the screening of the Guard Ring electrodes. However, it might also be possible to simply drive the magnetron amplitude to zero with a magnetron drive with a fixed amplitude and fixed phase relationship with

respect to the swapping pulse. Using a magnetron zeroing drive would be preferable to biasing the Guard Rings since the complexity of the cryogenic apparatus would not have to be increased.

Careful control of the swap pulses and alignment of the trap equilibrium positions as described above should allow the ions to be swapped between traps several times during a single cyclotron phase evolution period. Swapping will reduce the impact of changing magnetic field gradients on the measured cyclotron frequency ratio.

7.4.3 Technical Implementation

In the usual ICR lab hedging of bets, the double-trap scheme was initially pursued even while Michael P. Bradley and James V. Porto were still fighting noise pickup on the current apparatus. Given the trouble in getting the current single-trap apparatus to work, Simon and I thought it best to try the two-ion or single-trap technique first. I will give an overview of the current status, and discuss some of the technical issues that should be considered before construction begins again.

The double trap has been machined and is ready for assembly. The two traps are identical to the current traps, but the Middle Endcap has been made slightly thinner in order to move the trap centers to a separation of 2.5 cm. This separation is as small as possible while still maintaining the geometry and size of our present trap. The insert tube has been machined with supports for the cryogenic filter stages as well as the brass tongue-in-groove piece for forming the indium solder joint with the mating OFHC vacuum can [20]^G. The parts for assembling the central wire harness have also been machined. The main parts that are missing are the cryogenic electronics and all of the actual wiring.

There are several decisions which should be made before proceeding with construction. The first is where on the traps should we make the connection to the self-resonant transformer. The choices are a single connection to the Middle Endcap or two connections with one on each Outer Endcap. I believe that the Middle Endcap is the clear choice. In previous work, attaching the detector to the Lower Endcap, which is near the FEP (and which must still be located below the Lower Endcap), significantly dropped the Q of the axial detector. In addition, using the Middle Endcap as the pickup seems safer for avoiding noise pickup.*

Choosing the Middle Endcap as the pickup dictates that the outer endcaps should be pulsed in order to swap the ions between traps. The voltage adder in the current trap voltage source, or VBox, allows for voltage pulses of duration slightly less than a ms to pass through to the Ring. This should allow the Ring voltages to be adiabatically reduced just before applying the swap pulse. In order to apply the swap voltages to the outer endcaps, it might be necessary to add an external voltage adder (similar to the Guard Ring add on GBox).†

*With the Middle Endcap as the pickup, the Upper Endcap could also be used to shut the barn door if an external ion source were implemented for creating difficult ion species.

†One could be tempted to simply rely on the Dip capability of the VBox. The timing of the sequence

One must also decide how many independent voltages are needed. It would be nice to have independent Ring voltages for the two traps. This would allow the axial motion of each ion to be independently tuned to resonance with the detector. The down side is that the voltages can drift with respect to one another. This ought not be a serious problem if all of the solder connections are methodically heat sunk to one another so that any temperature variation causes only common changes in the contact potentials. It will be necessary to have two independent Guard Ring voltages to tune out C_4 in both traps. In addition, if it is necessary to move the trap equilibrium positions before swapping the ions, two independent bias voltages will be needed to accomplish this. It does not appear necessary to have independent Outer Endcap voltages. All told, this adds up to five new voltage sources and lines, all of which must avoid dumping noise into the insert. In reality, the current trap voltage source or VBox already produces two independent sets of Ring and Guard Ring voltages. It is simply a matter of modifying the VBox to output both pairs of voltages at the same time.

7.4.4 Disadvantages

There are disadvantages associated with the double-trap compared to the single-trap technique. The greatest disadvantages are the increased complexity of the cryogenic apparatus and the large number of additional stable trap voltages. Complexity of the cryogenic apparatus is not trivial since a lot of time can be burned cycling the apparatus from room temperature to 4 K. In addition, there will be many new noise paths associated with the increased number of electrodes and connections. Additionally, it might not be possible with the current superconducting shims to achieve adequate shimming of the lowest order magnetic field inhomogeneities B_1 and B_2 at both trap centers.

The double-trap technique can be used to compare non-doublets, i.e., ions with significantly different m/q. But the large reduction of sensitivity to magnetic field noise no longer holds. Generalizing the results of Sect. 5.1 to ions with possibly different charge, simultaneous cyclotron frequency comparison reduces the impact of magnetic field noise on the ratio by the fractional difference in the mass to charge $\Delta(m/q)/(m/q)$ of the ions being compared. The reason for this is that we do not actually perform simultaneous frequency comparisons. Instead we measure the difference in phase accumulated by the two ions in some time interval. This fact limits the possible comparisons for which magnetic field noise would not be a problem. If one were to compare $CH_4{}^+$ to C^+ in order to determine the atomic mass of hydrogen, the impact of magnetic field noise on the measured ratio would be down by only 0.3. Hence, even in the double-trap technique, it will be necessary to form reasonable doublets. Assuming fractional magnetic field fluctuations of $\sim 10^{-9}$, it will be necessary to use doublets with fractional mass to charge difference $\leq 10^{-2}$ in order to

of events in the VBox is not understood at the moment, and should be explored first. If using the Dip capability of the VBox works, then this will be fantastic.

reduce the fluctuations of the measured ratio to $\leq 10^{-11}$. This is not a terribly difficult constraint to meet, but it is important to understand.

One must also pay more attention to the odd order terms in the multipole expansion of the fields. In the single-trap technique, a uniform electric field along the axial direction, as characterized by a C_1, causes a common displacement of both ions along the axial direction. In the double-trap technique, if different trap voltages are used during the phase evolution period of the PNP measurement, the uniform electric field will cause a relative displacement of the two ions. This will cause a relative cyclotron frequency shift (and hence a systematic error) in the presence of a linear magnetic field gradient along the axial direction, such as that characterized by B_1. One must either use the same trap voltage (in a given trap) for both ions during the phase evolution time or use good doublets that do not suffer from this shift, since the trap voltages that make the ions resonant with the axial detector are very similar. Odd order field imperfections could also be eliminated using our SOF technique described in [46][G].

7.4.5 Techniques in the Balance

If one's goal is to have a flexible mass spectrometer that can measure masses in the range of 1 u to 133 u (i.e., H to Cs), then clearly the double-trap technique wins. The engineering problems are just that—problems that can be solved by careful design and avoidance of noise pickup. Once the double-trap scheme is working, one can produce many mass measurements very quickly and with accuracies of $\sim 10^{-12}$. In addition, the double-trap is probably the best route for obtaining fractional mass accuracies beyond 10^{-12}. Lastly, the double-trap technique has the advantage that it could work with highly charged ions for measuring very heavy masses. There is no fundamental obstacle for the double-trap technique, and its implementation would clearly advance the general application of precision mass spectrometry.

On the other hand, if one's interest is to determine masses in the range of 1 u to 40 u with accuracies of $\sim 10^{-12}$, our single-trap technique can most likely do the trick. The single-trap technique will work especially well for comparing light ions such as $^3He^+/^3H^+$ or antiproton/H^-. For making another MIT mass table (I should say FSU mass table!) over the range 1 u to 40 u, almost all of the necessary mass comparisons have fractional mass differences of $\leq 3\times10^{-3}$. There are a few nondoublet comparisons and comparisons of ions with different charge states that can easily be replaced by doublet comparisons.[‡] Our single-trap technique holds promise for achieving accuracies of $\sim 10^{-12}$. Additionally, it looks promising that the technique can be extended to ions with fractional mass differences $\sim 3\times10^{-3}$ using techniques proposed in this thesis.[§]

[‡]For instance, the comparisons Ar^+/Ne^+, $CD_4{}^+/C^+$, and Ar^{++}/Ne^+ could be replaced by the doublet comparisons $C_2D_6{}^+/C_3{}^+$ and $Ar^+/C_3H_4{}^+$.

[§]Specifically, the proposals include using ions with smaller mass to charge or using lower axial frequencies (Sect. 7.3.3), axial detection with FM sidebands or alternate axial readout (Sect. 5.3.1), and tuning the

If I were designing a mass spectrometer from scratch and had one to three years to make it work and two to five years to perform mass measurements, I would strongly consider building the double-trap. On the other hand, the single-trap technique holds great promise for performing most mass comparisons of current interest. I believe our two-ions-in-one-trap technique ought to be pursued as long as possible, since it is a proven technique and holds the possibility of accomplishing mass comparisons with fractional accuracies of 10^{-12}.

imbalance in the magnetron radii of the two ions δ_{mag} to zero by Stark shifting the magnetron modes into resonance with one another (Sect. 7.3.2).

Bibliography

[1] S. Rainville, Ph.D. thesis, Massachusetts Institute of Technology, 2003.

[2] E. Cornell, K. Boyce, D. Fygenson, and D. Pritchard, "2 Ions in a Penning trap—implications for precision mass-spectroscopy," Phys. Rev. A **45**, 3049 (1992).

[3] B. D'Urso, B. Odom, and G. Gabrielse, "Feedback cooling of a one-electron oscillator," Phys. Rev. Lett. **90**, 043001 (2003).

[4] J. Verdu *et al.*, "The magnetic moment anomaly of the electron bound in hydrogen-like oxygen $^{16}O^{7+}$," J. Phys. B **36**, 655 (2003).

[5] M. Amoretti *et al.*, "Production and detection of cold antihydrogen atoms," Nature **419**, 456 (2002).

[6] G. Gabrielse *et al.*, "Background-free observation of cold antihydrogen with field- ionization analysis of its states," Phys. Rev. Lett. **89**, 213401 (2002).

[7] R. VanDyck, D. Farnham, S. Zafonte, and P. Schwinberg, "Ultrastable superconducting magnet system for a penning trap mass spectrometer," Rev. Sci. Instrum. **70**, 1665 (1999).

[8] R. VanDyck, S. Zafonte, and P. Schwinberg, "Ultra-precise mass measurements using the UW-PTMS," Hyperfine Interact. **132**, 163 (2001).

[9] D. Farnham, R. Vandyck, and P. Schwinberg, "Determination of the electron's atomic mass and the proton/electron mass ratio via Penning trap mass-spectroscopy," Phys. Rev. Lett. **75**, 3598 (1995).

[10] T. Beier *et al.*, "New determination of the electron's mass," Phys. Rev. Lett. **88**, 011603 (2002).

[11] G. Gabrielse, A. Khabbaz, D. Hall, C. Heimann, H. Kalinowsky, and W. Jhe, "Precision mass spectroscopy of the antiproton and proton using simultaneously trapped particles," Phys. Rev. Lett. **82**, 3198 (1999).

[12] I. Bergstrom, T. Fritioff, R. Schuch, and J. Schonfelder, "On the masses of ^{28}Si and the proton determined in a Penning trap," Phys. Scr. **66**, 201 (2002).

[13] G. Douysset, T. Fritioff, C. Carlberg, I. Bergstrom, and M. Bjorkhage, "Determination of the Ge-76 double beta decay Q value," Phys. Rev. Lett. **86**, 4259 (2001).

[14] M. Bradley, J. Porto, S. Rainville, J. Thompson, and D. Pritchard, "Penning trap measurements of the masses of ^{133}Cs, ^{87}Rb, ^{85}Rb, and ^{23}Na with uncertainties ≤ 0.2 ppb," Phys. Rev. Lett. **83**, 4510 (1999).

[15] F. DiFilippo, V. Natarajan, K. Boyce, and D. Pritchard, "Accurate atomic masses for fundamental metrology," Phys. Rev. Lett. **73**, 1481 (1994).

[16] B. Fogelberg, K. Mezilev, H. Mach, V. Isakov, and J. Slivova, "Precise atomic mass values near ^{132}Sn: The resolution of a puzzle," Phys. Rev. Lett. **82**, 1823 (1999).

[17] G. Greene, M. Dewey, E. Kessler, and E. Fischbach, "Test of special relativity by a determination of the Lorentz limiting velocity—Does $E = mc^2$?," Phys. Rev. D **44**, R2216 (1991).

[18] J. Bonn *et al.*, "Newest results from the Mainz neutrino-mass experiment," Phys. Atom. Nuclei **63**, 969 (2000).

[19] V. Lobashev, "The search for the neutrino mass by direct method in the tritium beta-decay and perspectives of study it in the project KATRIN," Nuc. Phys. A **A719**, 153c (2003).

[20] M. Bradley, Ph.D. thesis, Massachusetts Institute of Technology, 2000.

[21] H. Stolzenberg *et al.*, "Accurate mass determination of short-lived isotopes by a tandem Penning-trap mass-spectrometer," Phys. Rev. Lett. **65**, 3104 (1990).

[22] G. Audi and A. Wapstra, "The 1995 update to the atomic mass evaluation," Nucl. Phys. A **595**, 409 (1995).

[23] D. Pritchard, M. Bradley, J. Porto, S. Rainville, and J. Thompson, in *ICAP, Atomic Physics 17* (AIP Conference Proceedings 2001, 551, Florence, Italy, 2000), pp. 73–85.

[24] E. Williams, R. Steiner, D. Newell, and P. Olsen, "Accurate measurement of the Planck constant," Phys. Rev. Lett. **81**, 2404 (1998).

[25] B. Taylor, "Determining the Avogadro constant from electrical measurements," Metrologia **31**, 181 (1994).

[26] T. Udem, A. Huber, B. Gross, J. Reichert, M. Prevedelli, M. Weitz, and T. Hansch, "Phase-coherent measurement of the hydrogen 1S-2S transition frequency with an optical frequency interval divider chain," Phys. Rev. Lett. **79**, 2646 (1997).

[27] R. VanDyck, D. Farnham, S. Zafonte, and P. Schwinberg, in *Trapped Charged Particles and Fundamental Physics* (AIP, Asilomar, CA, 1998), Vol. 457, pp. 101–110.

[28] H. Haffner *et al.*, in *Abstracts of 17th International Conference on Atomic Physics*, edited by F. Fuso and F. Cervelli (AIP, Firenze, Italy, 2000), pp. 27–28.

[29] P. Mohr and B. Taylor, "CODATA recommended values of the fundamental physical constants: 1998," Rev. Mod. Phys. **72**, 351 (2000).

[30] A. Wicht, J. Hensley, E. Sarajlic, and S. Chu, "A preliminary measurement of the fine structure constant based on atom interferometry," Phys. Scr. **T102**, 82 (2002).

[31] M. George, L. Lombardi, and E. Hessels, "Precision microwave measurement of the 2(3)P(1)-2(3)P(0) interval in atomic helium: A determination of the fine- structure constant," Phys. Rev. Lett. **87**, 173002 (2001).

[32] R. Battesti *et al.*, "Acceleration of ultracold atoms: towards a measurement of h/m-Rb," J. Opt. B-Quantum Semicl. Opt. **5**, S178 (2003).

[33] S. Gupta, K. Dieckmann, Z. Hadzibabic, and D. Pritchard, "Contrast interferometry using Bose-Einstein condensates to measure h/m and α," Phys. Rev. Lett. **89**, 140401 (2002).

[34] E. Kessler, M. Dewey, R. Deslattes, A. Henins, H. Borner, M. Jentschel, and H. Lehmann, "The GAMS4 flat crystal facility," Nucl. Instrum. Methods A **457**, 187 (2001).

[35] M. Haugan and C. Will, "Modern tests of special relativity," Phys. Today **40**, 69 (1987).

[36] P. Linstrom and W. Mallard, eds., NIST Chemistry WebBook, NIST Standard Reference Database Number 69, March 2003, National Institute of Standards and Technology, Gaithersburg MD 20899 (http://webbook.nist.gov).

[37] E. Kessler *et al.*, "The deuteron binding energy and the neutron mass," Phys. Lett. A **255**, 221 (1999).

[38] L. Brown and G. Gabrielse, "Geonium theory—physics of a single electron or ion in a Penning trap," Rev. Mod. Phys. **58**, 233 (1986).

[39] E. Cornell, R. Weisskoff, K. Boyce, and D. Pritchard, "Mode-coupling in a Penning trap—π-pulses and a classical avoided crossing," Phys. Rev. A **41**, 312 (1990).

[40] E. Cornell, R. Weisskoff, K. Boyce, R. Flanagan, G. Lafyatis, and D. Pritchard, "Single-ion cyclotron-resonance measurement of $M(CO^+)/M(N_2^+)$," Phys. Rev. Lett. **63**, 1674 (1989).

[41] R. Weisskoff, Ph.D. thesis, Massachusetts Institute of Technology, 1988.

[42] R. Nguyen, B.S. thesis, Massachusetts Institute of Technology, 1998.

[43] F. DiFilippo, Ph.D. thesis, Massachusetts Institute of Technology, 1994.

[44] J. Jackson, *Classical Electrodynamics*, 2nd ed. (Wiley and Sons, New York, 1975).

[45] V. Natarajan, Ph.D. thesis, Massachusetts Institute of Technology, 1993.

[46] V. Natarajan, K. Boyce, F. DiFilippo, and D. Pritchard, "Precision Penning trap comparison of nondoublets—Atomic masses of H, D, and the neutron," Phys. Rev. Lett. **71**, 1998 (1993).

[47] T. Dixon and R. Woods, "Microwave absorption spectrum of the CO^+ ion," Phys. Rev. Lett. **34**, 61 (1975).

[48] P. Martin and M. Feher, "CASSCF calculations of the multipole moments and dipole polarisability functions of the $X^2\Sigma^+$ and $A^2\Pi$ states of CO^+," Chem. Phys. Lett. **232**, 491 (1995).

[49] P. Rosmus and H. Werner, "*Ab initio* calculations of radiative transition probabilities in the $X^2\Sigma^+$ and $A^2\Pi$ electronic states of CO^+," Molecular Phys. **47**, 661 (1982).

[50] P. Certain and R. Woods, "On the dipole moment of CO^+," J. Chem. Phys. **58**, 5837 (1973).

[51] C. Townes and A. Schawlow, *Microwave Spectroscopy*, 2nd ed. (Dover Publications Inc., New York, NY, 1975).

[52] G. Herzberg, *Molecular Spectra and Molecular Structure: 4. Constants of Diatomic Molecules*, 2nd ed. (D. Van Nostrand Company, Inc., NewYork, NY, 1965), Vol. 4.

[53] C. Ekstrom, J. Schmiedmayer, M. Chapman, T. Hammond, and D. Pritchard, "Measurement of the electric polarizability of sodium with an atom interferometer," Phys. Rev. A **51**, 3883 (1995).

[54] T. Miller and B. Bederson, *Advances in Atomic, Molecular, and Optical Physics*, Vol. 13 (Academic Press, New York, 1977).

[55] A. Bhatia and R. Drachman, "Polarizability of helium and the negative hydrogen ion," J. Phys. B **27**, 1299 (1994).

[56] A. Bhatia and R. Drachman, "Static properties and the Stark effect of the ground state of the HD molecular ion," Phys. Rev. A. **61**, 032503/1 (2000).

[57] A. Kalemos, A. Mavridis, and A. Metropoulos, "An accurate description of the ground and excited states of SiH," J. Chem. Phys. **116**, 6529 (2002).

[58] J. Senekowitsch, H. Werner, P. Rosmus, E. Reinsch, and S. Oneil, "*Ab initio* calculations of radiative transition probabilities in SH, SH^+, and SH^-," J. Chem. Phys. **83**, 4661 (1985).

[59] H. Werner, P. Rosmus, and E. Reinsch, "Molecular properties from MCSCF-SCEP wave-functions. 1. Accurate dipole-moment functions of OH, OH^-, and OH^+," J. Chem. Phys. **79**, 905 (1983).